Late Alpine cooling histories of tectonic blocks along the central part of the Transalp-Traverse (Inntal – Gadertal): constraints from geochronology

DISSERTATION

zur Erlangung des Grades eines Doktors
der Naturwissenschaften

der Geowissenschaftlichen Fakultät der
Eberhardt-Karls-Universität Tübingen

vorgelegt von

Petra Most
aus Göppingen

2003

Tag der mündlichen Prüfung: 3. Februar 2003

Dekan: Prof. Dr. Dr. h.c. Muharrem Satir

1. Berichterstatter: Prof. Dr. Wolfgang Frisch

2. Berichterstatter: Priv. Doz. Dr. Joachim Kuhlemann

Vorwort

Mein Dank gilt an erster Stelle Prof. Dr. Wolfgang Frisch, der mir die Durchführung dieser Arbeit ermöglicht hat. Er war stets bereit mit mir zu diskutieren und hat damit sehr zum Gelingen dieser Arbeit beigetragen. Auch möchte ich mich dafür bedanken, daß er mir die Möglichkeit zum Erwerb von Lehrerfahrung gab, und mir die Teilnahme an Fortbildungskursen und an vielen internationalen Tagungen ermöglichte. Dank seiner Unterstützung konnte ich auch Erfahrungen in Arbeitsgebieten außerhalb der Alpen machen. Die gemütlichen Abende in diversen Tavernen und Berggasthöfen nach gemeinsamer Geländearbeit werden unvergessen bleiben.

PD Dr. Joachim Kuhlemann möchte ich für die Übernahme des Korreferats und für die vielen Anregungen und Diskussionen danken.

Dr. István Dunkl danke ich für die Einweisung in die Spaltspurendatierung. Bei den zahlreichen Reaktorproblemen war er immer der ruhende Pol, der sich um Lösungen kümmerte. Für seine tatkräftige Unterstützung, vor allem in der Endphase dieser Arbeit, möchte ich mich bei Ihm und auch seiner Frau Judith bedanken.

Dr. Kadosa Balogh (Institute of Nuclear Research, Debreccen, Ungarn) führte die K/Ar Messungen durch.

Dr. Wolfgang Siebel möchte ich für die Rb/Sr Datierungen danken. Seine Diskussionsbereitschaft hat mir bei der Interpretation sehr geholfen.

Bei Dr. Mathias Westphal möchte ich mich für die Einführung in die Bedienung der Mikrosonde bedanken, und dafür, daß er mir die Vorteile der WDX nähergebracht hat. Auch stand er immer mit Rat und Tat zur Seite, wenn die Sonde beschloß Ihr Eigenleben zu entwickeln und zu streiken. Er war immer bereit meine Daten mit mir zu diskutieren.

PD Dr. Thomas Wenzel danke ich für die Hilfe bei den Mikrosondenanalysen der Apatite.

Mein besonderer Dank gilt unseren TA´s Gerlinde Höckh, Dagmar Kost und Doris Mühlbayer Renner. Ohne deren tatkräftige Unterstützung bei der Probenaufbereitung für die Altersdatierungen hätte ich nur die Hälfte meiner vielen Proben bearbeiten können. Dazu haben auch Thomas Piepenbrink (Grobpräparation) und Steffi Braun (Mineralseparation) beigetragen. Danke. Frau Indra Gill-Kopp hat die Dünn- und Mikrosondenschliffe hergestellt.

Der Deutschen Forschungsgemeinschaft danke ich für die finanzielle Unterstützung des Projektes. Der Start des Projektes wurde durch finanzielle Hilfe der Universität Tübingen in Form von wiss. Hilfskraft-Mitteln durch Prof. Dr. Wolfgang Frisch erleichtert.

Für Diskussionen und Gespräche, aber auch für die Ablenkung von der Wissenschaft danke ich Ines Dünkel, Uwe Dünkel, Horst Hann, Franz Moser, Martina Schwab und Conny Spiegel.

Mein ganz besonderer Dank gilt meinem Mann Thomas Most, der mich auch bei den Geländearbeiten in den Alpen begleitet und unterstützt hat. Ohne seine tatkräftige Hilfe würde manche Gesteinsprobe immer noch auf 3000m liegen. Die regen Diskussionen im Gelände, aber auch die schönen Hüttenabende werde ich nicht vergessen.

Abstract

The present structure of the Alps is a result of continuous convergence between the European and African plates during the Alpine Orogeny. Even today this still ongoing mountain-building process is not fully understood. The Transalp project is an international and multidisciplinary research program for investigating the orogenic processes driven by the collision of the European and Adriatic continental lithospheric plates. The seismic reflecting profile along the transect Munich (Germany) – Venice (Italy) was designed to unravel the deep structures and developmental history of the Eastern Alps.

This study is part of the Transalp project and aims to reconstruct the Late Alpine cooling and exhumation history of different blocks and units along the central part of the Transalp-Traverse (Inntal – Gadertal). Therefore 61 samples were collected for geochronological investigations, mainly for fission track dating. The sampling strategy was to extend a pre-existing dataset into areas without data, as well as to collect samples from vertical relief profiles.

Geochronological data based on Rb/Sr white mica, K/Ar white mica, K/Ar biotite, Rb/Sr biotite and zircon and apatite fission track data are used to construct and model several time-temperature paths. Out of this data exhumation rates were calculated.

For the Austroalpine units with pre-Alpine or partly Alpine rejuvenated mica ages, the zircon fission track ages indicate Early Cretaceous cooling below 240° C of the Upper Austroalpine Northern Greywacke Zone and the Upper Austroalpine Altkristallin southern block. Whereas the Lower Austroalpine Innsbruck Quartzphyllite and the Schwazer Augengneis cooled not until Paleocene times below the closure temperature of zircons. Final cooling below 100° C occurred in the Northern Greywacke Zone in Eocene, and in the Altkristallin southern block, the Innsbruck Quartzphyllite and the Schwazer Augengneis in the Middle-Late Miocene as indicated by the apatite fission track age.

In the Penninic units and the Upper Austroalpine Altkristallin northern block Oligocene-Miocene mica cooling ages are predominant. The zircon fission track ages indicate common Miocene cooling below 225° C. In the Zentralgneis of the western Tauern window the zircon fission track ages, and also the apatite fission track ages, depend on the altitude. In contrast to the Penninic units, the ages obtained in the Altkristallin northern block have a narrow range around 22 Ma and show no correlation with the altitude, which indicates rapid exhumation of this block. The apatite fission track ages show ongoing Middle-Late Miocene cooling.

Apatite fission track ages together with track length distributions are used for thermal modelling. The thermal histories show different trends and reflect regional variations in the rate of cooling.

It is not possible to convert cooling paths, estimated from geochronological data, directly into exhumation histories. Therefore the program EXHUME was used to model some P-T-t paths, but the results were not convincing. The problem is that assumptions must be made about the geothermal gradient. Therefore exhumation rates were calculated with the altitude dependence method. This method gives reliable exhumation rates for the Penninic Zentralgneis in the order of 1.1 mm/a for the time between 14 and 12 Ma, and 0.6 mm/a for the time interval 9-5 Ma.

Zusammenfassung

Die heutige Struktur der Alpen ist das Ergebnis anhaltender Konvergenz zwischen der europäischen und der afrikanischen Platte während der alpinen Orogenese. Bis heute ist dieser immer noch andauernde Gebirgsbildung nicht vollständig verstanden. Das Transalp Projekt ist ein internationales und multidisziplinäres Forschungsvorhaben zur Untersuchung von Prozessen der Gebirgsbildung bei der Kollision kontinentaler Lithosspärenplatten. Mit Hilfe des reflexionsseismischen Profil zwischen München (Deutschland) und Venedig (Italien) sollen die Tiefenstrukturen und die Entwicklungsgeschichte der Ostalpen weiter entschlüsselt werden.
Diese Arbeit ist Teil des Transalp Projekts und hat die Rekonstruktion der Abkühlungs- und Hebungsgeschichte der unterschiedlichen Blöcke und Einheiten entlang des Zentralabschnitts der Transalp-Traverse (Inntal – Gadertal) als Ziel. Dafür wurden 61 Proben für geochronologische Untersuchungen, hauptsächlich für Spaltspurendatierungen, gesammelt. Die Proben wurden hauptsächlich in Gebieten gesammelt, aus denen bislang kaum Daten existieren um die Lücken zu schließen. Auch wurde auf eine Beprobung entlang von vertikalen Höhenprofilen geachtet.
Geochronologische Daten basierend auf Rb/Sr Hellglimmeralter, K/Ar Hellglimmeralter, K/Ar Biotitalter, Rb/Sr Biotitalter und Spaltspurendatierungen an Zirkon und Apatit wurden für die Konstruktion und Modellierung von Zeit-Temperatur Pfaden verwendet. Mit Hilfe dieser Pfade wurden Hebungsraten ermittelt.

Für die ostalpinen Einheiten mit vor-alpidischen oder teilweise alpidisch verjüngten Glimmeraltern, zeigen die Zirkonspaltspurendatierungen eine frühkretazische Abkühlung unter 240° C für die oberostalpine Nördliche Grauwackenzone und den oberostalpinen Altkristallinen Südblock. Der unterostalpine Innsbrucker Quarzphyllit und der Schwazer Augengneis hingegen sind erst im Paläozen unter die Schließungstemperatur des Zirkons abgekühlt. Die weitere Abkühlung unter 100° C erfolgte in der Nördlichen Grauwackenzone im Eozän, hingegen im Altkristallinen Südblock, dem Innsbrucker Quarzphyllit und dem Schwazer Augengneis erst im mittleren bis späten Miozän. Dies wird durch die Apatitspaltspurenalter angezeigt.

In den penninischen Einheiten und dem oberostalpinen Altkristallinen Nordblock sind oligozäne-miozäne Glimmerabkühlalter weit verbreitet. Die Zirkonspaltspurenalter ergeben eine gemeinsame miozäne Abkühlung unterhalb 225° C. Im Zentralgneis des westlichen Tauernfensters konnte eine höhenabhänige Altesverteilung der Spaltspurenalter festgestellt werden. Im Gegensatz dazu ergibt die Spaltspurendatierung im Altkristallinen Nordblock einen engen Bereich der Zirkonalter um 22 Ma. Eine Korrelation mit der Höhe ist nicht erkennbar. Dies zeigt an, daß dieser Block sehr schnell herausgehoben wurde. Die Apatitspaltspurenalter zeigen die weitere mittel bis spät miozäne Abkühlung.

Die Apatitspaltspurenalter wurden zusammen mit den Spaltspurenlängenverteilungen für die thermische Modellierung benutzt. Die thermischen Geschichten zeigen unterschiedliche Trends und reflektieren die regionalen Unterschiede in den Abkühlungsraten.

Es ist nicht möglich Abkühlungspfade, die aus den geochronologischen Daten ermittelt wurden, direkt in Hebungsgeschichten zu konvertieren. Daher wurde das Programm EXHUME verwendet um einige P-T-t Pfade zu modellieren, aber die Ergebnisse waren nicht überzeugend. Das Problem bei der Modellierung ist, daß ein geothermischer Gradient angenommen werden muß. Daher wurden die Hebungsraten mit der höhenabhängigen

Methode berechnet. Diese Methode ergibt verläßliche Hebungsraten für den penninischen Zentralgneis in der Größenordnung von 1.1 mm/a für die Zeit zwischen 14 und 12 Ma, und 0.6 mm/a für den Zeitraum 9-5 Ma.

Contents

Appendix

1 Introduction and aim of the study

The Transalp project is an international and multidisciplinary research program for investigating orogenic processes driven by the collision of the European and Adriatic continental lithospheric plates. The project consists of two main parts:

- (A) Active and passive seismological experiments (main part).
- (B) Accompanying multidisciplinary geoscience projects.

The aim of the main part is to provide a continuous seismic reflecting profile through the Eastern Alps along the transect Munich (Germany) – Venice (Italy). This seismic profile should help to unravel the deep structures and developmental history of the Eastern Alps. It fills a gap of detailed seismic knowledge between the Eastern Swiss Alps and the Carpathians. Head of the German seismic group is H. Gebrande (University of Munich, Germany). B. Lammerer (University of Munich, Germany) is responsible for the interpretation of the deep structures in combination with the surface geology of the German and Austrian sector, A. Castellarin (University of Bologna; Italy) of the Italian sector.

In the frame of the Transalp project, this study focuses on geochronological investigations along the central part (Inntal – Gadertal) of the Transalp-Traverse. The aim is the reconstruction of the exhumation and cooling history of the different units and blocks of the study area. Therefore the following methods are applied:

- The main subject is the zircon and apatite fission track dating method. Zircon fission track ages are rare. Existing apatite fission track ages are based on the internal detector method. In this study the reproducible external detector method is used.
- In regions with a lack of mica ages, additionally K/Ar and Rb/Sr analysis are performed to complete the data set.
- Of prime importance are the apatite fission track lengths distributions. Until now, they are missing in the study area. They provide an important tool for modelling the low temperature cooling history.
- Microprobe analysis of white micas used for K/Ar dating and of apatites used for thermal modelling.
- Additional geothermobarometrical investigations.

From the data above, time-temperature paths of the different units will be reconstructed to lead to a better understanding of Alpine orogeny.

2 Geology

2.1 Geological setting

Field work was mainly carried out along the central part of the Transalp-Traverse (Fig. 2.1) which, in the study area, crosscuts from north to south the following Austroalpine, Penninic and Southalpine units (Tab. 2.1):

North	Austroalpine units	Upper Austroalpine Northern Greywacke Zone Lower Austroalpine Innsbruck Quartzphyllite and Schwazer Augengneis
↓	Penninic units	South Penninic Glockner Nappe complex Middle Penninic Venediger Nappe complex South Penninic Glockner Nappe complex
	Austroalpine unit	Upper Austroalpine crystalline basement complex
South	Southalpine unit	Southalpine Brixen Quartzphyllite

Tab. 2.1: Austroalpine, Penninic and Southalpine units in the study area.

Additionally samples of the Rensen and Rieserferner intrusions, situated east and west of the Traverse, were included.
A generalised geological and tectonic overview, mainly based on the map of Brandner (1985) is shown in Fig. 2.1.

2.1.1 Penninic units

In the Eastern Alps, Penninic rocks are only exposed in tectonic windows, e.g., the Tauern window and the Rechnitz window.
The Tauern window is nearly 30 km wide and 160 km long in W-E extension from the Brenner Pass in the west to the Katschberg Pass in the east. There are large-scale low-angle normal faults (extensional shear zones) at the western and eastern boundaries of the Tauern window (Behrmann 1988; Selverstone 1988; Genser & Neubauer 1989), which were mainly active in Early to Middle Miocene times (Fügenschuh 1995). To the north, the eastern and central Tauern window is limited by a high-angle fault, the Salzach fault or "Tauern-Nordrandstörung". It has been active in the Oligocene-Miocene as a (ductile-brittle) sinistral strike-slip fault with a supposed offset of 60-100 km (Ratschbacher et al. 1991). The prolongation of the Salzach fault to the western end of the window is not known. Splay fault zones probably partition the amount of displacement and enter the Penninic realm of the western Tauern window (Frisch et al. 2000). The frame of the Tauern window is formed by the structurally higher Austroalpine units. In the Tauern window two main lithological and tectonic units are exposed (Fig. 2.1): the Middle Penninic Venediger Nappe (Frisch 1976) and the overlying South Penninic Glockner Nappe (Frisch 1974, 1976).

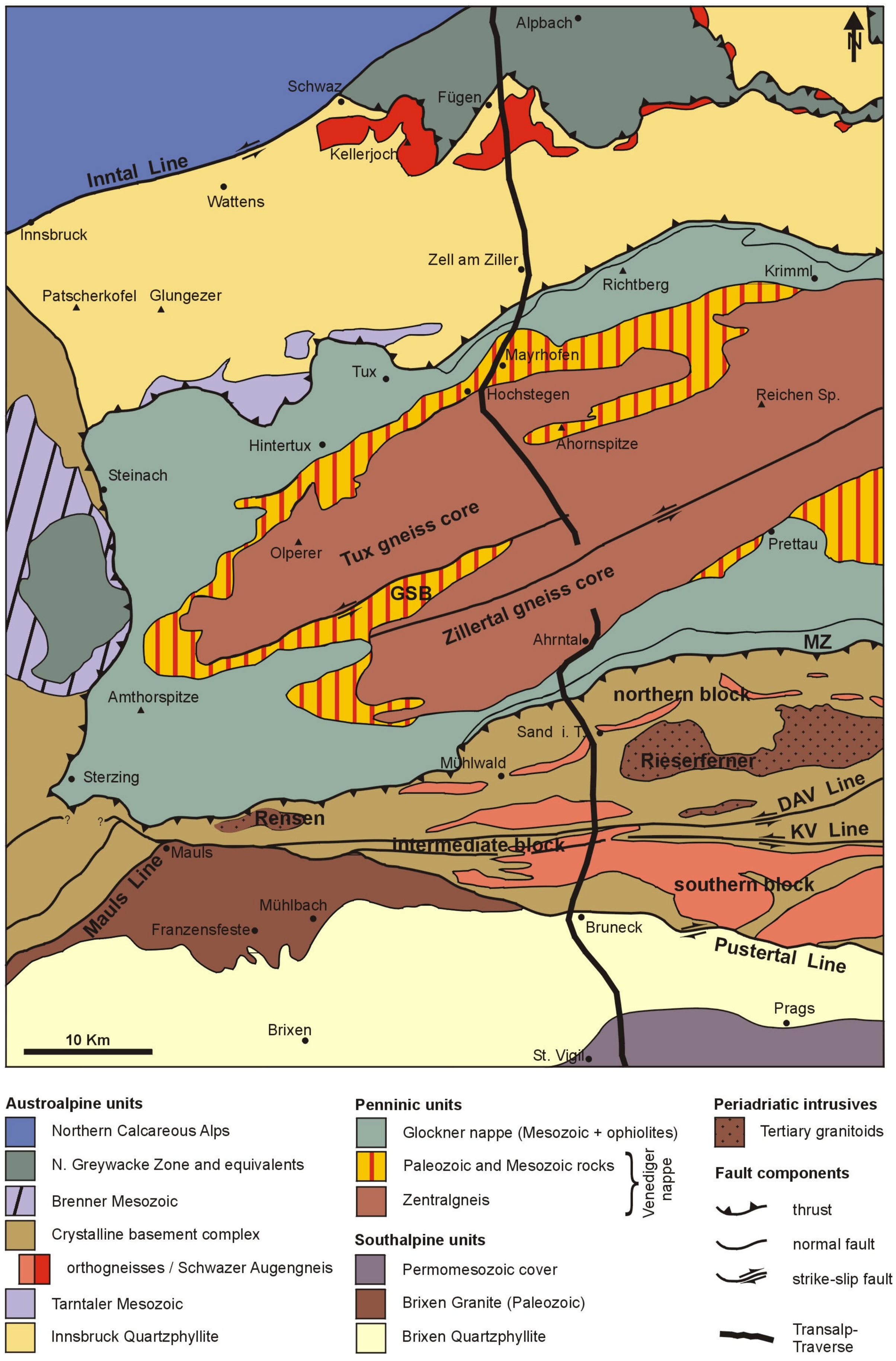

Fig. 2.1: Simplified geological map of the study area. Redrawn and modificated after (Brandner, 1985). GSB = Greiner schist belt; MZ = Matrei Zone; DAV = Defereggen-Antholz-Vals Line; KV = Kalkstein-Vallarga Line.

In the western Tauern window the Venediger Nappe complex comprises pre-Variscan polymetamorphic basement sequences consisting of amphibolites, hornblende garbenschists, migmatites and micaschists (exposed e.g. in the Greiner schist belt (GSB)) which are intruded by Late Variscan granitoids (Fig. 2.1). These granitoids were transformed to the Zentralgneis (Fig. 2.1) during Alpine deformation and occurs in the western Tauern window in the form of the Tux gneiss core and the Zillertal gneiss core (Fig. 2.1). A parautochthonous Mesozoic metasedimentary cover consisting of calcitic and dolomitic marbles (Jurassic Hochstegen Zone), calcareous micaschists, quartzites and metaarkoses (Cretaceous Kaserer Formation (Thiele 1970)) superimposes the Zentralgneis (Fig. 2.1). After Frisch (1974) and Ledoux (1982) part of the Jurassic Hochstegen Zone and the mainly clastic sequences of the Cretaceous Kaserer Formation form the Wolfendorn Nappe. The latter is considered as a thrust nappe bounded by mylonitic zones (Ledoux 1984) and is restricted to the western Tauern window (Frisch 1980).

The polymetamorphic basement sequences and the Mesozoic cover rocks of the Venediger Nappe were summarised as the Lower Schieferhülle (LSH) by authors of the first half of the 20th century. The term, although not properly defined as a tectono-stratigraphic unit, is used until recent times (e.g. Blanckenburg et al. 1989; Selverstone 1993; Zimmermann et al. 1994). Tollmann (1977) defined the “Untere Schieferhülldecke” as a tectonic term.

The Glockner Nappe represents the higher Penninic nappe complex (Fig. 2.1). In the western Tauern window the Glockner Nappe consists of a mainly Mesozoic sequence of metasediments (greenish phengite-quartzites, metaarkoses, micaceous calcitic and dolomitic marbles, carbonate-free and calcareous schists) intercalated with MORB-type metabasitic rocks (greenschists and amphibolites) (Höck & Milller 1987). The lowest part are the rocks of the Permoscytian Wustkogel Series (Frasl & Frank 1966), followed by Middle Triassic carbonate rocks and the Upper Triassic (?) - Cretaceous rocks of the Bündner Schiefer Series (Ledoux 1984).

In the hangingwall of the Glockner Nappe, in the southern part of the Tauern window, the Matrei Zone (MZ) is exposed (Fig. 2.1). The Matrei Zone is a zone of intense imbrication of Penninic rocks with parts of the lower Austroalpine Mesozoic and even with elements of the Austroalpine Altkristallin (Morteani 1974). The Matrei Zone is interpreted to reflect the trench-slope situation of the Penninic-Austroalpine active continental margin during the Cretaceous (Frisch et al. 1987). Due to their inhomogeneous composition it is uncertain, whether the Matrei Zone belongs to the lower Austroalpine unit or the Penninic unit (Tollmann 1977; Bögel & Schmidt 1976). Following Frisch et al. (1987) the Matrei Zone represents the uppermost part of the Bündner Schiefer of the Glockner Nappe and is according to Frisch & Popp (1881) also found along the northern margin of the Tauern window.

The Glockner Nappe including the Matrei Zone is often summarised as the Upper Schieferhülle (USH) by various authors (e.g. Blanckenburg et al. 1989; Selverstone 1993), the tectonic term “Obere Schieferhülldecke” was defined by Tollmann (1977).

Generally the terms Upper and Lower Schieferhülle should be omitted to avoid misunderstandings and misinterpretations (Frisch 1974; Kurz et al. 1996). In this study the terms LSH and USH are only used by referring to literature. For a better understanding a correlation of names of the Penninic nappes in the western Tauern window, modified after Kurz et al. (1996), is presented in Tab. 2.2.

Glockner Nappe complex	Upper Schieferhülle	Matrei Zone Glockner Nappe
Venediger Nappe complex	Lower Schieferhülle	Wolfendorn Nappe Intruded basement and part of the Mesozoic cover
	Zentralgneis	Tux and Zillertal gneiss core

Tab. 2.2: Correlation of names of Penninic nappes in the western Tauern window, modified after Kurz et al. (1996).

According to Frank et al. (1987) three Alpine metamorphic events can be distinguished in the Tauern window:

- An eclogite facies metamorphism (P = up to 20 kbar, T = 550-600° C) is documented for the central part of the Tauern window, outside the studied area (Miller et al. 1980). The age of this metamorphic event is still unknown.
- Subsequent blueschist facies metamorphism (P > 10 kbar, T < 400-450° C) overprinted the eclogites and affected also metabasites and metasediments of the USH and LSH (Zimmermann et al. 1994). According to them, the age of the blueschist facies metamorphic event in the central Tauern window is not older than Upper Eocene, derived from blueschist facies phengites Ar/Ar ages between 36 and 32 Ma.
- Finally, a greenschist to amphibolite facies metamorphism affected all units in the Tauern window.

In the studied area the metamorphic grade increases from greenschist to amphibolite facies conditions towards to the central areas of the Tauern window, as indicated by the mineral isograd patterns and oxygen isotope temperatures (Hoernes & Friedrichsen 1974; Morteani 1974). In Fig. 2.2 the isotherms and isograds of the Alpine regional metamorphism in the western Tauern window are shown according to Morteani (1974), Hoernes & Friedrichsen (1974) and Raase & Morteani (1976).

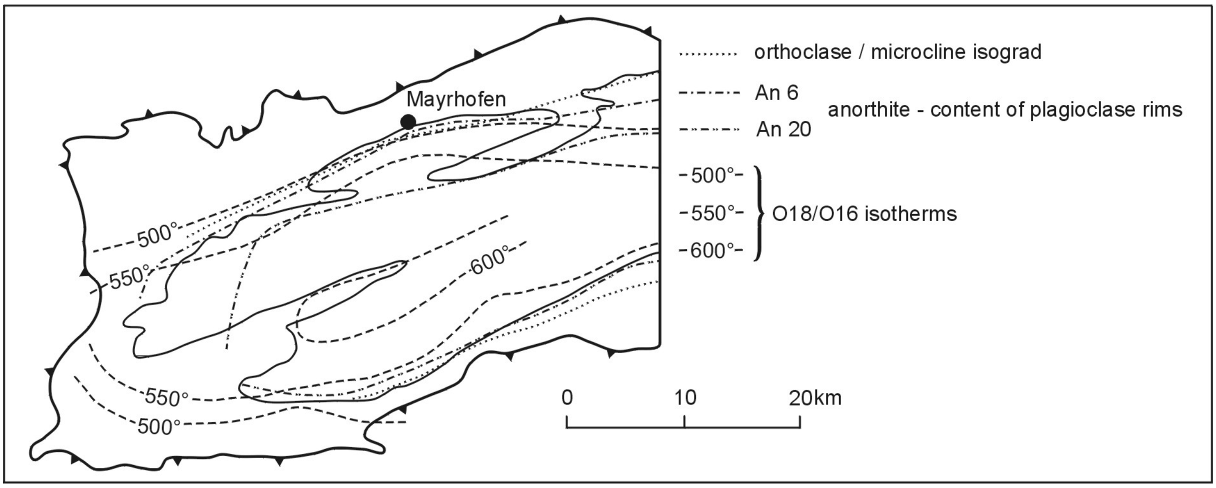

Fig. 2.2: Isotherms and isograds of the Alpine regional metamorphism in the western Tauern window. Redrawn after Grundmann & Morteani (1985).

First pressure estimations are in the 5-7 kbar range (Morteani 1974). Evidence for high pressure metamorphism in the hornblende garbenschists of the GSB was found by Selverstone et al. (1984) and Selverstone & Spear (1985). Garnet-biotite geothermometry yields temperatures of final equilibration of ~550° C, and garnet-plagioclase-kyanite-quartz geobarometry indicates pressures of 6-8 kbar for the matrix assemblage and 9-10 kbar for plagioclase inclusions in garnet. Quantitative modelling of zoned garnet, hornblende and plagioclase indicates growth and equilibration along a decompression path from ~530° C and 10 kbar (mineral cores) to ~550° C and 7 kbar (mineral rims). Petrologic data of the Glockner Nappe indicate pressures of ~7 kbar and T ~450-500° C. The PT-paths reconstructed on these petrologic data together with geochronological data are shown in Fig. 4.7. Frisch (1984) estimated a pressure around 4 kbar at 500° C for the Kaserer Formation according to microprobe analyses of an epidote-amphibolite.

2.1.2 Austroalpine units

The Austroalpine units can be divided in two subunits, the Lower Austroalpine unit and the Upper Austroalpine unit (Bögel & Schmidt 1976). Tollmann (1977) suggests a further subdivision. He separates the Upper Austroalpine unit in a Middle Austroalpine unit and an Upper Austroalpine unit. But this trisection is controversially discussed, and is not used in this study.

2.1.2.1 Lower Austroalpine unit

The Lower Austroalpine unit in the study area is largely built up of the Innsbruck Quartzphyllite north of the Tauern window (Fig. 2.1). The rocks are mainly quartzphyllites of Palaeozoic age.

There are no modern detailed data on the metamorphic grade and the structural evolution of the Innsbruck Quartzphyllite. A detailed study performed by Rockenschaub & Kolenprat (1998) is in process. For parts of the quartzphyllite area, middle greenschist facies metamorphism was suggested from the occurrence of chloritized biotite and garnet (Hoschek et al. 1980). It is generally accepted, that there were polyphase deformation events under similar greenschist facies conditions. Until now it is a problem to differentiate between Variscan and Alpine metamorphic events (Mostler 1986). First results of the investigations of Piber & Tropper (2001) yield pressure variations from 2.5 to 6.4 kbar and 300-400° C for the assemblage muscovite-chlorite-albite. No biotite could be found in the samples.

Many bodies of crystalline rocks occur along the border between the Innsbruck Quartzphyllite and the Northern Greywacke Zone. These bodies consist mainly of augengneisses, which are known as Schwazer Augengneis or Kellerjochgneis (Fig. 2.1). Over the years the Schwazer Augengneis were attributed either to the Lower or the Middle Austroalpine unit (Tollmann 1977; Satir & Morteani 1979).
The Rb/Sr whole rock age and microscopic investigations of the Schwazer Augengneiss indicate, that these rocks were metamorphosed around 325 Ma by a prograde metamorphism of amphibolite facies conditions and succeeding retrogressive metamorphism under greenschist facies conditions. During a metamorphic event around 90 Ma a maximum temperature of about 350° C was attained (Satir & Morteani 1979). First results with the empirically calibrated stilpnomelane-muscovite-chlorite thermobarometer for low-grade rocks (Currie & Van Staal 1999) yield P = 5.8-7.5 kbar and T = 310-400° C (Piber & Tropper 2001).

2.1.2.2 *Upper Austroalpine unit*

The Upper Austroalpine unit occupies vast areas of the central part of the Eastern Alps. In the study area this unit is formed by: (a) the so called Austroalpine Altkristallin or crystalline basement complex south of the Tauern window and (b) the Northern Greywacke Zone (Fig. 2.1).

The Altkristallin south of the Tauern window consists of predominantly pre-Upper Ordovician micaschists and paragneisses with amphibolites, marbles and graphitic gneisses. Upper Ordovician granitoids, the later orthogneisses, intruded into these sedimentary sequences (Borsi et al. 1973) (Hammerschmidt 1981).

Two major shear zones have been identified within the Altkristallin (Bianchi 1934): the Kalkstein-Vallarga (KV) Line and the Defereggen-Antholz-Vals (DAV) Line. These lines subdivide the Altkristallin into three distinct blocks (Fig. 2.1), referred to as southern block, intermediate block and northern block (Borsi et al. 1973). In the studied area the DAV Line is a mylonitic sinistral strike-slip fault and the KV Line a cataclastic sinistral strike-slip fault (Kleinschrodt 1987). Both have been simultaneously active in the Oligocene-Miocene, between about 35 and 25 Ma. (Schulz 1989) assumed 30 km sinistral displacement for the DAV Line.

For all three blocks the Variscan evolution was nearly identical. According to Stöckhert (1982, 1985) the formation of a foliation and folding during the Variscan orogeny was accompanied by metamorphism under amphibolite facies conditions (P = 5.5 ± 1 kbar and T = 575 ± 30° C). In the southern part of the northern block, partial melting occurred during a later high temperature amphibolite facies stage (P = 6 ± 1 kbar, T = 650 ± 30° C). The anatectic melts intruded into already foliated metamorphic rocks (Stöckhert 1987) and formed aplitic and pegmatitic rocks with Late Variscan Rb/Sr whole rock ages around 260 Ma (Borsi et al. 1978).
The southern block cooled below 300° C (P = 2-3 kbar) at around 300 Ma (Borsi et al. 1978) whereas a polyphase Alpine deformation and coeval greenschist to amphibolite facies metamorphism affected the northern block. According to Stöckhert 1982, 1985) the Early Alpine deformation was accompanied by greenschist facies metamorphism (P = 7.5 ± 1.5 kbar, T = 450 ± 50° C). The Late Alpine deformation was limited in its extent and reached P < 4.5 ± 1.5 kbar and T = 300 ± 50° C (Stöckhert 1987). But these data are only based on critical facies estimates and not on geothermobarometrical investigations. Angelmaier (1997) suggests an Early Alpine metamorphism under amphibolite facies conditions (P = 6-7 kbar, T = 580-600° C) followed by a retrograde greenschist facies overprint. This is based on garnet zonation profiles and on various garnet-biotite geothermometers after Ferry & Spear (1978), Perchuk & Lavrent'eva (1983), Indares & Martignole (1985) and Hoinkes (1986).

The Northern Greywacke Zone consists of Paleozoic (sub)greywackes with minor carbonates, lydites, slates and volcanic intercalcations (mainly greenschists).

A polymetamorphic history of the Northern Greywacke Zone is inferred from observations of mineral assemblages. The Variscan metamorphism reached lowest greenschist facies conditions (Hoescheck 1973). A probably flat thermal peak of the Early Alpine metamorphism was reached in Cretaceous times. Mineralogical and geochronological data allow an estimation for the temperature in the range of 250-300° C (Kralik 1983).

Along the Inn valley a major fault, the Inntal Line, forms the southern limit of the Northern Calcareous Alp (Fig. 2.1). It is generally considered as a sinistral strike-slip fault (Ratschbacher et al. 1989) with a ~80 km displacement during Oligocene-Miocene times (Frisch et al. 1998). The ongoing activity of the Inntal Line is displayed by periodic earthquakes in the Inn valley.

2.1.3 Southalpine units

In the studied area along the Transalp–Traverse only one Southalpine unit, namely the Brixen Quartzphyllite, is exposed (Fig. 2.1). The Brixen Quartzphyllite is part of the pre-Permian basement of the Southern Alps and comprises mainly quartzphyllites and minor amounts of quarzites.

The whole Southalpine basement underwent a complex Variscan tectonic evolution including thrusting and folding. The metamorphic grade does not exceed greenschist facies conditions in the Brixen Quartzphyllite (Sassi et al. 1994). For the Brixen Quartzphyllite the garnet-biotite geothermometry yields temperatures of 420-520° C at pressures of 2-4.5 kbar. Alpine metamorphic overprints do not occur.

The most prominent strike-slip fault, the Periadriatic Lineament, separates the Eastern Alps from the Southern Alps and marks the southern limit of Alpine metamorphism by definition. It consists of several different segments with different names (e.g. Pustertal Line, Mauls Line; Fig. 2.1). For a discussion of the Periadriatic Lineament the reader is referred to Bögel (1975). For this work, only the Pustertal Line is of interest.
The Pustertal Line is a mostly cataclastic dextral strike-slip fault. In contrast to the definition mentioned above, the southern boundary of Alpine metamorphism does not occur along the Pustertal Line but further to the north along the DAV Line (Fig. 2.1). Activity of the Pustertal Line in Early Oligocene times (around 30 Ma) and Early and Middle Miocene times (19-16 Ma) was dated on newly formed white mica by the K/Ar and Ar/Ar methods (Müller 1996; Läufer et al. 1997). The palinspastic reconstruction of the pre-Miocene situation shows, that the Periadriatic Lineament restores to a straight line (Frisch et al. 1998, 2000). This straight line allows to postulated pre-Miocene dextral displacement of about 100 km (Schmidt & Kissling 1997).

2.1.4 Tertiary Intrusives

Tonalites and granodiorites of the Oligocene Rieserferner and Rensen intrusions to the north of the DAV Line forms two W-E trending plutonic bodies with a contact metamorphic aureole. For a detailed description of the mineral zones the reader is referred to Prochaska (1981), Mager (1985), Cesare (1992, 1994).

Syntectonic emplacement of the Rieserferner Pluton along the north side of the DAV Line is indicated by sheared contact metamorphic andalusite (Mager 1985).

3 Mineral chemistry and geothermobarometry

3.1 Mineral chemistry

3.1.1 Analytical procedure

The electron microprobe analyses of the minerals were performed using wavelength-dispersive methods on a JEOL JXA 8900 Superprobe at the Institute of Geosciences, University of Tübingen (Germany). Analyses were carried out with an accelerating voltage of 15 kV, a probe current of 20 nA and a beam diameter between 1 and 10 µm (depends on the measured mineral). For the calibration of the analysed elements the ASTIMEX standards were used. Raw count data were corrected with a ZAF correction program. The analyses of the minerals are presented in Appendix Tab. A1-A4. Weight percentages were converted to molar percentages by assuming a fixed number of oxygen (O) per formula unit.

3.1.2 Garnet

Garnet was analysed in sample 45AnTA (Zentralgneis). The analyses are presented in Appendix Tab. A1.

The general formula for garnet is $A_3B_2[SiO_2]_3$. The A-position can be replaced by calcium, magnesium, ferrous iron or manganese, the B-position by aluminium, ferrous iron or chromium. The formula was calculated on the basis of 12 oxygens. Fe^{3+} was calculated according to Ryburn et al. (1976).

According to Rickwood (1968) the end-members of garnets were calculated in the following order: andradite $Ca_3Fe_2[SiO_4]_3$, pyrope $Mg_3Al_2[SiO_4]_3$, spessartine $Mn_3Al_2[SiO_4]_3$, grossular $Ca_3Al_2[SiO_4]_3$ and almandine $Fe_3Al_2[SiO_4]_3$ (see Appendix Tab. A1). All analysed garnets are almandine-rich garnets (X_{Fe} is 0.60-0.63). The pyrope and the grossular components are very similar. X_{Mg} is 0.14-0.19 and X_{Ca} is 0.16-0.20. The spessartine component is low (X_{Mn} is 0.02-0.07).

Zoning profiles were examined to determine the metamorphic evolution from the chemical composition. Several models have been proposed to explain the compositional zoning in garnet, among them element fractionation models (Hollister 1966; Tracy et al. 1976; Crawford 1977; Thompson et al. 1977; Trzciensky jr. 1977; Tracy 1982) and diffusion models (Anderson & Buckley 1973; Woodsworth 1977; Yardley 1977; Dempster 1985). In Fig 3.1 some typical garnet zoning profiles are schematically illustrated.

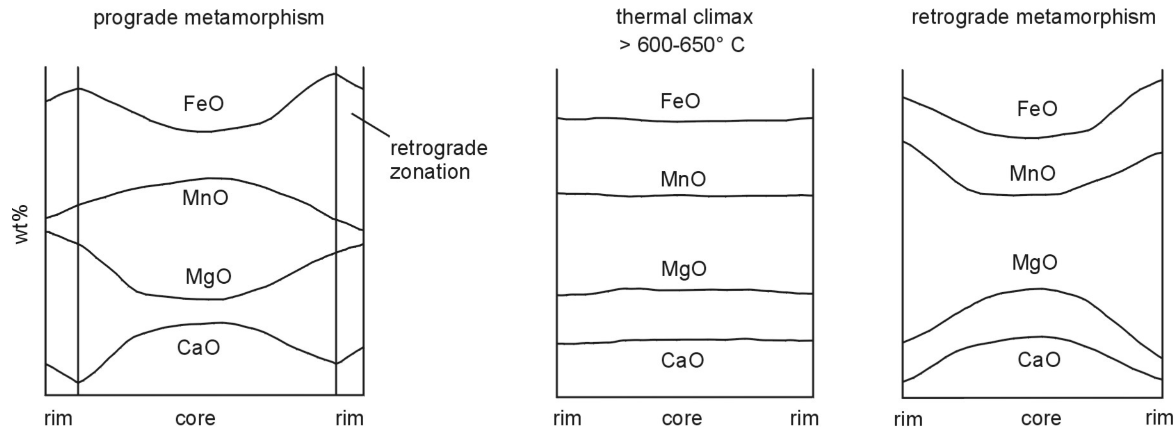

Fig. 3.1: Schematic garnet zoning profiles according to Hollister (1966), Tracy et al. (1976), Thompson et al. (1977), Woodsworth (1977), Yardley (1977), Tracy (1982) and Dempster (1985).

Some representative zoning profiles of the investigated garnets are shown in Fig. 3.2.

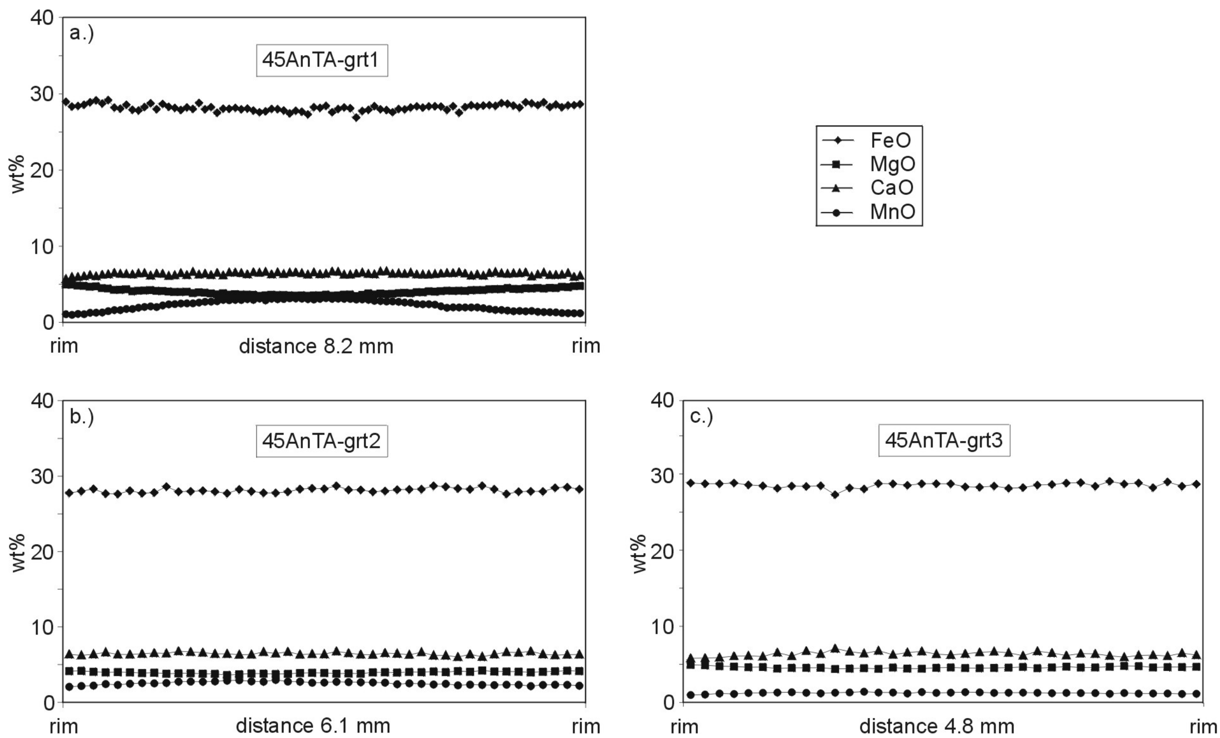

Fig. 3.2: Characteristic rim-core-rim zoning profiles of FeO (wt%), MgO (wt%), CaO (wt%) and MnO (wt%) in garnets from the Zentralgneis (sample 45AnTA).

Only one garnet displays a weak zoning trend by decreasing MnO content from core to rim (Fig. 3.2a). According to Hollister (1966) this prograde MnO zonation is attributed to fractionation processes (Rayleigh fractionation) and is generated by constant removal of Mn from a homogeneous reservoir as the garnet crystallises. This MnO zonation was not generated by diffusion, but it is the original zonation developed during the garnet growth. The other two garnets (Fig. 3.2b+c) show no zoning, which indicates homogenisation by diffusion processes above 600-650° C (Anderson & Buckley 1973; Tracy et al. 1976; Woodsworth 1977).

3.1.3 Biotite

In addition to garnet, biotite was analysed in sample 45AnTA (Zentralgneis). The analyses are presented in Appendix Tab. A2.

Biotite belongs to the group of trioctahedral micas and the general formula is $K_2R^+_6[Al_2Si_6O_{20}/(OH)_4]$. The formula was calculated on the basis of 11 oxygens (water-free).

Most specimens fall within a field outlined by four end-members: phlogopite, annite, eastonite and siderophyllite. Thus in biotite, as compared with phlogopite, magnesium is replaced by ferrous iron. A subdivision of biotites themselves is made in meroxene, lepidomelane and siderophyllite. The chemistry of the analysed biotites is plotted in the variation diagram according to Foster (1960). This variation diagram is based on the different occupation in octahedral sites. All analysed biotites plot in the meroxene field (Fig. 3.3). The biotites are unzoned, and their Mg/(Mg+Fe) ratios range from 0.62 to 0.66. The Ti content is between 0.04 and 0.07.

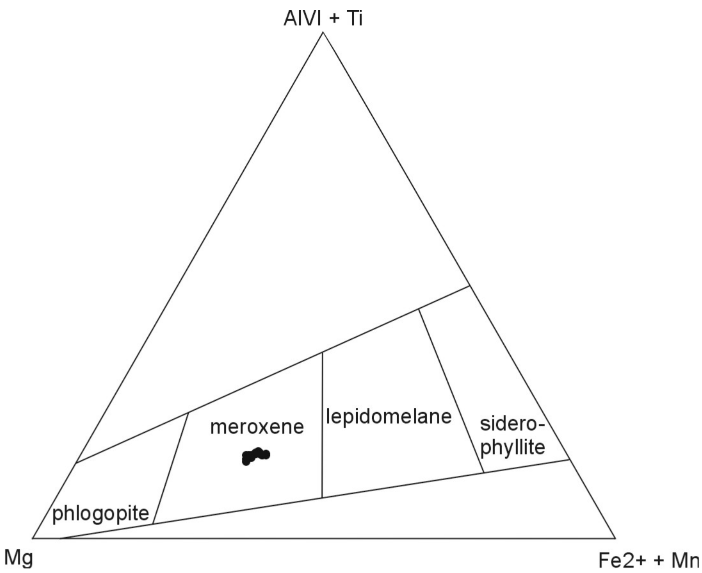

Fig. 3.3: Variation diagram according to Foster (1960).

3.1.4 White mica

Microprobe analyses of white mica were performed on some selected samples used for K/Ar age determinations. The analyses of samples 29AnTA (Wustkogel Series), 2AnTA and 51AnTA (Kaserer Formation) and 45AnTA (Zentralgneis) are presented in Appendix Tab. A3.

White mica belongs to the group of dioctahedral micas and the general formula is $KAl_2[AlSi_3O_{10}/(OH)_2]$. The formula was calculated on the basis of 11 oxygens (water-free).

There are varieties of white mica, which results from various substitutions. Increasing pressure leads to an increase of the Si content according to following substitution (Massonne & Schreyer 1987):

$$Al^{IV} + Al^{VI} <=> Si^{IV} + (Fe, Mg)^{VI}$$

This results in the formation of a celadonite or phengite component, respectively. The calculation of end-members was according to Schliestedt (1980), whereas the mineral phases (mol%) were calculated in the following way:

$$\text{paragonite} = Na/(Na*K)*100$$
$$\text{celadonite} = (Si\text{-}3)*100$$
$$\text{muscovite} = 100\text{-}(\text{paragonite}+\text{celadonite})$$

Muscovite is the main component in all analysed white micas with a content between 54.73 and 67.92 mol% (Appendix Tab. A 3.1). The paragonite contents of the samples 29AnTa, 2AnTA and 51AnTA are very low (0.88-2.71 mol%) and the celadonite contents are in the range 27.49-45.56 mol%. Only sample 45AnTA has a higher paragonite content (12.22-18.67 mol%) and a lower celadonite content (16.10-28.47 mol%).

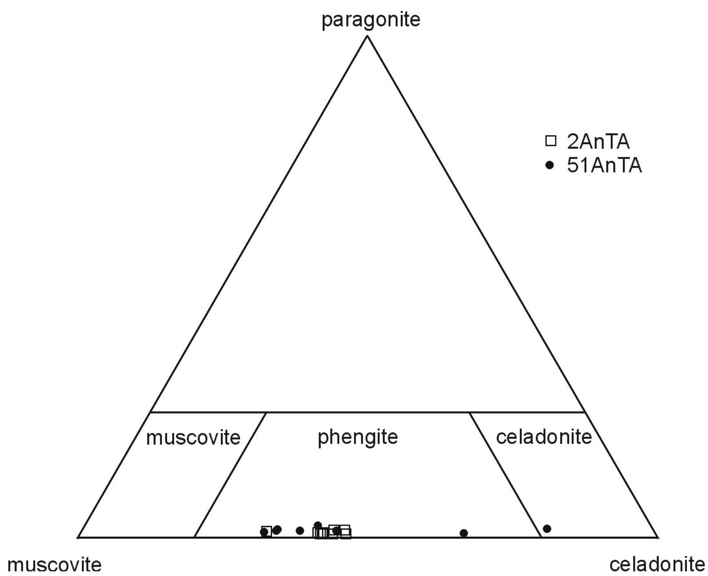

Fig 3.4: Compositional variation of white mica (sample 2AnTA and 51AnTA (Kaserer Formation)) according to Schliestedt (1980).

Due to the high Si content (3.16-3.79) the samples plot in or near the phengite field (Fig. 3.4 and 3.5). The analyses of two white micas (sample 51AnTA) differ from the rest in the way, that the main component here is celadonite (65.69 mol% and 78.49 mol%). A possible explanation might be the presence of two mica generations. But it is not possible to distinguish two mica generations under the microscope due to intensive crenulation. Massonne & Schreyer (1987) noted, that phengites frequently do not completely equilibrate with the matrix, but retain their original composition over long periods of time. Therefore, phengites with vastly different compositions may occur within a single rock.

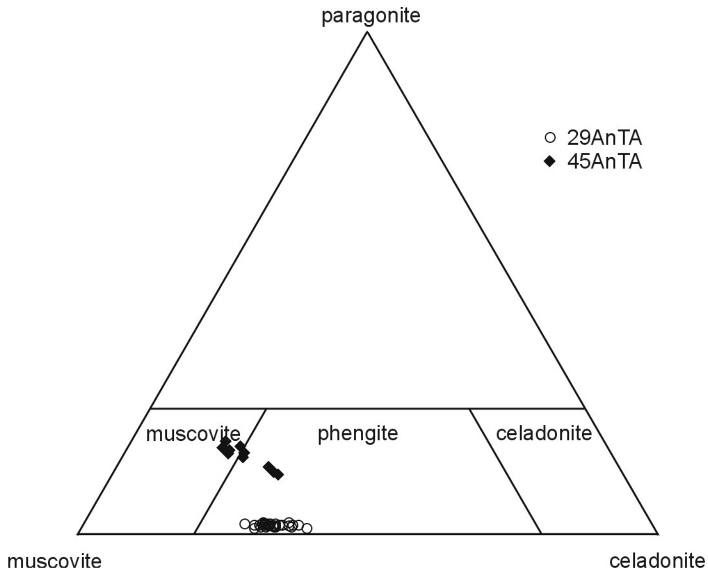

Fig 3.5: Compositional variation of white mica (sample 29AnTA (Wustkogel Series) and 45AnTA (Zentralgneis)) according to Schliestedt (1980).

3.1.5 Feldspar

Feldspar was analysed in sample 2AnTA and 51AnTA (Kaserer formation) and the analyses are presented in Appendix Tab. A4.

The general formula for feldspar, is $XAl_{(1-2)}Si_{(3-2)}O_8$. The formula was calculated on the basis of 8 oxygens.

The feldspars are classified chemically as members of the ternary system $NaAlSi_3O_8$ (albite) – $KalSi_3O_8$ (orthoclase) – $CaAl_2Si_2O_8$ (anorthite). All analysed feldspars of both samples have a similar composition with an orthoclase content of 94.30-97.40 mol%. The albite content is low (2.59-6.46 mol%) and the anorthite content is negligible (max. 1.18 mol%). Representative analyses are plotted in Fig. 3.6.

Due to the same chemistry of K-feldspars, a differentiation is only possible by their different crystal structures or, in case of microcline, by the cross-hatched twinning. Such twinning is visible under the microscope in some feldspar grains.

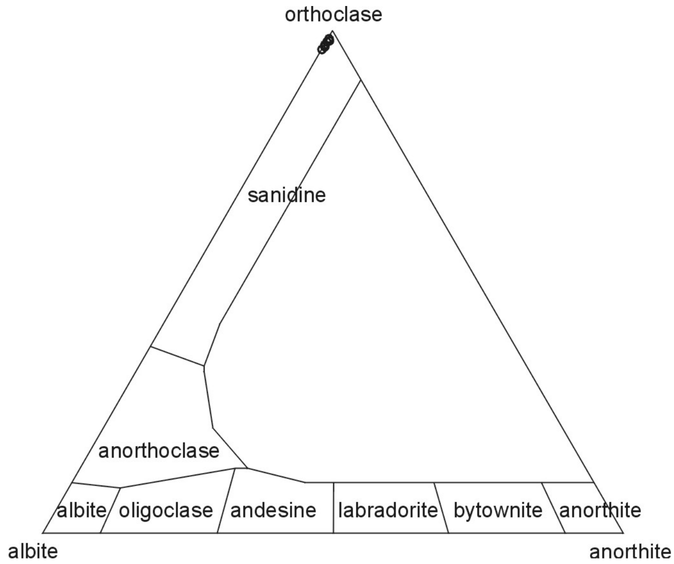

Fig. 3.6: Feldspar compositions (mol%) in the system orthoclase-albite-anorthite.

3.2 Geothermobarometry

To gain information about the temperature and pressure condition, which prevailed during the formation of metamorphic rocks, numerous experimentally and empirically calibrated geothermometers and barometers had been developed. They are based on the pressure and/or temperature dependence of exchange reactions between different mineral phases.

3.2.1 Geothermometry

3.2.1.1 Garnet–biotite geothermometers

The widely used garnet-biotite geothermometer is based on the temperature-sensitive Fe/Mg distribution between coexisting garnet and biotite according to the following cation exchange reaction:

$$Fe_3Al_2[SiO_4]_3 + KMg_3[AlSi_3O_{10}/(OH)_2] \rightleftharpoons Mg_3Al_2[SiO_4]_3 + KFe_3[AlSi_3O_{10}/(OH)_2]$$

almandine + phlogopite ⇌ pyrope + annite

With increasing temperature garnet becomes Mg- and biotite Fe-richer. The pressure dependence of the reaction is negligible (Ferry & Spear 1978). There are many calibrations for this geothermometer. The most popular calibration is that of Ferry & Spear (1978), which is used among the calibrations of Perchuk & Lavrent'eva (1983), Hoinkes (1986) and Indares & Martignole (1985).

The garnet-biotite geothermometer was experimentally calibrated on synthetic garnet and biotite by Ferry & Spear (1978). The temperature is calculated according to equation 3.1:

$$T[°C] = \frac{(12454 + 0.057 * P_{[bars]})}{(4.662 - 3R * \ln K_D)} - 273 \qquad (3.1)$$

$$K_D = ((Mg / Fe)_{grt} / (Mg / Fe)_{bt})$$

$$R = 1.987 cal / molK$$

The Fe/Mg exchange between garnet and biotite depends on the Ca and Mn content of garnet and the Ti and Al^{VI} concentrations of biotite (Ferry & Spear 1978). Thus this thermometer is only valid for garnets containing less than 20 mol% grossular and spessartine. The (Al^{VI}+Ti)/(Al^{VI}+Ti+Fe+Mg) ratio in biotite should not exceed 0.15.

The calibration of Perchuk & Lavrent'eva (1983) is based on the experimental reactions of Mg-, Fe- and Al-oxalates using amorphous SiO_2. The temperature can be estimated from equation 3.2.

$$T[°C] = \frac{(7843.7 + \Delta V * (P_{[bars]} - 6000))}{(R * \ln K_D + 5.699)} - 273 \qquad (3.2)$$

$$K_D = ((Mg / Fe)_{grt} / (Mg / Fe)_{bt})$$

$$R = 1.987 cal / molK$$

According to Hoinkes (1986) small grossular concentrations (below 10 mol%) lead to significant temperature variations. He recalibrated the garnet-biotite geothermometer by taking into account, that increasing Ca contents of garnet decrease the distribution coefficient K_D. The temperature can be calculated from equation 3.3.

$$T[°C] = \frac{(2089 + 0.00956 * P_{[bars]})}{(0.7821 - \ln K_D - 2.978 * XCa + 5.906 * (XCa_{grt})^2)} - 273 \qquad (3.3)$$

$$XCa_{grt} = Ca / (Fe + Mg + Ca + Mn)$$

$$K_D = ((Mg / Fe)_{grt} / (Mg / Fe)_{bt})$$

Hodges & Spear (1982) corrected the garnet-biotite geothermometer of Ferry & Spear (1978) by taking the influence of Ca into account. Based on this work, Indares & Martignole (1985) suggested a garnet-biotite geothermometer which considers also the Ti and Al^{VI} content in biotite. The model is a combination of thermodynamical and empirical data. The outcome of this is the following formula for the calculation of the temperature (eq. 3.4):

$$T[°C] = \frac{(12454 + 0.057 * P_{[bars]} - 4770 * XAl_{bt} - 22353 * XTi_{bt} + 9000 * XCa_{grt} + Mn_{grt})}{(4.662 - 3 * R * \ln K_D)} - 273 \qquad (3.4)$$

$$K_D = \left((Mg/Fe)_{grt} / (Mg/Fe)_{bt}\right)$$

$$R = 1.987 cal/molK$$

$$XAl^{VI}{}_{bt} = Al^{VI} / \left(Al^{VI} + Ti + Fe + Mg + Mn\right)$$

$$XTi_{bt} = Ti / \left(Ti + Al^{VI} + Fe + Mg + Mn\right)$$

$$XCa_{grt} = Ca / (Fe + Mg + Ca + Mn)$$

$$XMn_{grt} = Mn / (Mn + Ca + Mg + Fe)$$

3.2.1.2 Results

In sample 45AnTa (Zentralgneis) the composition of the garnet rim, together with the composition of the adjacent biotite rim were used to obtain temperature data of the crystallisation of the rims (Appendix Tab. A5) A summary of the temperatures calculated by the garnet-biotite geothermometers according to Ferry & Spear (1978), Perchuk & Lavrent'eva (1983), Hoinkes (1986) and Indares & Martignole (1985) is presented in Fig. 3.7. For a better comparison all temperatures shown in Fig. 3.7 were calculated at a given pressure of 6 kbar.

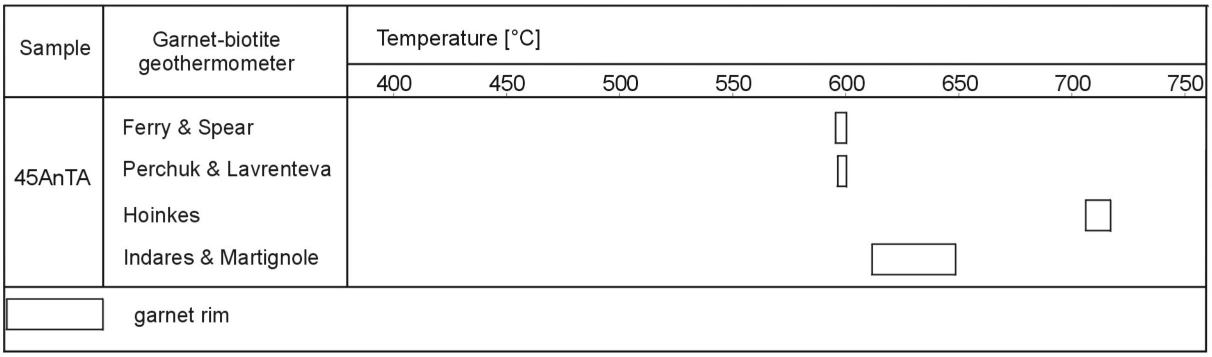

Fig. 3.7: Summary of the temperatures calculated by the garnet-biotite geothermometers according to Ferry & Spear (1978), Perchuk & Lavrent'eva (1983), Hoinkes (1986) and Indares & Martignole (1985).

The garnet-biotite thermometer of Ferry & Spear (1978) gave temperatures between 580 and 600° C for the rim assemblage. Similar results were derived with the garnet-biotite thermometer according to Perchuk & Lavrent'eva (1983). The Ca correction of Hoinkes (1986) yielded temperatures of 710 to 730° C for the rim assemblage. These temperatures seem to be too high. With the garnet-biotite geothermometer according to Indares & Martignole (1985), the temperatures are in the range 620-650° C (rim).

These results with maximum temperatures around 600° C fit very well to the oxygen isotope temperatures obtained by Hoernes & Friedrichsen (1974) in the western Tauern window (Fig. 2.2).

3.2.2 Geobarometry

3.2.2.1 Phengite geobarometer

Numerous workers have observed increases in the Si content in phengites with increasing pressure and decreasing temperature (e.g. Ernst 1963; Guidotti 1978). This observation is confirmed and quantified experimentally for phengites coexisting with K-feldspar, quartz and biotite in the KMASH (K_2O + MgO + Al_2O_3 + SiO_2 + H_2O) system (Velde 1965; Massonne & Schreyer 1987). The Si isopleths given in Fig. 3.8 can be used for pressure estimates.

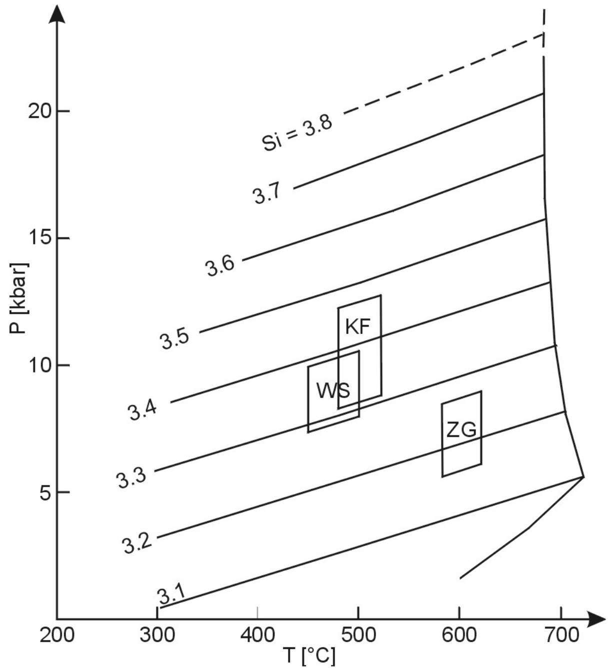

Fig. 3.8: P-T plot with Si isopleths for phengite Si contents in the limiting assemblage with K-feldspar, quartz and biotite after Massonne & Schreyer (1987). Abbreviations: KF = Kaserer Formation, WS = Wustkogel Series and ZG = Zentralgneis.

3.2.2.2 Results

White micas with various amounts of phengite component were analysed in samples 29AnTA (Wustkogel Series), 2AnTA and 51AnTA (Kaserer Formation) and 45AnTA (Zentralgneis). The pressures obtained with phengite barometry are presented together with P-T data from literature and from this study in Tab. 3.3.

Unit	P	T	Source	Si	P_{MSc}
Zentralgneis	6-7 kbar	~600° C	this study	3.16-3.28	5.5-8.5 kbar
Kaserer Formation	~4 kbar	500° C	2, 3	3.31-3.46	8.0-12.5 kbar
Wustkogel Series	~7 kbar	~450-500° C	1, 3	3.29-3.39	7-10.5 kbar

Tab. 3.3: Pressures (P_{MSc}) estimated on the basis of the Massonne & Schreyer (1987) KMASH isopleths. Sources: 1 (Selverstone et al. 1984); 2 (Frisch 1984); 3 (Hoernes & Friedrichsen 1974).

For sample 29An TA (Wustkogel Series) and sample 45AnTA (Zentralgneis), the results obtained with phengite barometry are in good agreement with the existing pressure estimations (Tab. 3.3). The other two samples of the Kaserer Formation yield higher pressures than the pressures estimated by Frisch (1984) according to microprobe analyses of a low-grade epidote-amphibolite. But he also found relict amphiboles, which point to an early phase of metamorphism with a higher P/T ratio than the later low-grade metamorphism. Maybe the pressures between 8 and 12.5 kbar obtained by applying phengite barometry on metaarkoses (samples 2AnTA and 51AnTA) belongs to an early (high pressure ?) phase of metamorphism.

4 Geochronology

4.1 Sampling strategy and sample preparation

During field trips in 1999 and 2000, 61 samples were collected along the central part of the Transalp-Traverse for geochronological investigations, mainly for fission track dating. The sampling strategy was to extend a pre-existing dataset into areas without data, as well as to collect samples from vertical relief profiles. Such 3-dimensional sampling (valley, intermediate and on peak) was performed in high relief areas (e.g. Zillertaler Alps).
Four samples of the Rieserferner and Rensen intrusive bodies were obtained from C. Rosenberg (FU Berlin). Sample numbers and localities except sample MA22 are shown in Fig. 4.1. The locality of this sample is near St. Jakob in Defereggen and the results are presented in Fig. 4.8 and Fig. 4.12.

The sample preparation was carried out at the fission track laboratory at the Institute of Geosciences, University of Tübingen (Germany). Between 1 to 8 kg of unweathered rock material were taken for the separation of micas, zircon and apatite. All samples were crushed and ground. In two cases, sample splits were selected and powdered in a tungsten carbide mill for Rb/Sr whole rock analysis. Then the samples were sieved in different size fractions and the fraction < 250 µm or < 200 µm was further separated using a GEMENY shaking table. The two fractions richest in heavy minerals were treated by 5 % acetic acid to dissolve carbonates and by heavy liquid separation (poly-tungstenate, $\rho = 2.9$ g/cm^3) to remove quartz and feldspar, followed by magnetic separation. The heavy liquid separation by methyleniodide ($\rho = 3.3$ g/cm^3) leads to ± pure zircon and apatite concentrates. If necessary, handpicking completed the mineral separation.

4.2 K/Ar geochronology

4.2.1 Theory

The K/Ar method is based on the decay of naturally occurring ^{40}K to stable radiogenic ^{40}Ar* (11.2 %) and radiogenic ^{40}Ca* (88.8 %). ^{40}Ca* is generally not used for radiometric dating. The method is applicable to certain K-bearing minerals and rocks.

The amount of ^{40}K can be directly calculated from the K concentration because the isotopic composition of K in natural terrestrial samples is believed to be constant. After the measurement of the K concentration and the amount of radiogenic ^{40}Ar*, the age of the mineral can be determined after the following equation:

$$t = \frac{1}{\lambda}\ln\left[\frac{^{40}\mathrm{Ar}^*}{^{40}\mathrm{K}}\left(\frac{\lambda}{\lambda e}\right)+1\right] \qquad (4.1)$$

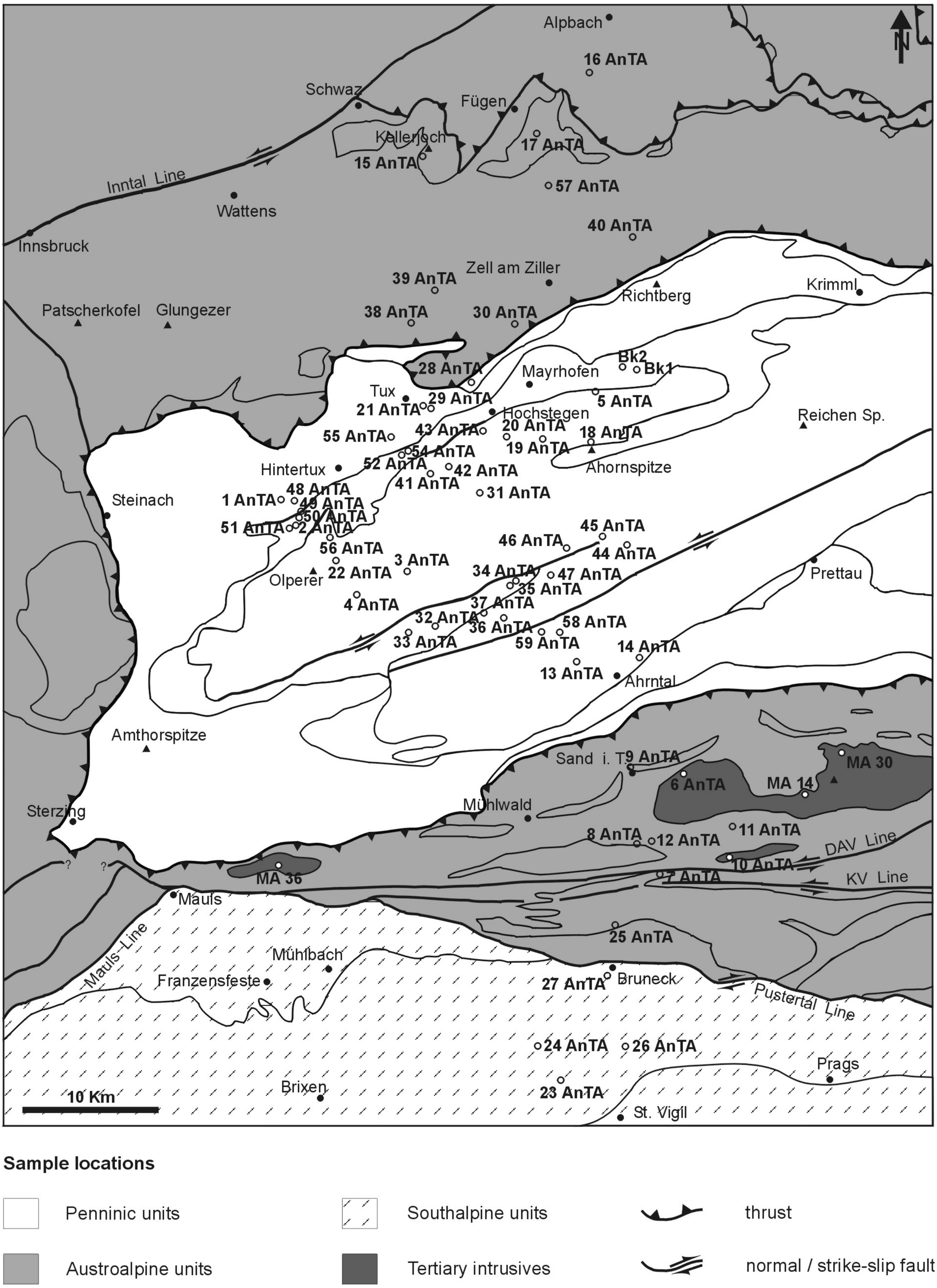

Fig. 4.1: Sample locations

where:	t	= time elapsed since the system was closed
	λ	= total decay constant of ^{40}K
	λe	= decay constant of ^{40}K to $^{40}Ar^*$

The value of t is the age of the mineral under the assumption that no radiogenic $^{40}Ar^*$ produced by the decay of ^{40}K has escaped from the mineral and no $^{40}Ar^*$ was incorporated into the mineral either at the time of its formation or during a later metamorphic event.

Also the mineral have become closed with respect to $^{40}Ar^*$ soon after its formation, which means that it must have cooled rapidly after crystallisation. These assumptions require careful evaluation in each case and must be kept in mind for the interpretation of K/Ar dates.

4.2.2 Analytical methods

The K/Ar age determinations were carried out at the Institute of Nuclear Research in Debrecen (Hungary). Analyses were made on separated white mica and biotite concentrates. Each sample was splitted, whereby at one aliquot K was determined by flame photometry with lithium as internal standard and a sodium buffer. For the argon measurements the other aliquot was degassed by high frequency heating and Ar was separated from the evolved gases with SAES St 707 ion getter pumps using a titanium sponge. The isotopic ratios were measured with a mass spectrometer, using an enriched ^{38}Ar spike.

4.2.3 Results

The results of K/Ar dating of 11 biotite, 10 phengite and 1 white mica samples are listed in Tab. 4.1. The regional distribution of the ages are presented together with previously published age data in Fig. 4.5 and Fig. 4.7.

Penninic units

The K/Ar biotite ages of the Zentralgneis samples range between 20 ± 1 Ma and 14 ± 1 Ma with a maximum frequency around 17 to 14 Ma. The phengite ages are between 23 ± 1 Ma and 18 ± 1 Ma and are systematically older as the biotite ages. Sample (32AnTA) of the Greiner schist belt yields a biotite K/Ar age of 15 ± 1 Ma and a phengite K/Ar age of 21 ± 1 Ma.

Unexpectedly high K/Ar phengite ages were obtained from rocks of the Kaserer Formation (Frauenwand area). Sample 51AnTA yields an age of 40 ± 2 Ma and the other sample (2AnTA) gives an age of 82 ± 3 Ma (125-200 µm) and 78 ± 3 Ma (200-315 µm). Both are micaschists with only a few meters distance in sample location. The two size fractions of sample 2AnTA yield nearly identical ages, so there is no indication of mixed ages. Any loss or gain of radiogenic argon can be estimated with the graphical solution presented by Harper (1970). The two ages of sample 2AnTA were plotted in an ^{40}Ar versus K concentration diagram (Fig. 4.2), which shows that there is loss of argon. Under the assumption that both samples have the same amount of argon loss, the recalculated weighted mean K/Ar isochron age is 107 ± 2 Ma.

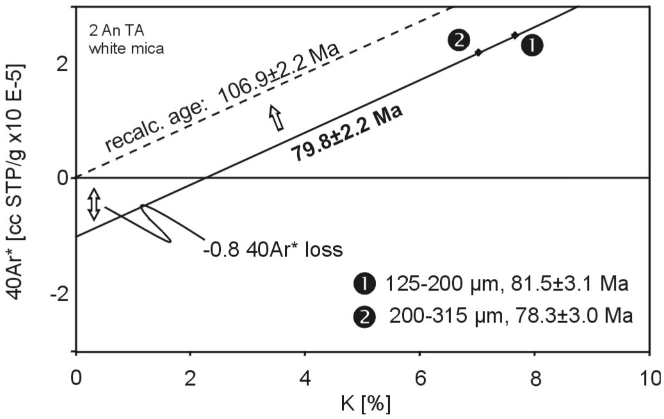

Fig. 4.2: K/Ar isochron data for sample 2AnTA.

Sample	Mineral	Grain size [µm]	% K	40 Ar rad. [cc STP/g]	% rad. Ar	Age [Ma]
Penninic samples						
2 An TA	phengite	125-200	7.685	2.492x10-5	80.6	81.5 ± 3.1
	phengite	200-315	7.046	2.193x10-5	94.8	78.3 ± 3.0
3 An TA	biotite	250-355	7.850	4.390x10-6	69.6	14.3 ± 0.6
	phengite	250-355	8.429	5.772x10-6	51.3	17.5 ± 0.7
13 An TA	biotite	250-315	7.31	4.642x10-6	72.3	16.3 ± 0.6
14 An TA	biotite	<250	6.977	4.929x10-6	57.0	18.0 ± 0.8
	phengite	250-355	8.770	7.357x10-6	73.4	22.6 ± 0.9
18 An TA	biotite	<200	7.14	4.733x10-6	87.2	17.0 ± 0.7
20 An TA	biotite	<200	7.42	4.900x10-6	65.9	16.9 ± 0.7
22 An TA	biotite	<200	7.242	4.740x10-6	62.7	16.8 ± 0.7
29 An TA	phengite	100-200	7.456	7.304x10-6	65.3	25.0 ± 1.0
32 An TA	biotite	200-315	7.572	4.524x10-6	57.2	15.3 ± 0.6
	phengite	200-315	8.893	7.175x10-6	50.6	20.6 ± 0.9
37 An TA	biotite	250-355	7.402	4.095x10-6	80.5	14.2 ± 0.6
44 An TA	biotite	<250	7.626	5.804x10-5	82.5	19.5 ± 0.8
46 An TA	biotite	<250	7.624	4.331x10-6	85.6	14.4 ± 0.6
48 An TA	phengite	<200	9.131	9.461x10-6	84.6	26.1 ± 1.0
51 An TA	phengite	100-200	8.080	1.253x10-5	90.6	39.5 ± 1.5
55 An TA	phengite	63-125	8.888	9.188x10-6	80.5	26.4 ± 1.0
Austroalpine samples						
9 An TA	phengite	250-315	8.99	1.365x10-5	84.0	38.6 ± 1.5
16 An TA	white mica	10-20	3.426	3.795x10-5	86.9	264.4 ± 10.7
Tertiary intrusive samples						
MA 22	biotite	<200	6.591	8.009x10-6	64.9	31.0 ± 1.2

Tab. 4.1: K/Ar data. The calculations are based on the recommended constants given by Steiger & Jäger (1977).

Further to the north, K/Ar dating of the phengite samples of the Wustkogel Series gives ages of 26 ± 1 Ma and 25 ± 1 Ma.

Austroalpine units

The fine-grained white mica sample of the Northern Greywacke Zone yields an K/Ar age of 264 ± 11 Ma.

South of the Tauern window, in the so called “Altkristallin”, a K/Ar phengite age of 39 ± 2 Ma is obtained from an orthogneiss near Sand in Taufers.

Tertiary intrusives

K/Ar dating on biotite from the Rieserferner intrusion yields an age of 31 ± 1 Ma.

4.3 Rb/Sr geochronology

4.3.1 Theory

The decay of naturally occurring ^{87}Rb to stable ^{87}Sr in Rb-bearing minerals can be used to calculate the radiometric age of minerals from measurements of the concentrations of Rb and Sr and of the ^{87}Sr/^{86}Sr ratio after the basic equation:

$$\left(\frac{^{87}\mathrm{Sr}}{^{86}\mathrm{Sr}}\right)=\left(\frac{^{87}\mathrm{Sr}}{^{86}\mathrm{Sr}}\right)_i+\frac{^{87}\mathrm{Rb}}{^{86}\mathrm{Sr}}\left(e^{\lambda t}-1\right) \tag{4.2}$$

which is solved for t:

$$t=\frac{1}{\lambda}\ln\left[\frac{\frac{^{87}\mathrm{Sr}}{^{86}\mathrm{Sr}}-\left(\frac{^{87}\mathrm{Sr}}{^{86}\mathrm{Sr}}\right)_i}{\frac{^{87}\mathrm{Rb}}{^{86}\mathrm{Sr}}}+1\right] \tag{4.3}$$

where:	t	= time elapsed since the system was closed
	λ	= decay constant
	^{87}Sr/^{86}Sr	= measured ratio
	(^{87}Sr/^{86}Sr)$_i$	= initial ratio
	^{87}Rb/^{86}Sr	= initial ratio of the sample

Such calculated “dates” may represent the age of the mineral, provided that it remained closed for Rb and Sr after crystallisation and that an appropriate value was chosen for the initial $^{87}Sr/^{86}Sr$ ratio.

To reduce the error, the isochron method was introduced by Nicolaysen (1961) and is generally used since then. In this method different minerals from one rock sample with varying amounts of Rb and the whole rock are analysed and their $^{87}Sr/^{86}Sr$ ratios (y-axis) are plotted versus the $^{87}Rb/^{86}Sr$ ratios (x-axis) in an Rb/Sr isochron diagram. Then the basic equation 3.2 is also the equation for a straight line in the slope-intercept form:

$$y=b+mx \tag{4.4}$$

At time zero (t_o) of the system (= the time of the last strontium isotope homogenisation), all of the cogenetic minerals and thus also the whole rock sample lie on a horizontal line and have the same $^{87}Sr/^{86}Sr$ ratio (= initial strontium isotope ratio) but, depending on the mineral, different $^{87}Rb/^{86}Sr$ ratios. Assume that the system is closed to loss or gain of Rb and Sr and the number of atoms of stable ^{86}Sr remains the same. As time passes, ^{87}Rb decays to ^{87}Sr, the points for the different cogenetic minerals move on parallel lines with a slope of –1. At any time t they all lie along a straight line (called an isochron), whose slope is a function of the time since t_o and whose y-intercept is the initial strontium isotope ratio.

An age determined in this way is called an isochron age. A number of mathematical procedures based on the principle of the least squares are available for calculating the isochrons and their standard deviations (e.g. York 1966).

4.3.2 Analytical methods

The Rb/Sr isotopic compositions were analysed at the Institute of Geosciences, University of Tübingen (Germany). The samples were spiked with a mixed ^{87}Rb-^{84}Sr tracer solution. Micas and whole rocks were decomposed in a HF-$HClO_4$ (2 ml HF, 20 drops of $HClO_4$) solution at 100° C for three days. For isotope analyses, Rb and Sr were separated on quartz columns by conventional ion exchange chromatography with a 5 ml resin bed of Bio Rad AG 50W-X12, 200-400 mesh. All isotopic measurements were made on a Finnigan MAT 262 mass spectrometer. Sr was loaded with a Ta-HF activator on a single W filament. Rb was loaded with ultra-pure H_2O on pre-conditioned Re filaments and measurements were performed in a Re double filament configuration. The $^{87}Sr/^{86}Sr$ isotope ratios are normalised to $^{86}Sr/^{88}Sr = 0.1194$. Analyses of the NBS 987 Sr standard yielded a mean $^{87}Sr/^{86}Sr$ of 0.710248 ± 0.000010 (n = 240). Total procedure blanks (chemistry and loading) were <200 pg for Sr.

The Rb/Sr age calculations are based on a two-point isochron (e.g. Wendt 1986) and were calculated by using the program ISOPLOT rev. 2.49 (Ludwig 2001).

4.3.3 Results

Penninic units

The Rb/Sr isotope analyses were carried out on two samples from the Frauenwand area (Kaserer Formation) in order to better constrain their unexpectedly high K/Ar ages. The analytical data of the whole rock samples and white mica is given in Tab. 4.2, and the regional distribution of the ages is presented together with ages from the literature in Fig. 4.4.

Sample	Mineral	Grain size [µm]	Rb [ppm]	Sr [ppm]	$^{87}Rb/^{86}Sr$	$^{87}Sr/^{86}Sr$	Age [Ma]
2 An TA	whole rock		97.78	20.43	13.875	0.728776±11	
	phengite	125-200	309.4	17.47	52.022	0.860209±09	242.2 ± 1.4
51 An TA	whole rock		75.03	18.53	11.74	0.729975±10	
	phengite	100-200	283.8	13.14	62.87	0.767308±08	51.4 ± 0.8

Tab. 4.2: Rb/Sr isochron data. The calculations are based on the recommended constants given by Steiger & Jäger (1977).

Rb/Sr phengite dating of the two samples yield different ages although there is only a few meters distance between them in the field and both are micaschists. The isochron age is calculated with the whole rock and phengite isotope compositions. Sample 2AnTA (125-200 µm) yields an age of 242 ± 4 Ma and sample 51AnTA (100-200 µm) yields an age of 51 ± 1 Ma. As the grain size is very similar, this can not be the explanation for the differences in the ages.

4.4 Interpretation and discussion of published and new Rb/Sr and K/Ar mica ages

The concept of closure temperatures is the keystone for discussion and interpretation of radiometric data and thermal histories. Dodson (1973) offered the simple definition of closure temperature as being “the temperature of a system at the time represented by its apparent age”.

For biotite Purdy & Jäger (1976) suggested a closure temperature of 300 ± 50° C for the Rb/Sr and K/Ar systems, based on their empirical study in the Central Alps. For white micas, they proposed a closure temperature of 500 ± 50° C for the Rb/Sr system and 350 ± 50° C for the K/Ar system. The radioactive clock of a mineral begins to “tick”, when its temperature falls below its closure temperature. In a cooling rock unit the Rb/Sr and K/Ar clock of the various minerals starts at different times (cooling ages) making it possible to reconstruct the cooling process. Blanckenburg et al. (1989) found an undisturbed age sequence in the Tauern window and they determined a closure temperature of 550° C for the phengite Rb/Sr system by linear extrapolation and a closure temperature of 410° C for the phengite K/Ar system by linear interpolation between biotite and hornblende (Fig. 6.1).

However, the concept of closure temperatures has been a matter of debate (Blanckenburg et al. 1989; Villa 1998). Often mineral ages are interpreted as cooling ages, but they could also represent crystallisation ages. If during progressive or retrograde metamorphism crystallisation of a datable mineral occurs below its closure temperature and if this temperature is not reached during the further course of metamorphism, the Rb/Sr and K/Ar dates correspond to the metamorphic crystallisation age.

Another problem of dating minerals and interpreting the ages is that the parent and daughter nuclides in all radiometric dating systems are of different elements. The most extreme case is the K/Ar system where the parent isotope, ^{40}K, is an alkali element and the daughter, $^{40}Ar^*$, is a noble gas. The result is that Argon loss from minerals may occur because the gas does not form bonds with other atoms in a crystal lattice and tends to diffuse and gets lost from the system (Villa 1998).

Metamorphosed samples may yield a disorted age value if the radiogenic $^{40}Ar^*$ that had previously accumulated in the mineral has not been completely driven out before recooling (= excess Argon). In this case, a mixed age without geological significance is obtained. In contrast, loss of $^{40}Ar^*$ leads to reduction of the radiometric age (Villa 1998). The same is valid for the Rb/Sr system.

This all must be kept in mind for the interpretation of Rb/Sr and K/Ar mica ages.

4.4.1 Penninic units

In the literature, data on the age of the metamorphic climax of the Penninic units are controversial. For a discussion, see Blanckenburg et al. (1989). The investigations of Christensen et al. (1994) on garnet growth (Rb/Sr geochronology) from different structural levels within the Tauern window lead to the following results. Garnet growth in the sample from the greenschist facies Glockner Nappe complex (USH in Fig. 4.3) occurred between 35 and 30 Ma, the garnet from the amphibolite facies Greiner schist belt (LSH in Fig. 4.3) grew between 62 and 30 Ma. The thermal maxima in the Penninic units of the western Tauern window appear to have occurred at about 30 Ma (Fig. 4.3).

In the Venediger Nappe complex, the Rb/Sr phengite ages of the Zentralgneis range from 31 to 16 Ma (Fig. 4.4). (Satir 1975) interpreted his six Rb/Sr phengite ages obtained from the Tuxer-Tunnel (in the Zentralgneis) as crystallisation ages with an average of 29 Ma. This is in good agreement with the results of Christensen et al. (1994). Blanckenburg et al. (1989) suggest a continuation of the thermal peak of metamorphism in the Zentralgneis until some 20 Ma ago without knowing the results of Christensen et al. (1994). This interpretation is based on their Rb/Sr phengite age of 20 Ma obtained in the Greiner schist belt and the Zentralgneis (Fig. 4.4). An Rb/Sr phengite age of 21 Ma is also reported from Satir (1975) for the Greiner schist belt and interpreted as cooling age.

In the Zentralgneis the K/Ar phengite ages decrease from east to west. Raith et al. (1978) published K/Ar phengite ages in the range 21 to 18 Ma for the Reichenspitz area. From there westward the K/Ar phengite ages are between 19 and 14 Ma (Fig. 4.5). The decreasing ages are according to Blanckenburg et al. (1989) the result of westward tilting of the Tauern window during uplift. The K/Ar phengite ages of the Greiner schist belt show ages from 21 to 14 Ma (Fig. 4.5).

The trend of decreasing ages towards the west is also recorded in the K/Ar biotite ages of the Zentralgneis (Fig. 4.7). Near Krimml the ages are around 22 Ma and in the western part of the Zentralgneis around 13 Ma. Raith et al. (1978) attributed this age pattern to updoming along an E-W axis, subsequent to the cooling caused by uplift and erosion.

The Rb/Sr biotite ages of the Zentralgneis (Fig. 4.6) are nearly identical with the above mentioned K/Ar biotite ages. Also the K/Ar and Rb/Sr biotite ages of the Greiner schist belt have a narrow range of 15 to 13 Ma. These ages were all interpreted as cooling ages after the Tauern metamorphism.

In the Glockner Nappe complex the K/Ar white mica ages (phengites and muscovites) are between 32 and 17 Ma with a maximum around 25 Ma (Fig. 4.5) and are generally interpreted as formation or crystallisation ages at peak metamorphism (Blanckenburg et al. 1989). According to Christensen et al. (1994) they could mark the beginning of cooling after the peak metamorphism at ~30 Ma.

In summary, the pressure-temperature evolution of rocks from the Venediger Nappe complex (LSH in Fig. 4.3) and Glockner Nappe complex (USH in Fig. 4.3) in the western part of the Tauern window in combination with some of the age data described before is presented in Fig. 4.3. For a discussion, see Selverstone (1993).

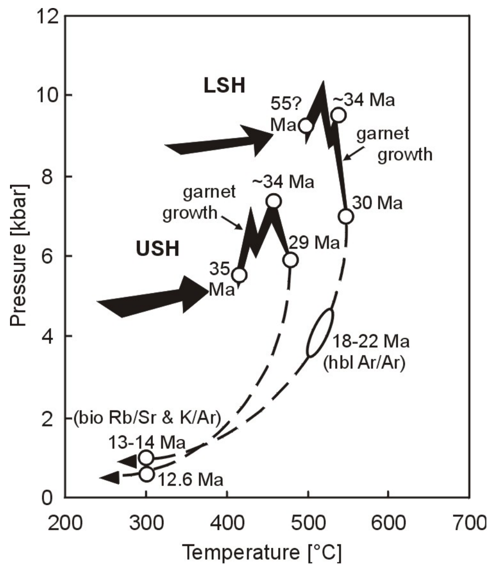

Fig. 4.3: Pressure-temperature diagram summarising the P-T-t histories of the LSH and USH from the SW corner of the Tauern window after Selverstone (1993). P-T paths are from Selverstone et al. (1984) and Selverstone & Spear (1985); garnet growth ages are from Christensen et al. (1994); hornblende ages are from Blanckenburg et al. (1989); other age data are reviewed by Selverstone 1985, 1988).

At the moment, it is not clear how to interpret the Rb/Sr phengite ages of 242 Ma and 51 Ma (Fig. 4.4) and the corresponding K/Ar phengite ages of ~80 Ma (recalc. Age: 107 ± 2 Ma) and 40 Ma (Fig. 4.5). Both samples are from locations near the Frauenwand in the Kaserer Formation, which represents a metamorphic clastic series in the western part of the Tauern window. With respect to its position above the at least in part Upper Jurassic Hochstegen marble, a Lower to Middle Cretaceous age is assigned to it (Frisch 1984).

The pre-Alpine Rb/Sr phengite age of 242 Ma is interpreted in the way, that no significant recrystallisation and thus no rejuvenation of the phengite occurred during Alpine deformation and metamorphism. This indicates also, that Alpine metamorphism did not reached temperatures above 500° C, which are required for a homogenisation of the Rb/Sr system. Based on oxygen isotope data, Hoernes & Friedrichsen (1974) determined temperatures of 500° C near the Tuxer Joch. Frisch (1984) estimated also a temperature of 500° C for the Kaserer Formation according to microprobe analyses of an epidote-amphibolite. As Fig. 4.2 shows, there is no significant incorporation of excess $^{40}Ar^{*}$ in the sample, which could explain the K/Ar phengite age of ~80 Ma, but, in contrast, there is a loss of argon. It is not clear to what extent this age has a geologically significant meaning. Either the age is related to the subduction of the South Penninic oceanic domain and the resulting internal Penninic nappe stacking. Or it represents incomplete homogenisation during Alpine deformation and metamorphism. In the latter case the age is meaningless.

The Rb/Sr phengite age of 51 Ma is potentially a mixed age of a pre-Alpine and an Alpidic phengite. According to the microprobe analyses (chapter 3.1.4) it seems, that the occurrence of two different mica generations in sample 51AnTA is possible. If it is true, that there are two mica generations, then the K/Ar phengite age of 40 Ma must also be interpreted as a mixed age.

However, these are the first geochronological data, which are available for the Kaserer Formation. More detailed investigations are required (e.g. $^{40}Ar/^{39}Ar$ dating).

4.4.2 Austroalpine units

$^{40}Ar/^{39}Ar$ dating of white mica from the Northern Greywacke Zone record disturbed Ar-release spectra with ages of ~180 Ma in low-temperature gas release steps, which increase to 267 ± 6 Ma in medium- and high-temperature gas release steps (Handler et al. 2001). These data fit very well to the K/Ar white mica age of 264 Ma of the present study (Fig. 4.5). These ages are interpreted to record Late Variscan cooling and an Early Jurassic tectonothermal overprint (Handler et al. 2001).

Nearly all $^{40}Ar/^{39}Ar$ age spectra of the Innsbruck Quartzphyllite show staircase patterns due to polyphase tectonothermal events (Handler et al. 2001). Three events can be clearly deduced: (1) Late Variscan metamorphic imprint (e.g. 283 ± 3 Ma); (2) possible Early Jurassic rejuvenation is indicated by ages between 200 and 180 Ma; (3) Cretaceous overprint is indicated by a weakly defined age of ~93 ± 5 Ma. After Handler et al. (2001) these data show that the Cretaceous metamorphic overprint, which was associated with ductile thrusting, did not significantly exceed the Ar retention temperature in white mica (375 ± 50° C).

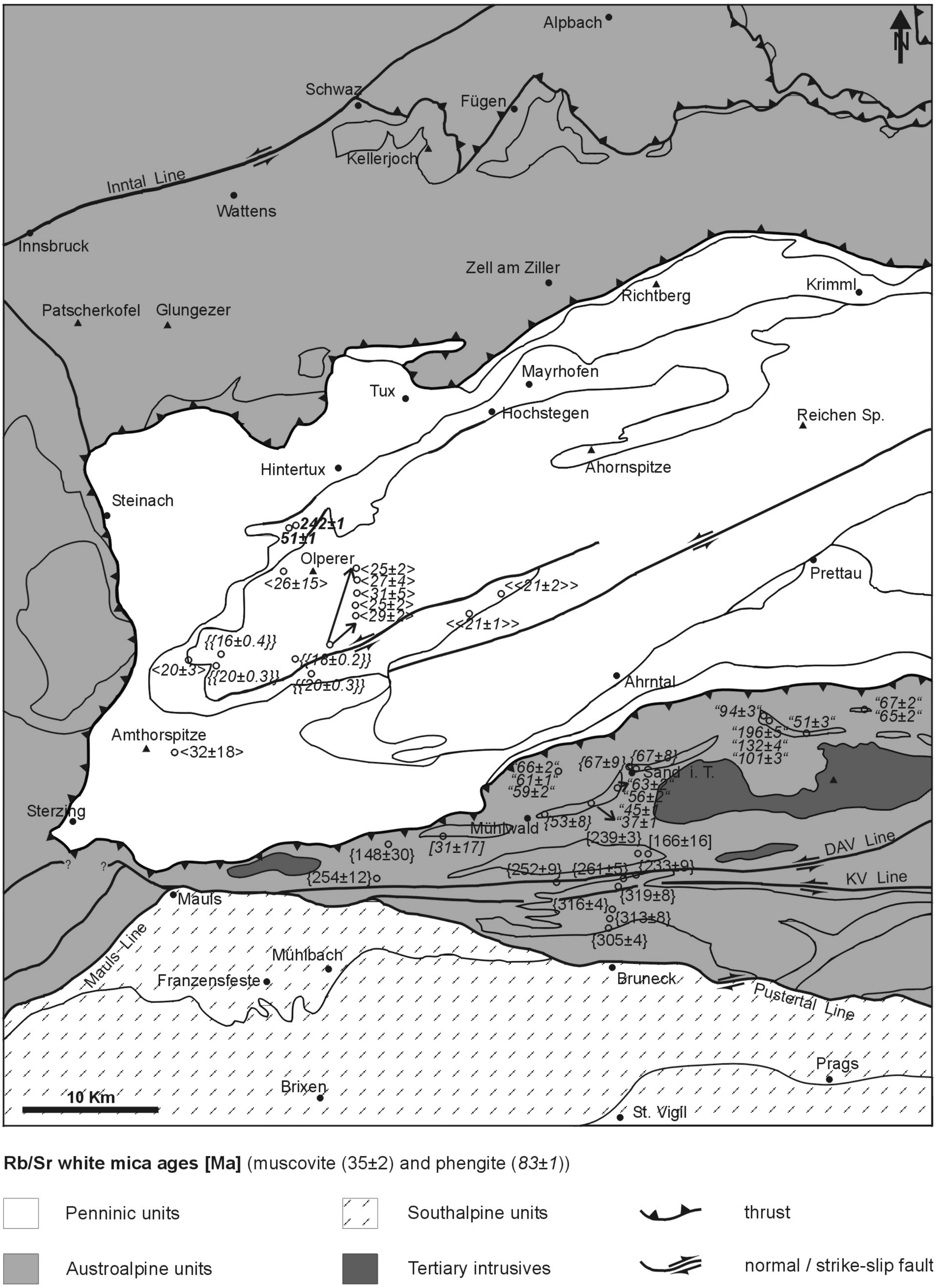

Data derived from: Borsi et al. (1973) { }; Satir (1975) < >; Borsi et al. (1978) [ ]; Hammerschmidt (1981) " "; Satir & Morteani (1981) << >>; Blanckenburg et al. (1989) {{ }}; **this study**

Fig. 4.4: Compilation of published and new Rb/Sr white mica ages.

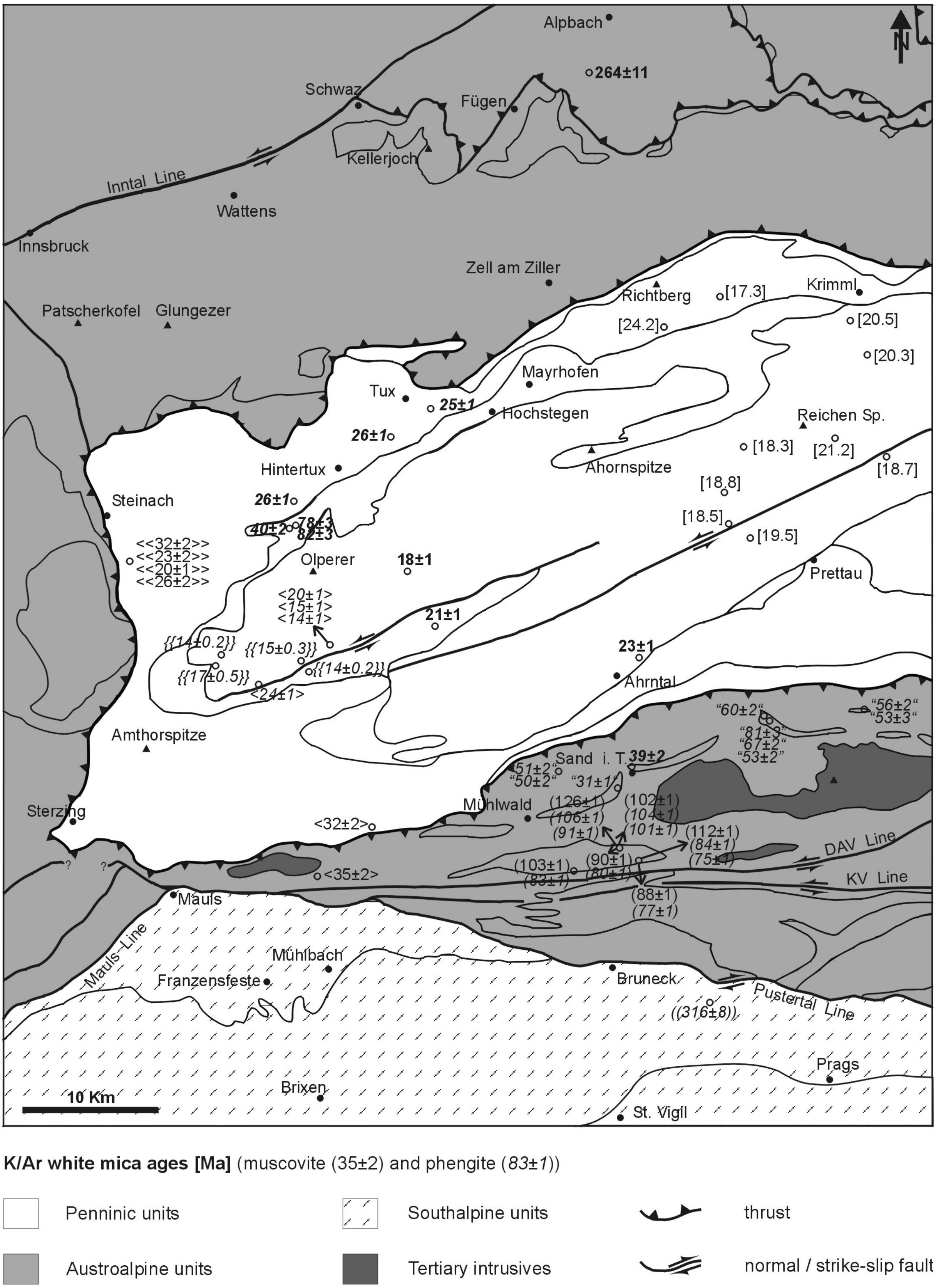

Data derived from: Satir (1975) < >; Raith et al. (1978) [ ]; Hammerschmidt (1981) " "; Thöni (1981) << >>; Stöckhert (1984) ( ); Hammerschmidt & Stöckhert (1987) (( )); Blanckenburg et al. (1989) {{ }}; **this study**

Fig. 4.5: Compilation of published and new K/Ar white mica ages.

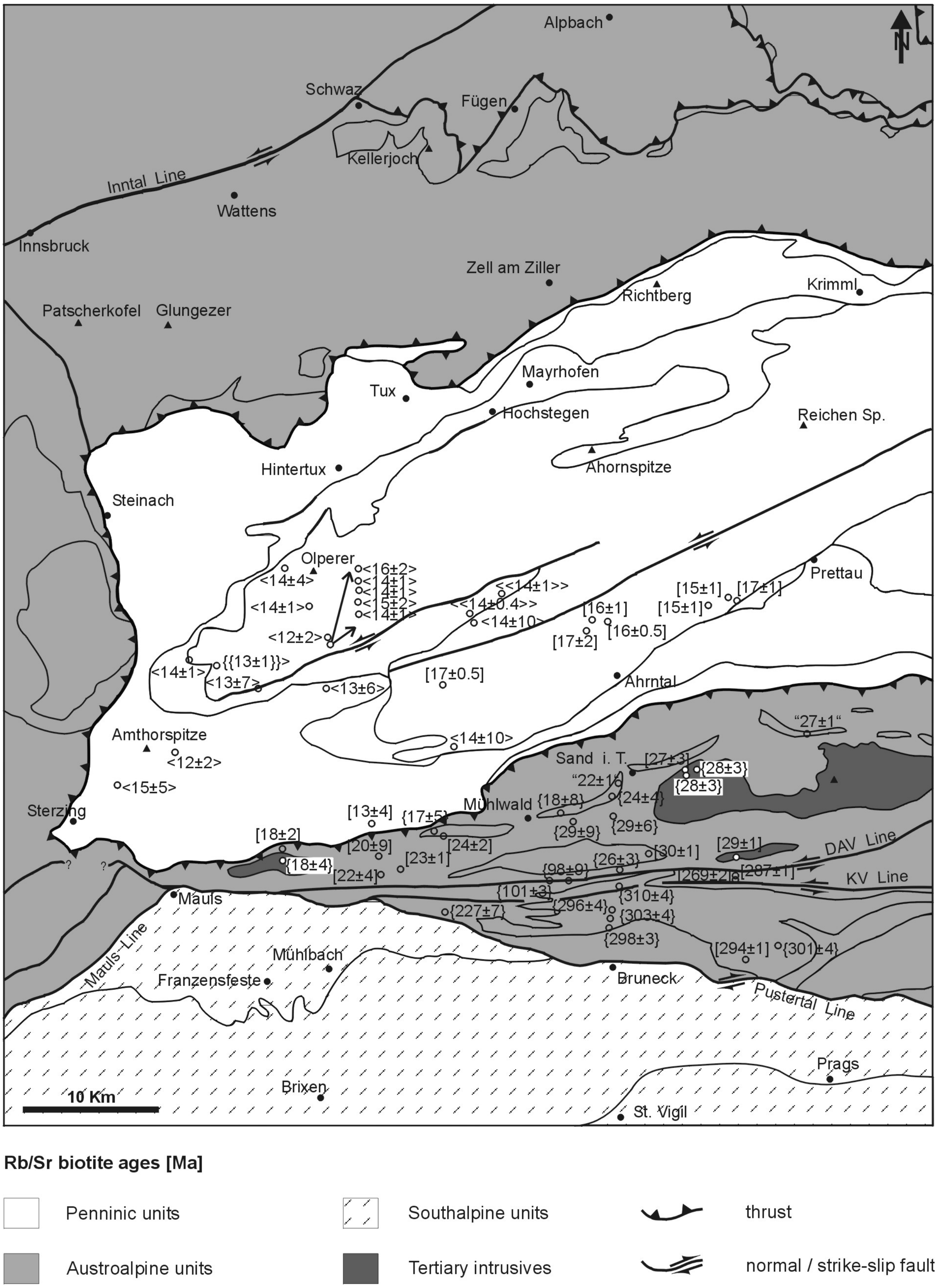

Data derived from: Borsi et al. (1973) { }; Satir (1975) < >; Borsi et al. (1978) [ ]; Hammerschmidt (1981) " "; Satir & Morteani (1981) << >>; Blanckenburg et al. (1989) {{ }}

Fig. 4.6: Compilation of published and new Rb/Sr biotite ages.

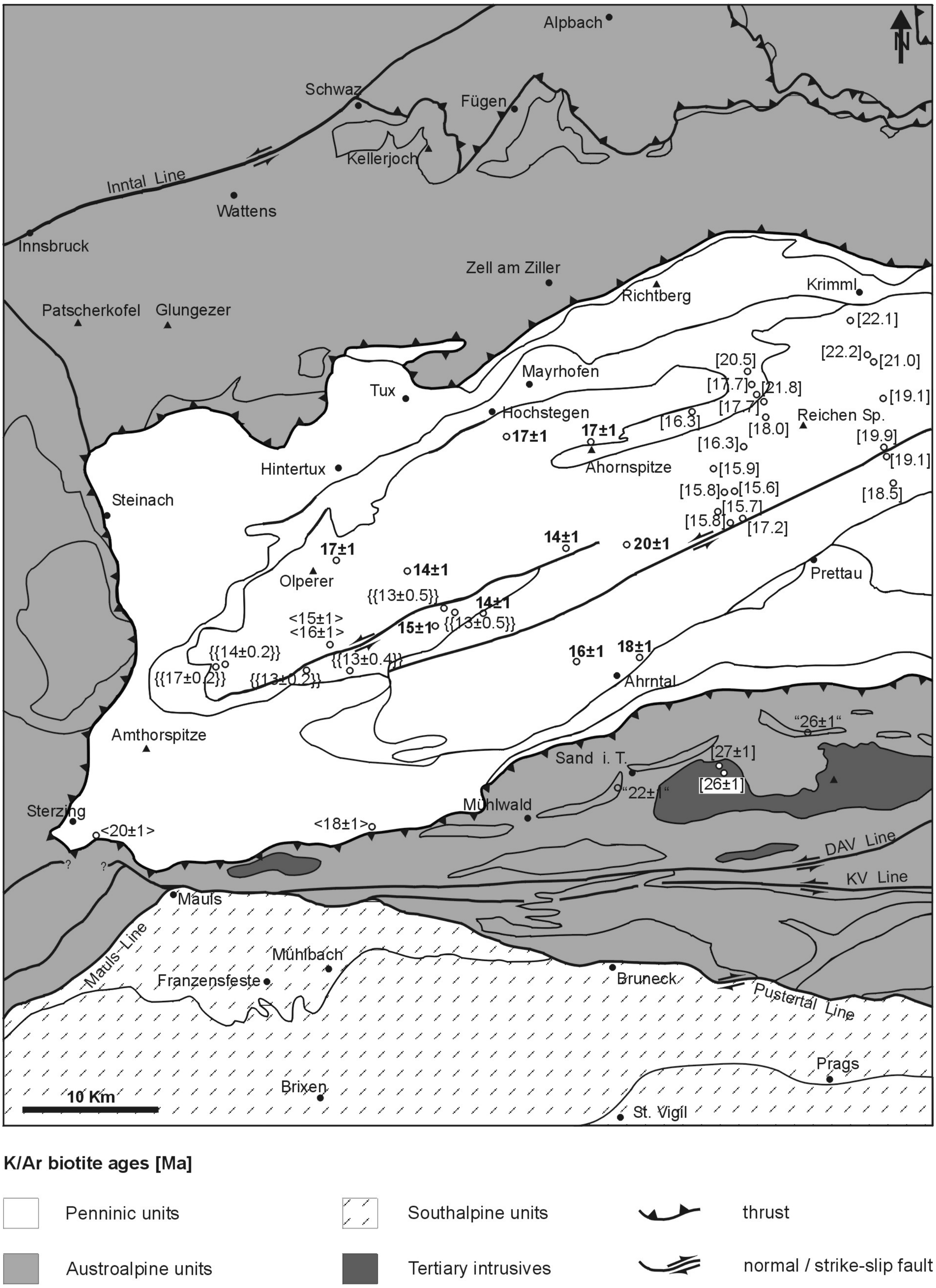

Data derived from: Satir (1975) < >; Raith et al. (1978) [ ]; Hammerschmidt (1981) “ ”; Blanckenburg et al. (1989) {{ }}; **this study**

Fig. 4.7: Compilation of published and new K/Ar biotite ages.

In the Altkristallin south of the Tauern window the published Rb/Sr white mica ages of the southern block have a narrow range between 316 and 305 Ma (Fig. 4.4). The Rb/Sr biotite ages are systematically younger and are between 303 and 294 Ma (Fig. 4.6).
Nearly the same age distribution is visible in the intermediate block between the KV Line and DAV Line (Fig. 4.4 and 4.6). These Late Variscan or Carboniferous mica ages indicate that these blocks did not experience temperatures high enough to reset the ages during the Alpine history. They can be related to regional cooling after the Variscan metamorphism (Borsi et al. 1973).

Only the northern block underwent intense Alpine deformation and metamorphism which is reflected in the younger mica ages (Fig. 4.4–4.7). The Rb/Sr white mica ages (muscovite and phengite) in the northern block show considerable variations from 254 to 37 Ma (Fig. 4.4). The oldest Rb/Sr muscovite ages (254 and 239 Ma) were obtained near the DAV Line (in pegmatitic gneisses). These ages are clearly pre-Alpine, but they are too young to be referable to the Variscan event. Hammerschmidt (1981) interpreted his Rb/Sr phengite ages (196-37 Ma) all as mixed ages. In some cases this can be proven by analysing different grain size fractions from the same sample showing that the smaller grain size yields the younger "age" (Fig. 4.4). But this is not generally the case. There are also samples with a narrow age range of the different size fractions between 67 and 60 Ma (Fig. 4.3) and therefore these ages can not be interpreted as mixed ages. Rb/Sr phengite ages around 67 Ma were also obtained by Borsi et al. (1973). They interpreted these ages in terms of Alpine metamorphic events. In particular the Rb/Sr phengite ages could be referred to an Early Alpine phase (well known in the Eastern Alps with cooling ages around 80 Ma), with partial rejuvenation linked to the Late Alpine phase (Borsi et al. 1973, 1978). Such an interpretation is also proposed by Hawkesworth (1976) for a more eastward part of the Altkristallin near the border of the Tauern window. By petrographic and radiometric investigations he ascertained Late Cretaceous metamorphism of amphibolite facies. Early Alpine deformation and metamorphism of amphibolite facies followed by a greenschist facies overprint is also proposed by Angelmaier (1997) for the Altkristallin north of the DAV Line in the area E of St. Jakob in Defereggen.

Compared to these results, the K/Ar determinations on muscovites and phengites from deformed pegmatites by Stöckhert (1984) give different ages (Fig. 4.5), leading to another interpretation. In one sample, which shows strong Early Alpine deformation but lacks later Alpine overprint, both generations of white mica (coarse muscovite and fine phengite) yield ages of ~102 Ma. This uniform age is interpreted as a cooling age after the Early Alpine deformation and metamorphism in greenschist facies (Stöckhert 1984). After his opinion the thrusting of the Altkristallin onto the Penninic rocks of the Tauern window must have taken place prior to 100 Ma. This age is in contrast to the younger Rb/Sr phengite ages and their interpretation, and it is not clear to what extent this age has a geologically significant meaning.

The other samples dated by Stöckhert (1984) show obvious effects of younger deformation. The coarse muscovites (with a pre-Alpine Rb/Sr age of 239 Ma; Borsi et al. (1973)) yield K/Ar muscovite ages between 126 and 88 Ma. The fine fractions, mainly phengites formed during the Early Alpine deformation and metamorphism, and partly some minor amounts of white mica (re)crystallised during Late Alpine overprint, give ages between 106 and 75 Ma. These ages are all interpreted as mixed ages (Stöckhert 1984). In the northernmost part of the Altkristallin the K/Ar phengite ages range between 81 and 31 Ma (Fig. 4.5). The extreme scatter of ages was explained by Stöckhert (1984) with an episode lasting about 70 Ma during which temperatures remained around or slightly above the closure temperature. So it seems that these ages were rejuvenated during Late Alpine greenschist facies conditions.

Handler et al. (2001) reported $^{40}Ar/^{39}Ar$ white mica ages of 60 and 45 Ma (integrated plateau ages) with subsequent rejuvenation (<40 Ma) of mylonitic rocks close to the DAV Line.

The concordant K/Ar and Rb/Sr biotite ages of the northern block are believed to date cooling below the 300° C isotherm at ~29 to ~18 Ma (Fig. 4.8). These Oligocene to Miocene ages are interpreted as the effect of the Tauern metamorphism (Hammerschmidt 1981) or the result of a strong Late Alpine uplift and correspondingly deep level of erosion (Stöckhert 1984). Borsi et al. (1978) recognised an increase in the biotite cooling ages from west to east. They believe that this gradual change is the result of the variation in the erosion level caused by a tilt of the northern block, with uplift of its western part.

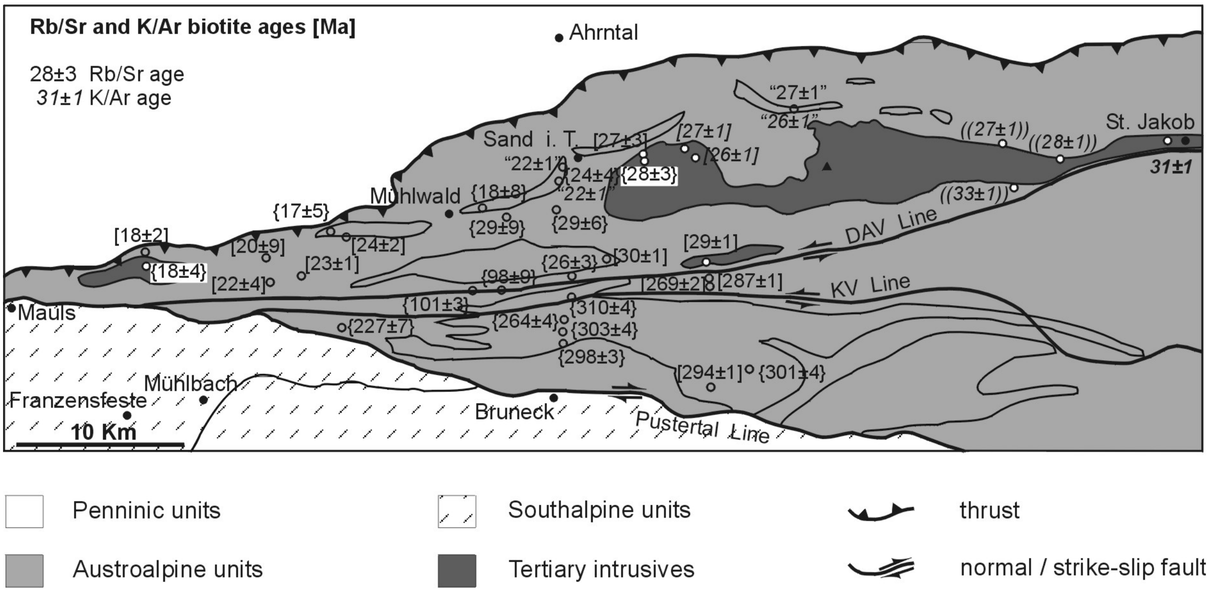

Data derived from: Borsi et al. (1973) { }; Borsi et al. (1978) [ ]; Hammerschmidt (1981) " "; Steenken et al. (2002); **this study**

Fig. 4.8.: Compilation of published and new Rb/Sr and K/Ar biotite ages of the Altkristallin.

4.4.3 Tertiary intrusives

The new K/Ar and Rb/Sr biotite ages of the Rieserferner intrusion are in the range 31 to 26 Ma (Fig. 4.8) and thus very close to the intrusion age of 31 ± 3 Ma (Borsi et al. 1978). The Rensen intrusion yielded a Rb/Sr biotite age of 18 Ma (Borsi et al. 1973). The trend of younger ages in the west to older ages in the east reflect that the Rieserferner pluton intruded in different levels and that there is a common cooling history with the surrounding Altkristallin since the Oligocene.

4.4.4 Southalpine units

The only available data of the Brixen Quartzphyllite are from Hammerschmidt & Stöckhert (1987). They yield K/Ar phengite ages in the range 316 ± 8 Ma (Fig. 4.5), which correspond to the $^{40}Ar/^{39}Ar$ plateau age of 319 ± 5.5 Ma within the error limits. After Hammerschmidt & Stöckhert (1987) the ages obtained for the phengites of the Brixen Quartzphyllite give the time of cooling below a certain temperature after progressive deformation and metamorphism. This evolution must have been completed during an early stage of the Late Carboniferous, prior to the intrusion of the Brixen Granite at 280 Ma (Borsi et al. 1972).

4.5 Fission track dating

4.5.1 Theory

The fission track dating method is based on the formation of damage zones or tracks resulting from the spontaneous fission of ^{238}U in zircons and apatites. Fission occurs continuously so the fission tracks accumulate with time. Tracks produced by spontaneous fission of ^{235}U, ^{232}Th and ^{244}Pu are negligible in number compared to those from ^{238}U. For a detailed discussion of the theory of track formation see Fleischer et al. (1965).

The basic equation for isotope dating methods, including the fission track dating method, is:

$$N_D = N_P\,(e^{\lambda t} - 1) \tag{4.5}$$

where:
- N_D = number of daughter atoms
- N_P = number of parent atoms
- λ = decay constant

Entering the density of spontaneous tracks $\rho_s = \frac{\lambda_f}{\lambda_d}{}^{238}N(e^{\lambda_d t} - 1)$ for N_D and the density of induced tracks $\rho_i = {}^{238}N I \sigma \phi$ for N_P finally gives

$$t = \frac{1}{\lambda_\alpha}\left(\ln \frac{\rho_s \lambda_\alpha}{\rho_i \lambda_f} I\sigma\phi + 1\right) \tag{4.6}$$

for the fission track age equation (Price & Walker 1963; Naeser 1967) with:

λ_α = α-decay constant of ^{238}U (1.55125 x 10^{-10} a^{-1}; (Jaffrey et al. 1973)
λ_f = decay constant for the spontaneous fission of ^{238}U
λ_d = total decay constant = $\lambda_\alpha + \lambda_f$ of ^{238}U
I = $^{235}U/^{238}U$ isotope ratio (7.2527 x 10^{-3}; (Cowan & Adler 1976)

σ = cross-section for neutron fission reaction of ^{235}U (580.2×10^{-24} cm^{-2}; (Hanna et al. 1969)

ϕ = thermal neutron fluence (n/cm^2)

ρ_s = density of spontaneous tracks ($tracks/cm^2$)

ρ_i = density of induced tracks ($tracks/cm^2$)

In order to eliminate a number of variables (e.g. the decay constant, the neutron fluence, differences in the etching procedure and individual counting statistics), the ζ-calibration method was introduced by Hurford & Green (1983), whereby a ζ- calibration factor is derived for each dosimeter glass (of known uranium concentrations) by repeated analyses of age standards (of known age) and can be determined by the following equation:

$$\zeta = \frac{(e^{\lambda_\alpha t_{std}} - 1)}{\lambda_\alpha \left(\frac{\rho_s}{\rho_i}\right)_{std} G\rho_d} \tag{4.7}$$

where:	G	= geometry factor (0.5 for the external detector method)
	ρ_d	= dosimeter track density
	t_{std}	= age of the standard
	$(\rho_s / \rho_i)_{std}$	= track density ratio in the standard

After the ζ-calibration factor has been determined, the age of a sample can be determined from the following equation:

$$t_s = \frac{1}{\lambda_\alpha} \ln\left[\lambda_\alpha \left(\frac{\rho_s}{\rho_i}\right)_s \rho_d G\zeta + 1\right] \tag{4.8}$$

where:	t_s	= age of the sample
	$(\rho_s / \rho_i)_s$	= track density ratio in the sample

4.5.2 Analytical methods

The zircon grains were mounted in PFA Teflon (Gleadow et al. 1976) and the apatite grains were embedded in ARALDITE-D epoxy resin on glass slides. The mineral mounts were grinded using emery papers (1200 and 2500 mesh). To expose the internal grain surfaces, the mineral surfaces were polished in three steps using 9 µm, 3 µm and 1 µm oil based diamond suspension. The zircon mounts were etched in a KOH-NaOH eutectic melt at 215° C (Gleadow et al. 1976) for 8 to 81 hours. This time variation is dependent on the uranium content, age and the grade of metamictization of the individual grains. The apatite mounts were etched in 5.5 Mol HNO_3 for 20 sec at 21° C (Donelick et al. 1999). Special care was taken to avoid exposure of the apatite samples to temperatures above 50° C to avoid track shortening and track density reduction (Green et al. 1986).

Zircon and apatite fission track dating was carried out using the external detector method (Gleadow 1981). Therefore the mineral mounts were covered with muscovite sheets, which served as detectors for the induced fission tracks of the samples.
After irradiation the muscovite sheets (detector and dosimeter) were etched in 40 % HF at room temperature for 20 min in case of zircons and for 30 min in case of apatites. The etching was stopped by washing the mineral mounts and muscovite sheets with distilled water.

The samples were irradiated at the RISØ reactor, Roskilde (Denmark), the ANSTO reactor, Lucas Heights (Australia) and the Oregon State University TRIGA reactor, Corvallis (USA). The neutron fluence for zircon was $1.4x10^{15}$ n/cm^2 or $1.6x10^{15}$ n/cm^2 and for apatite $4.0x10^{15}$ n/cm^2. For each sample batch two dosimeter glasses (zircon: CN2; apatite: CN5) and two or three age standards (zircon: Fish Canyon Tuff, Tardree Rhyolithe, Buluk Member; apatite: Fish Canyon Tuff, Durango, Mt. Dromedary) were included and used for the determination of the ζ-factor after equation 4.7.

Only well-etched zircon and apatite crystals with sections parallel to the crystallographic c-axis are selected for track counting. The spontaneous and induced fission tracks were counted under a Zeiss optical microscope (Axioscop), equipped with a positioning tablet controlled by the computer program ”FT Stage” (version 3.12b) developed by Dumitru (1993). The spontaneous fission tracks within the zircon grains were counted at 1000x magnification under oil. The spontaneous fission tracks within the apatite grains and the induced tracks in the muscovites were counted dry at the same magnification.
A lot of grains (mainly apatites) contain dislocations in the crystal lattice which are difficult to distinguish from fission tracks. Therefore only those tracks are counted fulfilling the following criteria: (1) fission tracks are straight and not curved, (2) fission tracks have a maximum length of 20 µm and a defined end, and (3) fission tracks are randomly oriented (Fleischer et al. 1965).

All fission track ages were calculated using the ζ-calibration method (Hurford & Green 1983). The ζ-factor of 124.64 ± 1.80 for zircon (Tab. 4.3) is based on 10 zircon standards irradiated during 5 different irradiations. The ζ-factor of 373.73 ± 7.59 for apatite (Tab. 4.4) is based on 10 apatite standards irradiated during 4 different irradiations.

All ages are reported as central ages with standard errors of ± 1 σ (Galbraith 1981). The χ^2 test (Galbraith 1981) has been applied to each data set with the aim to see if there is any additional uncertainty, other than that allowed by Poisson variation in track counts. If the χ^2 probability ($P\chi^2$) is larger than 5 %, the single grain ages are considered to represent a Poissonian distribution. The fission track data were evaluated by using the TRACKKEY 4-0C Program of Dunkl (2002). For a presentation of the histograms and the radial plots see Appendix Fig. B1 and Fig. B2.

Age standard	Number of grains	Spontaneous		Induced		P_{χ}^2 (%)	Dosimeter		ζ ± 1s
		ρ_s	N_s	ρ_i	N_i		ρ_d	N_d	
ZF-5	25	60.6	(643)	72.4	(769)	100	5.51	(5412)	120.82 ± 7.01
ZT-2	20	64.2	(593)	37.2	(344)	98	5.51	(5412)	124.44 ± 8.91
ZF-4	25	54.1	(1298)	64.0	(1536)	100	5.39	(5303)	122.78 ± 5.4
ZT-4	25	59.8	(1410)	33.8	(798)	78	5.39	(5303)	123.83 ± 6.19
ZB-3	25	11.5	(433)	20.5	(772)	99	5.37	(5276)	109.21 ± 6.86
ZF-4	25	50.3	(737)	65.0	(952)	99	5.37	(5276)	135.24 ± 7.31
ZB-3	25	9.7	(997)	23.3	(2391)	100	6.29	(6184)	125.21 ± 5.21
ZF-5	25	59.7	(3829)	85.8	(5500)	96	6.29	(6184)	127.75 ± 3.89
ZT-3	25	67.3	(2006)	44.7	(1332)	96	6.32	(6215)	123.91 ± 5.2
ZF-5	25	58.3	(2990)	83.2	(4267)	100	6.32	(6215)	126.22 ± 4.09
weighted mean									**124.64 ± 1.80**

Tab. 4.3: Determination of the ζ-factor for zircon. Track densities (ρ) are as measured (x10^5 tr/cm^2); number of tracks counted (N) shown in brackets; ρs = spontaneous track density, ρi = induced track density, ρd = track density of dosimeter glass (CN2); Pχ^2: probability obtaining chi-square value for n degree of freedom (where n = no. crystals -1). ZB = Buluk Member zircon, ZF = Fish Canyon Tuff zircon, ZT = Tardree Rhyolithe zircon.

Age standard	Number of grains	Spontaneous		Induced		P_{χ}^2 (%)	Dosimeter		ζ ± 1s
		ρ_s	N_s	ρ_i	N_i		ρ_d	N_d	
AD-4	28	2.3	(558)	6.1	(1501)	99	4.38	(4307)	386.37 ± 20.96
AF-3	25	1.7	(348)	5.3	(1073)	100	4.38	(4307)	394.05 ± 26.02
AF-3	29	1.5	(321)	5.5	(1184)	98	5.75	(5650)	358.87 ± 23.96
AD-2	25	2.2	(535)	7.7	(1861)	61	5.75	(5650)	381.48 ± 20.32
AD-6	25	2.5	(484)	6.2	(1215)	95	4.01	(3940)	394.45 ± 22.99
AF-4	25	2.2	(362)	5.6	(928)	70	4.01	(3940)	357.57 ± 23.76
AF-7	25	2.6	(310)	5.8	(769)	99	4.01	(3940)	346.04 ± 24.71
AF-3	25	1.9	(337)	6.2	(1103)	100	4.86	(4782)	376.02 ± 24.92
AD-4	25	2.8	(596)	9.0	(1956)	93	5.66	(5559)	364.67 ± 18.68
AMD-1	25	6.9	(393)	6.4	(363)	99	4.86	(4782)	377.93 ± 28.05
weighted mean									**373.73 ± 7.59**

Tab. 4.4: Determination of the ζ-factor for apatite. Track densities (ρ) are as measured (x10^5 tr/cm^2); number of tracks counted (N) shown in brackets; ρs = spontaneous track density, ρi = induced track density, ρd = track density of dosimeter glass (CN5); Pχ^2: probability obtaining chi-square value for n degree of freedom (where n = no. crystals -1). AD = Durango apatite, AF = Fish Canyon Tuff apatite, Mt. Dromedary apatite.

4.5.3 Zircon fission track ages

Zircon fission track age determinations were carried out on 57 samples. The analytical data are listed in Tab. 4.5 and the regional distribution of the ages are presented together with ages from literature in Fig. 4.10.

4.5.3.1 Results

Penninic units

The samples of the Zentralgneis yield zircon fission track ages between 17 ± 1 Ma and 11 ± 1 Ma. From two samples of the Greiner schist belt ages of 15 ± 1 Ma and 14 ± 1 Ma are obtained. An increase of the ages with altitude is visible. Also the ages continuously increase towards to the northern margin of the Tauern window. In the Wolfendorn Nappe the zircon fission track ages are 18 ± 1 Ma and in the Glockner nappe complex the zircon fission track dating yield ages between 22 ± 1 Ma and 18 ± 1 Ma.

Austroalpine units

In the Innsbruck Quartzphyllite the zircon fission track ages range from 70 ± 5 Ma to 56 ± 3 Ma. Zircon fission track dating of the Schwazer Augengneis yields ages between 64 ± 4 Ma and 58 ± 3 Ma. A zircon fission track age of 118 ± 14 Ma is obtained in the Northern Greywacke Zone. In the Altkristallin between the southern border of the Tauern window and the Pustertal Line, the zircon fission track ages increase from 21 ± 1 Ma over 48 ± 3 Ma to 122 ± 7 Ma towards to the south with clear jumps of the ages by crossing the DAV and KV Lines.

Tertiary intrusives

The zircon fission track dating of the Rensen pluton yields an age of 15 ± 1 Ma, while ages between 26 ± 1 Ma and 20 ± 1 Ma are obtained from the Rieserferner pluton. They display a clear trend to older ages from west to east (Fig. 4.12).

Southalpine units

In the Brixen Quartzphyllite the zircon fission track ages range between 224 ± 15 Ma and 209 ± 11 Ma.

Sample	Alt. [m]	Number of grains	Spontaneous ρ_s	N_s	Induced ρ_i	N_i	P_{χ}^2 (%)	Dosimeter ρ_d	N_d	Central age [Ma] ±1s
Penninic samples										
1 An TA	2450	19	19.1	(316)	32.3	(534)	93	5.39	(5303)	19.8 ± 1.5
2 An TA	2490	23	25.1	(477)	44.1	(836)	67	5.19	(5103)	18.4 ± 1.1
3 An TA	1380	20	52.8	(903)	301.1	(5150)	76	11.89	(12030)	13.0 ± 0.5
4 An TA	1790	20	63.3	(1300)	171.1	(3515)	50	5.8	(5697)	13.4 ± 0.5
5 An TA	925	20	56.2	(1011)	159.8	(2875)	98	5.8	(5697)	12.7 ± 0.5
13 An TA	2010	21	70.8	(1308)	346.7	(6407)	37	11.89	(12030)	15.1 ± 0.5
14 An TA	1110	21	67.6	(997)	341.1	(5029)	8	11.53	(11334)	14.2 ± 0.6
18 An TA	2950	19	48.4	(609)	116.3	(1463)	97	5.39	(5303)	14.0 ± 0.7
19 An TA	1980	20	49.4	(529)	119.6	(1282)	99	5.19	(5103)	13.3 ± 0.7
20 An TA	900	18	54.5	(653)	149.7	(1795)	89	5.39	(5303)	12.2 ± 0.6
21 An TA	1200	21	46.5	(521)	88.6	(993)	100	5.83	(5733)	19.0 ± 1.1
22 An TA	3250	20	32.2	(412)	67.9	(868)	97	5.39	(5303)	15.9 ± 1.0
28 An TA	2095	21	47.3	(1010)	79.3	(1692)	86	5.8	(5697)	21.5 ± 1.0
29 An TA	1200	21	40.4	(624)	162.1	(2501)	97	11.89	(12030)	18.5 ± 0.9
31 An TA	905	20	57.2	(1102)	190.3	(3666)	85	6.29	(6184)	11.8 ± 0.5
32 An TA	3100	22	87.5	(1152)	218.5	(2878)	99	6.04	(5941)	15.0 ± 0.6
35 An TA	2840	20	75.2	(2063)	199.9	(5483)	45	6.07	(5974)	14.2 ± 0.5
36 An TA	2700	21	93.3	(1192)	263.2	(3363)	92	6.29	(6184)	13.9 ± 0.5
37 An TA	2050	20	20.0	(326)	60.4	(985)	100	6.29	(6184)	13.0 ± 0.9
41 An TA	2750	20	59.2	(786)	167.6	(2224)	99	6.29	(6184)	13.8 ± 0.6
42 An TA	2135	22	56.0	(550)	163.6	(1608)	100	6.29	(6184)	13.4 ± 0.7
43 An TA	777	8	89.3	(79)	301.8	(267)	97	6.04	(5941)	11.1 ± 1.4
44 An TA	2185	20	126.1	(1624)	361.8	(4659)	87	5.83	(5733)	12.7 ± 0.4
46 An TA	2701	20	116.4	(984)	295.7	(2500)	42	5.58	(5492)	13.7 ± 0.6
47 An TA	2210	14	55.8	(159)	144.5	(412)	100	5.58	(5492)	13.4 ± 1.3
48 An TA	2345	22	86.5	(850)	160.7	(1580)	99	5.83	(5733)	19.5 ± 0.9
50 An TA	2460	20	41.5	(535)	80.3	(1034)	92	5.58	(5492)	18.0 ± 1.0
51 An TA	2500	21	53.5	(1041)	100.7	(1960)	99	5.58	(5492)	18.4 ± 0.8
54 An TA	2250	18	87.8	(561)	167.3	(1069)	87	5.58	(5492)	18.2 ± 1.0
55 An TA	2195	21	97.2	(898)	177.4	(1639)	98	5.83	(5733)	19.9 ± 0.9
56 An TA	2605	20	86.3	(738)	232.8	(1991)	81	5.83	(5733)	13.5 ± 0.6
58 An TA	2920	20	82.4	(1166)	174.8	(2475)	100	5.58	(5492)	16.4 ± 0.7
59 An TA	3360	20	172.6	(1968)	385.3	(4394)	83	6.07	(5974)	16.9 ± 0.6
Austroalpine samples										
7 An TA	960	19	101.0	(1132)	67.6	(758)	99	5.19	(5103)	48.1 ± 2.5
8 An TA	890	20	45.0	(1181)	67.2	(1764)	95	5.34	(5251)	22.2 ± 0.9
9 An TA	890	21	37.9	(906)	132.0	(3153)	52	11.53	(11334)	20.6 ± 0.9
11 An TA	2800	20	51.4	(657)	77.6	(992)	99	5.19	(5103)	21.4 ± 1.2
12 An TA	1410	20	36.4	(544)	54.4	(813)	72	5.39	(5303)	22.4 ± 1.3
15 An TA	2250	20	76.3	(833)	38.1	(416)	82	5.19	(5103)	64.4 ± 4.1
16 An TA	2110	5	77.2	(357)	21.0	(97)	92	5.19	(5103)	118.0 ± 13.7
17 An TA	570	20	103.2	(1592)	57.4	(886)	81	5.19	(5103)	57.9 ± 2.7
25 An TA	990	20	331.4	(1694)	99.8	(510)	99	6.04	(5941)	123.8 ± 6.7
30 An TA	905	20	177.9	(1556)	118.9	(1040)	99	6.07	(5974)	56.3 ± 2.5
38 An TA	2755	21	263.9	(1686)	139.8	(893)	95	5.83	(5733)	68.2 ± 3.1
39 An TA	2180	20	143.1	(1266)	81.0	(717)	91	5.8	(5697)	63.5 ± 3.2
40 An TA	2550	20	146.6	(807)	72.1	(397)	97	5.58	(5492)	70.3 ± 4.5
57 An TA	610	10	91.6	(117)	54.8	(70)	99	5.58	(5492)	57.9 ± 8.8

Southalpine samples										
23 An TA	1085	20	505.7	(1889)	73.6	(275)	79	5.34	(5251)	224.6 ± 15.2
24 An TA	990	20	472.2	(1346)	77.9	(222)	94	5.83	(5733)	216.6 ± 16.3
26 An TA	2260	20	316.9	(3053)	55.1	(531)	97	6.04	(5941)	212.9 ± 10.8
Tertiary intrusive samples										
6 An TA	1200	20	62.2	(2091)	115.3	(3876)	100	5.8	(5697)	19.5 ± 0.7
10 An TA	2400	21	77.3	(745)	114.6	(1104)	99	5.19	(5103)	21.8 ± 1.1
MA 14	2740	20	46.5	(535)	67.4	(776)	89	5.19	(5103)	22.3 ± 1.3
MA 22	1460	20	93.7	(967)	114.7	(1184)	100	5.19	(5103)	26.4 ± 1.3
MA 30	2325	9	47.0	(341)	70.7	(513)	99	5.19	(5103)	21.5 ± 1.6
MA 30 *	2325	11	54.1	(691)	194.7	(2488)	95	11.53	(11334)	19.9 ± 0.9
MA 36	1675	20	50.7	(873)	106.2	(1827)	87	5.19	(5103)	15.4 ± 0.7

Tab. 4.5: Analytical data of zircon fission track dating. Track densities (ρ) are as measured (x10^5 tr/cm^2); number of tracks counted (N) shown in brackets; ρs = spontaneous track density, ρi = induced track density, ρd = track density of dosimeter glass; Zircon ages calculated using dosimeter glass: CN2 with ζ-CN2 = 124.6±1.8; Pχ^2: probability obtaining chi-square value for n degree of freedom (where n = no. crystals -1).

4.5.4 Apatite fission track ages

Apatite fission track age determinations were carried out on 52 samples. The analytical data are listed in Tab. 4.6 and the regional distribution of the ages are presented together with previously published age data in Fig. 4.11.

4.5.4.1 Results

Penninic units

The samples of the Zentralgneis yield apatite fission track ages between 11 ± 1 Ma and 5 ± 1 Ma. In the Greiner schist belt the ages are 9 ± 1 Ma and 8 ± 1 Ma. A clear correlation of the apatite ages with altitude is visible. The ages increase towards to the northern margin of the Tauern window. In the Wolfendorn Nappe the apatite fission track ages are between 13 ± 2 Ma and 12 ± 1 Ma. From the Glockner Nappe complex, zircon fission track ages of 14 ± 2 Ma and 13 ± 2 Ma are obtained.

Austroalpine units

In the Innsbruck Quartzphyllite the apatite fission track ages range from 14 ± 4 Ma to 10 ± 3 Ma. The apatite fission track dating of the Schwazer Augengneis yields an age of 13 ± 1 Ma. A significantly older apatite fission track age of 39 ± 5 is obtained from the Northern Greywacke Zone (sample 16AnTA). In the Altkristallin between the southern border of the Tauern window and the Pustertal Line, the apatite fission track ages show a uniform pattern of 11 ± 1 Ma to 9 ± 1 Ma with a maximum of 10 ± 1 Ma. In contrast to the zircon fission track ages there are no jumps in ages across the DAV and KV Lines.

Sample	Alt. [m]	Number of grains	Spontaneous		Induced		P_{χ}^{2} (%)	Dosimeter		Central age [Ma] ±1s	Mean track length [µm]	Standard deviation [µm]	Number of tracks
			ρ_s	N_s	ρ_i	N_i		ρ_d	N_d				
Penninic samples													
2 An TA	2490	31	1.4	(236)	11.7	(1911)	99	5.75	(5650)	13.3 ± 1.0	12.49 ± 0.49	2.43	25
3 An TA	1380	30	0.4	(76)	6.7	(1251)	100	5.75	(5650)	6.5 ± 0.8	-	-	-
4 An TA	1790	32	0.5	(90)	7.7	(1413)	100	5.71	(5615)	6.8 ± 0.8	12.94 ± 0.53	1.75	11
5 An TA	925	30	0.8	(148)	16.9	(2982)	100	5.71	(5614)	5.3 ± 0.5	13.70 ± 0.21	1.66	60
13 An TA	2010	31	0.6	(75)	6.3	(800)	100	5.75	(5650)	10.1 ± 1.2	-	-	-
14 An TA	1110	30	0.7	(52)	7.9	(601)	100	5.75	(5650)	9.3 ± 1.4	-	-	-
18 An TA	2950	30	1.0	(225)	12.0	(2808)	100	5.75	(5650)	8.6 ± 0.6	13.40 ± 0.27	1.8	45
19 An TA	1980	31	1.2	(233)	18.3	(3493)	99	5.75	(5650)	7.2 ± 0.5	14.00 ± 0.19	1.33	47
20 An TA	900	30	0.8	(176)	16.6	(3690)	100	5.75	(5650)	5.1 ± 0.4	-	-	-
22 An TA	3250	30	2.9	(629)	31.9	(6882)	100	5.71	(5615)	9.7 ± 0.5	13.90 ± 0.19	1.33	50
28 An TA	2095	19	1.3	(59)	8.8	(404)	99	5.26	(5170)	14.3 ± 2.0	-	-	-
29 An TA	1200	15	0.9	(25)	7.4	(215)	100	5.75	(5650)	12.5 ± 2.7	-	-	-
31 An TA	1150	30	2.8	(500)	46.8	(8259)	65	5.26	(5170)	5.9 ± 0.3	13.38 ± 0.18	1.44	63
32 An TA	3100	30	1.2	(102)	12.9	(1115)	100	5.46	(5364)	9.3 ± 1.0	14.65 ± 0.66	1.61	6
33 An TA	2255	4	0.9	(7)	11.2	(88)	82	5.46	(5364)	8.1 ± 3.2	-	-	-
35 An TA	2840	30	1.7	(300)	19.6	(3389)	98	5.06	(4976)	8.4 ± 0.5	14.10 ± 0.25	1.97	60
36 An TA	2700	31	1.0	(115)	12.2	(1444)	100	5.66	(5559)	8.4 ± 0.8	13.93 ± 0.35	1.72	24
37 An TA	2050	33	0.4	(71)	5.4	(925)	95	5.46	(5364)	7.8 ± 1.0	13.62 ± 0.38	1.84	23
41 An TA	2750	30	1.4	(313)	18.7	(4078)	42	5.66	(5559)	8.1 ± 0.5	13.48 ± 0.29	2.03	48
42 An TA	2135	30	1.1	(260)	16.2	(3757)	99	5.46	(5364)	7.1 ± 0.5	13.52 ± 0.44	1.65	14
43 An TA	777	30	0.5	(81)	10.6	(1807)	95	5.46	(5364)	4.6 ± 0.5	13.91 ± 0.16	1.23	59
44 An TA	2185	30	3.2	(675)	37.1	(7760)	89	5.06	(4976)	8.2 ± 0.4	13.66 ± 0.17	1.56	81
46 An TA	2701	32	0.6	(73)	5.6	(732)	89	5.06	(4976)	9.4 ± 1.2	13.85 ± 0.37	1.82	24
47 An TA	2210	30	0.8	(143)	9.8	(1684)	100	4.86	(4782)	7.7 ± 0.7	14.00 ± 0.26	1.18	21
48 An TA	2345	27	0.8	(102)	6.2	(756)	93	5.06	(4976)	12.7 ± 1.4	-	-	-
49 An TA	2430	24	1.2	(54)	8.7	(394)	100	5.06	(4976)	12.9 ± 1.9	-	-	-
51 An TA	2500	30	1.8	(211)	13.4	(1602)	100	4.86)	(4782)	12.0 ± 0.9	12.51 ± 0.88	3.17	13
54 An TA	2250	15	1.2	(102)	9.8	(806)	100	5.26	(5170)	12.4 ± 1.3	10.80 ± 1.11	2.48	5
55 An TA	2195	15	1.3	(89)	9.7	(645)	99	5.06	(4976)	13.0 ± 1.5	13.29 ± 0.69	1.82	7
56 An TA	2605	30	0.9	(112)	11.4	(1371)	100	4.86	(4782)	7.4 ± 0.8	-	-	-

58 An TA	2920	30	1.0	(121)	8.7	(1107)	100	5.06	(4976)	10.3 ± 1.0	14.16 ± 0.30	1.31	19
59 An TA	3360	30	0.6	(71)	5.3	(590)	100	4.86	(4782)	10.9 ± 1.4	-	-	-
Austroalpine samples													
7 An TA	960	26	1.1	(74)	12.3	(789)	100	5.75	(5650)	10.1 ± 1.2	-	-	-
8 An TA	890	30	0.7	(139)	8.1	(1578)	99	5.75	(5650)	9.5 ± 0.9	13.63 ± 0.38	1.51	16
9 An TA	890	30	0.6	(117)	5.7	(1208)	100	5.75	(5650)	10.4 ± 1.1	13.39 ± 0.97	2.75	8
11 An TA	2800	31	1.7	(315)	19.0	(3615)	100	5.75	(5650)	9.4 ± 0.7	13.67 ± 0.20	1.56	60
12 An TA	1410	32	0.5	(97)	5.6	(1102)	100	5.75	(5650)	9.5 ± 1.0	13.68 ± 0.20	1.37	46
16 An TA	2110	15	3.5	(74)	9.8	(206)	100	5.75	(5650)	38.5 ± 5.3	13.44 ± 0.26	1.72	43
17 An TA	570	25	3.0	(228)	24.7	(1896)	100	5.71	(5615)	12.8 ± 1.0	11.92 ± 0.49	2.09	18
25 An TA	990	30	1.1	(152)	11.1	(1573)	96	5.26	(5170)	9.5 ± 0.8	14.08 ± 0.15	1.12	55
30 An TA	905	4	0.9	(11)	9.4	(112)	97	5.46	(5364)	10.0 ± 3.2	-	-	-
38 An TA	2755	22	1.4	(107)	12.4	(935)	99	5.66	(5559)	12.1 ± 1.3	12.80 ± 1.51	3.7	6
39 An TA	2180	18	1.5	(96)	12.6	(782)	100	5.06	(4976)	11.6 ± 1.3	-	-	-
40 An TA	2550	8	1.5	(18)	11.2	(134)	93	5.46	(5364)	13.7 ± 3.5	11.64 ± 0.75	2.48	11
57 An TA	610	13	2.0	(44)	17.1	(378)	95	5.06	(4976)	11.0 ± 1.8	11.63 ± 0.49	2.29	22
Southalpine samples													
23 An TA	1085	19	1.2	(27)	9.5	(217)	100	5.75	(5650)	13.4 ± 2.7	11.05 ± 0.84	2.06	6
24 An TA	990	8	2.0	(23)	17.9	(211)	97	5.26	(5170)	10.7 ± 2.4	-	-	-
26 An TA	2260	27	1.8	(184)	12.9	(1293)	82	5.66	(5559)	15.0 ± 1.3	13.54 ± 0.37	1.76	23
Tertiary intrusive samples													
6 An TA	1200	31	0.6	(130)	6.0	(1394)	100	5.71	(5615)	9.9 ± 0.9	13.07 ± 0.29	2.17	58
MA 22	1460	30	1.3	(140)	13.5	(1449)	100	5.75	(5650)	10.4 ± 1.0	-	-	-
MA 30	2325	30	0.8	(163)	8.4	(1641)	100	5.75	(5650)	10.7 ± 0.9	13.57 ± 0.28	1.61	33
MA 36	1675	29	0.4	(79)	4.2	(875)	100	5.75	(5650)	9.7 ± 1.2	13.42 ± 0.22	1.4	41

Tab. 4.6: Analytical data of apatite fission track dating. Track densities (ρ) are as measured ($x10^5$ tr/cm^2); number of tracks counted (N) shown in brackets;
ρs = spontaneous track density, ρi = induced track density. ρd = track density of dosimeter glass;
Apatite ages calculated using dosimeter glass: CN5 with zCN5 = 373.7±7.6
P_{χ}^{2}: probability obtaining chi-square value for n degree of freedom (where n = no. crystals -1)

Tertiary intrusives

Apatite fission track ages obtained from the Rensen and the Rieserferner intrusion display a homogeneous age pattern of 11 to 10 ± 1 Ma. A trend to increasing apatite ages towards to the east, as previously recorded by the mica and zircon fission track ages, is not visible.

Southalpine units

In the Brixen Quartzphyllite the apatite fission track ages are between 15 ± 1 Ma and 11 ± 2 Ma.

4.5.5 Interpretation and discussion of zircon and apatite fission track ages

During the past decade, zircon and apatite fission track dating have become a routine part of tectonic and low temperature thermal history investigations. The zircon and apatite fission track age determinations yield cooling histories for rocks below the respective closure temperature for each mineral. The closure temperature or effective retention temperature for fission tracks is defined as the temperature at which 50 % of the original number of fission tracks are preserved. The zircon closure temperature has been determined to be 240 ± 50° C for slow cooling rates (Hurford 1986). For faster cooling rates, as in Alpine systems (>10° C/Ma), a value of 225 ± 25° C has been proposed by Hurford et al. (1989, 1991). For apatite, a closure temperature of 100 ± 20° C is generally used (Wagner 1968; Naeser & Faul 1969; Hurford 1986).

Experiments have shown that partial annealing of fission tracks is a gradual process which occurs over a wide temperature zone (Naeser & Faul 1969; Green et al. 1986; Laslett et al. 1987). This temperature zone is called “partial annealing zone” (PAZ) (see Wagner & Van den Haute 1992). The lower limit of the PAZ is defined as the temperature where a maximum decrease in the gradient of track stability appears. The upper limit of the PAZ is represented by the temperature where complete annealing of the tracks occurs. The zircon partial annealing zone (ZPAZ) has temperature limits of ~190 to 260° C (Zaun & Wagner 1985) and the apatite partial annealing zone (APAZ) is at temperatures of ~70 to 125° C (Gleadow et al. 1983).

All zircon and apatite samples passed the χ^2 test with a $P\chi^2$ probability of >80 % in most case. Furthermore all individual grain ages plot within the 2σ range of the appropriate radial plots (Appendix Fig. B1 and Fig. B2). This clearly denotes the occurrence of multiple age populations within a sample.

4.5.5.1 Penninic units

The zircon fission track ages of the Zentralgneis range between 18 and 11 Ma (Fig. 4.10), which indicates Miocene cooling below ~225° C. As expected, the ages depend on the altitude in the way that the topographic highest samples display the oldest ages. A trend to older ages in the west, as indicated by the mica ages, is not visible. But it seems that there is a slight trend to increasing ages at the southern border of the Zentralgneis.

The apatite fission track ages are in the range of 11 to 5 Ma (Fig. 4.11) and show ongoing Miocene cooling. An increase of the apatite ages with altitude is observable.

Towards to the northern margin of the Tauern window a rise of zircon fission track ages of 18 Ma in the Wolfendorn Nappe to ages of 22 Ma in the Glockner Nappe complex is visible (Fig. 4.10). The zircon fission track age of 22 Ma of the Penken area confirm the opinion of Miller (1984) to assign the Penken-breccia to the Penninic units (Bündner-Schiefer Formation).
Also the apatite fission track ages increase from 12 Ma in the Wolfendorn Nappe to 14 Ma in the Glockner Nappe complex (Fig. 4.11).

This observation is evidence that first the Glockner Nappe complex cooled below 225° C followed by the Wolfendorn Nappe and finally by the Zentralgneis during the Miocene updoming of the Tauern window. Two NW-SE profiles (Fig. 4.9) in which all samples derived from nearly the same altitude (~2300 m), clarify this age distribution.

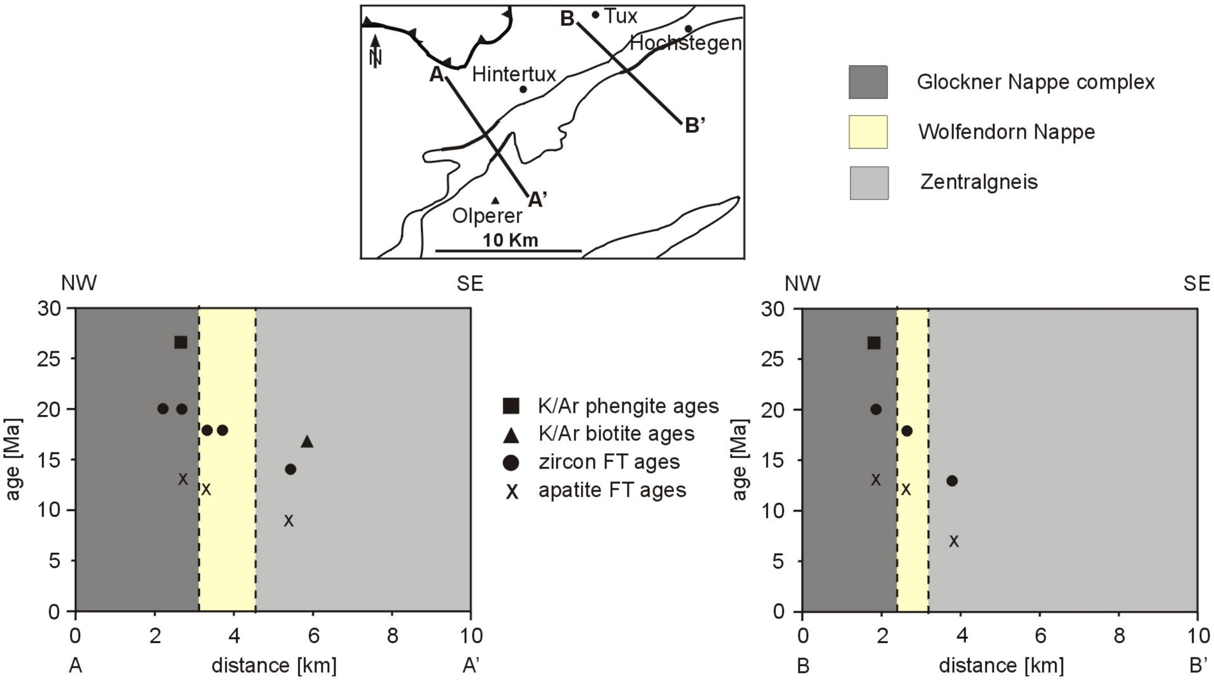

Fig. 4.9: Thermochronological profiles.

4.5.5.2 *Austroalpine units*

One zircon fission track age of 118 Ma is gained in the Northern Greywacke Zone and indicates the Early Cretaceous cooling of this Upper Austroalpine unit to 240 ± 50° C.
The rather high apatite fission track ages of 39 Ma (Fig. 4.10) and 22 Ma are interpreted by Grundmann & Morteani (1985) as probable cooling ages of the eo-Alpine event. But due to the lack of enough data a final interpretation is not possible.

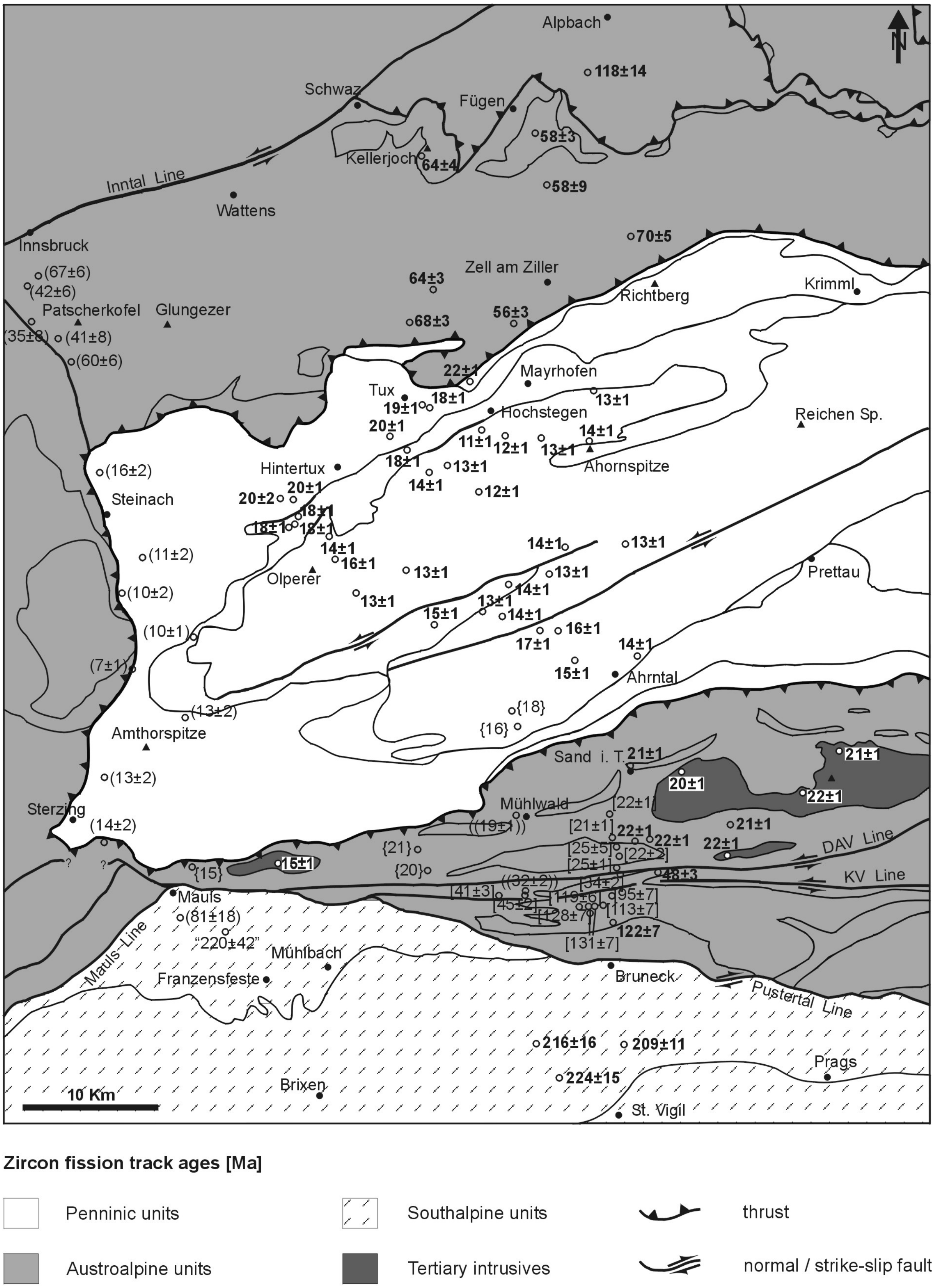

Data derived from: Fügenschuh (1995) ( ); Brix et al. (1996) { }; Elias (1998) " "; Stöckhert et al. (1999) [ ]; Steenken et al. (2002) (( )); **this study**

Fig. 4.10: Compilation of published and new zircon fission track ages.

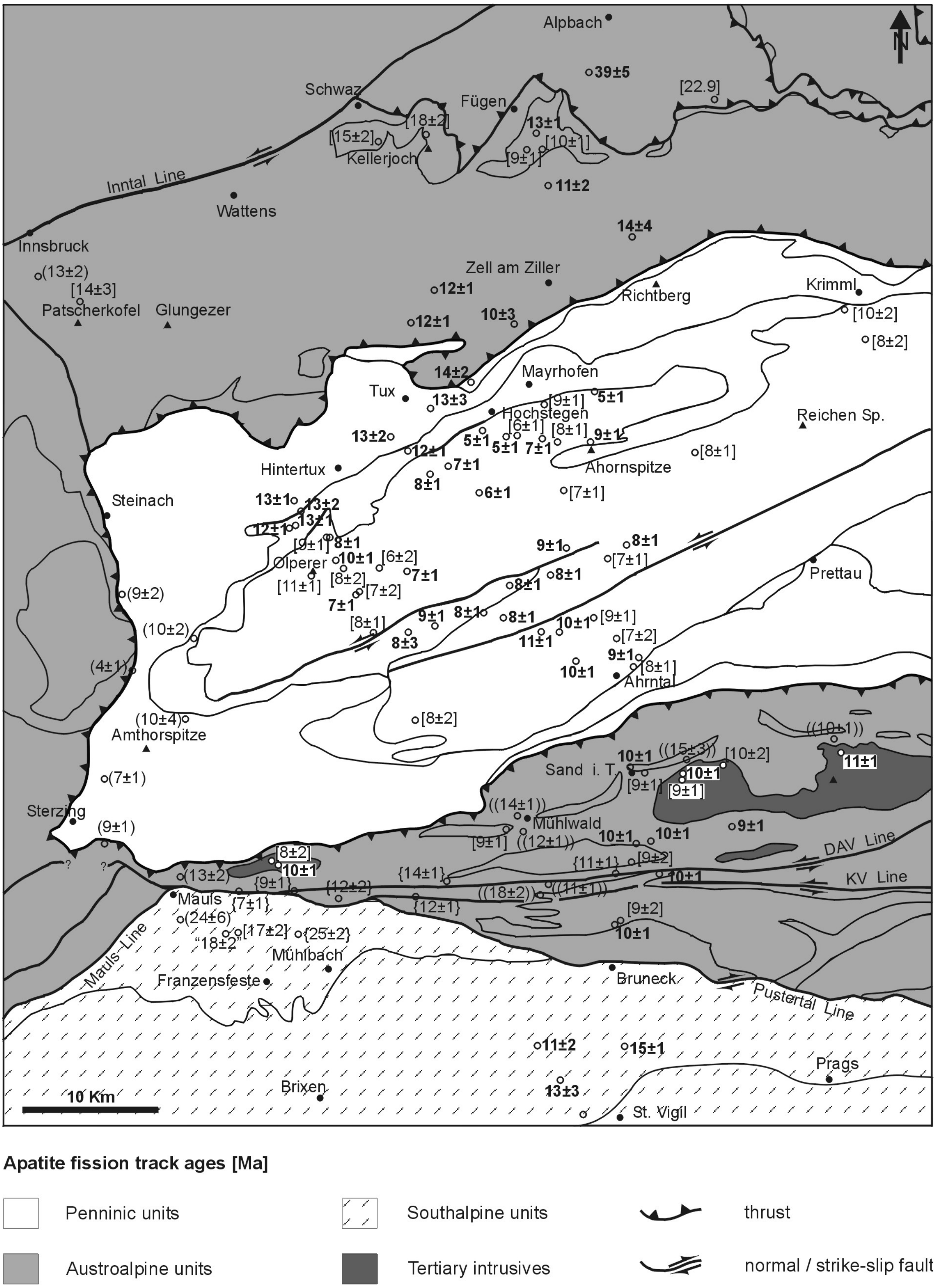

Data derived from: Grundmann & Morteani (1985) [ ]; Coyle (1994) { }; Fügenschuh (1995) ( ); Elias (1998) “ ”; Steenken et al. (2002) (( )); **this study**

Fig. 4.11: Compilation of published and new apatite fission track ages.

In the Innsbruck Quartzpyllite the zircon fission track ages are between 70 and 56 Ma (Fig. 4.10). Nearly the same age distribution (64 to 58 Ma) is observable in the samples of the Schwazer Augengneis (Fig. 4.10). The origin of the Schwazer Augengneis is still a matter of debate. It has been attributed over the years to either the Lower or the Middle Austroalpine units (Handler et al. 2001). The zircon fission track ages show clearly that the Schwazer Augengneis is part of the Lower Austroalpine units and can be interpreted as the inverted basement of the Innsbruck Quartzphyllite. This is in contrast to the classical concept in which the Schwazer Augengneis is the basement of the Northern Greywacke Zone. The zircon fission track ages reflect cooling after the Cretaceous metamorphic overprint.
Final cooling below ~100° C was between 18 and 9 Ma, whereby the data of this study have a narrower range of 14 to 10 Ma (Fig. 4.11).

In the Altkristallin south of the Tauern window the zircon fission track ages of the southern block are between 131 and 95 Ma (Fig. 4.12). This suggests that the southern block cooled below 240 ± 50° C in the Early Cretaceous. There is no indication for reheating, and so it seems that the southern block remained in a temperature range of ~200-100° C throughout the Oligocene/Miocene tectonic activity (Stöckhert et al. 1999).
In the intermediate block the zircon fission track ages are younger and in the range of 48–34 Ma (Fig. 4.12). This indicates that the temperature, in contrast to the southern block, was high enough for track annealing (>260° C) and cooling below 240 ± 50° C took place in the Eocene.
From mica ages (Fig. 4.4–4.7) it is known that the northern block underwent intense Alpine deformation and metamorphism. The zircon fission track ages are systematically younger as the Rb/Sr and K/Ar biotite ages and scatter between 25 Ma and 15 Ma with a frequency maximum around 22 Ma, but close to the biotite ages (Fig. 4.8). This indicates a) rapid cooling during the tectonic activity of the DAV Line and b) that movements along the DAV Line occur longer as suggested by the Rb/Sr white mica microchron ages of 33 to 30 Ma obtained by Müller et al. (2000).
The homogeneous apatite data at around 10 Ma (Fig. 4.12) show that the late cooling history below ~100° C is identical for the three blocks, indicating stagnation of vertical displacement along the DAV and KV Lines.

After Stöckhert et al. (1999) the age pattern across the DAV Line indicates that the largest portion of displacement took place within a few million years around 30 Ma, when the northern block was still above the closure temperature of biotite, whereas the intermediate block was around or just below the closure temperature for fission tracks in zircon. A vertical displacement of about 1.5-2 km across the DAV Line was estimated by Stöckhert et al. (1999) from the initial temperature contrast of ca. 50° C and by using a thermal gradient of about 30° C/km.

4.5.5.3 Tertiary intrusives

The zircon fission track ages of the Oligocene Rieserferner pluton give a trend from 22 Ma in the western part to 26 Ma in the eastern part (Fig. 4.12). For the Rensen pluton, zircon fission track dating yields an age of 15 Ma (Fig. 4.12). These ages are similar to those obtained from the northern block, indicating a common cooling his-

tory since the Oligocene. Like the biotite ages, the zircon fission track ages show also a trend to higher ages in the east and suggest W-E tilting of the northern block.
The maximum of the apatite fission track ages are ~10 Ma (Fig. 4.12) and are identical to the ages obtained from the country rocks of the plutons. This leads to the conclusion that there is no more tilting of the northern block at that time.

Two apatite fission track ages from Coyle (1994) yield much higher ages of 20 Ma and 16 Ma. Also Steenken et al. (2002) published apatite ages between 19 and 10 Ma for the northern and intermediate block (Fig. 4.12), and interpret a weak tendency of increasing apatite fission track ages towards to the east. One reason of those anomalous high ages could be the reactor (ANSTO reactor, Lucas Heights, Australia) used for the irradiation. It came out during an intralaboratory study of the Tübingen fission track working group, that the flux of the reactor has high spatial variation. This leads to a gradient in the sample batch and therefore to a gradient of the ages depending on the sample position. No apatite sample of this study was irradiated in Australia.

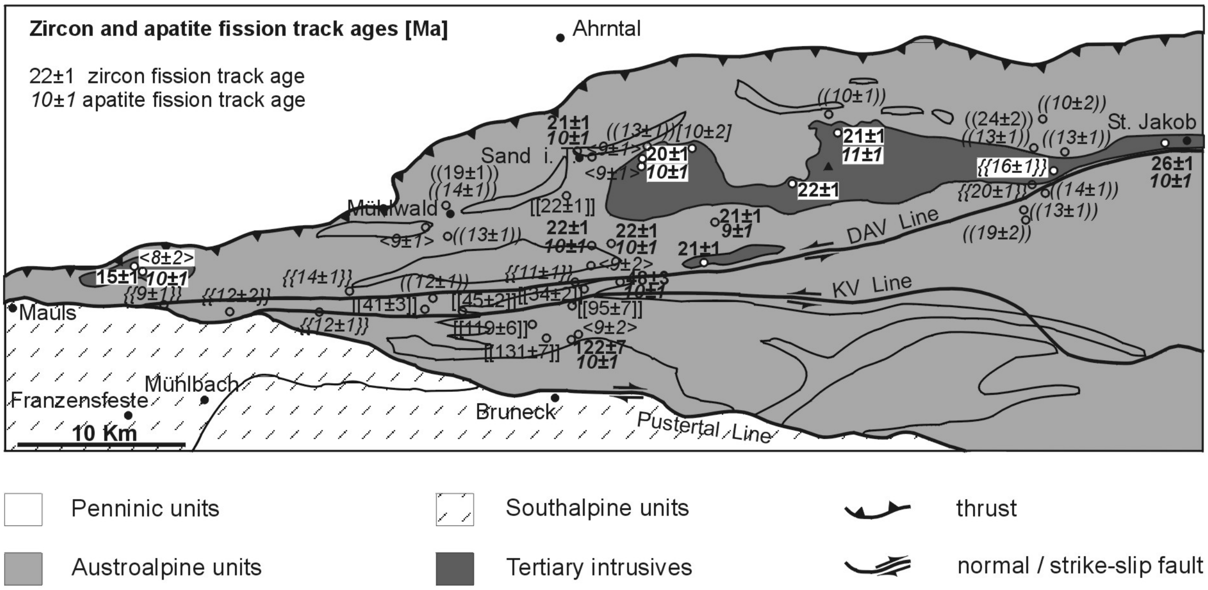

Data derived from: Grundmann & Morteani (1985) < >; Coyle (1994) {{ }}; Stöckhert (1999) [[ ]]; Steenken et al. (2002) (( )); **this study**

Fig. 4.12: Compilation of published and new zircon and apatite fission track ages of the Altkristallin.

4.5.5.4 Southalpine units

Most of the samples south of the Periadriatic lineament give Late Triassic zircon fission track ages between 224 and 209 Ma (Fig. 4.10). They indicate (ongoing ?) slow cooling of this area, which starts around 316 Ma (K/Ar white mica cooling ages; Hammerschmidt & Stöckhert 1987). For the more westward central Southern Alps (Lake Como region) similar zircon fission track ages are obtained by Bertotti et al. (1999). The existence of a Late Triassic thermal event in this region, which is possible related to magmatism, is documented by several Rb/Sr, K/Ar and Ar/Ar age determinations (Ferrara & Innocenti 1974; Bertotti et al. 1999). This thermal event is followed by a period of crustal extension, which has been constrained between the Early Norian (220 Ma) and

the Late Liassic (186 Ma) by the sedimentary record (Bertotti et al. 1993). The measured Late Triassic fission track ages are maybe also related to this thermal event, whereas the mica ages in the study area are not rejuvenated. This indicates, that the temperature did not exceed >350° C. Fügenschuh (1995) reported a Late Cretaceous zircon fission track age of 81 Ma for a sample of the Brixen Granite (formation age 280 Ma; Borsi et al. 1972) which is obviously meaningless due to bad statistic values.
In the Brixen Quartzphyllite the apatite fission track ages range from 15 to 11 Ma and thus they are slightly higher as the ages obtained north of the Periadriatic lineament (Fig. 4.11). The apatite fission track ages of the Brixen Granite are a bit older and scatter from 25 to 17 Ma. Hammerschmidt & Stöckhert (1987) propose on the basis of their petrological and geological informations an onset of Late Alpine exhumation and erosion at ~40 Ma by a temperature of ~150° C.

4.6 Summary

According to the large amount of geochronological data presented before, the age data are summarised in different age groups. The fission track data were additionally evaluated in fission track age distribution maps (Fig. 4.13).
To point out the remarkable differences in the cooling history of different blocks of the Altkristallin south of the Tauern window, a comprehensive compilation of these data is given at the end of this chapter (Fig. 4.14).

Mica ages

~300 Ma
Mica ages from regions with very weak or no Alpine overprint cluster in the range of 300 ± 20 Ma. Such ages can be found in the Southalpine Brixen Quartzphyllite and the Austroalpine Altkristallin southern block. They are interpreted as a record of Variscan cooling in pre-Alpine basement rocks.

270-230 Ma
This group may comprise pre-Alpine ages that are partly rejuvenated by the Alpine event. Such ages can be found in the Austroalpine Northern Greywacke Zone, in the Austroalpine Altkristallin intermediate block and in the southern area of the Austroalpine Altkristallin northern block.

~100 Ma
This younger age in the Austroalpine units is restricted to the southern area of the Altkristallin northern block. This age and the data accumulation in the range of 90-80 Ma from Austroalpine basement rocks are generally interpreted to correlate with the beginning of thrusting of the Austroalpine on the cooler Penninic rock series due to the subduction of the South Penninic oceanic domain. Maybe the Late Cretaceous age around 80 Ma obtained in the Kaserer Formation could be also related to the same event. The internal Penninic nappe stacking is a result of the underthrusting of the Venediger Nappe beneath the Glockner Nappe.

70-40 Ma

Ages in this time span occur in the northern area of the Austroalpine Altkristallin northern block. They are interpreted to refer to an Early Alpine metamorphic event, with partial rejuvenation linked to the Late Alpine metamorphic event.

30-10 Ma

These ages are interpreted to reflect Late Alpine cooling. Such ages are obtained in the Penninic units of the Tauern window, the Austroalpine Altkristallin northern block and the Tertiary intrusives.

Zircon fission track ages

~220 Ma

These very old ages are preserved in the Southalpine Brixen Quartzphyllite, where no or only very low grade Alpine overprint has occurred.

130-90 Ma

This age group can be found in the Austroalpine Northern Greywacke Zone and in the Austroalpine Altkristallin southern block. It indicates common cooling below 240 ± 50° C in the Cretaceous.

~60 Ma

This age cluster occurs in the Austroalpine Innsbruck Quartzphyllite and the Austroalpine Schwazer Augengneis. These ages reflect cooling after the Cretaceous metamorphic overprint. The nearly identical ages of both units show clearly that the Schwazer Augengneis is part of the Lower Austroalpine units and not of the Upper Austroalpine units.

~40 Ma

Only the samples of the Austroalpine Altkristallin intermediate block yield such ages. This indicates that the temperatures, in contrast to the southern block, was high enough for track annealing (>260° C) and cooling below 240 ± 50° C took place in the Eocene.

22-10 Ma

This age group can be found in the Penninic units of the Tauern window, the Austroalpine Altkristallin northern block and the Tertiary intrusives. The ages indicate Miocene cooling below ~225° C. In the Zentralgneis of the western Tauern window the ages depend on the altitude in the way that the topographic highest samples display the oldest ages. In contrast the ages obtained in the Altkristallin northern block have a narrow range around 22 Ma and show no correlation with the altitude, which indicates rapid exhumation. The ages of the Glockner Nappe and the Altkristallin northern block are nearly identical and display common cooling below 225° C.

Apatite fission track ages

~40 Ma

Only in the Austroalpine Northern Greywacke Zone such rather high age is measured. It is interpreted as probable cooling age of the eo-Alpine event. But due to the lack of enough data a final interpretation is not possible.

25-10 Ma

This age group is restricted to the Southalpine Brixen Granite and the Brixen Quartzphyllite. These ages mark cooling below ~100° C.

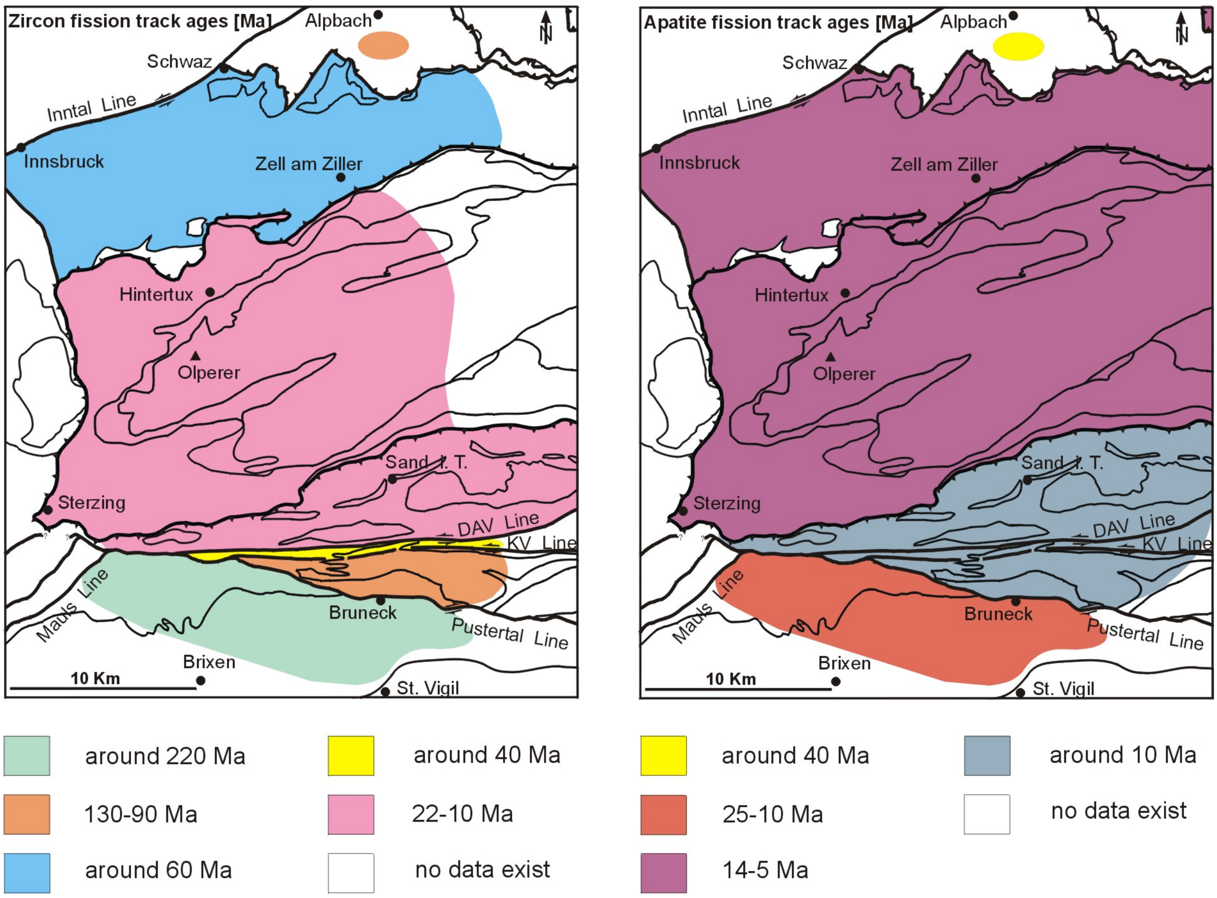

Fig. 4.13: Fission track age distribution maps.

14-5 Ma

These ages can be found in the Austroalpine Innsbruck Quartzphyllite and the Penninic units of the Tauern window. For the Tauern window they show ongoing Miocene cooling. This final cooling below ~100° C occurred contemporaneously with the Innsbruck Quartzphyllite and the Altkristallin south of the Tauern window (see below). An increase of the apatite ages with altitude is observable.

~10 Ma

Such homogeneous ages were obtained in the Austroalpine Altkristallin northern block, intermediate block and southern block. They show that the late cooling history is identical for the three blocks and no more vertical displacement occured along the DAV and KV Line (Fig. 4.14).

Compilation of age data of the Altkristallin south of the Tauern window

Due to the number of age data available for the Austroalpine Altkristallin, it is possible to draw a thermochronological N-S profile. The age distribution along the Transalp-Traverse is shown in Fig. 4.14.

The DAV Line separates the southern block with Variscan mica ages from the northern block with Alpine mica ages. In the area directly north of the DAV Line, a Rb/Sr white mica age of 239 Ma and a K/Ar white mica age of ~100 Ma are reported. These ages possibly indicate a further shear zone in this area, which was active before the DAV Line (Fig. 4.14). Stöckhert (1982) assumed that the location of the DAV Line west of the Tauferer valley was considerably further north, near Uttenheim. This requires a N-S trending dextral fault with an offset of ~2 km, as was subsequently proposed, for example, on the sketch map of Stöckhert et al. (1999). However, evidence from field control is missing due to bad outcrop conditions. The shear zone described by Stöckhert (1982) and Stöckhert et al. (1999) is possibly the suggested older shear zone.

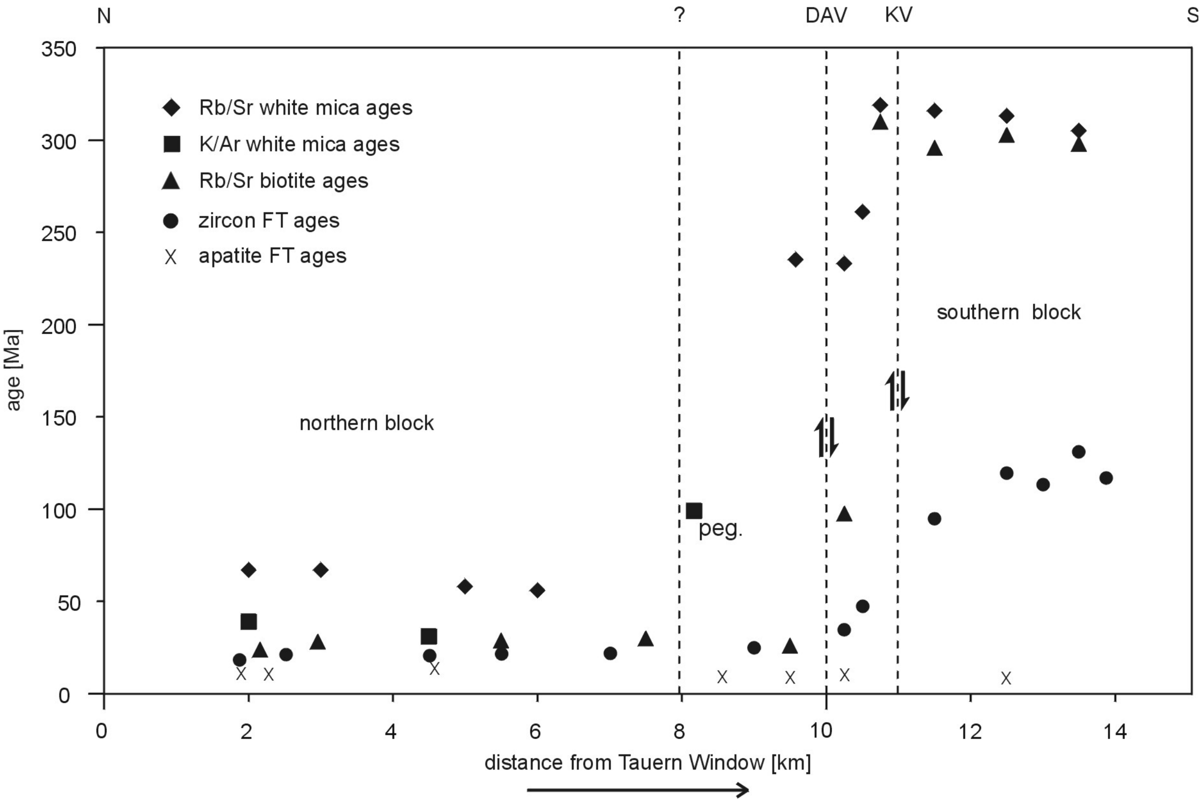

Fig. 4.14: Thermochronological profile of the Austroalpine Altkristallin south of the Tauern window. The compilation of the age data along the Transalp-Traverse is after Borsi et al. (1973), Hammerschmidt (1981), Stöckhert (1984), Grundmann & Morteani (1985), Stöckhert et al. (1999) and this study.

The zircon fission track ages along the Transalp-Traverse increase from 21 Ma to 131 Ma towards the south with clear jumps of the ages by crossing the DAV and KV Line.

In contrast to the zircon fission track ages the apatite fission track ages show a uniform age pattern of 11-9 Ma. The homogeneous ages of the three blocks indicate that, after 10 Ma, the exhumation is only controlled by erosion. Vertical displacements caused by tectonics became negligible.

Stöckhert et al. (1999) suggested a vertical displacement of about 1.5-2 km across the DAV Line around 30 Ma (cf. chapter 4.5.5.2). But this can be only a minimum value. One problem in their estimation is, that they did not consider the whole time of activity of the DAV Line, which lasted longer (cf. chapter 4.5.5.2). Another problem is the horizontal displacement (30 km; Schulz 1989) in addition to the vertical displacement along the DAV Line.

In principle it is possible to calculate the amount of vertical displacement (d) on a fault from the different cooling ages (t_1 and t_2) across the fault (Wagner & Van den Haute 1992). A constant geothermal gradient for both tectonic blocks must be assumed. The amount of vertical displacement can be calculated from the age difference t_2-t_1, the difference between the closure temperature (T_c) and the ambient surface temperature (T_{amb}), and the geothermal gradient according to eq. 4.9

$$d = \frac{(T_c - T_{amb})*(t_2 - t_1)}{\text{geotherm.gradient}*t_2} \qquad (4.9)$$

For the calculation of the displacement the fault has to be obviously younger than the youngest age found on either side (Wagner & Van den haute 1992). The activity of the DAV Line is dated to begin around 30 Ma (Müller et al. 2000) and the youngest zircon ages are 22 Ma (cf. 4.5.3.1 and Fig. 4.14). Therefore this method is not applicable.

The only method to estimate a vertical displacement rate between the two blocks is by treating each block separately. According to Kleinschrodt (1987), Schulz (1988) and Most (1997) vertical displacement along the DAV Line occurred mainly during brittle deformation as indicated by steep dipping slickensides. Out of the fission track data it is possible to calculate the vertical displacement of the low temperature history for the area along the Transalp-Traverse.
In the northern block the zircon fission track ages are around 22 Ma and the apatite ages are around 10 Ma. In the intermediate block, the zircon fission track age is 48 Ma and the apatite fission track age is also 10 Ma. This difference in ages and the difference in closure temperatures (= 125° C) is used to calculate a cooling rate of 10.4° C/Ma for the northern block and 3.3° C/Ma for the intermediate block. Under the assumption of a geothermal gradient of 28° C/km (e.g. Bellieni & Visona 1981) a vertical displacement of ~3 km of the northern block relative to the intermediate block can be estimated for the time between 22 and 10 Ma.

Additionally a vertical displacement of ~2 km of the northern block relative to the intermediate block is also estimated for the time between ~28 Ma (biotite cooling ages) and 22 Ma. Due to the uncertainties of the concept of closure temperatures (cf. chapter 4.4), this can only be a rough estimation.

For the area of the Transalp-Traverse a vertical displacement of ~5 km of the northern block relative to the intermediate block for the time between ~30 Ma and 10 Ma can be assumed. Due to insufficient fission track ages along the whole DAV Line, further conclusions can not be drawn.

5 Fission track length distribution in apatites

5.1 Background

Confined track length measurements in apatite yield track length distributions that can be used, together with the apatite fission track age, to model the cooling history of a rock below ~100° C (e.g. Ketcham et al. 1999).

Confined tracks are fully enclosed in the crystal, and they are etched out via cleavage planes or cracks (track in cleavage, TINCLE) or via surface tracks (track in track, TINT). The criteria for track length measurements are: (1) both ends are defined, sharp and well visible, and (2) the track is at least close to parallel to the surface (± 10 deg is usually considered horizontal; Donelick et al. (1999)).

Annealing experiments (Green et al. 1986, 1989) and track length studies of apatites with different cooling histories have established characteristic track length distributions (Gleadow et al. 1986), which are shown in Fig. 5.1.

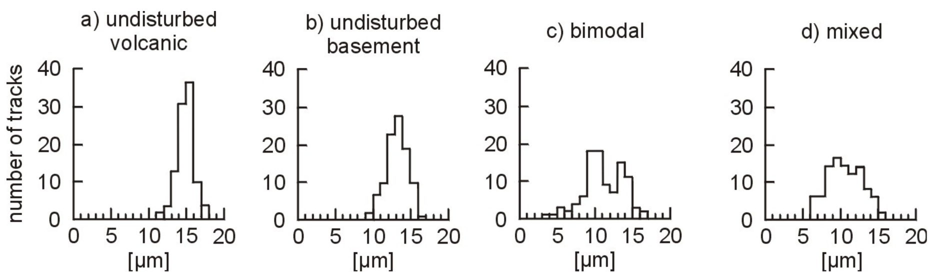

Fig. 5.1: Typical track length distributions of confined tracks in apatite. Diagrams show track length distributions of a) undisturbed volcanic rocks, b) undisturbed basement rocks, c) bimodal and d) mixed distributions after Gleadow et al. (1986).

The mean track length together with the track length distribution of confined tracks can supply information on the temperature history of a sample (Fig. 5.2). It has been qualitatively shown that apatites from undisturbed volcanic rocks and rapid cooled (intrusive) rocks yield long mean track lengths and small standard deviations ranging from 14 to 15 (± 0.8–1.3) µm (Fig. 5.1a). In contrast, apatites from rocks that have cooled slowly will yield shorter mean track lengths and larger standard deviations in the range of 12 to 14 (± 1–2) µm. Also the distribution becomes broader and shows a negative skewness. This is the typical track length distribution of an undisturbed basement (Fig. 5.1b). Reduced lengths indicate that the sample remained for some time in the partial annealing zone. A more complex thermal history with reheating, e.g. magmatic heating or burial, may cause partial annealing of the tracks accumulated before reheating, and a so-called mixed age and mixed track lengths distribution (Fig. 5.1d) are the result. The contribution of small tracks will increase and bimodal distributions can be obtained (Fig. 5.1c).

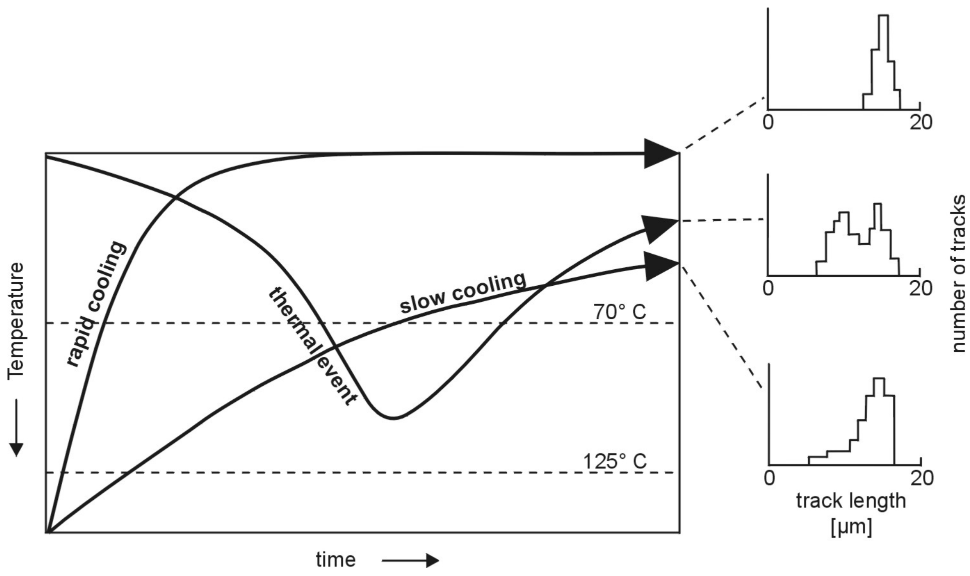

Fig. 5.2: Typical apatite fission track length distributions with different time-temperature paths after Seward (1993).

5.1.1 Analytical methods

Due to their low uranium content confined track length measurements were not possible in all apatite samples. In this case, the probability that the tracks intersect the tracks or cracks which emerge at crystal surface (TINT's and TINCLE's) is so low that a significant number of horizontal confined tracks cannot be revealed by etching. To increase the number of observable confined tracks, it is necessary to create artificially induced host tracks or cracks. For this, three experimental techniques can be applied: (a) irradiation of ^{252}Cf spontaneous fission fragments to the mineral surface, (b) irradiation of heavy ions using an accelerator and (c) artificial fracturing of apatite crystals (for a comparison see Yamada et al. (1998)).

In this study the heavy ion irradiation technique was applied. The apatite grains were embedded in ARALDITE-D epoxy resin on glass slides in vacuum and polished (see 4.5.1). The irradiation with $^{136}Xe^{19+}$ ions (11.4 MeV/nucleon; 2×10^6 ions/cm^2) using a universal linear accelerator was performed by the Gesellschaft für Schwerionenforschung, Darmstadt (Germany). After the irradiation, the mounts were etched in 5.5 Mol HNO_3 for 20 sec at 21° C (Donelick et al. 1999).

The microscope used for the fission track age determinations is equipped with a drawing tube and a digitising tablet which was calibrated to a micrometer scale for length measurements (Dumitru 1993). All length measurements were made on horizontal confined tracks (TINT's and TINCLE's) and were measured under dry conditions at 1000x magnification. Length calibration on a micrometer scale was done several times.

5.1.2 Results

The track length measurements of apatites were carried out on 36 samples and presented in Fig. 5.3 and 5.4.

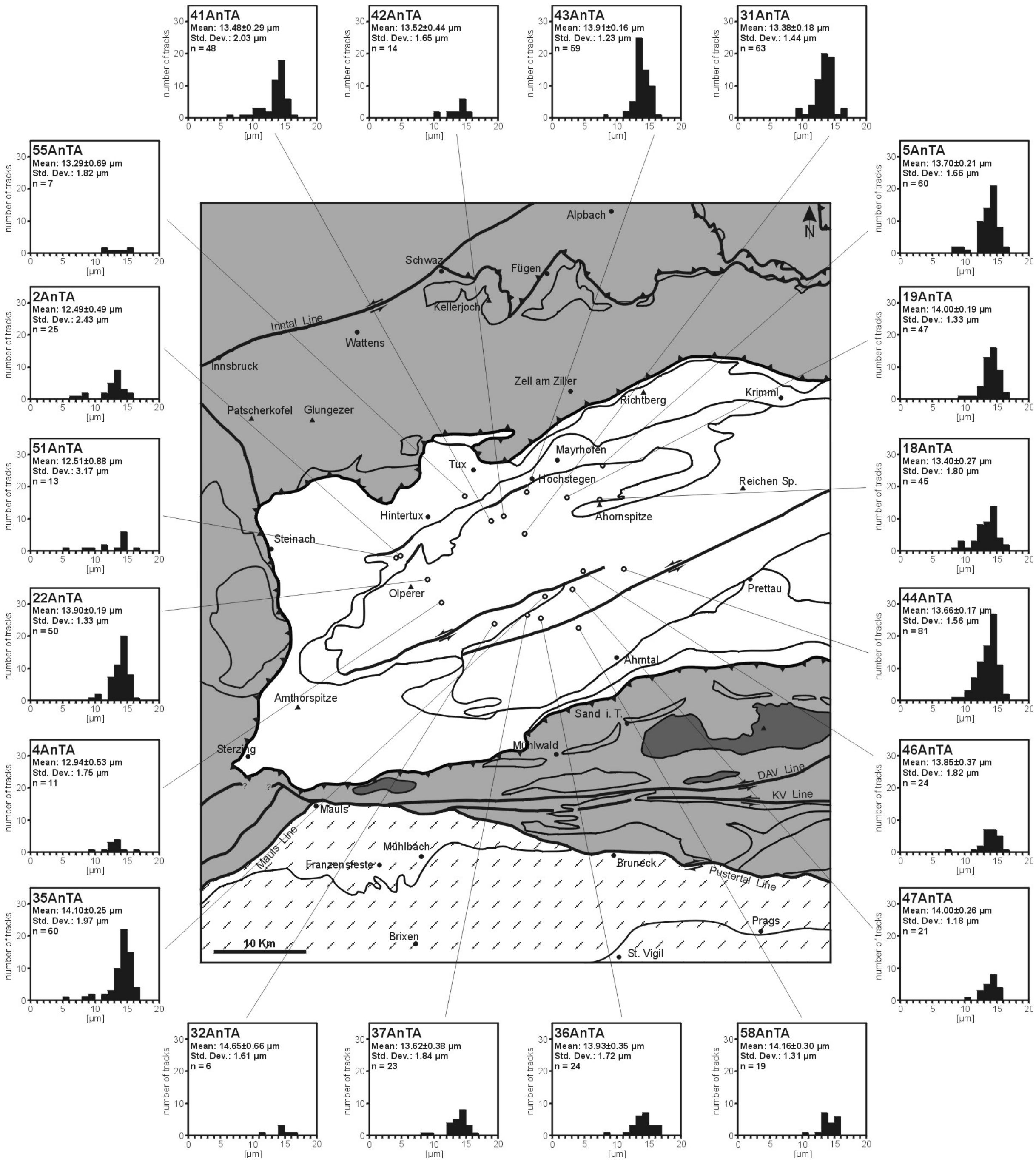

Fig. 5.3: Track length histograms of confined horizontal tracks in apatites from Penninic units.

Penninic units

Most samples of the Zentralgneis yield uniform track length distributions (Fig. 5.3) and the mean track lengths of 12.9 to 13.9 (± 1.2-1.8) µm indicate monotonous slow cooling like the undisturbed basement type of Gleadow et al. (1986). Sample 44AnTA (Fig. 5.3) is a good example for a typical undisturbed basement with a broad distribution of track lengths and a negative skewness. The mean track lengths of >14 µm obtained from some samples of the Zentralgneis and in the Greiner schist belt point to faster cooling through the PAZ. The shortened mean track lengths of 12.5 (± 2.4-3.1) µm in apatite samples of the Kaserer Formation also belongs to the undisturbed basement type but indicate slower cooling as the samples of the Zentralgneis. The only sample (55AnTA) of the Wustkogel Series has a mean track length of 13.3 (± 1.8) µm. Due to the low number of measured confined tracks no further interpretation is possible.

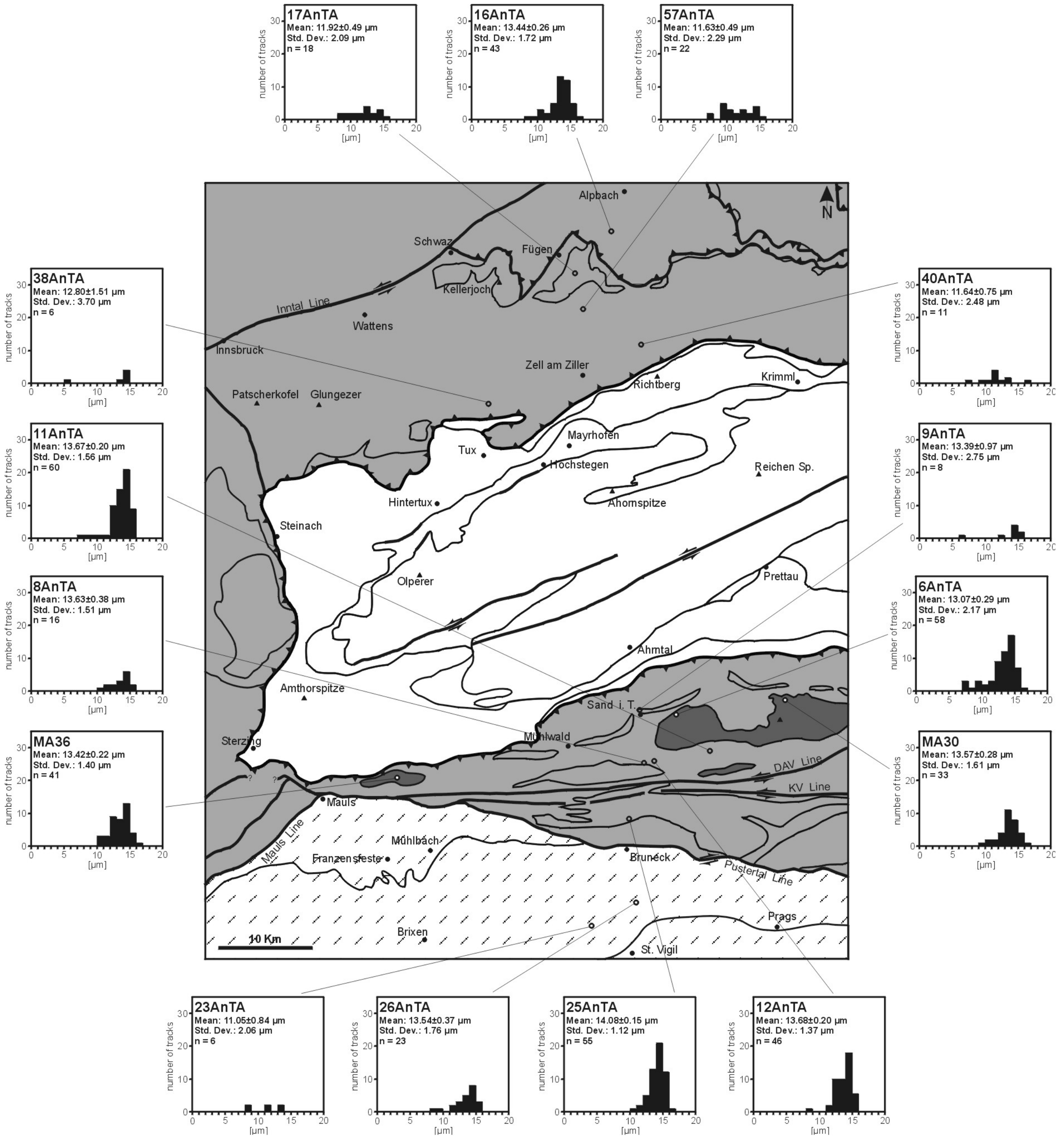

Fig. 5.4: Track length histograms of confined horizontal tracks in apatites from Austroalpine units.

Austroalpine units

The shortest mean track lengths are recorded by samples of the Innsbruck Quartzphyllite and Schwazer Augengneis (Fig. 4.21), whose mean track lengths of 11.6 to 12.8 (± 2.4-3.7) are rather of the mixed type according to Gleadow et al. (1986). However, they are weakly constrained because of the low number of measured confined tracks. Sample 16AnTA of the Northern Greywacke Zone has a mean track length of 13.4 (± 1.7) µm and is a typical example for undisturbed basement distribution and slow cooling. The samples of the Altkristallin south of the Tauern window yield uniform track length distributions (Fig. 5.4) and the mean track lengths of 13.4 to 13.7 (± 1.4-2.7) µm indicate slow and steady cooling. The track length distributions are similar to the undisturbed basement type of Gleadow et al. (1986). One sample (25AnTA) has a mean track length of 14.1 (± 1.4) µm and can be interpreted in terms of faster cooling.

Tertiary intrusives

The mean track length of the Rensen pluton is 13.4 (± 1.4) µm and of the Rieserferner pluton 13.1 to 13.6 (± 1.6-2.2) µm (Fig. 5.4). They are identical with the samples from the Altkristallin and display slow cooling.

Southalpine units

Out of the two samples only one (26AnTA) contains sufficient horizontal confined tracks. The mean track length is 13.5 (± 1.8) µm, and the track length distribution is that of an undisturbed basement (Gleadow et al. 1986). The negative skewness indicates that the sample remained in the partial annealing zone for some time and therefore cooled slowly.

5.2 Chemical composition of apatites

In order to get more information about the annealing behaviour, the chemical composition of apatite (generally written as: $Ca_5(PO_4)_3[F,Cl,OH]$) has to be determined. F, Cl and OH mutually substitute between the end-members fluorapatite, chlorapatite and hydroxyapatite.

Experimental studies showed that the mean track length depends on the chemical composition of the apatite grains. Fission tracks in chlorine-rich apatites are more resistant to annealing than tracks in fluorine-rich apatites (Green et al. 1989, Crowley et al. 1991, Donelick et al. 1999). Thus the annealing properties strongly depend on the Cl/F ratio (Green et al. 1985).

5.2.1 Analytical methods

The electron microprobe analyses of the apatites were performed using wavelength-dispersive methods on a JEOL JXA 8900 Superprobe at the Institute of Geosciences, University of Tübingen (Germany). Analyses were made with an accelerating voltage of 15 kV, a probe current of 20 nA and a beam diameter of 20 µm. A ZAF correction was used for data reduction.

For the calibration of the analysed elements the ASTIMEX standards (fluorite A for F; sanidine for Si; tugtupite for Cl and rhodonite for Mn) and MAC 4570"S" standards (apatite S for P and Ca) were used. The ASTIMEX standard apatite A was not used because of the insufficient information about the element concentrations (Appendix Tab. B1).

5.2.2 Results

To get an overview of the chemical compositions of the dated apatites, 24 apatite mounts derived from different units were analysed. The total sum of the element concentrations is higher than 100 wt% in some analyses. One reason could be that the chemically etched apatite mounts from the fission track age determination were used and their surfaces are not flat and smooth as required for quantitative analysis. Another reason could be that the apatite S standard is insufficiently known and not well chemically analysed. The given element concentrations of the apatite S standard (Appendix Tab. B1) are based on electron microprobe analyses. But element concentrations are calculated from the ratios of specimen and standard intensities and the known concentrations in the standard. Analyses of F and Cl in apatite were also problematic, because F and Cl may diffuse out irregularly under increasing duration of exposure to the electron beam (Stormer et al. 1993).

The analyses of this study yield stoichiometric excess of P, and therefore it seems that the values for P are systematically too high. The cause of this error may be the result of an inaccurate value for P in the used standard. The outcome of this is a low value for Ca.

The measurements are not suitable for quantitative statements but the Cl concentrations between 0.00 and 0.15 and the high F concentrations allow to say that the analysed apatites are near end-member fluorapatites (Appendix Tab. B1), the most common variety of apatite in nature.

5.3 Thermal modelling

5.3.1 Theory

Modelling of the thermal history was carried out with the computer program AFTSolve (version 1.2.2) of Ketcham et al. (2000). The program uses the multi-kinetic annealing model of Ketcham et al. (1999) as a default, but also implements the mono-kinetic models of Laslett et al. (1987) and Crowley et al. (1991) for Durango apatite, and of Crowley et al. (1991) for fluorapatite. Input parameters are the apparent apatite fission track age, the fission track length distribution and additionally the chlorine content of the apatites. Time-temperature constraints, such as geochronological data of other minerals (e.g., zircon fission track age) are considered.

The program uses a Monte Carlo algorithm to simulate a best fit thermal evolution path for an apatite sample with known apparent age and track length distribution. The operator can determine the number of simulation runs, and the modelled output parameters are compared to the input parameters. Two statistics are used to evaluate how well the data and the model results fit. The Kolmogorov-Smirnov test ("K-S Test") is used to compare the measured fission track length distribution to the track length distribution predicted by the model. The "Age GOF" is the goodness-of-fit between the age data and the age predicted by the model. For each of these statistics, a "good" result corresponds to a value of 0.50 or higher, which is the expected value if the time-temperature path and kinetic model are in fact the correct ones. The program provides a graphic display of the modelling results showing the best fit evolution trend (= solid line) and statistically acceptable limits (dark grey: better fit; light grey: acceptable fit). In order to constrain the significance of the model results other geological data like metamorphic events are necessary to decide which thermal history fits best the geological situation of the region.

The use of mono-kinetic models implicitly assumes that the studied apatites have the same kinetic behaviour as the apatite the model is based on, which is rarely the case, especially when a model based on the Durango apatite (Laslett et al. 1987) is employed (Ketcham et al. 1999). In this study the model of Crowley et al. (1991) for fluorapatite is used due to the chemical composition of the analysed apatites. The input parameters for the time-temperature calculations are the zircon and apatite fission track ages and the corresponding temperature intervals. In case of zircon the closure temperature of 225 ± 25° C for fast cooling or 240 ± 50° C for slower cooling and for the apatites the partial annealing zone (70-125° C) were chosen for the temperature ranges. The vertical bold lines represent these temperature intervals. A present day temperature of 20° C was assumed by the model. The modelled thermal history of the samples is based on 50000 simulation runs.

The track length measurements of apatites were carried out on 36 samples but only 25 samples were suitable for thermal modelling, because for statistical reasons it needs more than 20 track length measurements.

The thermal histories calculated for the apatite samples show different trends and reflect regional variations in the rate of cooling. In nearly all modelled time-temperature histories the "K-S Test" and the "Age GOF" have a value above 0.50 (mostly above 0.90). This shows the good agreement between the observed and modelled data.

5.3.2 Results

Penninic units

The best fit model suggests a similar time-temperature evolution for all samples of the Zentralgneis (Fig. 5.5a-m). The characteristic time-temperature path first indicates slow cooling, followed by rapid cooling. After entering the apatite PAZ the samples from the Ahornspitze area (Fig. 5.5a-f) show relatively uniform and continuous cooling up to the present at average cooling rates between ~10 and 22° C/Ma with no indication of prolonged residence in the PAZ. This result is in good agreement with the track length distributions of the samples. The highest average cooling rates were obtained from the valley samples. Only for sample 31AnTA (Fig. 5.5d) the model suggests that the sample remained for some time (~4 Ma) at a temperature of around 90° C in the PAZ

before final cooling. Sample 22AnTA (Fig. 5.5g) from the Olperer area shows also continuous cooling from a temperature of 115° C to the present at an average cooling rate of 10° C/Ma. Such time-temperature paths were also calculated for the area of the Zillertaler Hauptkamm (Fig. 5.5h-m) where average cooling rates of ~10-13° C/Ma are obtained.
The time-temperature history of sample 35AnTA (Fig. 5.5n) of the Greiner schist belt is similar to the samples of the Zentralgneis. First there is slow cooling between 14 Ma and 10 Ma followed by rapid cooling to 125° C at ~9 Ma, which slows down to the present. The average cooling rate of 12° C/Ma for the time between 9 Ma and present is nearby identical with those of the Zentralgneis of the same altitude.

In contrast sample 2AnTA (Kaserer Formation) shows another cooling history. The modelled time-temperature path (Fig. 5.5o) indicates first rather rapid cooling to 125°C, followed by very slow cooling until the final faster cooling which starts at ~3 Ma. The average cooling rate for the time between 13 Ma and present is ~8° C/Ma. Some shortened tracks (see histogram) indicate that the sample stayed for some time in the PAZ.

Austroalpine units

The modelled time-temperature path for sample 16AnTA (Fig. 5.5p) of the Northern Greywacke Zone indicates very slow cooling for the time between 118 Ma and 58 Ma. This time span is followed by faster cooling through the apatite PAZ. The final cooling history, which starts around 30 Ma, is characterised by a more or less slow cooling with an average cooling rate of ~3° C/Ma.

The samples of the Schwazer Augengneis (Fig. 5.5q) and Innsbruck Quartzphyllite (Fig. 5.5r) yield similar time-temperature paths. The model suggests for both samples slow cooling for the time between 58 Ma and entering the apatite PAZ (~12 Ma). The samples remained for some time at the same temperature in the PAZ before the final faster cooling. This is also indicated by the mixed type track length distribution and the shortened mean track lengths around 12 µm, but the number of counted tracks are too low for a clear statement. The average cooling rates for the time between entering the PAZ and the present are 7° C/Ma and 9° C/Ma, respectively.

The best fit model for the three samples of the Altkristallin south of the Tauern window shows two different time-temperature paths. For the two samples of the northern block (Fig. 5.5s-t) the model suggests for the temperature between ~230° C and 125° C at first slow cooling followed by faster cooling. For the same temperature range the model suggest for sample 25AnTA (Fig. 5.5u) from the southern block continuous slow cooling. The reason is the older zircon fission track age of 122 Ma and the resulting longer time span. After cooling below 125° C, the three samples underwent the same history. They cooled continuously during passing the apatite PAZ followed by more rapid cooling during final exhumation. They have an average cooling rate of ~10° C/Ma since 10 Ma.

Tertiary intrusives

The two samples of the Rieserferner pluton (Fig. 5.5v-w) and sample MA36 (Fig. 5.5x) of the Rensen pluton have similar thermal histories as the Altkristallin north of the DAV Line (Fig. 5.5s-t). Monotonic slow cooling in Early to Middle Miocene time is followed by faster cooling in the Late Miocene. After entering the PAZ at 120° C the time-temperature paths shows uniform cooling to the present at an average cooling rate of ~10° C/Ma with no indication of a prolonged stay in the PAZ. This result is in good agreement with the track length distributions of the samples.

Southalpine units

For sample 26AnTA (Fig. 5.5y) the model suggests very slow cooling for the time from 209 Ma to 66 Ma. But this time-temperature path is only a rough estimation due to the lack on further information (e.g., zircon track lengths distributions). At ~16 Ma the sample enters the apatite PAZ and cooled below 125° C. Final cooling occurred at an average cooling rate of 6° C/Ma.

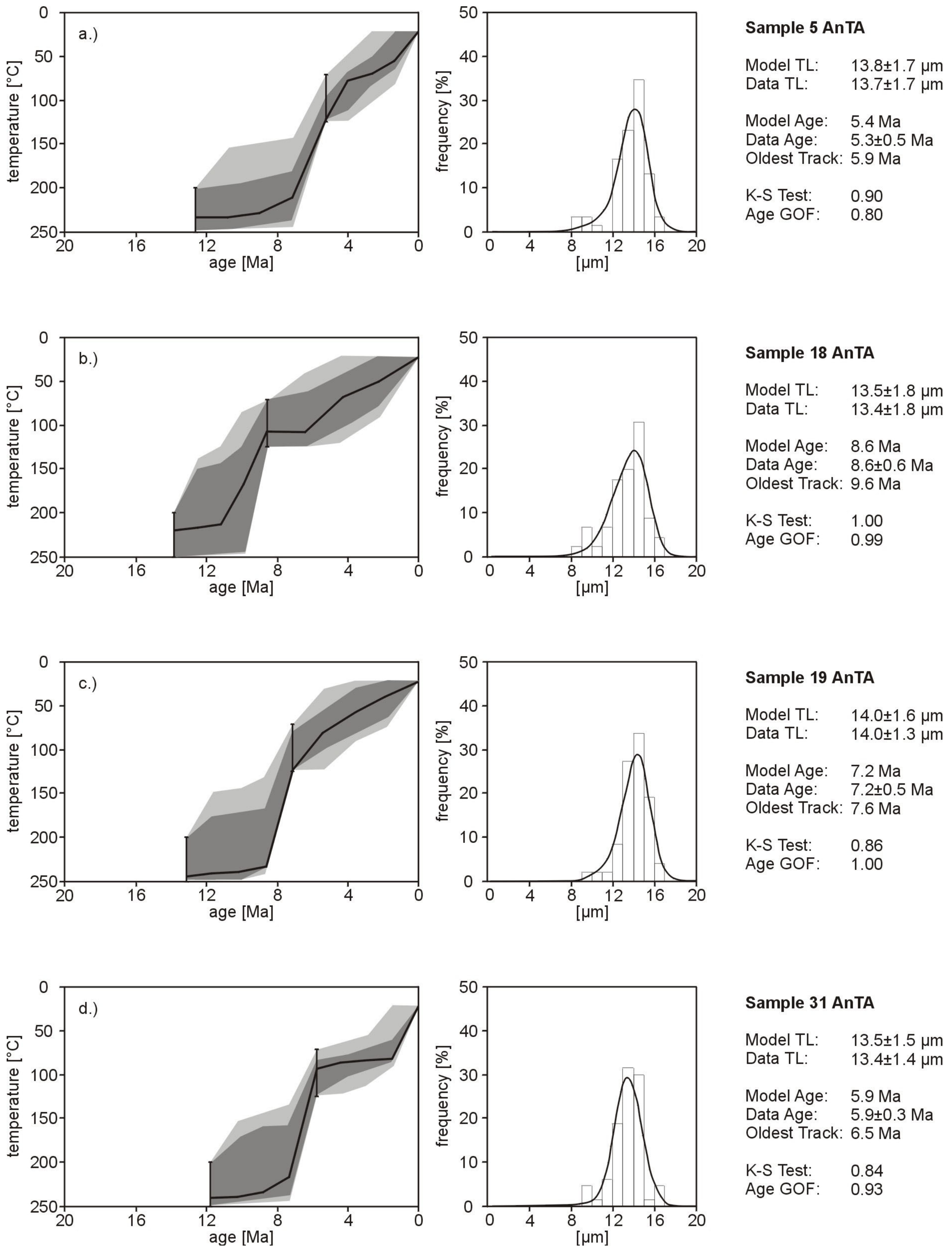

Fig. 5.5a-d: Modelled time-temperature paths and fission track length distributions (normalized to n = 100).

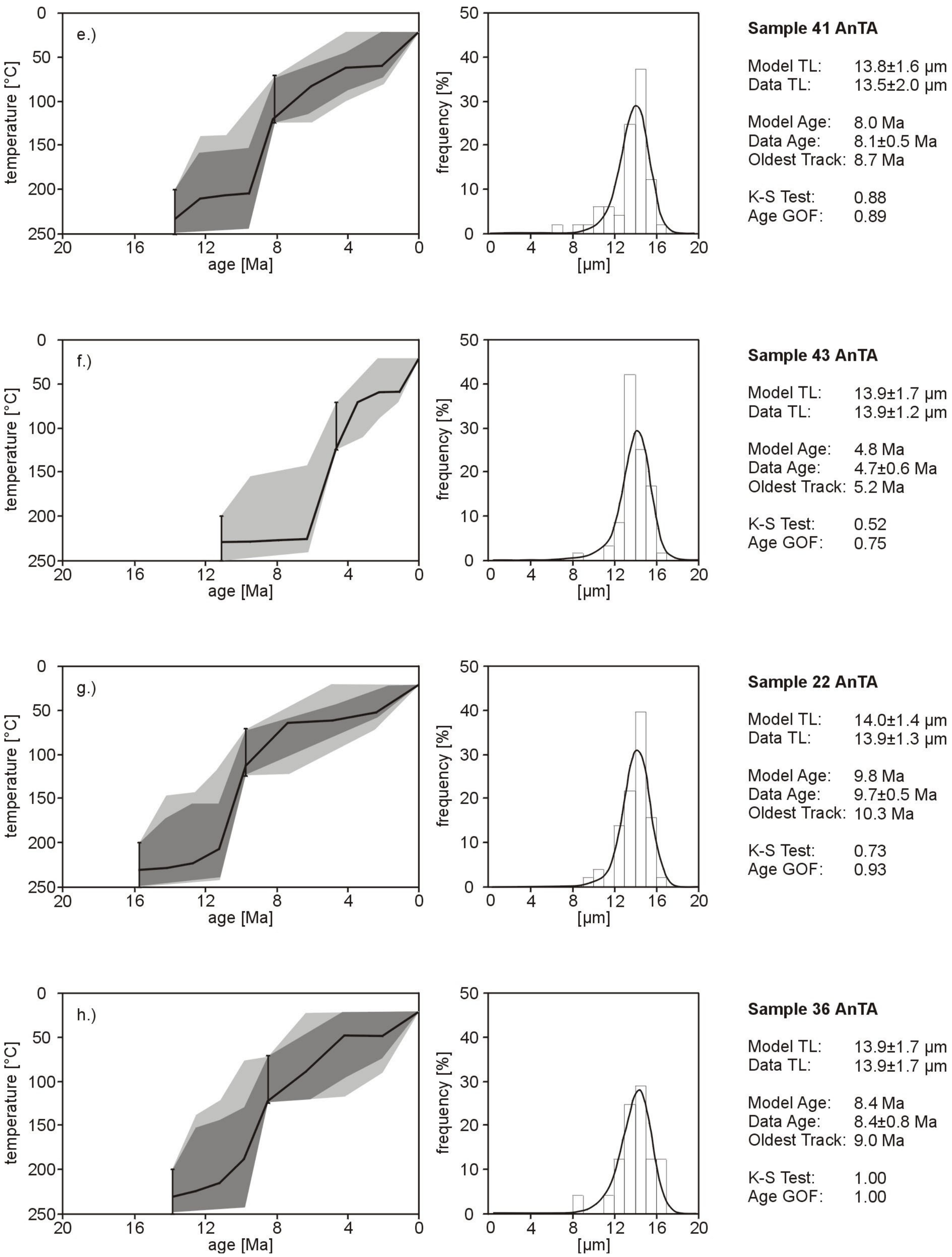

Fig. 5.5e-h: Modelled time-temperature paths and fission track length distributions (normalized to n = 100).

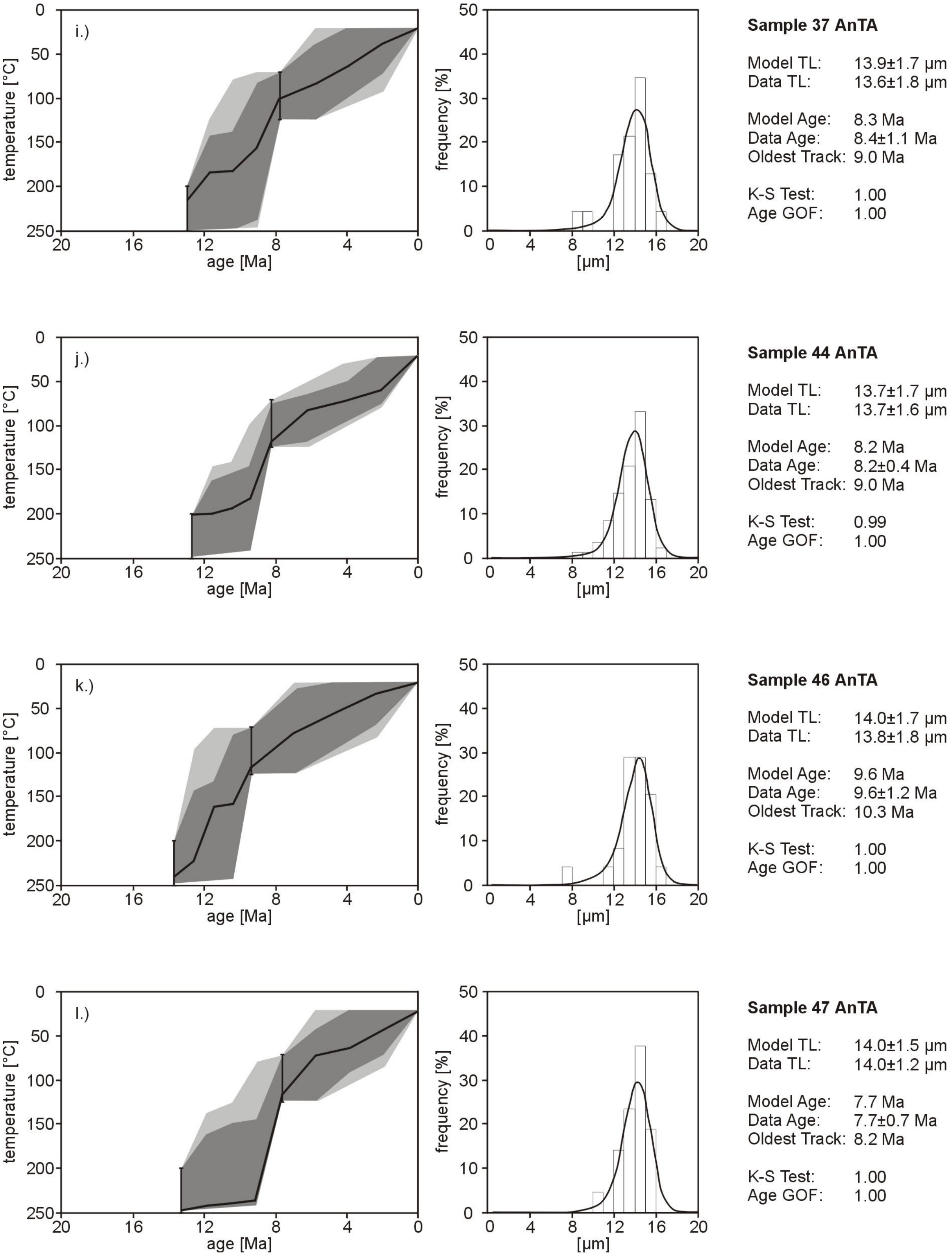

Fig. 5.5i-l: Modelled time-temperature paths and fission track length distributions (normalized to n = 100).

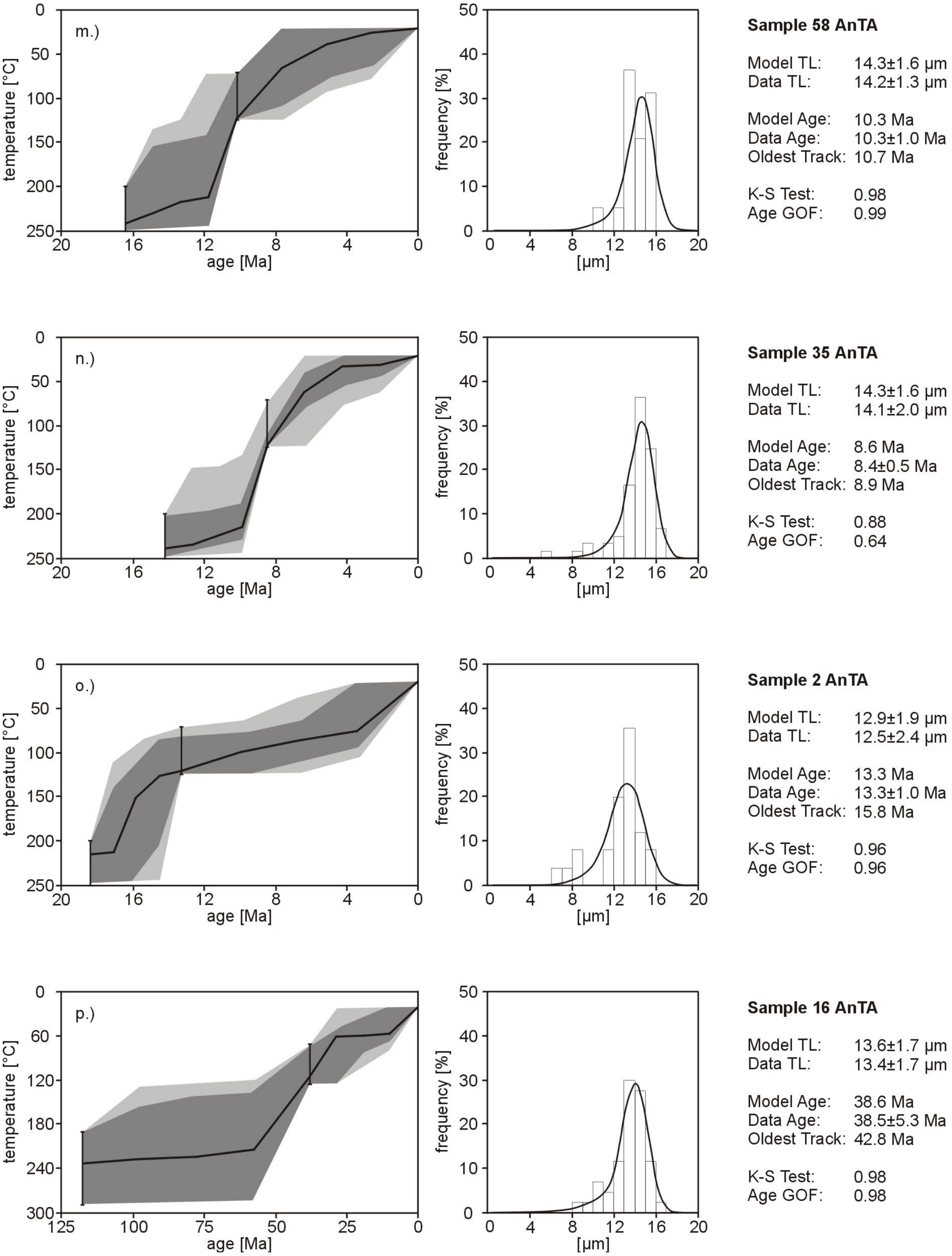

Fig. 5.5m-p: Modelled time-temperature paths and fission track length distributions (normalized to n = 100).

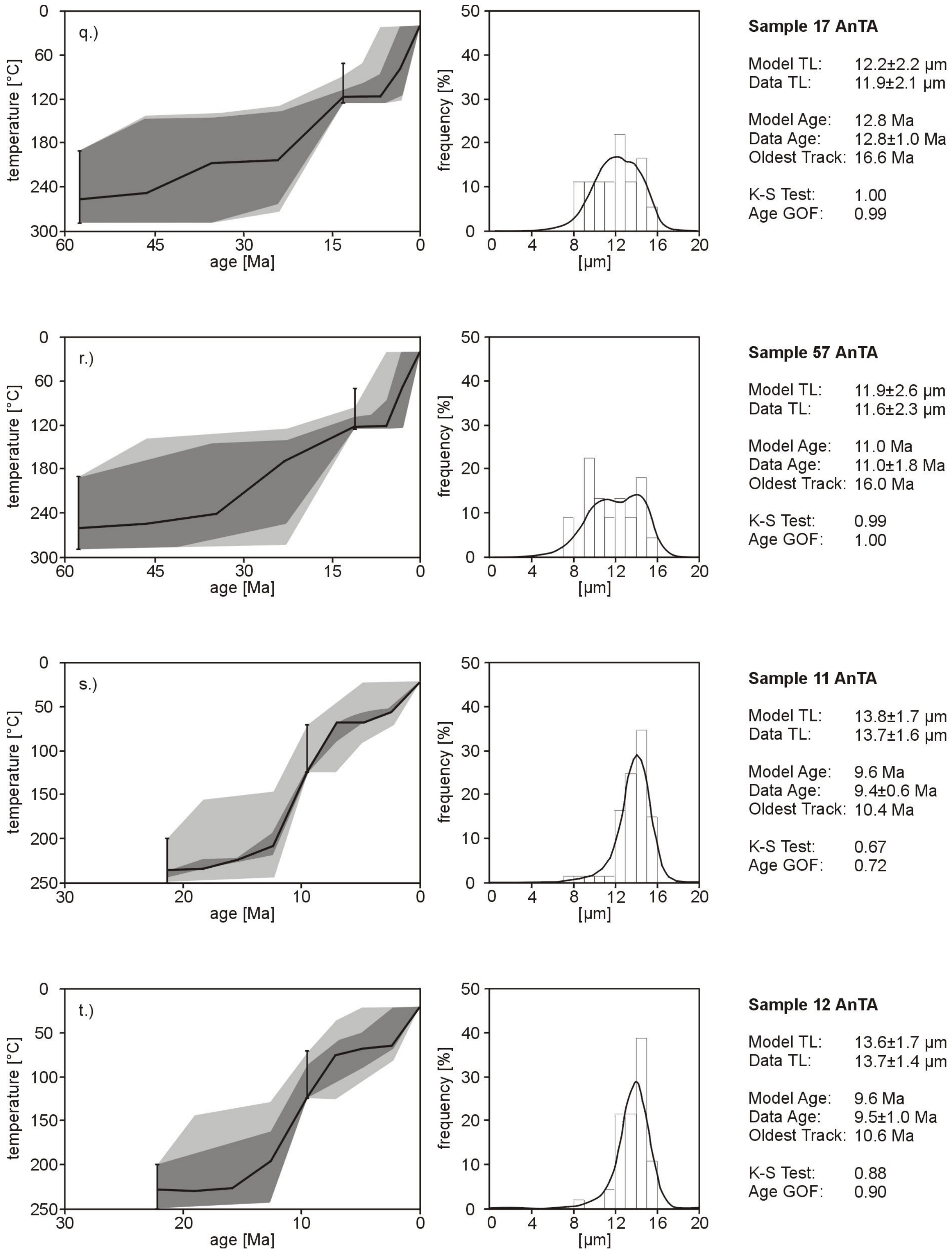

Fig. 5.5q-t: Modelled time-temperature paths and fission track length distributions (normalized to n = 100).

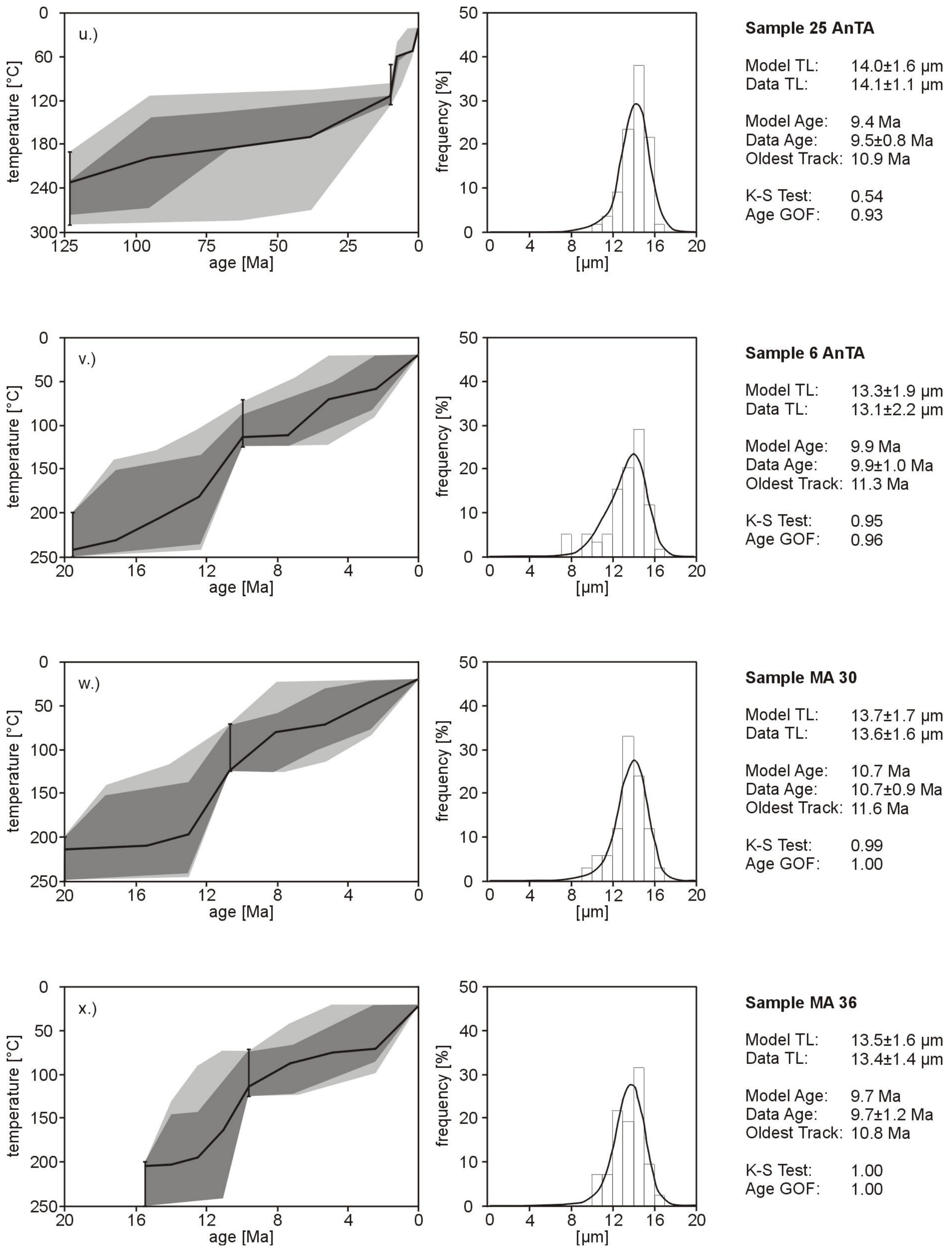

Fig. 5.5u-x: Modelled time-temperature paths and fission track length distributions (normalized to n = 100).

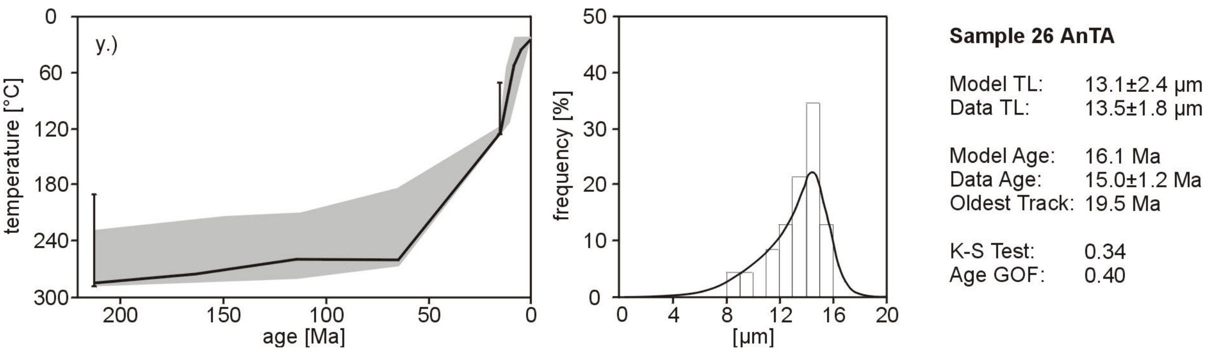

Fig. 5.5y: Modelled time-temperature paths and fission track length distributions (normalized to n = 100).

6 Exhumation and cooling histories

The terms uplift and exhumation are often used in an unprecise manner. Therefore it is necessary to define the usage of these terms. In this study the definitions of England & Molnar (1990) are used.

1) Surface uplift: Displacement of Earth`s surface with respect to the geoid.
2) Uplift of rocks: Displacement of rocks with respect to the geoid.
3) Exhumation: Displacement of rocks with respect to the surface. The rate of exhumation is simply the rate of erosion or the rate of removal of overburden by tectonic processes.

Often the terms uplift or uplift rate are regarded to be identical to the term exhumation rate by numerous authors. Critical reading of papers dealing with this definition is mandatory.

Based on the concept of closure temperatures (Dodson 1973) geochronological data can provide information on the cooling history of rocks. For the calculation of exhumation rates from the cooling history several assumptions should be fulfilled. The critical isotherms must have been horizontal and must remain at a constant depth with respect to the surface, and the uplift rate must be equal to the rate of erosion (Parrish 1983).

Exhumation rates can be calculated in two different ways:

- The mineral pair method (Wagner et al. 1977) using different blocking temperatures of two minerals or isotope systems in the same sample. The exhumation rate is calculated from

  $$\text{exhumation rate} = \Delta z/\Delta t$$

  where:
  $$\Delta z = \text{depth}_{\text{blocking temperature1}} - \text{depth}_{\text{blocking temperature2}}$$
  $$\Delta t = \text{time}_{\text{blocking temperature1}} - \text{time}_{\text{blocking temperature2}}$$

  under the assumption of a static and constant geothermal gradient.

- The altitude dependence method (Fitzgerald & Gleadow 1988) using the same dating method (e.g. apatite or zircon fission track dating) in two rock samples from different altitudes. One advantage of this method is that it does not require the knowledge of the geothermal gradient and the closure temperature. The exhumation rate is calculated directly from the slope of age-altitude profiles according to

  $$\text{exhumation rate} = \Delta z/\Delta t$$

  where:
  Δz = known vertical distance between the two samples in m
  Δt = differences in age of the two samples

under the assumption that the two samples have undergone the same tectonic and thermal history. Stüwe et al. (1994) showed that exhumation rates calculated from apatite fission track ages could be too high because of topographic effects, but this is mainly valid for fast exhumation in the order of >1 mm/a.

For the western Tauern Window both methods of calculating exhumation rates have been used in the past. Blanckenburg et al. (1989) used the mineral pair method and calculated continuously decreasing rates of exhumation from 3.6 to 0.1 mm/a for the time between 20 Ma and present (Fig. 6.1). They place cooling ages at their corresponding closure temperatures on the pressure-temperature path determined by Selverstone et al. (1984). Grundmann & Morteani (1985) calculated an exhumation rate of 0.5 mm/a for the time between 10 and 5 Ma by using the altitude dependence method. The exhumation rates calculated by Grundmann & Morteani (1985) and Blanckenburg et al. (1989) for the last stages of cooling differ. It seems that is not possible to convert cooling paths, estimated from geochronological data, directly into exhumation histories.

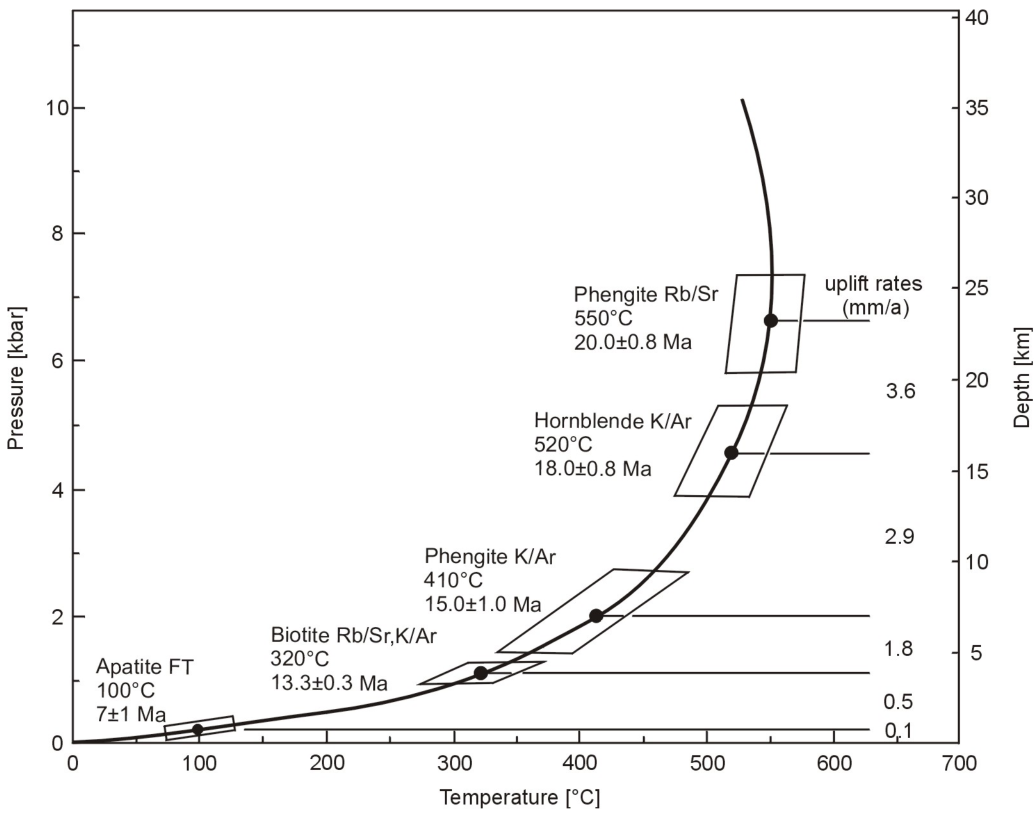

Fig. 6.1: P-T-t path for the western Tauern Window from Blanckenburg et al. (1989).

One problem of the mineral pair method is the validity of the fixation of the closure temperatures (e.g., exactly 300° C for the biotite Rb/Sr system). The main problem arises from the fact, that the development of the geothermal gradient during cooling is based on assumptions. A common practice is to assume some estimated static and constant geothermal gradient (e.g. 30° C/km). The calculated exhumation rate is clearly dependent on this assumed value (Mancktelow & Grasemann 1997).

A more realistic solution includes heat advection and the time-dependent progressive increase of the geothermal gradient. The latter can be modelled with the program EXHUME. This program for 1-dimensional, semi-analytical modelling of geotherms and cooling histories during exhumation is developed by Mancktelow (1998).

With this program Fügenschuh (1995) modelled a P-T-t path for the western Tauern window by using the exhumation rates and mineral ages (cf. Fig. 6.1) as proposed in Blanckenburg et al. (1989). The zircon fission track age is from Fügenschuh (1995). Predicted temperatures for the first three time points (Rb/Sr phengite, K/Ar hornblende, K/Ar phengite) are in good agreement with the suggested closure temperatures. No satisfactory fit of the Rb/Sr biotite and the zircon and apatite fission track ages with the lower temperature part of the modelled P-T-t path could be found. The closure temperatures predicted by the model are significantly too low (Fig 6.2).

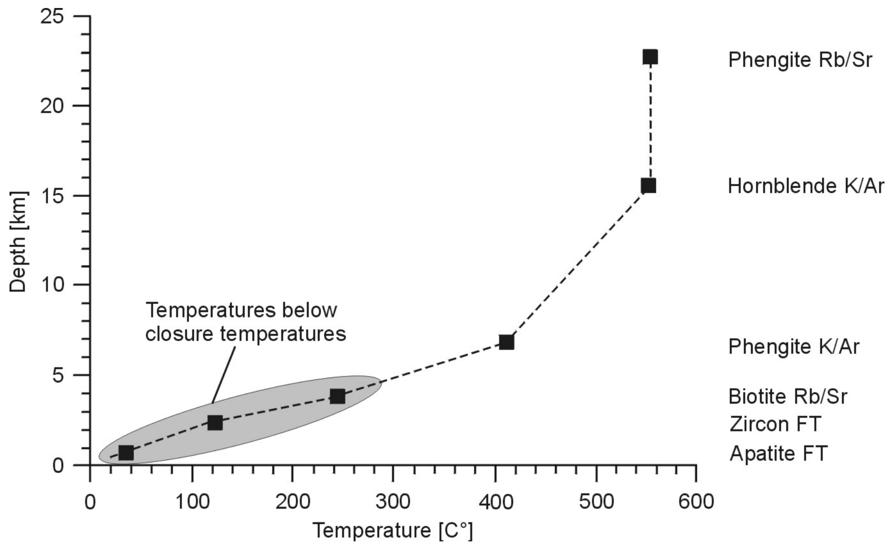

Fig. 6.2: Modelled P-T-t path from Fügenschuh (1995) of the western Tauern window according to mineral ages and exhumation rates as proposed in Blanckenburg et al. (1989). Zircon fission track age from Fügenschuh (1995).

Fügenschuh (1995) presented also a modified P-T-t path. A short period (1.7 Ma) of almost no exhumation at 15 Ma would allow the Rb/Sr biotite point to fall into the right temperature interval at around 300° C. Also the zircon fission track age plots around 200° C, but the proposed temperature for the apatite point is too high.

The program EXHUME was also used in this study to model some P-T-t paths. But for the low temperature part of the P-T-t paths it was not possible to achieve satisfactory results and geological meaningful solutions (Fig. 6.4). The proposed temperatures for the zircon and apatite points are always too high. Therefore the results of the modelling should not be overinterpreted. One problem is, that an initial geotherm must always be input to start the modelling and the constraints on this geotherm are usually poor (Mancktelow 1998). For the modelling a geothermal gradient of 24° C/km is used. The same value is proposed by Blanckenburg et al. (1989).

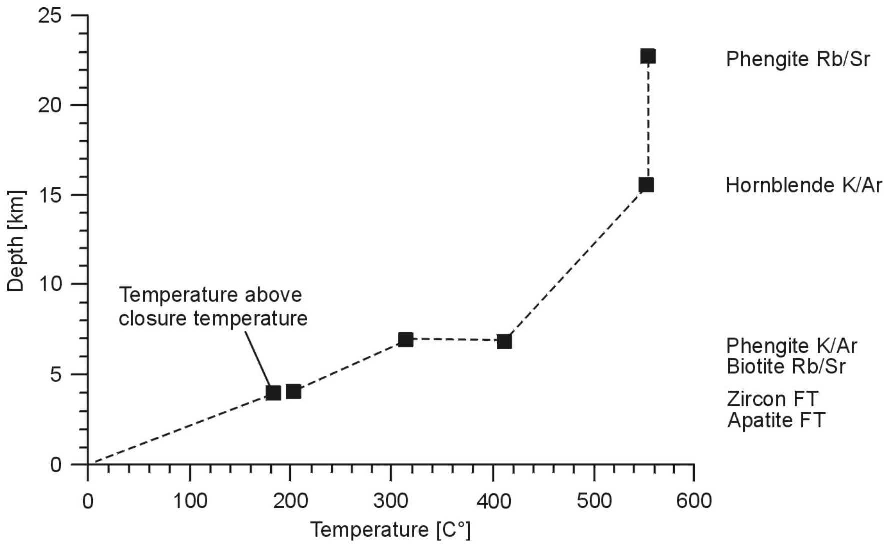

Fig. 6.3: Modified P-T-t path (cf. Fig. 6.2) of the western Tauern window after Fügenschuh (1995).

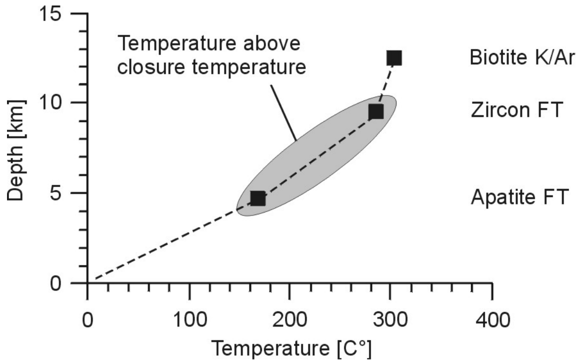

Fig. 6.4: Modelled P-T-t path of sample 18AnTA (Ahornspitze profile; cf. Fig. 6.6). Used parameters: surface temperature of 0° C; depth to base of lithosphere of 100 km; temperature at base of lithosphere at 1300° C; thermal diffusivity of $1x10^{-6}$ m^2/s; surface volumetric heat production of $2.2x10^{-6}$ W/m^3; depth at which heat production drops to 1/e of 30 km; heat capacity of 1100 J/kg/° C; density of 2800 kg/m^3.

According to the uncertainties of the EXHUME program described above, it is clear that exhumation rates calculated by the altitude dependence method would provide more realistic values. Because this method does not require the knowledge of the geothermal gradient and the closure temperature.

Due to the high topographic relief in the Zillertaler Alps it was possible to calculate some exhumation rates with the altitude dependence method. Fig. 6.5 shows the location and the results of the two profiles. Both are located in the Zentralgneis. For the time between 14 Ma and 12 Ma an exhumation rate of 1.1 mm/a (Ahornspitze) and 1.2 mm/a (Grinbergspitze) was calculated. The exhumation rate decreases to 0.6 mm/a for the time interval of 9-5 Ma. These rates are similar to those obtained by Grundmann & Morteani (1985).

Both erosion and surface topography cause a time-dependent variation in isotherm geometry that can result in significant errors in calculating exhumation rates from geochronological data (Stüwe et al. 1994; Mancktelow & Grasemann 1997). Closure of the apatite fission track system occurs at depths where isotherms may be perturbed by topographic effects. The isotherms will be elevated under ridges and depressed under valleys (Stüwe et al.

1994). The question is how far the isotherms can rise into the ridges. The critical parameters are the topographic wavelength and amplitude. Mancktelow & Grasemann (1997) presented analytical solutions and numerical models and drew the following conclusions. With a topographic wavelength < 6000 m, a relief of ~3000 m and exhumation rates in the order of 1 mm/a, the lateral cooling effect of the steep V-shaped valleys is too large to allow isotherms of ≥ 100° C to rise into the ridges. With increasing wavelengths and the same vertical relief, valleys become more open and the slopes shallower, and the 100° C isotherm can rise into the ridges. The result is an overestimation of the calculated exhumation rates.

For the two profiles the maximum topographic wavelength is 7000 m, the relief is 2000 m and the calculated exhumation rate is 0.6 mm/a. According to Mancktelow & Grasemann (1997) the error which results from using the altitude dependence method to calculate exhumation rates is geologically insignificant in these cases.

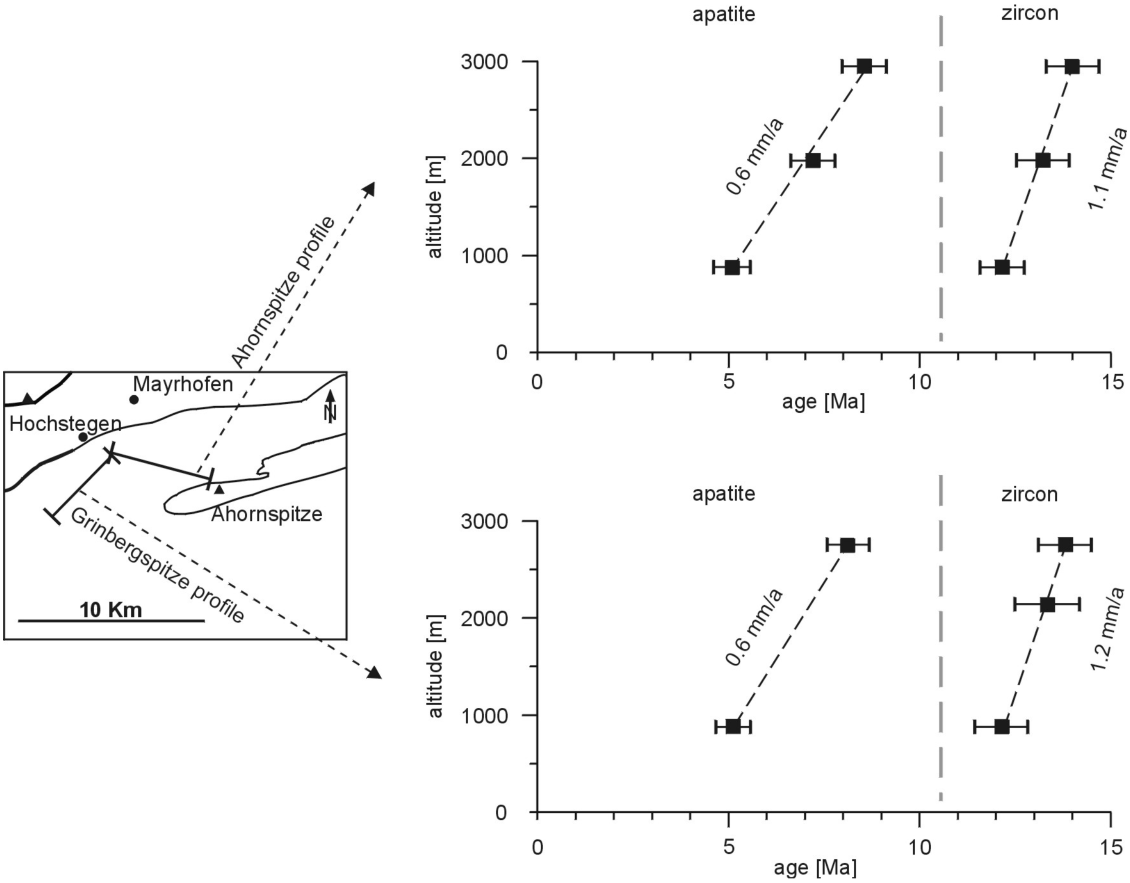

Fig. 6.5: Exhumation rates calculated with the altitude dependence method.

Three time-temperature paths of the Ahornspitze are presented in Fig. 6.6. It comes out that there is continuous cooling during the Miocene but with differences in each time-temperature path. The cooling rate for sample 18AnTa (top) is first ~25° C/Ma and then ~23° C/Ma, for sample 19AnTA (middle) ~21° C/Ma and for sample 18AnTA (valley) first ~16° C/Ma and then ~18° C/Ma. The data shows a change of higher cooling rates at the top to lower cooling rates in the valley.

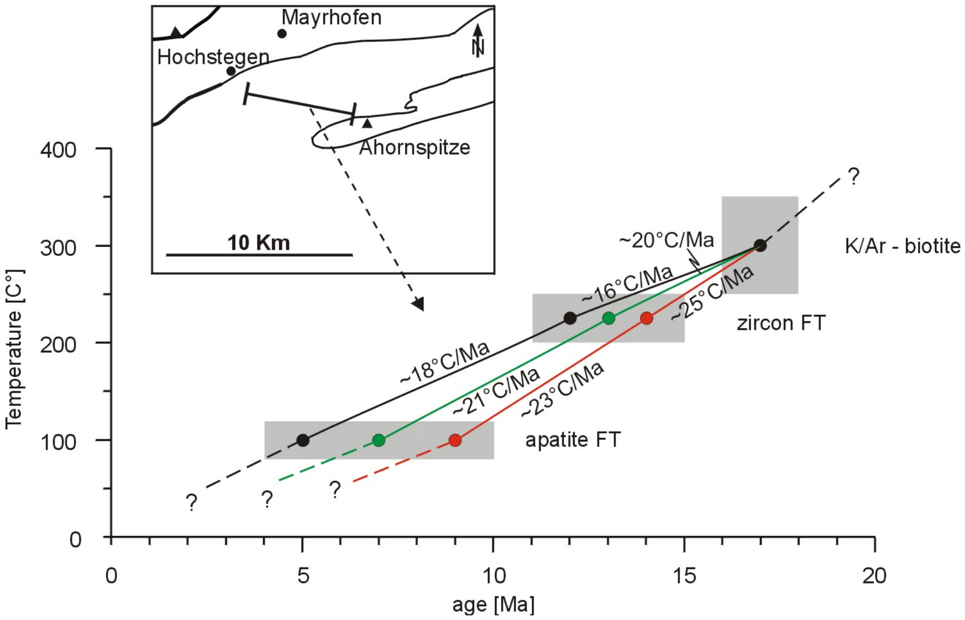

Fig. 6.6: T-t paths of sample 18AnTA (top = red), 19AnTA (middle = green) and 20AnTA (valley = black).

For the Austroalpine units it was not possible to calculate any exhumation rates with the altitude dependence method. Due to the smooth relief of the Innsbruck Quartzphyllite area, only a rough estimation of the exhumation rate (~0.2 mm/a in average) is possible. No correlation between age and altitude is observed in the Altkristallin. But the time-temperature paths of the Altkristallin (Fig. 6.7 and 6.8) point out the differences in the cooling histories of the southern and northern block.

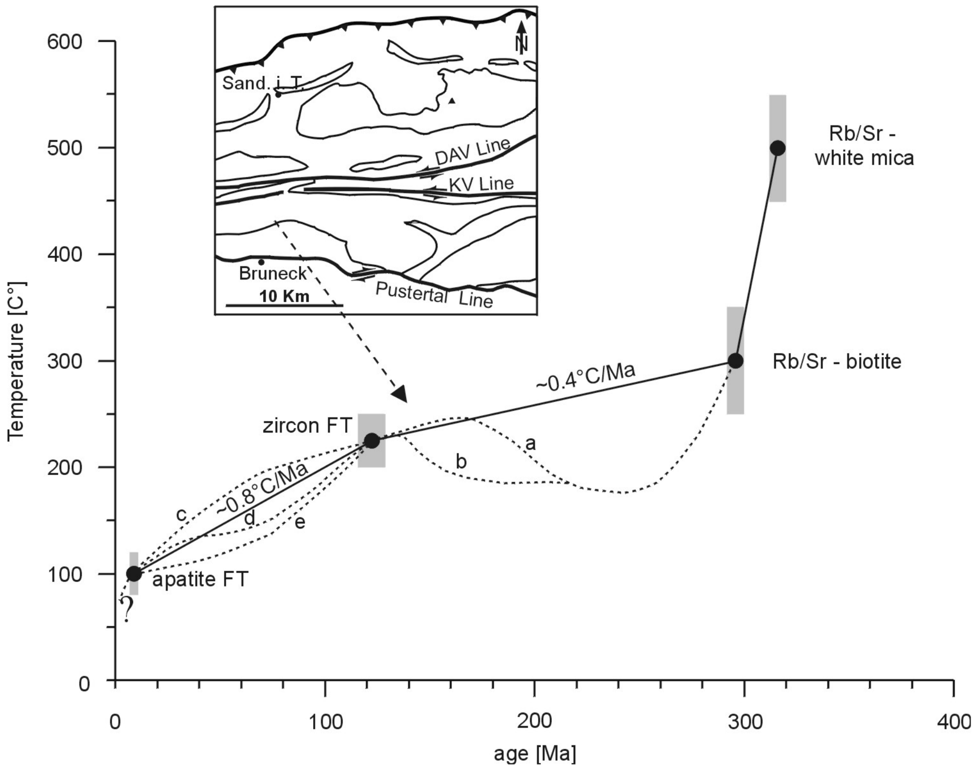

Fig. 6.7: T-t path of the Austroalpine Altkristallin southern block. Mica ages are from Borsi et al. (1973). Geologically more realistic solutions are represented by the dashed lines a-e).

The time-temperature path (black line) of the southern block (Fig. 6.7) indicates fast Variscan cooling, followed by a period of very slow cooling with an average cooling rate of 0.4° C/Ma and increased Alpine cooling with an average cooling rate of 0.8° C/Ma. The black line marks the cooling path if continuous linear cooling between the figure points is assumed. But it is unrealistic to believe that over a period of ~170 Ma nothing should be happen. More realistic cooling paths are suggested by the dashed lines (Fig. 6.7a-e). Cooling path a) suggests post-Variscan cooling and reheating due to rifting of the Penninic ocean in Jurassic time (cf. Dunkl et al. 1999). Whereas cooling path b) takes the reheating due to an Early Alpine metamorphic event in Cretaceous time into account. The cooling paths c-e) show some possible variations in the cooling history of the last 100 Ma. However, the data is not sufficient to provide a final solution. Additional informations like zircon track lengths measurements are required.

The time-temperature path of the northern block (Fig. 6.8) indicates at first slow cooling during the Early Tertiary (average cooling rate of ~6° C/Ma) and faster cooling from the Oligocene/Miocene boundary on (average cooling rate of ~14° C/Ma). The dashed line marks the time-temperature path, when the closure temperatures of 410° C (K/Ar) and 550° C (Rb/Sr) for phengites suggested by Blanckenburg et al. (1989) are used.

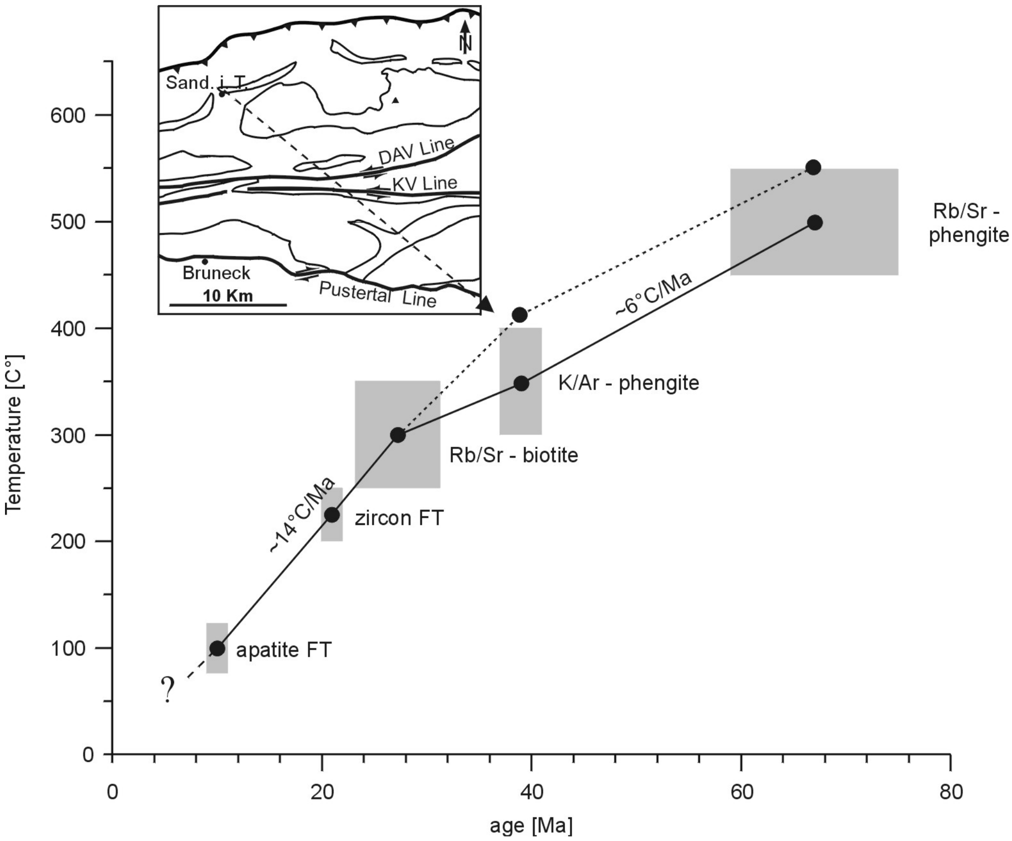

Fig. 6.8: T-t path of the Austroalpine Altkristallin northern block. Rb/Sr data are from Borsi et al. (1973). The dashed line marks the time-temperature path, when the closure temperatures for phengites suggested by Blanckenburg et al. (1989) are used.

7 Fission track age tomography

A new type of visualisation and evaluation of fission track ages was performed, the fission track age tomography. Therefore along a profile between Hochstegen and Sand in Taufers all new zircon and apatite fission track ages obtained inside the western Tauern window were projected into this vertical profile. The vertical distance of the sample localities exceeds 2500m. Also the profile was chosen to be perpendicular to the main WSW-ENE structures of the western Tauern window (e.g. Frisch 1977; Lammerer 1988) and close to the Transalp-Traverse (cf. Fig. 2.1). Age isolines were computed using the Kriging method (Fig. 7.1).

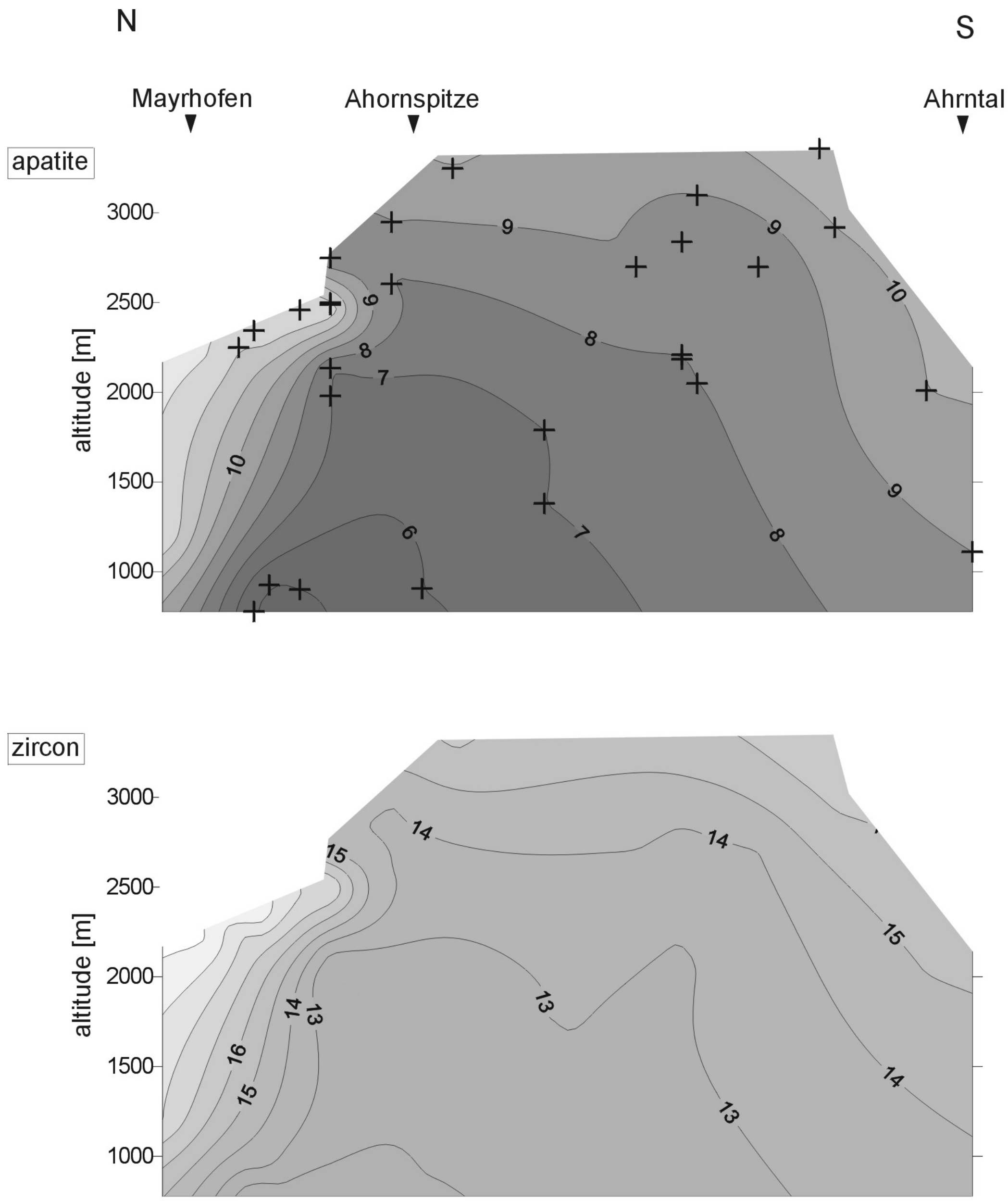

Fig. 7.1: Fission track age tomography of the western Tauern window along the Transalp-Traverse. The crosses marks the projected sample points. The top contour of the profile is an envelope curve of the local topograpy.

The validity of this procedure is confirmed by the monotonous upward increase of the fission track ages. Their projection to a vertical plane is reliable.

The zircon and apatite fission track age tomographic profiles display very similar pattern. In both profiles the vertical age gradients at the northern border of the Tauern window are high (Fig. 7.1). This indicates a gradual, slow vertical displacement during updoming of the Tauern window (cf. Fig. 8.1). In the central part of the profile the zircon and apatite age isolines show a plateau like arrangement (Fig. 7.1). This means that the central part of the western Tauern window was exhumed relative homogeneous "en block". Some visible irregularities in the age isolines are due to missing data points and have no meaning for the interpretation. The vertical age gradient is very low and indicates, that the central part displays a significantly higher exhumation rate than the northern part of the profile. In the southern part of the profile both age isolines are oblique (Fig. 7.1). The vertical age gradient is also very low, indicating faster exhumation.

These zircon and apatite age tomography profiles show that the central part of the western Tauern window underwent a more significant exhumation (average exhumation rate between 500 and 1500 m/Ma) than the northern part (average exhumation rate between 100 and 300 m/Ma).

8 Geodynamic evolution

The Eastern Alps have a complex history of repeated extension and compression related to the movement of the African plate and several microplates (e.g. Adriatic plate) against the European plate. Alpine orogeny of the Eastern Alps is generally interpreted to result from two continent-continent collisions. The first collision occurred between the Middle Penninic microcontinent and the Austroalpine upper continental plate after the subduction of the South Penninic oceanic domain. The second collision resulted from the ongoing convergence between the European lower continental plate and the Austroalpine upper continental plate after the subduction of the North Penninic basin (e.g.Dietrich & Franz 1976; Frisch 1976, 1979, 1981; Frank 1987). There are many different and controversial data and models about the exact time and the kinematics of the continent-continent collisions. Especially about the time of the first collision many different statements exist. They range from the Middle Cretaceous (Frisch 1979; Frank 1987; Ratschbacher et al. 1989) to Early Tertiary (Neubauer 1994). New models were developed, which take into account an independent evolution of stacking in the Austroalpine and Penninic units of the Eastern Alps (Neubauer 1994; Kurz et al. 1996, 1998). In the following the possible geodynamic evolution of the central part of the Transalp-Traverse since the Early Cretaceous is summarised.

1. Early Cretaceous

Shortening within the Austroalpine units is related to the subduction of the Hallstatt-Meliata oceanic domain, and the subsequent continent-continent collision of African derived tectonic units (future Upper Juvavic nappe complex) with the Austroalpine continental units in a footwall position (Neubauer 1994; Dallmeyer et al. 1998). The Early Cretaceous age of the internal Austroalpine nappe stacking is documented by geochronological age data around 130 Ma (Frank et al. 1987; Dallmeyer et al. 1996). The zircon fission track ages around 120 Ma (cf. chapter 4.5.3.1) indicate Early Cretaceous cooling below 225° C of the Upper Austroalpine Altkristallin southern block. A similar zircon fission track age is obtained in the Upper Austroalpine Northern Greywacke Zone (cf. chapter 4.5.3.1).

2. Middle-Late Cretaceous

Stacking in the Penninic domain is related to the southward subduction of the South Penninic oceanic domain and subsequent collision of Penninic continental units with the already assembled Austroalpine Nappe complex (Dallmeyer et al. 1998; Kurz et al. 1998). Ledoux (1984) argued for internal Penninic nappe stacking in the Late Cretaceous. Maybe the age data around 80 Ma obtained in the Kaserer Formation (cf. chapter 4.2.3) and also the high pressure metamorphism found in the same Formation and the Wustkogel Series (cf. chapter 3.2.2.2) could be related to the Late Cretaceous subduction process in the South Penninic basin resulting in the underthrusting of the Venediger Nappe beneath the Glockner Nappe. Thrusting to the N is indicated by top to the N sense of shear (Lammerer 1988; Kurz et al. 1996). This succession of events resulted in a nappe pile with the Austroalpine units at the top of the Penninic units before the end of the Cretaceous. Mica ages between 100 and 60 Ma in the Upper Austroalpine Altkristallin northern block reflect regional cooling after nappe stacking in the course of continent-continent collision and resulting metamorphism.

High crustal levels of Austroalpine units were affected by E-W extension, which resulted in the formation of the Gosau basins in the Late Cretaceous (Ratschbacher et al. 1989; Kurz et al. 1996). The age of the sedimentary succession of the Gosau basins constrains age of unroofing extension in the Austroalpine east of the Tauern Window to about 90-60 Ma (Ratschbacher et al. 1989).

During Cretaceous time the Adriatic microplate performs an anticlockwise rotation and was pressed towards W-NW against the European plate (Dercourt et al. 1986). Displacement analyses based on microstructures in mylonites confirm transpressional NW directed motions in the Austroalpine during early stages of the Alpine orogeny (Ratschbacher et al. 1987).

3. Paleocene

In Early Tertiary time the motion direction changed to N-S and frontal (e.g. Ratschbacher et al. 1989). Ongoing N-S compression in the Paleocene resulted in northward thrusting of the Cretaceous Austroalpine nappe pile over the Penninic units. The zircon fission track ages around 60 Ma of the Innsbruck Quartzphyllite (cf. chapter 4.5.3.1) indicates, that this lower Austroalpine unit cooled through 225° C during Paleocene time.

4. Eocene

In the Eocene important ongoing movements occurred, which result in the collision of the Austroalpine nappe pile with the European continent after the closure of the North Penninic basin (Frisch 1978). Final nappe stacking was reached. The Northern Greywacke Zone cooled below 100° C around 40 Ma as indicated by the apatite fission track age (cf. chapter 4.5.4.1).

5. Oligocene

In the Oligocene the maximum burial was reached. The maximum pressures (> 10 kbar) attained by the Venediger Nappe complex indicate burial to a depth of 35-40 km and for the base of the Glockner Nappe complex to 25-30 km (cf. chapter 3.2.2.2) and Selverstone & Spear (1985). These data imply a total thickness of ~25 km for the Austroalpine nappe pile (Selverstone & Spear 1985).

A change from dominantly shortening and overthrusting to transpression is documented by 1) subhorizontal E-W stretching lineations in the deeply buried and therefore highly metamorphic Penninic rocks and 2) top to the W sense of shear (e.g. Frisch 1968; Lammerer 1988; Ratschbacher et al. 1989; Ratschbacher et al. 1991; Kurz et al. 1996; Weger 1997). Extension, crustal thinning and decompression in the Penninic nappe pile developed at or slightly prior to the thermal peak of regional metamorphism around 30 Ma (Selverstone 1988; Selverstone 1993; Christensen et al. 1994). The investigations of this study gave maximum temperatures around 600° C for the central part of the western Tauern window (cf. chapter 3.2.1.2).
The Oligocene-Miocene activity of the sinistral DAV Line south of the Tauern Window and the sinistral Salzach fault at the northern margin of the central and eastern Tauern Window was related to E-W extension

(Ratschbacher et al. 1991; Frisch et al. 1998). The emplacement of the E-W elongated Rieserferner intrusion along the active DAV Line took place around 30 Ma (Borsi et al. 1978).

Exhumation and updoming of the later Tauern Window was initiated by continuous compression and accompanied by tectonic denudation and erosion (Frisch et al. 1998, 2000). It seems that the relative uplift of the Tauern Window together with the Austroalpine Altkristallin northern block was between these faults with respect to the other Austroalpine units (cf. Neubauer et al. 1999; Frisch et al. 2000). The similar geochronological data of both units confirm this assumption. Subsequent exhumation of the later western Tauern window under amphibolite to greenschist facies conditions occurred between 30 and 13 Ma, depending on the structural level (cf. chapter 4.2.3 and 4.4).

6. Miocene

The Early and Middle Miocene time was dominated by the so called lateral extrusion (Ratschbacher et al. 1991; Frisch et al. 1998). Lateral extrusion is ascribed to a combination of gravity-driven orogenic collaps triggered by an overthickened and thermally equilibrating lithosphere, and tectonic crustal escape along conjugate strike-slip faults. The crustal escape is driven by tangential forces due to continuing N-S convergence between the Adriatic microplate and the European plate. This means eastward movement of upper crustal blocks of the central Eastern Alps along the sinistral Inntal Line and the dextral Pustertal Line (Fig. 8.1a). The western border of the extrusion channel is a large-scale low-angle normal fault, the Brenner Line. Early Miocene fault activity is proven by geochronological data (Fügenschuh 1995; Müller 1996; Müller et al. 2001). The escape of these blocks was linked with ongoing and distinct E-W directed extension, crustal thinning and exhumation of the later Tauern Window together with the Altkistallin northern block (Fig. 8.1.a). The narrow zircon fission track age cluster around 21 Ma in the Altkristallin northern block (cf. chapter 4.5.3.1) indicates rapid exhumation of this block. At that time, a high exhumation rate (3.6 mm/a; Fig. 6.1) is reported by Blanckenburg et al. (1989) for the central part of the western Tauern window. The Early Miocene fast exhumation was mainly attained by tectonic denudation due to the lateral removal of the Austroalpine units above the Penninic units, and only to a minor part by erosion (Frisch et al. 2000; Kuhlemann et al. 2001). In the upper crustal levels of the Tauern window the zircon fission track ages are also around 20 Ma (cf. chapter 4.5.3.1) and clarify the above mentioned common cooling history. The zircon fission track ages get successively younger to lower crustal levels (cf. chapter 4.5.3.1). A drop of sediment discharge after 21 Ma is interpreted to result from a relief collapse in the course of lateral extrusion (Frisch et al. 1999; Kuhlemann 2000).

For the central part of the western Tauern window the exhumation rates decrease to ~1 mm/a and further to 0.5 mm/a (cf. chapter 6). Such slow cooling is also indicated by the apatite track length distributions and mean track lengths of 12.9 to 13.9 (± 1.2-1.8) µm (cf. chapter 5.1.2). The final cooling below 100° C starts for all investigated units, despite the Northern Greywacke Zone, around 13 Ma as indicated by the apatite fission track ages (cf. chapter 4.5.4.1). After entering the PAZ the modelled time-temperature paths suggest more or less slow cooling up to the present with average cooling rates between 22° C/Ma to 6° C/Ma (cf. chapter 5.3.2). The final exhumation history is dominated by erosion.

a) Middle Miocene

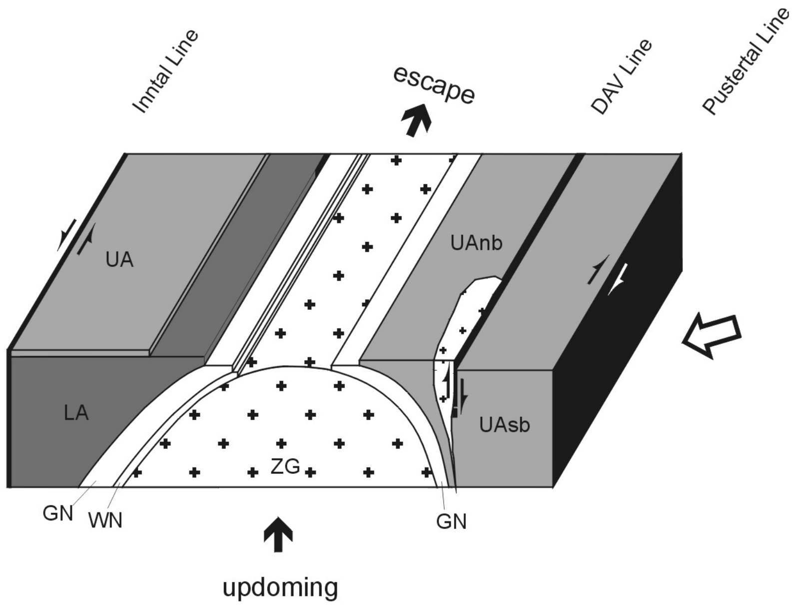

b) Late Miocene

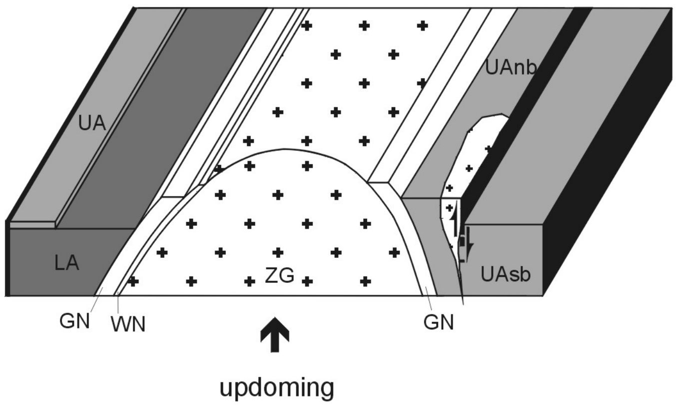

Fig. 8.1: Schematic block diagrams (N-S) display the a) Middle Miocene and b) Late Miocene evolution of the Tauern window as well as the surrounding units. The opening of the Tauern window due to exhumation occurred in the Middle Miocene as indicated by Zentralgneis pebbles in the Molasse (Brügel 1998). The arrow indicate the NW-SE compression field (Schulz 1994). The result is dextral movements or escape of blocks along the Pustertal Line (Ratschbacher et al. 1991). Sinistral movements along the DAV Line did not longer occur, but vertical displacement (cf. chapter 4.6). The Late Miocene is dominated by the ongoing exhumation of the Tauern window and further vertical displacement of the northern block relative to the southern block. Abbreviations: Glockner Nappe (GN); Lower Austroalpine unit (LA); Upper Austroalpine units (UA); Upper Austroalpine Altkristallin northern block (UAnb); Upper Austroalpine Altkristallin southern block (UAsb); Wolfendorn Nappe (WD); Zentralgneis (ZG).

A general observation are the differing age clusters (mica and zircon fission track) in the Tauern window and the Austroalpine Altkristallin northern block which show, that the eastern part was exhumed earlier than the western part. For the mica ages this was first described by Borsi et al. (1973) for the Austroalpine Altkristallin and by Raith et al. (1978) for the Tauern window. The results of this study display that this trend continued in the Austroalpine Altkristallin northern block during cooling below 225° C as indicated by the zircon fission track ages (cf. chapter 4.5.3.1). The conclusion is, that the tectonic denudation started in the eastern part by active eastward migration of Austroalpine tectonic blocks (Frisch et al. 2000).

7. Present

Fig. 8.2 shows two alternative models of the present day crustal structure along the Transalp-Traverse (Munich-Venice). They are the results and interpretations derived from deep seismic reflection profiling (TRANSALP Working Group 2002). Both models are widely identical except for the Tauern window and adjacent parts south of it. The bi-verging character is evident from the seismic sections. There are two major ramps: the southward dipping "Sub-Tauern Ramp" exposed at the Inn valley, and the northward dipping "Sub-Dolomites Ramp" which is exposed in the Valsugana-Agordo area. Along them crustal wedges have been upthrust.

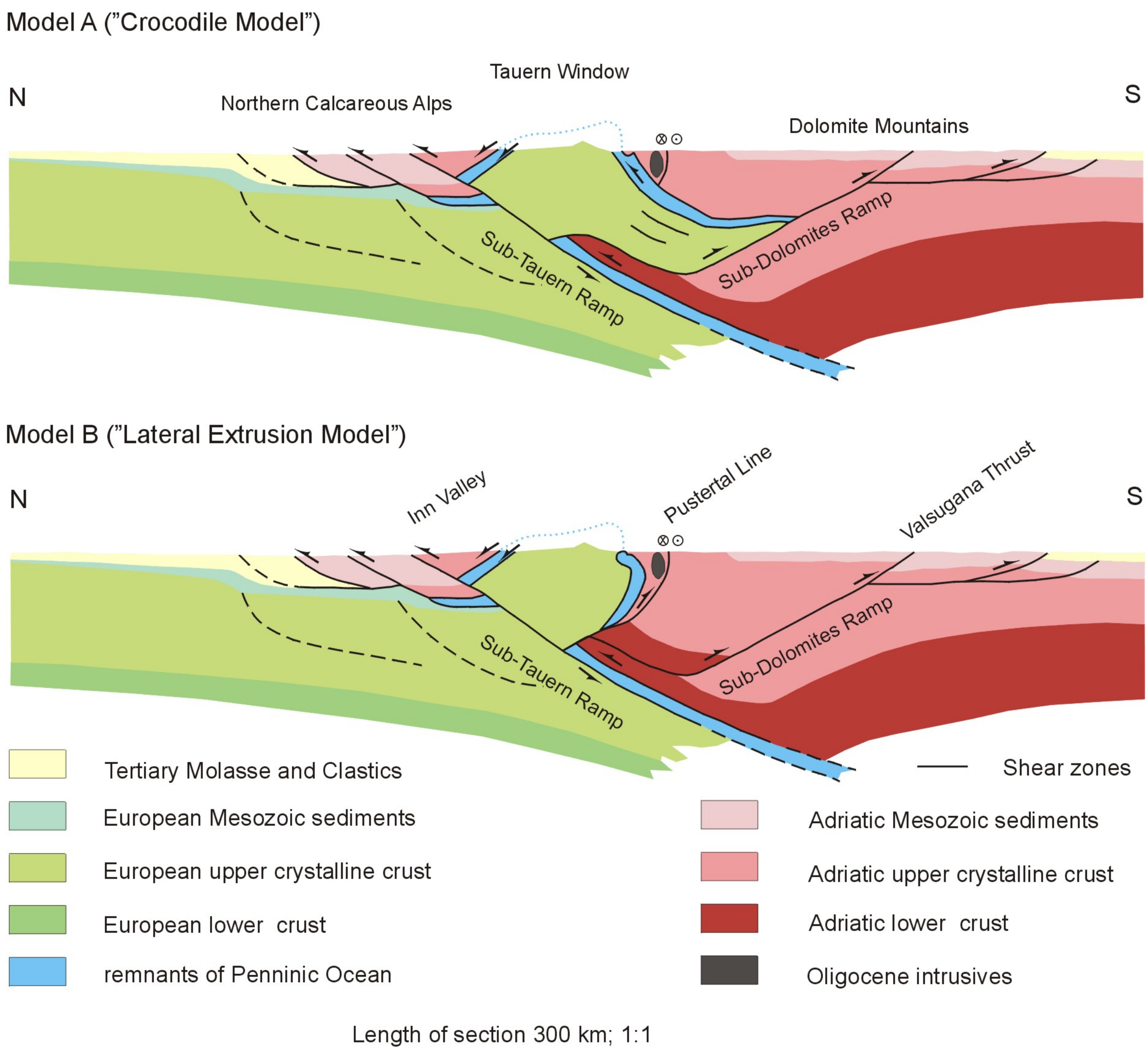

Fig. 8.2: Interpretational cartoon showing two controversial models according to TRANSALP Working Group (2002). Geographic terms and marked fault zones apply for both models.

The "Crocodile Model" (Lammerer et al. 2001) focuses on the bi-verging character (Fig. 8.2 A). The edge of the initially cooler Penninic units (supposed to represent the former European passive plate boundary) wedges deep into the approaching Adriatic plate. At the level of the brittle/ductile transition an upper and lower unit were split up. Thereby the Dolomite block was displaced to the South. The upper crust of the Adriatic plate was thrust as Austroalpine nappes over the Tauern window. With proceeding collision, the Adriatic lower crust subsequently pushed the Tauern window into its uplifted position. Consequently the Dolomite Mountains block was back-thrust to the South along the "Sub-Dolomites Ramp"

The "Lateral Extrusion Model" (Castellarin et al. 2001) describes the Eastern Alps according to earlier views in an indenter-style (Fig. 8.2 B). In contrast to model A, the steep northward dip of the Pustertal Line observed near the surface is interpreted to continue to greater depth. The Dolomite sector is rheologically considered as a rigid block, enforcing lateral extrusion. The model is supported by back folding and overturning of the Austroalpine Altkristallin at the southern border of the Tauern window.

Interpretation of seismic reflection records is a blend of quantitative science and visual art. An interpreter uses the rules of wave propagation, realistic limits on impedances of rocks and accepted principles of stratigraphic deposition and structural deformation to achieve a geologic understanding of a seismic section. The result is seldom a unique answer, but a lot of alternative interpretations. The seismic interpreter is heavily influenced by the quality and character of the seismic.

In the case of the Transalp project, the seismic investigations allow no clear interpretation of the deep structures in the study area. For instance, at the surface steeply dipping structures (e.g. Greiner shear zone, DAV and KV Line) were not recorded by the seismic. This means that they have to be also steep in the depth or the shear zones show no significant rheological differences in respect to the surrounding rocks. However these shear zones display an important role by the interpretation of the geochronological data and the geodynamic evolution. Both provided models can be interpreted out of the seismic data. The geochronological data of this study can only provide some additional information. Due to the before described geodynamic evolution and the reconstruction of the different exhumation and cooling histories of the investigated units, Model B seems more logic.
A Southalpine indenter (Dolomite sector) is required as a rigid block to enforce the proven lateral extrusion of the Austroalpine units and weak Penninic units along the Pustertal Line. Also the age tomographic profiles of the western Tauern window (cf. Fig. 8.1) and the fact, that the western later Tauern window and the Altkristallin northern block were squeezed in a kind of bench vice and exhumed together, requires the indentation of a rigid block.

9 Conclusions

In the frame of the Transalp project, this study focuses on geochronological investigations along the central part (Inntal – Gadertal) of the Transalp-Traverse. The aim is the reconstruction of the exhumation and cooling history of the different units and blocks of the study area. From north to south the following conclusions can be drawn:

- Upper Austroalpine unit

Early Cretaceous cooling of the Upper Austroalpine Northern Greywacke Zone below 240 ± 50° C is indicated by a zircon fission track age of 118 Ma. The rather high apatite fission track age of 39 Ma is interpreted as probable cooling age of the eo-Alpine event.

- Lower Austroalpine units

In terms of the Cenozoic exhumation history, the Schwazer Augengneis behaves as part of the Lower Austroalpine. This is supported by zircon fission track ages around 60 Ma, which are also derived of the Lower Austroalpine Innsbruck Quartzphyllite. The zircon fission track ages reflect cooling after the Cretaceous metamorphic overprint in greenschist facies. Final cooling below ~100° C happened between 14 and 10 Ma.
Mixed type apatite mean track length distributions recorded in the Innsbruck Quartzphyllite and Schwazer Augengneis, possibly indicate a later thermal event. An interpretation of them without additional investigations is impossible.

- Penninic units

For the western Tauern window, the phengite geobarometry indicates a high pressure metamorphism in the Wustkogel Series (Glockner Nappe) and the Kaserer Formation (Wolfendorn Nappe). This event could be related to the southward subduction of the South Penninic oceanic domain and the subsequent collision of Penninic continental units and the Austroalpine Nappe complex. The Late Cretaceous age of this process and the resulting internal Penninic nappe stacking is possibly reported by the K/Ar phengite age of 80 Ma obtained in the Kaserer Formation. Maximum temperatures of ~600° C were documented by garnet-biotite geothermometry for the central part of the western Tauern window at Oligocene time. Sequential cooling, indicated by zircon and apatite fission track data, from the hanging wall units (Glockner Nappe complex) towards to the footwall units (Wolfendorn Nappe and Zentralgneis) is related to the Miocene updoming of the western Tauern window. A common Early Miocene cooling below 225° C of the Glockner Nappe and the Austroalpine Altkristallin northern block is indicated by the nearly identical zircon fission track ages. This favours the assumption that the western Tauern window and the Altkristallin northern block were squeezed in a kind of bench vice and exhumed together. Also the Early Miocene zircon fission track ages of 22 Ma of the Penken area assign the Penken-breccia to the Penninic units (Bündner-Schiefer Formation).
The apatite mean track length distributions obtained from the investigated Penninic units are typical examples of the undisturbed basement type. They indicate slow to faster cooling with no prolonged residence in the PAZ.
The zircon and apatite fission track ages of the Zentralgneis depend on the altitude in the way, that the topographic highest samples display the oldest ages. Therefore it was possible to calculate some exhumation rates with the altitude dependence method. This method gives reliable exhumation rates in the order of 1.1 mm/a for

the time between 14 and 12 Ma, and 0.6 mm/a for the time interval 9-5 Ma. The mineral pair method is not applicable.
The apatite and zircon fission track age tomographic profiles show, that the central and southern part of the western Tauern window underwent more significant exhumation than the northern part in the last 16 Ma.

- Upper Austroalpine unit

In the Upper Austroalpine Altkristallin south of the western Tauern window, the zircon fission track ages show a trend to higher ages in the east and suggest W-E tilting of the northern block. This trend was first indicated by biotite cooling ages. Also the zircon fission track ages increase from 21 Ma to 131 Ma towards the south with clear jumps of the ages at the DAV (Defereggen-Antholz-Vals) Line and KV (Kalkstein-Vallarga) Line. For the area of the Transalp-Traverse a vertical displacement of ~5 km of the block north of the DAV Line relative to the block south of it can be assumed for the time between ~30 Ma and 10 Ma.
The homogeneous apatite fission track data around 10 Ma show that the late cooling history below 100° C is identical for the three blocks, indicating stagnation of vertical displacement along the DAV and KV Lines. After 10 Ma the exhumation is only controlled by erosion

- Southalpine units

The measured zircon fission track ages around 220 Ma obtained in the Southalpine units maybe related to a Late Triassic extensional event. Final cooling below 100° C occurred between 15 and 11 Ma as indicated by the apatite fission track ages. Further investigations, e.g. zircon fission track length measurements were needed for a final interpretation of the exhumation history.

10 References

Anderson, D. E. and G. R. Buckley (1973): Zoning in garnets - diffusion models. - Contrib. Mineral. Petrol. **40**: 87-104.

Angelmaier, P. (1997): Petrographische und geothermobarometrische Untersuchungen an Metapeliten und Metabasiten des Altkristallins S' des Tauernfensters (Osttirol/Österreich). - Georg-August-University, Göttingen, Germany, unpubl. Diploma thesis, pp131.

Behrmann, J. (1988): Crustal-scale extension in a convergent orogen: The Sterzing-Steinach mylonite zone in the Eastern Alps. - Geodynamica Acta (Paris) **2**: 63-73.

Bellieni, G. and D. Visona (1981): Metamorphic evolution of the Austroalpine schists outcropping between the intrusive masses of Vedrette di Ries (Rieserferner) and Cima di Vila (Zinsnock) (Eastern Alps, Italy). - N. Jb. Geol. Paläont. Mh **10**: 586-602.

Bertotti, G., V. Picotti, D. Bernoulli and A. Castellarin (1993): From rifting to drifting: Tectonic evolution of the South-Alpine upper crust from the Triassic to the Early Cretaceous. - Sediment. Geol. **86**: 53-76.

Bertotti, G., D. Seward, J. Wijbrans, M. ter Voorde and A. J. Hurford (1999): Crustal thermal regime prior to, during, and after rifting: A geochronological and modeling study of the Mesozoic South Alpine rifted margin. - Tectonics **18/2**: 185-200.

Bianchi, A. (1934): Studi petrografici sull` Alto Adige Orientale e regione limitrofe. - Mem. Ist. Geol. Min. Univ. Padova **X (5)**: 234.

Blanckenburg, v. F., I. M. Villa, H. Baur, G. Morteani and R. H. Steiger (1989): Time calibration of a PT-path from the Western Tauern Window, Eastern Alps: the problem of closure temperatures. - Contrib. Mineral. Petrol. **101/1-11**.

Bögel, H. (1975): Zur Literatur über die "Periadriatische Naht". - Verh. Geol. B.A. **2-3**: 163-199.

Bögel, H. and K. Schmidt (1976): Kleine Geologie der Ostalpen.Ott Verlag, pp.231.

Borsi, S., A. Del Moro and G. Ferrara (1972): Eta radiometriche delle rocce intrusive del massiccio di Bressanone-Ivigna-Monte Croce (Alto Adige). - Boll. Soc. Geol. Ital. **91**: 387-406.

Borsi, S., A. Del Moro, F. Pisa, F. P. Sassi and G. Zirpoli (1978): On the age of the Vedrette di Ries (Rieserferner) massif and its geodynamic significance. - Geol. Rundschau **68**: 41-60.

Borsi, S., A. Del Moro, F. P. Sassi, A. Zanferrari and G. Zirpoli (1978): New geopetrologic and radiometric data on the alpine history of the Austridic continental margin south of the Tauern Window. - Mem. Sci. Geol. (Padova) **32**: 1-17.

Borsi, S., A. Del Moro, F. P. Sassi and G. Zirpoli (1973): Metamorphic evolution of the Austridic rocks to the south of the Tauern Window (Eastern Alps): radiometric and geopetrologic data. - Mem. Soc. Geol. Ital. **12**: 549-571.

Brandner, R. (1985): Geologische und tektonische Übersichtskarte von Tirol: Sonderdruck aus Tiroler Heimat. - Jahrbuch für Geschichte und Volkskunde **48/49**.

Brügel, A. (1998): Provenances of alluvial conglomerates from the Eastalpine foreland: Oligo-/Miocene denudation history and drainage evolution of the Eastern Alps. - TGA, Series A **40**: 1-168.

Castellarin, A., G. V. Dal Piaz, G. B. Vai and TRANSALP Working Group (2001): The Transalp seismic profile: remarks and interpretation from the Italian side. - Geol. Paläont. Mitt. Innsb. **25**: 62.

Cesare, B. (1992): Metamorfismo di contatto di rocce pelitiche nell'aureola di Vedrette di Ries (Alpi Orientali - Italia). - Atti Tic. Sc. Terra **35**: 1-7.

Cesare, B. (1994): Hercynite as the product of staurolite decomposition in the contact aureole of Vedrette di Ries, eastern Alps, Italy. - Contrib. Mineral. Petrol. **116**: 239-246.

Christensen, J. N., J. Selverstone, J. L. Rosenfeld and D. J. De Paolo (1994): Correlation by Rb-Sr geochronology of garnet growth histories from different structural levels within the Tauern Window, Eastern Alps. - Contrib. Mineral. Petrol. **118**: 1-12.

Cowan, G. A. and H. H. Adler (1976): The variability of the natural abundance of 235U. - Geochimica et Cosmochimica Acta **40**: 1487-1490.

Coyle, D. A. (1994): The application of apatite fission track analysis to problems in tectonic. - La Trobe Univesity, Budoora, Victoria 3083, Australia, unpubl. Ph.D.

Crawford, M. L. (1977): Calcium zoning in almandine garnet, Wissahickon formation, Philadelphia, Pennsilvania. - Can. Mineral. **15**: 243-249.

Crowley, K. D., A. E. Cameron and R. L. Schaefer (1991): Experimental studies of annealing of etched fission tracks in fluorapatite. - Geochimica et Cosmochimica Acta **55**: 1449-1465.

Currie, K. L. and C. R. Van Staal (1999): The assamblage stilpnomelan-chlorite-phengitic mica: a geothermobarometer for blueschist and associated greenschist terranes. - J. Metamorphic Geol. **17**: 613-620.

Dallmeyer, R. D., R. Handler, F. Neubauer and H. Fritz (1998): Sequence of thrusting within a thick-skinned tectonic wedge: evidence from 40Ar/39Ar and Rb/Sr ages from the Austroalpine nappe complex of the eastern Alps. - J. Geol. **106**: 71-86.

Dallmeyer, R. D., F. Neubauer, R. Handler, H. Fritz, W. Müller, D. Pana and M. Putis (1996): Tectonothermal evolution of the internal Alps and Carpathians: Evidence from 40Ar/39Ar mineral and whole-rock data. - Eclogae geol. Helv. **89/1**: 203-227.

Dempster, T. J. (1985): Garnet zoning and and metamorphism of the barrovian type area, Scotland. - Contrib. Mineral. Petrol. **89**: 30-38.

Dercourt, J., L. P. Zonenshain and L.-E. Ricou (1986): Geological evolution of the Tethys belt from the Atlantic to the Pamirs since the Lias. - Tectonophysics **123**: 241-315.

Dietrich, V. J. and U. Franz (1976): Alpidische Gebirgsbildung in den Ostalpen: ein plattentektonisches Modell (Kurzfassung). - Geol. Rundschau **65**: 361-374.

Dodson, M. H. (1973): Closure temperature in cooling geochronological and petrological systems. - Contrib. Mineral. Petrol. **40**: 275-292.

Donelick, R. A., R. A. Ketcham and W. D. Carlson (1999): Variabillity of apatite fission-track annealing kinetics: II. Crystallographic orientation effects. - American Mineralogist **84**: 1224-1234.

Dumitru, T. A. (1993): A new computer-automated microscope stage system for fission-track analysis. - Nucl. Tracks Radiat. Meas. **21**: 575-580.

Dunkl, I. (2002): TRACKEY: a windows program for calculation and graphical presentation of fission track data. - Computers and Geosciences **28/2**: 3-12.

Dunkl, I., W. Frisch and J. Kuhlemann (1999): Fission track record of the thermal evolution of the Eastern Alps - review of the main zircon age cluster and the significance of the 160 Ma event. - TGA, Series A **52**: 77-78.

England, P. and P. Molnar (1990): Surface uplift, uplift of rocks, and exhumation of rocks. - Geology **18**: 1173-1177.

Ernst, W. G. (1963): Significance of phengitic micas from low-grade schists. - Am. Mineral. **12**: 25-62.

Ferrara, G. and F. Innocenti (1974): Radiometric age evidence of a Triassic thermal event in the Southern Alps. - Geol. Rundschau **63**: 572-581.

Ferry, J. M. and F. S. Spear (1978): Experimental calibration of the partitioning of Fe and Mg between biotite and garnet. - Contributions to Mineralogy and Petrology **66/2**: 113-117.

Fitzgerald, P. G. and A. J. W. Gleadow (1988): Fission-track geochronology, tectonics and structure of the Transantarctic Mountains. - Nucl. Tracks **17**: 351-357.

Fleischer, R. L., P. B. Price and R. M. Walker (1965): Effects of temperature, pressure and ionization of the formation and stability of fission tracks in minerals and glasses. - J. Geophys. Res. **70**: 1497-1502.

Fleischer, R. L., P. B. Price and R. M. Walker (1965): Tracks of charged particles in solids. - Science **149**: 383-393.

Foster, M. D. (1960): Interpretation of the composition of trioctahedral micas. - U.S. Geol. Survey Prof. Paper **354-B**: 24-29.

Frank, W. (1987): Evolution of the Austroalpine Elements in the Cretaceous. - in: FLÜGEL, H.W. & FAUPl, P. (eds.): Geodynamics of the Eastern Alps, Deuticke, Wien: 379-403.

Frank, W., V. Höck and C. Milller (1987): Metamorphic and tectonic history of the central Tauern Window. - in: FLÜGEL, H.W. & FAUPl, P. (eds.): Geodynamics of the Eastern Alps, Deuticke, Wien: 34-52.

Frasl, G. and W. Frank (1966): Einführung in die Geologie und Petrographie des Penninikums im Tauernfenster. - Aufschluß **Sonderheft 15**: 30-58.

Frisch, W. (1968): Zur Geologie des Gebietes zwischen Tuxbach und Tuxer Hauptkamm bei Lanersbach. - Mitt. Ges. Geol. Bergbaustud. Wien **18**: 287-336.

Frisch, W. (1974): Die stratigraphisch - tektonische Gliederung der Schieferhülle und die Entwicklung des penninischen Raumes im westlichen Tauernfenster (Gebiet Brenner - Gerlospaß). - Mitt. Geol. Ges. Wien **66/67**: 9-20.

Frisch, W. (1976): Ein Modell zur alpidischen Evolution und Orogenese des Tauernfensters. - Geol. Rundschau **65**: 375-393.

Frisch, W. (1978): A plate tectonics model of the Eastern Alps. - in: CLOSS, H.D.; ROEDER, D. & SCHMIDT, D. (eds.): Alps, Apennines, Hellenides: 167-172.

Frisch, W. (1979): Tectonic progradation and plate tectonic evolution of the Alps. - Tectonophysics **60**: 121-139.

Frisch, W. (1980): Tectonics of the western Tauern window. - Mitt. Österr. Geol. Ges. **71/72**: 65-71.

Frisch, W. (1981): Plate motions in the Alpine region and their correlation to the opening of the Atlantic ocean. - Geol. Rundschau **70/2**: 402-411.

Frisch, W. (1984): Metamorphic history and geochemistry of low-grade amphibolite in the Kaserer Formation (Marginal Bündner Schiefer of the Western Tauern Window, the Eastern Alps). - Schweiz. Mineral. Petrogr. Mitt. **64**: 193-214.

Frisch, W., S. B., J. Kuhlemann and I. Dunkl (2000): Geomorphological evolution of the Eastern Alps in response to Miocene tectonics. - Z. Geomorph. N. F. **44/1**: 103-138.

Frisch, W., A. Brügel, I. Dunkl, J. Kuhlemann and M. Satir (1999): Post-collisional large-scale extension and mountain uplift in the Eastern Alps. - Mem. Ist. Geol. Min. Univ. Padova **51**: 3-23.

Frisch, W., I. Dunkl and J. Kuhlemann (2000): Post-collisional orogen-parallel large-scale extension in the Eastern Alps. - Tectonophysics **327/3-4**: 239-265.

Frisch, W., K. Gommering, U. Kelm and F. Popp (1987): The upper Bündner Schiefer of the Tauern window - a key to understanding Eoalpine orogenic processes in the Eastern Alps. - in: FLÜGEL, H.W. & FAUPl, P. (eds.): Geodynamics of the Eastern Alps, Deuticke, Wien: 55-69.

Frisch, W., J. Kuhlemann, I. Dunkl and A. Brügel (1998): Palinspastic reconstruction and topographic evolution of the Eastern Alps during Late Tertiary tectonic extrusion. - Tectonophysics **297**: 1-15.

Frisch, W. and F. Popp (1881): Die Fortsetzung der "Nordrahmenzone" im Westteil des Tauernfensters. - Jahresber. 1980 Hochschulschwerpunkt **S 15**: 33-45.

Fügenschuh, B. (1995): Thermal and kinematik history of the Brenner area. - ETH Zürich, Swiss, unpubl. Ph.D., 225pp.

Galbraith, R. F. (1981): On statistical models for fission track counts. - Math. Geology **414**: 417-488.

Genser, J. and F. Neubauer (1989): Low angle normal faults at the eastern margin of the Tauern window (Eastern Alps). - Mitt. Österr. Geol. Ges. **81**: 233-243.

Gleadow, A. J. W. (1981): Fission track dating methods: What are the real alternatives? - Nucl. Tracks **5**: 3-14.

Gleadow, A. J. W., I. R. Duddy, P. F. Green and J. F. Lovering (1986): Confined fission track length in apatite: a diagnostic tool for thermal history analyses. - Contributions to Mineralogy and Petrology **94**: 405-415.

Gleadow, A. J. W., I. R. Duddy and J. F. Lovering (1983): Fission track analysis: a new tool for the evaluation of thermal histories and hydrocarbon potential. - Aust. Petrol. Explor. Assoc. J. **23**: 93-102.

Gleadow, A. J. W., A. J. Hurford and R. D. Quaife (1976): Fission track dating of zircon: improved etching techniques. - Earth and Planetary Science Letters **33**: 273-276.

Green, P. F., I. R. Duddy, A. J. W. Gleadow and P. R. Tingate (1985): Fission-track annealing in apatite: Track length measurements and the form of the arrhenius plot. - Nucl. Tracks **10/3**: 323-328.

Green, P. F., I. R. Duddy, A. J. W. Gleadow, P. R. Tingate and G. M. Laslett (1986): Thermal annealing of fission tracks in apatite: 1. A quantitative description. - Chemical Geology **59**: 237-253.

Green, P. F., I. R. Duddy, G. M. Lasslett, K. A. Hegarty, A. J. W. Gleadow and J. F. Lovering (1989): Thermal annealing of fission tracks in apatite. - Chemical Geology **79**: 155-182.

Grundmann, G. and G. Morteani (1985): The young uplift and thermal history of the central Eastern Alps (Austria/Italy), evidence from apatite fission track ages. - Jb. Geol. Bundesanst. **128**: 197-216.

Guidotti, C. V. (1978): Compositional variation of muscovite in medium- to high-grade pelites of northwestern Maine. - Am. Mineral. **63**: 878-884.

Hammerschmidt, K. (1981): Isotopengeologische Untersuchungen am Augengneis vom Typ Campo Tures bei Rain in Taufers, Südtirol. - Mem. Ist. Geol. Min. Univ. Padova **34**: 273-300.

Hammerschmidt, K. and B. Stöckhert (1987): A K-Ar and 40Ar/39Ar study on white micas from the Brixen Quarzphyllite, Southern Alps. - Contrib. Mineral. Petrol. **95**: 393-406.

Handler, R., F. Neubauer, G. Friedl, J. Genser, R. Heidorn, H. P. Steyer, H. Fritz and V. Tenczer (2001): Summary of new 40Ar/39Ar data along the Transalp-section. - Geol. Paläont. Mitt. Innsb. **25**: 112-113.

Hanna, G. C., C. H. Wescott, H. D. Lemmel, B. R. Leonard, J. S. Story and P. M. Attree (1969): Revision of values for the 2200 m/s neutron constants for four fissile nuclides. - At. Energ. Rev. **7**: 3-92.

Harper, C. T. (1970): Graphical solutions to the problem of radiogenic argon-40 loss from metamorphic minerals. - Eclogae geol. Helv. **63/1**: 119-140.

Hawkesworth, C. J. (1976): Rb/Sr geochronology in the Eastern Alps. - Contrib. Mineral. Petrol. **54**: 225-244.

Höck, V. and C. Miller (1987): Mesozoic Ophiolithic Sequences and Non-Ophiolithic Metabasites in the Hohe Tauern. - in: FLÜGEL, H.W. & FAUPl, P. (eds.): Geodynamics of the Eastern Alps, Deuticke, Wien: 16-33.

Hodges, K. V. and F. S. Spear (1982): Geothermometry, geobarometry and the Al2Si5 triple point at Mt. Moosilauke, New Hampshire. - Am. Mineral. **67**: 1118-1134.

Hoernes, S. and H. Friedrichsen (1974): Oxygen isotope studies on rocks of the Western Hohe Tauern area (Austria). - Schweiz. Mineral. Petrogr. Mitt. **54**: 769-788.

Hoescheck, G. (1973): Bericht über Untersuchungen an magmatischen Gesteinen aus der Grauwackenzone, Raum Kitzbühel. - Meet. Geotraverse I A, Salzburg.

Hoinkes, G. (1986): Effect of grossular content in garnet on the partitioning of Fe and Mg between garnet and biotite. - Contributions to Mineralogy and Petrology **92**: 393-399.

Hollister, L. S. (1966): Garnet zoning: an interpretation - based on the Rayleigh fractionation model. - Science **154**: 1642-1651.

Hoschek, G., E. C. Kirchner, H. Mostler and J. M. Schramm (1980): Metamorphism in the Austroalpine Units between Innsbruck and Salzburg (Austria) - A Synopsis. - Mitt. Österr. Geol. Ges. **71/72**: 335-341.

Hurford, A. J. (1986): Cooling and uplift patterns in the Lepontine Alps South Central Switzerland and age of vertical movement on the Insubric fault line. - Contrib. Mineral. Petrol. **92**: 413-427.

Hurford, A. J., M. Flisch and E. Jäger (1989): Unravelling the thermo-tectonic evolution of the Alps: a contribution from fission track analysis and mica dating. - Geological Society Special Publication **45**: 369-398.

Hurford, A. J. and P. F. Green (1983): The zeta callibration of fission-track dating. - Isotope Geoscience **1**: 285-317.

Hurford, A. J., J. C. Hunziker and B. Stöckhert (1991): Constraints on the late thermotectonic evolution of the Western Alps: Evidence for episodic rapid uplift. - Tectonics **10/4**: 758-769.

Indares, A. and J. Martignole (1985): Biotite.garnet geothermometry in the granulite facies: the influence of Ti and Al in biotite. - Am. Mineral. **70**: 272-278.

Jaffrey, A. H., K. F. Flynn, L. E. Glendenin, W. C. Bentley and A. M. Essling (1973): Precision measurement of half-lives and specific activities of 285U and 283U. - Phys. Rev. **4**: 1889-1906.

Ketcham, R. A., R. A. Donelick and W. D. Carlson (1999): Variabillity of apatite fission-track annealing kinetics: III. Extrapolation of geological time scales. - American Mineralogist **84**: 1235-1255.

Ketcham, R. A., R. A. Donelick and M. B. Donelick (2000): AFTSolve: A program for multi-kinetic modelling of apatite fission-track data. - Geological Materials Research **2/1**: 1-32.

Kleinschrodt, R. (1987): Quarzkorngefügeanalyse im Altkristallin südlich des Tauernfensters (Südtirol/Italien). - Erlanger Geol. Abh. **114**: 1-82.

Kralik, M. (1983): Interpretation of K-Ar and Rb-Sr data from fine fractions of weakly metamorphosed shales and carbonate rocks at the base of Northern Calcareous Alps. - Tschermaks Min. Petr. Mitt. **32**: 49-67.

Kuhlemann, J. (2000): Post-collisional sediment budget of circum-Alpine basins (Central Europe). - Mem. Ist. Geol. Min. Univ. Padova **52/1**: 1-91.

Kuhlemann, J., W. Frisch, I. Dunkl and B. Szekely (2001): Quantifying tectonic versus erosive denudation by the sediment budget; the Miocene core complexes of the Alps. - Tectonophysics **330**: 1-23.

Kurz, W., F. Neubauer and J. Genser (1996): Kinematics of Penninic nappes (Glockner Nappe and basement-cover nappes) in the Tauern Window (Eastern Alps, Austria) during subduction and Penninic-Austroalpine collision. - Eclogae geol. Helv. **89/1**: 573-605.

Kurz, W., F. Neubauer, J. Genser and E. Dachs (1998): Alpine geodynamic evolution of passiv and active continental margin sequences in the Tauern Window (eastern Alps, Austria, Italy): a review. - Geol. Rundschau **87**: 225-242.

Lammerer, B. (1988): Thrust-regime and transpression-regime tectonics in the Tauern Window (Eastern Alps). - Geol. Rundschau **77/1**: 143-156.

Lammerer, B., E. Lüschen, J. Schönrock and TRANSALP Working Group (2001): Interpretation of the Transalp section according to the "Crocodile Model". - Geol. Paläont. Mitt. Innsb. **25**.

Laslett, G. M., P. F. Green, I. R. Duddy and A. J. W. Gleadow (1987): Thermal annealing of fission tracks in apatite. - Chemical Geology **65**: 1-13.

Läufer, A. L., W. Frisch, G. Steinitz and J. Loeschke (1997): Exhumed fault-bounded Alpine blocks along the Periadriatic lineament: the Eder unit (Carnic Alps, Austria). - Geol. Rundschau **86**: 612-626.

Ledoux, H. (1982): Die Geologie des inneren Tuxertales (Tirol, Österreich). - Univ. Münster, Germany, unpubl. Ph.D., pp224.

Ledoux, H. (1984): Paläogeographie und tektonische Entwicklung im Penninikum des Tauern-Nordwestrandes im oberen Tuxer Tal. - Jb. Geol. Bundesanst. **126/3**: 359-368.

Ludwig, K. R. (2001): Isoplot / Ex rev 2.49, a geochronological toolkit for Microsoft Exel.

Mager, D. (1985): Geologische und petrographische Untersuchungen am Südrand des Rieserferner-Plutons (Südtirol) unter Berücksichtigung des Intrusionsmechanismus. - Universität Erlangen-Nürnberg, Germany, unpubl. Ph.D., pp182.

Mancktelow, N. (1998): A stepwise discrete fourier transform approach to 1D thermal modelling of exhumation by erosion and strechting. - Computers and Geosciences **24/9**: 829-837.

Mancktelow, N. and B. Grasemann (1997): Time-dependent effects of heat advection and topography on cooling histories during erosion. - Tectonophysics **270**: 167-195.

Massonne, H. J. and W. Schreyer (1987): Phengite geobarometry based on the limiting assemblage with K-feldspar, phlogopite and quartz. - Contributions to Mineralogy and Petrology **96**: 212-224.

Miller, H., M. Satir and W. Frank (1980): High-pressure metamorphism in the Tauern Window. - Mitt. Österr. Geol. Ges. **71/72**: 89-97.

Morteani, G. (1974): Petrology of the Tauern Window, Austrian Alps. - Fortschr. Miner. **52/1**: 195-220.

Most, T. (1997): Gefügekundliche Untersuchung und Fluid-/Gesteinswechselwirkungen der Kataklasite der Defereggen-Antholz-Vals (DAV) - Linie N' des Staller Sattels und S' von St. Veit in Defereggen (Osttirol/Österreich). - Georg-August-University, Göttingen, Germany, unpubl. Diploma thesis, pp154.

Mostler, H. (1986): Zur Geologie des Wipptales (Innsbrucker Quarzphyllit, unterostalpines Mesozoikum, Matreier Schuppenzone, Altkristallin, Steinacher Decke, Silltalstörung). - Jber. Mitt. Oberrhein. Geol. Ver. **68**: 29-42.

Müller, P., N. Mancktelow and M. Meier (2000): Rb-Sr michrochrons of synkinematik mica in mylonites: an example from the DAV fault of the Eastern Alps. - Earth and Planetary Science Letters **180**: 385-397.

Müller, W. (1996): Dating deformation along the Periadriatic fault system SW of the Tauern window using microsampling techniques. - 14. Schweiz. Tektonikertreffen (Basel), Abstracts: 25.

Müller, W., G. Prosser, N. Mancktelow, I. M. Villa, S. P. Kelley, G. Viola and F. Oberli (2001): Geochronological constraints on the evolution of the Periadriatic Fault System (Alps). - Geol. Rundschau **90**: 623-653.

Naeser, C. W. (1967): The use of apatite and sphene for fission-track age determinations. - Bulletin Geological Society of America **78**: 1523-1526.

Naeser, C. W. and H. Faul (1969): Fission track annealing in apatite and sphene. - J. Geophys. Res. **74**: 705-710.

Neubauer, F. (1994): Kontinentkollision in den Ostalpen. - Geowissenschaften **12**: 136-140.

Neubauer, F., J. Genser, W. Kurz and X. Wang (1999): Exhumation of the Tauern Window, Eastern Alps. - Phys. Chem. Earth **24/8**: 675-680.

Nicolaysen, L. O. (1961): Graphic interpretation of discordant age measurements on metamorphic rocks. - Anal. N.Y. Ac. Sci. **91/2**: 198-206.

Parrish, R. R. (1983): Cenozoic thermal evolution and tectonics of the Coast Mountains of British Columbia 1. Fission track dating, apparent uplift rates, and patterns of uplift. - Tectonics **2**: 601-631.

Perchuk, L. L. and I. V. Lavrent'eva (1983): Experimental investigation of exchange equilibria in the system cordierite-garnet-biotite. - in: SAXENA, S.K. (eds): Kinetics and equilibrium in mineral reactions. New York, Springer**:** 199-239.

Piber, A. and P. Tropper (2001): Is there a high-pressure low-temperature metamorphism in the Austroalpine basement north of the Tauern window, Eastern Alps? - Geol. Paläont. Mitt. Innsb. **25**: 161-162.

Price, P. B. and R. M. Walker (1963): Fossil tracks of charged particles in mica and the age minerals. - Journal of Geophysical Research, B, Solid Earth and Planets **68**: 4847-4862.

Prochaska, W. (1981): Einige Ganggesteine der Rieserfernerintrusion mit neuen radiometrischen Altersdaten. - Mitt. Ges. Geol. Bergbaustud. Wien **27**: 161-171.

Purdy, J. W. and E. Jäger (1976): K-Ar ages on rock forming minerals from the Central Alps. - Mem. Ist. Geol. Min. Univ. Padova **30**: 1-31.

Raase, P. and G. Morteani (1976): The potassic feldspar in metamorphic rocks of the western Hohe Tauern area, Eatern Alps. - Geol. Rundschau **65**: 422-436.

Raith, M., P. Raase, H. Kreuzer and P. Müller (1978): The age of the Alpidic metamorphism in the western Tauern window, Austrian Alps, according to radiometric dating. - in: CLOSS, H.D.; ROEDER, D. & SCHMIDT, D. (eds.): Alps, Apennines, Hellenides: 140-148.

Ratschbacher, L., W. Frisch, H. G. Linzer and O. Merle (1991): Lateral extrusion in the Eastern Alps, part 2: Structural analysis. - Tectonics **10**: 257-271.

Ratschbacher, L., W. Frisch, F. Neubauer, S. M. Schmid and J. Neugebauer (1989): Extension in compressional orogenic belts: The eastern Alps. - Geology **17**: 404-407.

Ratschbacher, L., W. Frisch and U. Ring (1987): Stacking, dispersion and extension as a consequence of Alpine transpression in the eastern Alps. - Terra Cognita **7**: 118.

Rickwood, P. C. (1968): On recasting analyses of garnet into end-member molecules. - Contrib. Mineral. Petrol. **18/2**: 175-198.

Rockenschaub, M. and B. Kolenprat (1998): Polyphase Entwicklung der Innsbrucker Quarzphyllite Zone und des Patscherkofel Kristallins (Ostalpen): Variszische, permische und alpine Metamorphose? - Tagung Tektonik Strukturgeologie Kristallingeologie (TSK) 7, Abstracts: 2.

Ryburn, R. J., A. Raheim and D. H. Green (1976): Determination of the P-T path of natural eclogites during metamorphism - record of subduction. - Lithos **9**: 161-164.

Sassi, F. P., F. Neubauer, C. Mazzoli, R. Sassi, R. Spiess and G. Zirpoli (1994): Tentative Comparison of the Paleozoic Evolution of the Austroalpine and Southalpine Quarzphyllites in the Eastern Alps. - Per. Mineral. **63**: 35-52.

Satir, M. (1975): Die Entwicklungsgeschichte der westlichen Hohen Tauern und der südlichen Ötztalmasse aufgrund radiometrischer Altersbestimmungen. - Mem. Ist. Geol. Min. Univ. Padova **30**: 1-84.

Satir, M. and G. Morteani (1979): Kaledonische, herzynische und alpidische Ereignisse im Mittelostalpin nördlich der westlichen Hohen Tauern, abgeleitet aus petrographischen und geochronologischen Untersuchungen. - Geol. Rundschau **68**: 1-40.

Schliestedt, M. (1980): Phasengleichgewichte in Hochdruckgesteinen von Sifnos, Griechenland. - TU Braunschweig, Germany, unpubl. Ph.D., pp143.

Schmidt, S. M. and E. Kissling (1997): A step towards a better understanding of the Alpine arc: The transition Central Alps - Western Alps in the light of new geological and geophysical data. - Quaderni di Geodinamica Alpina e Quaternaria **4**: 110-113.

Schulz, B. (1988): Deformation, Metamorphose und Petrographie im ostalpinen Altkristallin südlich des Tauernfensters (südliche Deferegger Alpen, Österreich). - Univ. Nürnberg-Erlangen, Germany, unpubl. Ph.D., pp134.

Schulz, B. (1989): Jungalpidische Gefügeentwicklung entlang der Defereggen-Antholz-Vals-Linie (Osttirol, Österreich). - Jb. Geol. Bundesanst. **132/4**: 775-789.

Schulz, B. (1994): Geologische Karte des Altkristallins östlich des Tauferer Tals (Südtirol). - Erlanger Geol. Abh. **124**: 1-28.

Selverstone, J. (1985): Petrologic constraints on imbrication, metamorphism and uplift in the SW Tauern Window, Eastern Alps. - Tectonics **4**: 687-704.

Selverstone, J. (1988): Evidence for east-west crustal extension in the Eastern Alps. - Tectonics **7**: 87-105.

Selverstone, J. (1993): Micro- to macroscale interactions between deformational and metamorphic processes, Tauern Window, Eastern Alps. - Schweiz. Mineral. Petrogr. Mitt. **73**: 229-239.

Selverstone, J. and F. S. Spear (1985): Metamorphic P-T paths from pelitic schists and greenstones in the southwest Tauern Window, Eastern Alps. - J. Metamorphic Geol. **3**: 439-465.

Selverstone, J., F. S. Spear, G. Franz and G. Morteani (1984): High-pressure metamorphism in the SW Tauern Window, Austria: P-T paths from hornblende-kyanite-staurolite schists. - J. Petrol. **25**: 501-531.

Seward, D. (1993): Fission-track analysis with special Reference to uplift/cooling histories of mountain belts. - Proceedings of the VI Summer School Earth and Planetary Sciences, Sienna.: 149-166.

Steenken, A., S. Siegesmund, T. Heinrichs and B. Fügenschuh (2002): Cooling and exhumation of the Rieserferner Pluton (Eastern Alps, Italy/Austria). - Geol. Rundschau **91**: 799-817.

Steiger, R. H. and E. Jäger (1977): Subcommission on Geochronology: Convention on the use of decay constants in geo- and cosmochronolgy. - Earth and Planetary Science Letters **36**: 359-362.

Stöckhert, B. (1982): Deformation und retrograde Metamorphose im Altkristallin S' des westlichen Tauernfensters (Südtirol). - Univ. Nürnberg-Erlangen, Germany, unpubl. Ph.D., pp214.

Stöckhert, B. (1984): K-Ar determinations on muscovites and phengites from deformed pegmatites, and the minimum age of the Old Alpine deformation in the Austridic basement to the south of the western Tauern Window (Ahrn valley, Southern Tyrol, Eastern Alps). - N. Jb. Miner. Abh. **150**: 103-120.

Stöckhert, B. (1985): Pre-Alpine history of the Austridic basement to the south of the western Tauern Window (Southern Tyrol, Italy) - Caledonian versus Hercynian event. - N. Jb. Geol. Paläont. Mh. **10**: 618-642.

Stöckhert, B. (1987): Das Uttenheimer Pegmatit-Feld (Ostalpines Altkristallin, Südtirol) Genese und alpine Überprägung. - Erlanger Geol. Abh. **114**: 83-106.

Stöckhert, B., M. R. Brix, R. Kleinschrodt, A. J. Hurford and R. Wirth (1999): Thermochronometry and microstructures of quartz - a comparison with experimental flow laws and predictions on the temperature of the brittle - plastic transition. - J. Struct. Geol. **21**: 351-369.

Stormer, J. C., M. L. Pierson and R. C. Tacker (1993): Variation of F and Cl X-ray intensity due to anisotropic diffusion in apatite during electron microprobe analysis. - American Mineralogist **78**: 641-648.

Stüwe, K., L. White and R. Brown (1994): The influence of eroding topography on steady-state isotherms: application to fission track analysis. - Earth Planet. Sci. Lett. **124**: 63-74.

Thiele, O. (1970): Zur Stratigraphie und Tektonik der Schieferhülle der westlichen Hohen Tauern. - Verh. Geol. B.A. **1970**: 230-244.

Thompson, A. B., R. J. Tracy, P. T. Lyttle and J. B. Thompson jr. (1977): Retrograde reaction histories deduced from compositional zonation and mineral inclusions in garnet from the Gassetts Schist, Vermont. - Am. J. Sci. **277**: 1152-1167.

Tollmann, A. (1977): Geologie von Österreich.,

Tracy, R. J. (1982): Compositional zoning and inclusions in metamorphic minerals. - in: FERRY, J.M. (eds.): Characterization of Metamorphism through Mineral Equilibria. Mineral. Soc. Am. Rev. Mineralogy **10**: 355-397.

Tracy, R. J., P. Robinson and A. B. Thompson (1976): Garnet composition and and zoning in the determination of temperature and pressure of metamorphism, central Massachusetts. - American Mineralogist **61**: 762-775.

TRANSALP Working Group (2002): First deep seismic reflection images of the Eastern Alps reveal giant crustal wedges and transcrustal ramps. - Geoph. Res. Letters **29/10**: 92-1 - 92-4.

Trzciensky jr., W. E. (1977): Garnet zoning - product of a continuous reaction. - Can. Mineral. **15**: 250-256.

Velde, B. (1965): Phengite micas: Synthesis, stability and natural occurence. - Am. J. Sci. **263**: 886-913.

Villa, I. M. (1998): Isotopic closure. - Terra Nova **10**: 42-47.

Wagner, G. A. (1968): Fission-track dating of apatites. - Earth and Planetary Science Letters **4**: 411-414.

Wagner, G. A., G. M. Reimer and E. Jäger (1977): Cooling ages derived by apatite fission-track, mica Rb-Sr and K-Ar dating: the uplift and cooling history of the Central Alps. - Mem. Ist. Geol. Min. Univ. Padova **30**: 1-27.

Wagner, G. A. and P. Van den Haute (1992): Fission-track dating. Enke, pp285.

Weger, M. (1997): Duktile Kinematik kontinentaler Kruste am Beispiel der Zentralgneise des westlichen Tauernfensters. - Univ. München, Germany, unpubl. Ph.D., pp254.

Wendt, I. (1986): Radiometrische Methoden in der Geochronologie. - C.T.H **23**: 1-170.

Woodsworth, G. J. (1977): Homogenization of zoned garnets from pelitic schists. - Can. Mineral. **15**: 230-242.

Yamada, R., T. Yoshioka, K. Watanabe, T. Tagami, H. Nakamura, T. Hashimoto and S. Nishimura (1998): Comparison of experimentel techniques to increase the number of measurable confined fission tracks in zircon. - Chemical Geology **149/2**: 99-107.

Yardley, B. W. D. (1977): An emirical study of diffusion in garnet. - American Mineralogist **62**: 793-800.

York, D. (1966): Leastsquares fitting of a straight line. - Can. J. Phys. **44**: 1079-1086.

Zaun, P. E. and G. A. Wagner (1985): Fission-track stability in zircons under geological conditions. - Nucl. Tracks **10**: 303-307.

Zimmermann, R., K. Hammerschmidt and G. Franz (1994): Eocene high pressure metamorphism in the Penninic units of the Tauern Window (Eastern Alps), evidence from 40Ar-39Ar dating and petrological investigations. - Contrib. Mineral. Petrol. **117**: 175-186.

Appendix Tab. A1: Electron microprobe analysis of garnet.

Sample	45AnTA	45AnTA	45AnTA	45AnTA	45AnTA	45AnTA	45AnTA	45AnTA	45AnTA	45AnTA	45AnTA	45AnTA	45AnTA	45AnTA	45AnTA	45AnTA	45AnTA	45AnTA	45AnTA
Analysis	grt1-1	grt1-2	grt1-3	grt1-4	grt1-5	grt1-6	grt1-7	grt1-8	grt1-9	grt1-10	grt1-11	grt1-12	grt1-13	grt1-14	grt1-15	grt1-16	grt1-17	grt1-18	grt1-19
SiO2	38.75	38.83	38.57	38.84	38.73	38.84	38.69	38.54	38.77	38.58	38.64	38.83	38.65	38.54	38.58	38.46	38.72	38.81	38.62
Al2O3	21.10	21.18	21.35	21.20	20.99	21.02	21.13	21.03	21.17	21.02	21.06	20.87	20.87	21.12	21.07	21.13	20.93	21.04	20.97
TiO2	0.00	0.01	0.04	0.09	0.03	0.05	0.03	0.06	0.14	0.07	0.05	0.06	0.07	0.04	0.07	0.14	0.10	0.02	0.07
FeO	28.97	28.34	28.42	28.58	28.90	29.15	28.74	29.19	28.20	28.07	28.58	27.91	27.83	28.28	28.77	27.99	28.68	28.30	28.17
MgO	4.97	4.96	4.82	4.79	4.68	4.73	4.49	4.45	4.27	4.28	4.35	4.08	4.16	4.19	4.23	4.13	4.12	4.05	3.99
CaO	5.69	5.95	5.96	6.07	6.21	6.06	6.25	6.32	6.50	6.38	6.35	6.30	6.44	6.47	6.15	6.41	6.38	6.10	6.19
MnO	1.07	0.98	1.11	1.08	1.26	1.28	1.30	1.48	1.62	1.61	1.76	1.76	1.93	2.03	2.11	2.02	2.23	2.37	2.40
Total	100.55	100.25	100.27	100.66	100.80	101.13	100.63	101.07	100.67	100.01	100.79	99.81	99.95	100.67	100.98	100.28	101.16	100.69	100.41
FeO Ox	28.97	28.34	28.42	28.58	28.81	29.05	28.74	28.80	28.20	28.07	28.58	27.91	27.83	28.28	28.68	27.99	28.63	28.30	28.17
Fe2O3 Ox	0.00	0.00	0.00	0.00	0.10	0.11	0.00	0.43	0.00	0.00	0.00	0.00	0.00	0.00	0.10	0.00	0.05	0.00	0.00
Summe Ox	100.55	100.25	100.27	100.66	100.81	101.14	100.63	101.11	100.67	100.01	100.79	99.80	99.94	100.67	100.99	100.27	101.16	100.69	100.41
Number of ions on the basis of 12 O																			
Si	3.03	3.04	3.02	3.03	3.03	3.03	3.03	3.01	3.03	3.04	3.02	3.06	3.04	3.02	3.02	3.02	3.03	3.04	3.04
Al tot.	1.95	1.95	1.97	1.95	1.93	1.93	1.95	1.94	1.95	1.95	1.94	1.94	1.94	1.95	1.94	1.96	1.93	1.94	1.94
Ti	0.00	0.00	0.00	0.01	0.00	0.00	0.00	0.00	0.01	0.00	0.00	0.00	0.00	0.00	0.00	0.01	0.01	0.00	0.00
Fe tot.	1.89	1.85	1.86	1.87	1.89	1.90	1.88	1.91	1.84	1.85	1.87	1.84	1.83	1.85	1.88	1.84	1.88	1.86	1.85
Fe3+	0.00	0.00	0.00	0.00	0.01	0.01	0.00	0.03	0.00	0.00	0.00	0.00	0.00	0.00	0.01	0.00	0.00	0.00	0.00
Fe2+	1.89	1.85	1.86	1.87	1.88	1.89	1.88	1.88	1.84	1.85	1.87	1.84	1.83	1.85	1.88	1.84	1.87	1.86	1.85
Mg	0.58	0.58	0.56	0.56	0.55	0.55	0.52	0.52	0.50	0.50	0.51	0.48	0.49	0.49	0.49	0.48	0.48	0.47	0.47
Ca	0.48	0.50	0.50	0.51	0.52	0.51	0.52	0.53	0.54	0.54	0.53	0.53	0.54	0.54	0.52	0.54	0.53	0.51	0.52
Mn	0.07	0.07	0.07	0.07	0.08	0.08	0.09	0.10	0.11	0.11	0.12	0.12	0.13	0.13	0.14	0.13	0.15	0.16	0.16
Total cat	8.00	7.99	7.99	7.99	8.00	8.00	8.00	8.01	7.98	7.98	8.00	7.97	7.98	8.00	8.00	7.99	8.00	7.98	7.99
Andradite	0.00	0.00	0.00	0.00	0.47	0.50	0.00	1.93	0.00	0.00	0.00	0.00	0.00	0.00	0.44	0.00	0.23	0.00	0.00
Pyrope	19.85	19.74	19.03	19.04	18.70	18.87	17.91	17.49	17.00	17.16	17.41	16.48	16.80	16.72	16.84	16.47	16.55	16.22	16.04
Spessartine	2.44	2.23	2.49	2.45	2.87	2.90	2.95	3.31	3.67	3.67	4.00	4.04	4.43	4.60	4.78	4.58	5.09	5.40	5.48
Grossular	16.34	17.02	16.91	17.35	17.37	16.88	17.92	15.93	18.60	18.39	18.27	18.29	18.70	18.56	17.17	18.38	18.20	17.57	17.89
Almandine	61.37	61.02	61.57	61.16	60.59	60.85	61.22	61.35	60.73	60.78	60.32	61.19	60.07	60.11	60.77	60.57	59.93	60.82	60.60
% Rest	2.70	2.18	1.34	2.34	2.85	2.96	2.45	1.29	2.24	2.31	2.81	2.69	2.86	2.37	2.36	1.94	3.31	2.61	2.64
Xprp = XMg	0.19	0.19	0.19	0.19	0.18	0.18	0.17	0.17	0.17	0.17	0.17	0.16	0.16	0.16	0.16	0.16	0.16	0.16	0.16
Xalm = XFe	0.63	0.62	0.62	0.62	0.62	0.63	0.62	0.62	0.62	0.62	0.62	0.62	0.61	0.61	0.62	0.61	0.62	0.62	0.62
Xsps = XMn	0.02	0.02	0.02	0.02	0.03	0.03	0.03	0.03	0.04	0.04	0.04	0.04	0.04	0.04	0.05	0.04	0.05	0.05	0.05
Xgrs = XCa	0.16	0.17	0.17	0.17	0.17	0.17	0.17	0.17	0.18	0.18	0.18	0.18	0.18	0.18	0.17	0.18	0.18	0.17	0.17
XAl	1.00	1.00	1.00	1.00	1.00	1.00	1.00	1.00	1.00	1.00	1.00	1.00	1.00	1.00	1.00	1.00	1.00	1.00	1.00

Appendix Tab. A1: Electron microprobe analysis of garnet.

Sample	45AnTA	45AnTA	45AnTA	45AnTA	45AnTA	45AnTA	45AnTA	45AnTA	45AnTA	45AnTA	45AnTA	45AnTA	45AnTA	45AnTA	45AnTA	45AnTA	45AnTA	45AnTA	45AnTA
Analysis	grt1-20	grt1-21	grt1-22	grt1-23	grt1-24	grt1-25	grt1-26	grt1-27	grt1-28	grt1-29	grt1-30	grt1-31	grt1-32	grt1-33	grt1-34	grt1-35	grt1-36	grt1-37	grt1-38
SiO2	38.60	38.38	38.53	38.70	38.62	38.76	38.29	38.33	38.78	38.90	38.65	38.38	38.39	38.42	38.34	38.51	38.47	38.42	38.63
Al2O3	20.75	20.85	21.07	21.13	20.94	21.10	20.99	20.69	21.02	21.15	20.97	21.00	21.29	21.26	21.05	21.12	21.09	20.99	20.82
TiO2	0.12	0.11	0.10	0.05	0.07	0.10	0.01	0.01	0.14	0.07	0.11	0.14	0.15	0.08	0.06	0.08	0.10	0.15	0.06
FeO	27.89	28.23	28.03	28.82	27.98	28.27	27.53	28.07	28.04	28.16	27.98	28.08	27.81	27.59	27.72	28.03	28.00	27.83	27.44
MgO	3.99	4.02	3.85	3.95	3.90	3.79	3.68	3.82	3.65	3.70	3.64	3.64	3.62	3.48	3.56	3.63	3.58	3.59	3.53
CaO	6.46	6.21	6.63	6.27	6.40	6.21	6.50	6.16	6.55	6.55	6.47	6.33	6.59	6.51	6.63	6.31	6.57	6.34	6.52
MnO	2.48	2.50	2.50	2.60	2.70	2.73	2.78	2.96	2.90	2.95	2.94	3.06	2.96	3.13	2.89	3.11	3.04	3.07	3.16
Total	100.29	100.30	100.71	101.52	100.61	100.96	99.78	100.04	101.08	101.48	100.76	100.63	100.81	100.47	100.25	100.79	100.85	100.39	100.16
FeO Ox	27.89	28.23	28.03	28.68	27.98	28.27	27.53	28.07	28.04	28.16	27.98	28.08	27.81	27.59	27.72	28.03	28.00	27.83	27.44
Fe2O3 Ox	0.00	0.00	0.00	0.15	0.00	0.00	0.00	0.00	0.00	0.00	0.00	0.00	0.00	0.00	0.00	0.00	0.00	0.00	0.00
Summe Ox	100.29	100.30	100.71	101.53	100.61	100.96	99.78	100.04	101.07	101.48	100.75	100.63	100.81	100.47	100.25	100.79	100.84	100.39	100.16
Number of ions on the basis of 12 O																			
Si	3.04	3.03	3.02	3.02	3.03	3.04	3.03	3.04	3.04	3.03	3.04	3.02	3.01	3.02	3.03	3.03	3.02	3.03	3.05
Al tot.	1.93	1.94	1.95	1.94	1.94	1.95	1.96	1.93	1.94	1.94	1.94	1.95	1.97	1.97	1.96	1.96	1.95	1.95	1.94
Ti	0.01	0.01	0.01	0.00	0.00	0.01	0.00	0.00	0.01	0.00	0.01	0.01	0.01	0.00	0.00	0.00	0.01	0.01	0.00
Fe tot.	1.84	1.86	1.84	1.88	1.84	1.85	1.82	1.86	1.84	1.84	1.84	1.85	1.83	1.82	1.83	1.84	1.84	1.83	1.81
Fe3+	0.00	0.00	0.00	0.01	0.00	0.00	0.00	0.00	0.00	0.00	0.00	0.00	0.00	0.00	0.00	0.00	0.00	0.00	0.00
Fe2+	1.84	1.86	1.84	1.87	1.84	1.85	1.82	1.86	1.84	1.84	1.84	1.85	1.83	1.82	1.83	1.84	1.84	1.83	1.81
Mg	0.47	0.47	0.45	0.46	0.46	0.44	0.43	0.45	0.43	0.43	0.43	0.43	0.42	0.41	0.42	0.43	0.42	0.42	0.42
Ca	0.55	0.52	0.56	0.52	0.54	0.52	0.55	0.52	0.55	0.55	0.54	0.53	0.55	0.55	0.56	0.53	0.55	0.54	0.55
Mn	0.17	0.17	0.17	0.17	0.18	0.18	0.19	0.20	0.19	0.19	0.20	0.20	0.20	0.21	0.19	0.21	0.20	0.21	0.21
Total cat	7.99	8.00	7.99	8.00	7.99	7.98	7.99	8.00	7.99	7.99	7.99	7.99	7.99	7.98	7.99	7.99	8.00	7.99	7.98
Andradite	0.00	0.00	0.00	0.69	0.00	0.00	0.00	0.00	0.00	0.00	0.00	0.00	0.00	0.00	0.00	0.00	0.00	0.00	0.00
Pyrope	16.21	16.25	15.40	15.65	15.70	15.14	14.78	15.56	14.63	14.74	14.63	14.61	14.33	13.79	14.25	14.48	14.31	14.41	14.29
Spessartine	5.72	5.74	5.68	5.85	6.18	6.20	6.34	6.85	6.61	6.68	6.72	6.98	6.66	7.05	6.58	7.05	6.90	7.01	7.27
Grossular	18.86	18.05	19.07	17.16	18.52	17.83	18.76	18.04	18.88	18.76	18.69	18.26	18.76	18.55	19.08	18.10	18.88	18.30	18.98
Almandine	59.21	59.96	59.85	60.65	59.61	60.83	60.12	59.55	59.88	59.81	59.96	60.15	60.26	60.60	60.09	60.36	59.91	60.28	59.47
% Rest	3.54	3.05	2.44	2.17	2.92	2.42	1.88	3.40	2.85	2.66	2.76	2.46	1.40	1.16	1.95	2.09	2.28	2.29	2.88
Xprp = XMg	0.16	0.16	0.15	0.15	0.15	0.15	0.14	0.15	0.14	0.14	0.14	0.14	0.14	0.14	0.14	0.14	0.14	0.14	0.14
Xalm = XFe	0.61	0.62	0.61	0.62	0.61	0.62	0.61	0.61	0.61	0.61	0.61	0.61	0.61	0.61	0.61	0.61	0.61	0.61	0.61
Xsps = XMn	0.05	0.06	0.06	0.06	0.06	0.06	0.06	0.07	0.06	0.06	0.07	0.07	0.07	0.07	0.06	0.07	0.07	0.07	0.07
Xgrs = XCa	0.18	0.17	0.18	0.17	0.18	0.17	0.18	0.17	0.18	0.18	0.18	0.18	0.18	0.18	0.19	0.18	0.18	0.18	0.18
XAl	1.00	1.00	1.00	1.00	1.00	1.00	1.00	1.00	1.00	1.00	1.00	1.00	1.00	1.00	1.00	1.00	1.00	1.00	1.00

Appendix Tab. A1: Electron microprobe analysis of garnet.

Sample	45AnTA	45AnTA	45AnTA	45AnTA	45AnTA	45AnTA	45AnTA	45AnTA	45AnTA	45AnTA	45AnTA	45AnTA	45AnTA	45AnTA	45AnTA	45AnTA	45AnTA	45AnTA	45AnTA
Analysis	grt1-39	grt1-40	grt1-41	grt1-42	grt1-43	grt1-44	grt1-45	grt1-46	grt1-47	grt1-48	grt1-49	grt1-50	grt1-51	grt1-52	grt1-53	grt1-54	grt1-55	grt1-56	grt1-57
SiO2	38.60	38.43	37.80	38.53	38.60	38.23	38.15	38.46	38.47	38.46	38.81	38.50	38.60	38.37	38.42	38.47	38.51	38.63	38.49
Al2O3	21.08	21.02	20.32	21.11	20.93	20.91	21.06	21.16	21.03	21.12	21.39	20.97	21.22	21.18	21.08	21.32	20.95	21.23	21.08
TiO2	0.12	0.03	0.10	0.16	0.09	0.09	0.06	0.04	0.13	0.10	0.62	0.11	0.06	0.06	0.02	0.16	0.05	0.10	0.11
FeO	27.79	27.66	27.31	28.25	28.16	28.43	27.59	28.02	28.23	28.12	26.90	27.75	27.92	28.39	27.99	27.88	27.59	28.01	27.97
MgO	3.52	3.54	3.49	3.55	3.55	3.65	3.51	3.54	3.65	3.66	3.44	3.62	3.81	3.67	3.78	3.71	3.76	3.85	3.88
CaO	6.58	6.45	6.28	6.56	6.33	6.39	6.66	6.64	6.26	6.27	6.41	6.54	6.36	6.33	6.68	6.70	6.38	6.44	6.36
MnO	3.14	3.12	3.05	3.00	3.09	3.18	3.09	3.12	3.09	3.08	3.00	3.02	2.97	2.83	2.81	2.74	2.75	2.71	2.62
Total	100.83	100.25	98.35	101.16	100.75	100.88	100.12	100.98	100.86	100.81	100.57	100.51	100.94	100.83	100.78	100.98	99.99	100.97	100.51
FeO Ox	27.79	27.66	27.31	28.25	28.16	28.06	27.59	28.02	28.23	28.12	26.90	27.75	27.92	28.39	27.88	27.88	27.59	28.01	27.97
Fe2O3 Ox	0.00	0.00	0.00	0.00	0.00	0.41	0.00	0.00	0.00	0.00	0.00	0.00	0.00	0.00	0.13	0.00	0.00	0.00	0.00
Summe Ox	100.82	100.25	98.35	101.16	100.75	100.92	100.12	100.98	100.85	100.81	100.57	100.51	100.94	100.83	100.80	100.97	99.99	100.96	100.51
Number of ions on the basis of 12 O																			
Si	3.03	3.03	3.04	3.02	3.04	3.01	3.02	3.02	3.02	3.02	3.04	3.03	3.02	3.02	3.02	3.01	3.04	3.02	3.03
Al tot.	1.95	1.96	1.93	1.95	1.94	1.94	1.96	1.96	1.95	1.96	1.97	1.95	1.96	1.96	1.95	1.97	1.95	1.96	1.95
Ti	0.01	0.00	0.01	0.01	0.01	0.01	0.00	0.00	0.01	0.01	0.04	0.01	0.00	0.00	0.00	0.01	0.00	0.01	0.01
Fe tot.	1.82	1.83	1.84	1.85	1.85	1.87	1.83	1.84	1.86	1.85	1.76	1.83	1.83	1.87	1.84	1.83	1.82	1.83	1.84
Fe3+	0.00	0.00	0.00	0.00	0.00	0.02	0.00	0.00	0.00	0.00	0.00	0.00	0.00	0.00	0.01	0.00	0.00	0.00	0.00
Fe2+	1.82	1.83	1.84	1.85	1.85	1.85	1.83	1.84	1.86	1.85	1.76	1.83	1.83	1.87	1.83	1.83	1.82	1.83	1.84
Mg	0.41	0.42	0.42	0.41	0.42	0.43	0.41	0.41	0.43	0.43	0.40	0.42	0.44	0.43	0.44	0.43	0.44	0.45	0.45
Ca	0.55	0.55	0.54	0.55	0.53	0.54	0.56	0.56	0.53	0.53	0.54	0.55	0.53	0.53	0.56	0.56	0.54	0.54	0.54
Mn	0.21	0.21	0.21	0.20	0.21	0.21	0.21	0.21	0.21	0.21	0.20	0.20	0.20	0.19	0.19	0.18	0.18	0.18	0.17
Total cat	7.99	7.99	7.99	8.00	7.99	8.01	8.00	8.00	8.00	7.99	7.94	7.99	7.99	8.00	8.00	7.99	7.98	7.99	7.99
Andradite	0.00	0.00	0.00	0.00	0.00	1.83	0.00	0.00	0.00	0.00	0.00	0.00	0.00	0.00	0.57	0.00	0.00	0.00	0.00
Pyrope	14.07	14.19	14.47	14.17	14.29	14.44	14.05	14.10	14.63	14.60	13.84	14.55	15.13	14.60	15.03	14.67	15.13	15.28	15.51
Spessartine	7.13	7.11	7.19	6.81	7.07	7.15	7.03	7.06	7.04	6.99	6.86	6.90	6.70	6.40	6.35	6.16	6.29	6.11	5.95
Grossular	18.91	18.59	18.73	18.83	18.33	16.35	19.16	19.01	18.04	17.99	18.55	18.90	18.16	18.11	18.52	19.04	18.45	18.38	18.28
Almandine	59.88	60.10	59.61	60.19	60.31	60.23	59.76	59.82	60.30	60.42	60.75	59.66	60.00	60.89	59.53	60.14	60.13	60.22	60.25
% Rest	2.29	2.05	3.39	2.43	2.84	1.25	1.75	2.08	2.52	2.10	2.73	2.55	1.92	1.87	1.86	1.50	2.27	1.94	2.19
Xprp = XMg	0.14	0.14	0.14	0.14	0.14	0.14	0.14	0.14	0.14	0.14	0.14	0.14	0.15	0.14	0.15	0.14	0.15	0.15	0.15
Xalm = XFe	0.61	0.61	0.61	0.61	0.62	0.61	0.61	0.61	0.62	0.61	0.61	0.61	0.61	0.62	0.61	0.61	0.61	0.61	0.61
Xsps = XMn	0.07	0.07	0.07	0.07	0.07	0.07	0.07	0.07	0.07	0.07	0.07	0.07	0.07	0.06	0.06	0.06	0.06	0.06	0.06
Xgrs = XCa	0.18	0.18	0.18	0.18	0.18	0.18	0.19	0.18	0.17	0.18	0.19	0.18	0.18	0.18	0.19	0.19	0.18	0.18	0.18
XAl	1.00	1.00	1.00	1.00	1.00	1.00	1.00	1.00	1.00	1.00	1.00	1.00	1.00	1.00	1.00	1.00	1.00	1.00	1.00

Appendix Tab. A1: Electron microprobe analysis of garnet.

Sample	45AnTA	45AnTA	45AnTA	45AnTA	45AnTA	45AnTA	45AnTA	45AnTA	45AnTA	45AnTA	45AnTA	45AnTA	45AnTA	45AnTA	45AnTA	45AnTA	45AnTA	45AnTA	45AnTA
Analysis	grt1-58	grt1-59	grt1-60	grt1-61	grt1-62	grt1-63	grt1-64	grt1-65	grt1-66	grt1-67	grt1-68	grt1-69	grt1-70	grt1-71	grt1-72	grt1-73	grt1-74	grt1-75	grt1-76
SiO2	38.49	38.75	38.13	38.49	38.30	37.94	38.20	38.07	38.08	38.16	38.28	38.14	37.91	37.77	37.95	38.18	38.19	38.45	38.73
Al2O3	21.10	21.08	21.34	21.22	21.13	21.39	21.34	21.17	21.32	21.18	21.26	21.16	21.25	21.40	21.45	21.37	21.32	21.29	21.48
TiO2	0.06	0.08	0.11	0.04	0.03	0.07	0.11	0.05	0.11	0.06	0.10	0.08	0.09	0.10	0.09	0.06	0.10	0.08	0.08
FeO	28.21	28.36	28.20	28.37	28.38	28.34	27.89	28.39	27.53	28.27	28.52	28.37	28.46	28.52	28.43	28.79	28.70	28.46	28.20
MgO	3.82	3.97	3.96	4.08	4.03	4.11	4.16	4.13	4.16	4.13	4.23	4.25	4.25	4.36	4.37	4.37	4.52	4.40	4.37
CaO	6.51	6.30	6.28	6.28	6.34	6.41	6.47	6.47	6.59	6.41	6.15	6.30	6.14	6.49	6.60	6.42	6.38	6.44	6.46
MnO	2.58	2.40	2.38	2.39	2.33	2.12	1.92	1.98	1.97	1.96	1.97	1.97	1.86	1.75	1.64	1.63	1.55	1.47	1.50
Total	100.77	100.94	100.40	100.87	100.54	100.38	100.09	100.26	99.76	100.17	100.51	100.27	99.96	100.39	100.53	100.82	100.76	100.59	100.82
FeO Ox	28.21	28.36	28.18	28.33	28.23	27.94	27.89	28.07	27.53	28.17	28.47	28.15	28.21	27.77	27.85	28.29	28.20	28.46	28.20
Fe2O3 Ox	0.00	0.00	0.01	0.04	0.16	0.44	0.00	0.36	0.00	0.11	0.05	0.24	0.28	0.83	0.65	0.55	0.55	0.00	0.00
Summe Ox	100.77	100.94	100.40	100.87	100.56	100.42	100.08	100.29	99.76	100.18	100.52	100.30	99.98	100.47	100.60	100.87	100.81	100.59	100.82
Number of ions on the basis of 12 O																			
Si	3.02	3.03	3.00	3.02	3.01	2.99	3.01	3.00	3.01	3.01	3.01	3.01	3.00	2.98	2.98	2.99	2.99	3.01	3.02
Al tot.	1.95	1.95	1.98	1.96	1.96	1.99	1.98	1.97	1.98	1.97	1.97	1.97	1.98	1.99	1.99	1.97	1.97	1.97	1.98
Ti	0.00	0.00	0.01	0.00	0.00	0.00	0.01	0.00	0.01	0.00	0.01	0.00	0.01	0.01	0.01	0.00	0.01	0.00	0.00
Fe tot.	1.85	1.86	1.86	1.86	1.87	1.87	1.84	1.87	1.82	1.86	1.87	1.87	1.88	1.88	1.87	1.89	1.88	1.86	1.84
Fe3+	0.00	0.00	0.00	0.00	0.01	0.03	0.00	0.02	0.00	0.01	0.00	0.01	0.02	0.05	0.04	0.03	0.03	0.00	0.00
Fe2+	1.85	1.86	1.86	1.86	1.86	1.84	1.84	1.85	1.82	1.86	1.87	1.85	1.86	1.83	1.83	1.85	1.85	1.86	1.84
Mg	0.45	0.46	0.46	0.48	0.47	0.48	0.49	0.49	0.49	0.49	0.50	0.50	0.50	0.51	0.51	0.51	0.53	0.51	0.51
Ca	0.55	0.53	0.53	0.53	0.53	0.54	0.55	0.55	0.56	0.54	0.52	0.53	0.52	0.55	0.56	0.54	0.54	0.54	0.54
Mn	0.17	0.16	0.16	0.16	0.16	0.14	0.13	0.13	0.13	0.13	0.13	0.13	0.12	0.12	0.11	0.11	0.10	0.10	0.10
Total cat	8.00	7.99	8.00	8.00	8.00	8.01	7.99	8.01	7.99	8.00	8.00	8.01	8.01	8.02	8.02	8.02	8.02	8.00	7.99
Andradite	0.00	0.00	0.07	0.17	0.74	1.98	0.00	1.59	0.00	0.49	0.23	1.10	1.24	3.74	2.88	2.45	2.45	0.00	0.00
Pyrope	15.26	15.87	15.63	16.18	15.96	16.14	16.43	16.18	16.44	16.35	16.73	16.74	16.71	17.20	17.16	17.06	17.64	17.42	17.15
Spessartine	5.86	5.45	5.34	5.39	5.24	4.73	4.31	4.41	4.43	4.41	4.43	4.41	4.16	3.92	3.66	3.62	3.44	3.31	3.34
Grossular	18.69	18.11	17.75	17.73	17.31	16.12	18.37	16.63	18.73	17.76	17.26	16.75	16.11	14.67	15.75	15.56	15.45	18.33	18.22
Almandine	60.19	60.57	61.21	60.54	60.76	61.02	60.89	61.19	60.40	60.99	61.35	61.01	61.78	60.46	60.54	61.31	61.02	60.95	61.29
% Rest	2.31	2.62	0.89	1.82	1.34	0.52	0.87	0.12	0.70	1.11	1.33	0.73	0.22	1.12	0.84	0.45	0.44	1.68	1.09
Xprp = XMg	0.15	0.15	0.15	0.16	0.16	0.16	0.16	0.16	0.16	0.16	0.16	0.16	0.17	0.17	0.17	0.17	0.17	0.17	0.17
Xalm = XFe	0.61	0.62	0.62	0.62	0.62	0.62	0.61	0.62	0.61	0.62	0.62	0.62	0.62	0.61	0.61	0.62	0.62	0.62	0.62
Xsps = XMn	0.06	0.05	0.05	0.05	0.05	0.05	0.04	0.04	0.04	0.04	0.04	0.04	0.04	0.04	0.04	0.04	0.03	0.03	0.03
Xgrs = XCa	0.18	0.18	0.18	0.17	0.18	0.18	0.18	0.18	0.19	0.18	0.17	0.18	0.17	0.18	0.18	0.18	0.18	0.18	0.18
XAl	1.00	1.00	1.00	1.00	1.00	1.00	1.00	1.00	1.00	1.00	1.00	1.00	1.00	1.00	1.00	1.00	1.00	1.00	1.00

Appendix Tab. A1: Electron microprobe analysis of garnet.

Sample	45AnTA	45AnTA	45AnTA	45AnTA	45AnTA	45AnTA	45AnTA	45AnTA	45AnTA	45AnTA	45AnTA	45AnTA	45AnTA	45AnTA	45AnTA	45AnTA	45AnTA	45AnTA	45AnTA
Analysis	grt1-77	grt1-78	grt1-79	grt1-80	grt1-81	grt1-82	grt1-83	grt1-84	grt1-85	grt1-86	grt2-1	grt2-2	grt2-3	grt2-4	grt2-5	grt2-6	grt2-7	grt2-8	grt2-9
SiO2	38.45	38.54	38.20	38.59	38.60	38.47	37.91	37.82	37.90	38.22	38.72	38.54	38.49	38.32	38.35	38.46	38.28	37.79	38.11
Al2O3	21.51	21.37	21.38	21.53	21.19	21.47	21.41	21.36	21.57	21.50	21.03	21.07	21.23	21.40	21.08	21.14	21.37	21.08	21.23
TiO2	0.07	0.06	0.07	0.03	0.01	0.05	0.05	0.08	0.06	0.01	0.04	0.08	0.01	0.08	0.10	0.06	0.07	0.07	0.07
FeO	28.90	28.75	28.52	28.91	28.28	28.60	28.25	28.49	28.52	28.65	27.77	28.01	28.31	27.68	27.63	28.08	27.74	27.83	28.61
MgO	4.48	4.46	4.52	4.45	4.53	4.51	4.67	4.62	4.76	4.79	4.13	4.18	4.05	3.97	4.01	3.96	3.87	3.93	3.78
CaO	6.56	6.02	6.29	6.52	6.22	6.24	6.26	6.48	5.98	6.12	6.36	6.22	6.37	6.62	6.35	6.34	6.44	6.53	6.48
MnO	1.45	1.50	1.39	1.35	1.34	1.32	1.23	1.22	1.20	1.21	2.06	2.16	2.21	2.42	2.31	2.46	2.55	2.51	2.57
Total	101.42	100.70	100.37	101.38	100.17	100.66	99.77	100.07	99.99	100.50	100.11	100.26	100.67	100.49	99.83	100.50	100.32	99.74	100.85
FeO Ox	28.42	28.75	28.31	28.65	28.28	28.60	27.94	27.85	28.18	28.29	27.77	28.01	28.31	27.68	27.63	28.08	27.74	27.50	28.20
Fe2O3 Ox	0.53	0.00	0.23	0.29	0.00	0.00	0.34	0.71	0.38	0.40	0.00	0.00	0.00	0.00	0.00	0.00	0.00	0.36	0.46
Summe Ox	101.47	100.70	100.39	101.41	100.17	100.66	99.80	100.14	100.02	100.54	100.11	100.26	100.67	100.49	99.83	100.50	100.32	99.78	100.89
Number of ions on the basis of 12 O																			
Si	2.99	3.02	3.00	3.00	3.03	3.01	2.99	2.98	2.98	2.99	3.04	3.03	3.02	3.01	3.03	3.02	3.01	3.00	3.00
Al tot.	1.97	1.97	1.98	1.97	1.96	1.98	1.99	1.99	2.00	1.99	1.95	1.95	1.96	1.98	1.96	1.96	1.98	1.97	1.97
Ti	0.00	0.00	0.00	0.00	0.00	0.00	0.00	0.00	0.00	0.00	0.00	0.00	0.00	0.00	0.01	0.00	0.00	0.00	0.00
Fe tot.	1.88	1.88	1.87	1.88	1.86	1.87	1.86	1.88	1.88	1.88	1.83	1.84	1.86	1.82	1.82	1.85	1.83	1.85	1.88
Fe3+	0.03	0.00	0.01	0.02	0.00	0.00	0.02	0.04	0.02	0.02	0.00	0.00	0.00	0.00	0.00	0.00	0.00	0.02	0.03
Fe2+	1.85	1.88	1.86	1.86	1.86	1.87	1.84	1.84	1.86	1.85	1.83	1.84	1.86	1.82	1.82	1.85	1.83	1.83	1.86
Mg	0.52	0.52	0.53	0.52	0.53	0.53	0.55	0.54	0.56	0.56	0.48	0.49	0.47	0.46	0.47	0.46	0.45	0.46	0.44
Ca	0.55	0.50	0.53	0.54	0.52	0.52	0.53	0.55	0.50	0.51	0.54	0.52	0.54	0.56	0.54	0.53	0.54	0.56	0.55
Mn	0.10	0.10	0.09	0.09	0.09	0.09	0.08	0.08	0.08	0.08	0.14	0.14	0.15	0.16	0.15	0.16	0.17	0.17	0.17
Total cat	8.02	8.00	8.01	8.01	7.99	8.00	8.01	8.02	8.01	8.01	7.98	7.99	8.00	8.00	7.98	7.99	7.99	8.01	8.01
Andradite	2.35	0.00	1.00	1.27	0.00	0.00	1.53	3.19	1.69	1.76	0.00	0.00	0.00	0.00	0.00	0.00	0.00	1.63	2.04
Pyrope	17.36	17.59	17.64	17.20	18.02	17.70	18.36	18.21	18.72	18.68	16.55	16.72	16.08	15.63	16.03	15.79	15.26	15.50	14.78
Spessartine	3.19	3.36	3.08	2.97	3.03	2.94	2.74	2.72	2.68	2.67	4.69	4.91	4.99	5.42	5.25	5.57	5.72	5.63	5.71
Grossular	15.93	17.07	16.64	16.84	17.79	17.61	16.16	15.17	15.22	15.40	18.32	17.89	18.18	18.74	18.25	18.17	18.26	16.88	16.18
Almandine	61.16	61.98	61.63	61.72	61.17	61.74	61.21	60.71	61.70	61.49	60.43	60.48	60.76	60.21	60.47	60.47	60.76	60.36	61.29
% Rest	0.42	1.38	0.11	0.09	1.83	0.99	0.42	0.88	0.66	0.33	2.28	2.19	1.79	0.89	1.69	1.97	0.77	0.18	0.24
Xprp = XMg	0.17	0.17	0.17	0.17	0.18	0.17	0.18	0.18	0.18	0.18	0.16	0.16	0.16	0.15	0.16	0.15	0.15	0.15	0.15
Xalm = XFe	0.62	0.63	0.62	0.62	0.62	0.62	0.62	0.62	0.62	0.62	0.61	0.61	0.62	0.61	0.61	0.61	0.61	0.61	0.62
Xsps = XMn	0.03	0.03	0.03	0.03	0.03	0.03	0.03	0.03	0.03	0.03	0.05	0.05	0.05	0.05	0.05	0.05	0.06	0.06	0.06
Xgrs = XCa	0.18	0.17	0.18	0.18	0.17	0.17	0.17	0.18	0.17	0.17	0.18	0.17	0.18	0.19	0.18	0.18	0.18	0.18	0.18
XAl	1.00	1.00	1.00	1.00	1.00	1.00	1.00	1.00	1.00	1.00	1.00	1.00	1.00	1.00	1.00	1.00	1.00	1.00	1.00

Appendix Tab. A1: Electron microprobe analysis of garnet.

Sample	45AnTA	45AnTA	45AnTA	45AnTA	45AnTA	45AnTA	45AnTA	45AnTA	45AnTA	45AnTA	45AnTA	45AnTA	45AnTA	45AnTA	45AnTA	45AnTA	45AnTA	45AnTA	45AnTA
Analysis	grt2-10	grt2-11	grt2-12	grt2-13	grt2-14	grt2-15	grt2-16	grt2-17	grt2-18	grt2-19	grt2-20	grt2-21	grt2-22	grt2-23	grt2-24	grt2-25	grt2-26	grt2-27	grt2-28
SiO2	38.26	38.03	37.86	38.23	38.15	38.21	37.95	37.99	37.69	38.26	38.06	37.60	38.24	37.96	38.36	38.40	38.15	38.06	37.80
Al2O3	21.26	21.16	21.14	21.15	21.21	21.15	21.29	21.30	20.90	21.16	20.97	21.07	21.00	21.06	21.10	20.99	21.19	21.25	21.22
TiO2	0.12	0.06	0.08	0.11	0.06	0.11	0.09	0.07	0.07	0.08	0.04	0.08	0.09	0.08	0.09	0.08	0.05	0.14	0.05
FeO	27.95	27.99	28.08	27.95	27.72	28.24	27.98	27.79	27.78	27.93	28.28	28.39	28.33	28.72	28.19	28.18	27.93	28.02	28.21
MgO	3.83	3.85	3.78	3.77	3.61	3.71	3.82	3.79	3.75	3.77	3.87	3.91	3.89	3.80	3.84	3.80	3.97	3.98	3.94
CaO	6.78	6.67	6.58	6.43	6.43	6.31	6.34	6.68	6.46	6.70	6.32	6.40	6.38	6.75	6.52	6.33	6.30	6.53	6.45
MnO	2.73	2.75	2.72	2.78	2.87	2.93	2.78	2.73	2.97	2.75	2.73	2.59	2.62	2.72	2.68	2.66	2.63	2.61	2.39
Total	100.93	100.51	100.24	100.42	100.05	100.66	100.25	100.35	99.62	100.65	100.27	100.04	100.55	101.09	100.78	100.44	100.22	100.59	100.06
FeO Ox	27.70	27.55	27.64	27.95	27.72	28.16	27.80	27.54	27.36	27.79	27.95	27.62	28.14	27.76	28.09	28.18	27.88	27.69	27.76
Fe2O3 Ox	0.27	0.48	0.49	0.00	0.00	0.09	0.20	0.28	0.46	0.15	0.37	0.85	0.21	1.06	0.11	0.00	0.06	0.36	0.50
Summe Ox	100.96	100.56	100.29	100.41	100.05	100.67	100.27	100.38	99.66	100.66	100.30	100.13	100.57	101.19	100.79	100.44	100.23	100.63	100.11
Number of ions on the basis of 12 O																			
Si	3.00	3.00	2.99	3.01	3.02	3.01	3.00	3.00	3.00	3.01	3.01	2.98	3.01	2.99	3.01	3.03	3.01	3.00	2.99
Al tot.	1.97	1.97	1.97	1.97	1.98	1.96	1.98	1.98	1.96	1.96	1.95	1.97	1.95	1.95	1.95	1.95	1.97	1.97	1.98
Ti	0.01	0.00	0.00	0.01	0.00	0.01	0.01	0.00	0.00	0.00	0.00	0.00	0.01	0.00	0.01	0.00	0.00	0.01	0.00
Fe tot.	1.83	1.85	1.86	1.84	1.83	1.86	1.85	1.83	1.85	1.84	1.87	1.88	1.87	1.89	1.85	1.86	1.84	1.84	1.87
Fe3+	0.02	0.03	0.03	0.00	0.00	0.01	0.01	0.02	0.03	0.01	0.02	0.05	0.01	0.06	0.01	0.00	0.00	0.02	0.03
Fe2+	1.82	1.82	1.83	1.84	1.83	1.85	1.84	1.82	1.82	1.83	1.85	1.83	1.85	1.83	1.85	1.86	1.84	1.82	1.84
Mg	0.45	0.45	0.45	0.44	0.43	0.44	0.45	0.45	0.45	0.44	0.46	0.46	0.46	0.45	0.45	0.45	0.47	0.47	0.46
Ca	0.57	0.56	0.56	0.54	0.54	0.53	0.54	0.56	0.55	0.56	0.54	0.54	0.54	0.57	0.55	0.53	0.53	0.55	0.55
Mn	0.18	0.18	0.18	0.19	0.19	0.20	0.19	0.18	0.20	0.18	0.18	0.17	0.17	0.18	0.18	0.18	0.18	0.17	0.16
Total cat	8.01	8.01	8.01	8.00	7.99	8.00	8.01	8.01	8.01	8.00	8.01	8.03	8.01	8.03	8.00	7.99	8.00	8.01	8.01
Andradite	1.22	2.15	2.18	0.00	0.00	0.39	0.89	1.24	2.07	0.67	1.65	3.83	0.95	4.74	0.52	0.00	0.25	1.60	2.23
Pyrope	15.00	15.09	14.88	15.02	14.34	14.72	15.00	14.87	14.83	14.91	15.30	15.50	15.46	14.92	15.26	15.26	15.75	15.58	15.53
Spessartine	6.08	6.13	6.09	6.30	6.48	6.61	6.21	6.09	6.67	6.18	6.13	5.83	5.92	6.07	6.05	6.07	5.93	5.81	5.36
Grossular	17.87	16.64	16.44	18.42	18.37	17.61	17.01	17.60	16.29	18.39	16.31	14.41	17.28	14.31	18.11	18.27	17.72	16.78	16.05
Almandine	59.84	59.99	60.41	60.26	60.81	60.66	60.89	60.20	60.13	59.84	60.61	60.43	60.39	59.96	60.06	60.40	60.35	60.22	60.83
% Rest	0.57	0.23	0.35	1.72	1.05	1.46	0.16	0.21	0.13	1.27	0.76	0.85	1.60	0.82	1.81	2.45	1.23	0.29	0.45
Xprp = XMg	0.15	0.15	0.15	0.15	0.14	0.14	0.15	0.15	0.15	0.15	0.15	0.15	0.15	0.14	0.15	0.15	0.15	0.15	0.15
Xalm = XFe	0.60	0.61	0.61	0.61	0.61	0.62	0.61	0.61	0.61	0.61	0.61	0.61	0.61	0.61	0.61	0.62	0.61	0.61	0.61
Xsps = XMn	0.06	0.06	0.06	0.06	0.06	0.06	0.06	0.06	0.07	0.06	0.06	0.06	0.06	0.06	0.06	0.06	0.06	0.06	0.05
Xgrs = XCa	0.19	0.19	0.18	0.18	0.18	0.18	0.18	0.19	0.18	0.19	0.18	0.18	0.18	0.18	0.18	0.18	0.18	0.18	0.18
XAl	1.00	1.00	1.00	1.00	1.00	1.00	1.00	1.00	1.00	1.00	1.00	1.00	1.00	1.00	1.00	1.00	1.00	1.00	1.00

Appendix Tab. A1: Electron microprobe analysis of garnet.

Sample	45AnTA	45AnTA	45AnTA	45AnTA	45AnTA	45AnTA	45AnTA	45AnTA	45AnTA	45AnTA	45AnTA	45AnTA	45AnTA	45AnTA	45AnTA	45AnTA	45AnTA	45AnTA	45AnTA
Analysis	grt2-29	grt2-30	grt2-31	grt2-32	grt2-33	grt2-34	grt2-35	grt2-36	grt2-37	grt2-38	grt2-39	grt2-40	grt2-41	grt2-42	grt2-43	grt3-1	grt3-2	grt3-3	grt3-4
SiO2	38.02	37.39	37.70	37.81	37.94	37.82	38.14	37.47	38.37	38.10	38.36	38.25	37.66	37.80	37.99	38.40	38.11	38.22	38.39
Al2O3	21.17	21.25	21.34	20.97	21.20	21.33	21.41	20.88	21.28	21.26	21.19	21.31	21.39	21.49	21.34	21.50	21.33	21.33	21.37
TiO2	0.05	0.04	0.06	0.12	0.05	0.07	0.04	0.07	0.06	0.13	0.09	0.03	0.09	0.10	0.03	0.02	0.05	0.03	0.08
FeO	28.24	28.27	28.72	28.60	28.37	28.26	28.73	28.27	27.65	27.95	27.99	27.97	28.46	28.54	28.27	28.82	28.72	28.72	28.82
MgO	4.02	3.99	4.09	4.00	4.14	4.05	4.22	4.09	4.08	4.06	3.97	4.05	4.11	4.19	4.14	4.93	4.89	4.76	4.71
CaO	6.29	6.64	6.20	6.21	6.01	6.36	6.03	6.36	6.65	6.58	6.77	6.38	6.24	6.32	6.33	5.80	5.82	5.89	6.07
MnO	2.51	2.45	2.35	2.45	2.25	2.34	2.30	2.28	2.33	2.32	2.15	2.31	2.33	2.32	2.20	0.98	1.04	1.17	1.12
Total	100.30	100.03	100.46	100.16	99.96	100.23	100.87	99.42	100.42	100.40	100.52	100.30	100.28	100.76	100.30	100.45	99.96	100.12	100.56
FeO Ox	27.90	27.18	27.92	28.03	28.16	27.78	28.29	27.50	27.65	27.76	27.99	27.97	27.77	27.76	27.91	28.75	28.49	28.58	28.72
Fe2O3 Ox	0.37	1.21	0.89	0.63	0.24	0.53	0.49	0.85	0.00	0.21	0.00	0.00	0.76	0.87	0.39	0.07	0.25	0.15	0.11
Summe Ox	100.33	100.15	100.55	100.22	99.98	100.28	100.92	99.50	100.41	100.42	100.52	100.30	100.35	100.84	100.34	100.46	99.98	100.14	100.57
Number of ions on the basis of 12 O																			
Si	3.00	2.97	2.98	2.99	3.00	2.99	2.99	2.99	3.01	3.00	3.01	3.01	2.98	2.97	2.99	3.00	3.00	3.01	3.01
Al tot.	1.97	1.99	1.99	1.96	1.98	1.99	1.98	1.96	1.97	1.97	1.96	1.98	1.99	1.99	1.98	1.98	1.98	1.98	1.97
Ti	0.00	0.00	0.00	0.01	0.00	0.00	0.00	0.00	0.00	0.01	0.01	0.00	0.01	0.01	0.00	0.00	0.00	0.00	0.00
Fe tot.	1.86	1.88	1.90	1.89	1.88	1.87	1.89	1.89	1.82	1.84	1.84	1.84	1.88	1.88	1.86	1.89	1.89	1.89	1.89
Fe3+	0.02	0.07	0.05	0.04	0.01	0.03	0.03	0.05	0.00	0.01	0.00	0.00	0.05	0.05	0.02	0.00	0.01	0.01	0.01
Fe2+	1.84	1.80	1.84	1.86	1.86	1.84	1.86	1.83	1.82	1.83	1.84	1.84	1.84	1.83	1.84	1.88	1.88	1.88	1.88
Mg	0.47	0.47	0.48	0.47	0.49	0.48	0.49	0.49	0.48	0.48	0.46	0.48	0.48	0.49	0.49	0.57	0.57	0.56	0.55
Ca	0.53	0.56	0.52	0.53	0.51	0.54	0.51	0.54	0.56	0.56	0.57	0.54	0.53	0.53	0.53	0.49	0.49	0.50	0.51
Mn	0.17	0.16	0.16	0.16	0.15	0.16	0.15	0.15	0.16	0.15	0.14	0.15	0.16	0.15	0.15	0.06	0.07	0.08	0.07
Total cat	8.01	8.04	8.03	8.02	8.01	8.02	8.01	8.03	8.00	8.01	8.00	8.00	8.02	8.03	8.01	8.00	8.01	8.00	8.00
Andradite	1.65	5.46	3.99	2.81	1.05	2.37	2.18	3.86	0.00	0.96	0.00	0.00	3.44	3.88	1.76	0.31	1.11	0.68	0.48
Pyrope	15.76	15.90	16.17	15.77	16.28	15.96	16.49	16.27	16.16	15.94	15.79	16.02	16.26	16.52	16.24	19.26	19.12	18.68	18.48
Spessartine	5.59	5.55	5.28	5.49	5.03	5.24	5.11	5.15	5.24	5.18	4.86	5.19	5.24	5.20	4.91	2.18	2.32	2.61	2.49
Grossular	16.07	13.57	13.63	14.79	15.94	15.65	14.76	14.33	18.94	17.62	19.36	18.14	14.32	14.04	16.10	15.98	15.25	15.93	16.64
Almandine	60.92	59.52	60.93	61.15	61.69	60.78	61.46	60.39	59.66	60.31	59.99	60.65	60.74	60.37	61.00	62.27	62.19	62.09	61.90
% Rest	0.10	1.52	1.10	0.40	0.17	0.62	0.42	0.70	1.43	0.47	1.85	1.11	1.08	1.23	0.32	0.54	0.09	0.52	0.93
Xprp = XMg	0.16	0.15	0.16	0.15	0.16	0.16	0.16	0.16	0.16	0.16	0.15	0.16	0.16	0.16	0.16	0.19	0.19	0.18	0.18
Xalm = XFe	0.61	0.61	0.62	0.62	0.62	0.61	0.62	0.61	0.60	0.61	0.61	0.61	0.62	0.61	0.61	0.63	0.63	0.63	0.62
Xsps = XMn	0.06	0.05	0.05	0.05	0.05	0.05	0.05	0.05	0.05	0.05	0.05	0.05	0.05	0.05	0.05	0.02	0.02	0.03	0.02
Xgrs = XCa	0.18	0.18	0.17	0.17	0.17	0.18	0.17	0.18	0.19	0.18	0.19	0.18	0.17	0.17	0.18	0.16	0.16	0.16	0.17
XAl	1.00	1.00	1.00	1.00	1.00	1.00	1.00	1.00	1.00	1.00	1.00	1.00	1.00	1.00	1.00	1.00	1.00	1.00	1.00

Appendix Tab. A1: Electron microprobe analysis of garnet.

Sample	45AnTA	45AnTA	45AnTA	45AnTA	45AnTA	45AnTA	45AnTA	45AnTA	45AnTA	45AnTA	45AnTA	45AnTA	45AnTA	45AnTA	45AnTA	45AnTA	45AnTA	45AnTA	45AnTA
Analysis	grt3-5	grt3-6	grt3-7	grt3-8	grt3-9	grt3-10	grt3-11	grt3-12	grt3-13	grt3-14	grt3-15	grt3-16	grt3-17	grt3-18	grt3-19	grt3-20	grt3-21	grt3-22	grt3-23
SiO2	38.20	38.23	38.12	37.61	37.73	37.69	37.86	37.81	37.89	37.85	38.13	38.01	37.73	37.95	37.92	37.86	38.38	38.28	38.24
Al2O3	21.15	21.25	21.22	21.53	21.44	21.28	21.37	21.40	21.41	21.31	21.24	21.43	21.41	21.15	21.28	21.23	21.18	21.43	21.21
TiO2	0.04	0.03	0.04	0.05	0.09	0.02	0.02	0.09	0.05	0.01	0.06	0.05	0.08	0.09	0.06	0.05	0.02	0.09	0.05
FeO	28.56	28.44	28.11	28.41	28.36	28.45	27.28	28.16	28.03	28.74	28.71	28.51	28.72	28.72	28.71	28.31	28.26	28.42	28.11
MgO	4.62	4.65	4.45	4.54	4.54	4.56	4.39	4.44	4.49	4.41	4.58	4.44	4.43	4.55	4.60	4.52	4.49	4.53	4.57
CaO	6.13	6.03	6.55	6.08	6.75	6.38	7.08	6.68	6.42	6.79	6.26	6.55	6.70	6.34	6.24	6.39	6.58	6.68	6.51
MnO	1.24	1.26	1.30	1.34	1.27	1.19	1.28	1.32	1.41	1.30	1.30	1.18	1.36	1.26	1.29	1.35	1.33	1.25	1.28
Total	99.94	99.89	99.79	99.56	100.17	99.57	99.28	99.90	99.70	100.41	100.28	100.17	100.43	100.06	100.10	99.71	100.24	100.68	99.97
FeO Ox	28.43	28.44	28.02	27.99	27.56	27.87	27.16	27.71	27.80	27.84	28.34	28.17	27.79	28.21	28.17	27.90	28.17	28.11	28.03
Fe2O3 Ox	0.15	0.00	0.10	0.47	0.88	0.64	0.13	0.50	0.25	1.00	0.41	0.38	1.03	0.57	0.60	0.45	0.10	0.34	0.09
Summe Ox	99.95	99.88	99.80	99.60	100.26	99.64	99.29	99.95	99.72	100.51	100.32	100.20	100.53	100.11	100.16	99.75	100.25	100.71	99.98
Number of ions on the basis of 12 O																			
Si	3.01	3.01	3.01	2.98	2.97	2.99	3.00	2.98	2.99	2.98	3.00	2.99	2.97	2.99	2.99	2.99	3.02	3.00	3.01
Al tot.	1.97	1.97	1.97	2.01	1.99	1.99	1.99	1.99	1.99	1.98	1.97	1.99	1.99	1.97	1.98	1.98	1.96	1.98	1.97
Ti	0.00	0.00	0.00	0.00	0.01	0.00	0.00	0.01	0.00	0.00	0.00	0.00	0.00	0.01	0.00	0.00	0.00	0.01	0.00
Fe tot.	1.88	1.87	1.85	1.88	1.87	1.88	1.81	1.86	1.85	1.89	1.89	1.88	1.89	1.90	1.89	1.87	1.86	1.86	1.85
Fe3+	0.01	0.00	0.01	0.03	0.05	0.04	0.01	0.03	0.01	0.06	0.02	0.02	0.06	0.03	0.04	0.03	0.01	0.02	0.01
Fe2+	1.87	1.87	1.85	1.85	1.82	1.85	1.80	1.83	1.84	1.83	1.86	1.85	1.83	1.86	1.86	1.85	1.85	1.84	1.85
Mg	0.54	0.55	0.52	0.54	0.53	0.54	0.52	0.52	0.53	0.52	0.54	0.52	0.52	0.54	0.54	0.53	0.53	0.53	0.54
Ca	0.52	0.51	0.55	0.52	0.57	0.54	0.60	0.56	0.54	0.57	0.53	0.55	0.57	0.54	0.53	0.54	0.55	0.56	0.55
Mn	0.08	0.08	0.09	0.09	0.08	0.08	0.09	0.09	0.09	0.09	0.09	0.08	0.09	0.08	0.09	0.09	0.09	0.08	0.09
Total cat	8.00	8.00	8.00	8.01	8.03	8.02	8.00	8.01	8.01	8.03	8.01	8.01	8.03	8.02	8.02	8.01	8.00	8.01	8.00
Andradite	0.66	0.00	0.44	2.12	3.96	2.89	0.59	2.25	1.12	4.47	1.84	1.69	4.61	2.53	2.70	2.01	0.44	1.52	0.40
Pyrope	18.29	18.44	17.60	17.99	17.93	18.03	17.28	17.50	17.66	17.36	17.90	17.41	17.50	17.87	18.08	17.79	17.79	17.64	18.09
Spessartine	2.80	2.84	2.92	3.02	2.84	2.68	2.86	2.96	3.15	2.91	2.89	2.62	3.05	2.80	2.88	3.02	2.99	2.76	2.88
Grossular	16.78	17.19	18.18	15.21	15.21	15.24	19.45	16.68	17.04	14.75	15.75	16.77	14.42	15.38	14.94	16.07	18.30	17.18	18.12
Almandine	61.47	61.52	60.86	61.67	60.05	61.15	59.82	60.61	61.03	60.50	61.62	61.50	60.42	61.43	61.41	61.10	60.48	60.90	60.52
% Rest	1.13	1.32	0.90	0.90	1.22	0.71	0.13	0.71	0.33	1.01	0.18	0.42	1.35	0.40	0.57	0.36	1.52	0.26	1.22
Xprp = XMg	0.18	0.18	0.17	0.18	0.17	0.18	0.17	0.17	0.18	0.17	0.18	0.17	0.17	0.18	0.18	0.18	0.17	0.17	0.18
Xalm = XFe	0.62	0.62	0.61	0.62	0.61	0.62	0.60	0.61	0.61	0.62	0.62	0.62	0.62	0.62	0.62	0.62	0.61	0.61	0.61
Xsps = XMn	0.03	0.03	0.03	0.03	0.03	0.03	0.03	0.03	0.03	0.03	0.03	0.03	0.03	0.03	0.03	0.03	0.03	0.03	0.03
Xgrs = XCa	0.17	0.17	0.18	0.17	0.19	0.18	0.20	0.19	0.18	0.19	0.17	0.18	0.18	0.18	0.17	0.18	0.18	0.18	0.18
XAl	1.00	1.00	1.00	1.00	1.00	1.00	1.00	1.00	1.00	1.00	1.00	1.00	1.00	1.00	1.00	1.00	1.00	1.00	1.00

Appendix Tab. A1: Electron microprobe analysis of garnet.

Sample	45AnTA	45AnTA	45AnTA	45AnTA	45AnTA	45AnTA	45AnTA	45AnTA	45AnTA	45AnTA	45AnTA	45AnTA	45AnTA
Analysis	grt3-24	grt3-25	grt3-26	grt3-27	grt3-28	grt3-29	grt3-30	grt3-31	grt3-32	grt3-33	grt3-34	grt3-35	grt3-36
SiO2	38.40	38.26	38.17	38.05	38.29	38.36	38.32	38.17	38.49	38.56	38.16	38.28	37.88
Al2O3	21.40	21.29	21.37	21.44	21.23	21.39	21.51	21.21	21.32	21.22	21.35	21.50	21.56
TiO2	0.04	0.11	0.03	0.02	0.01	0.05	0.03	0.05	0.04	0.05	0.06	0.05	0.06
FeO	28.21	28.54	28.62	28.80	28.87	28.39	29.03	28.68	28.82	28.20	28.96	28.39	28.66
MgO	4.66	4.49	4.59	4.70	4.58	4.59	4.68	4.80	4.77	4.60	4.65	4.64	4.69
CaO	6.14	6.73	6.49	6.16	6.41	6.38	6.13	5.93	6.17	6.21	6.09	6.48	6.21
MnO	1.29	1.27	1.22	1.25	1.22	1.23	1.14	1.24	1.16	1.18	1.17	1.12	1.14
Total	100.14	100.69	100.48	100.42	100.62	100.39	100.85	100.08	100.77	100.02	100.44	100.46	100.20
FeO Ox	28.21	28.14	28.16	28.25	28.41	28.34	28.68	28.41	28.59	28.20	28.59	28.21	28.14
Fe2O3 Ox	0.00	0.45	0.51	0.61	0.51	0.05	0.39	0.30	0.25	0.00	0.41	0.20	0.58
Summe Ox	100.14	100.74	100.53	100.48	100.67	100.39	100.88	100.11	100.80	100.02	100.48	100.48	100.26
Number of ions on the basis of 12 O													
Si	3.01	3.00	3.00	2.99	3.00	3.01	3.00	3.00	3.01	3.03	3.00	3.00	2.98
Al tot.	1.98	1.97	1.98	1.99	1.96	1.98	1.98	1.97	1.96	1.96	1.98	1.99	2.00
Ti	0.00	0.01	0.00	0.00	0.00	0.00	0.00	0.00	0.00	0.00	0.00	0.00	0.00
Fe tot.	1.85	1.87	1.88	1.89	1.89	1.86	1.90	1.89	1.88	1.85	1.90	1.86	1.89
Fe3+	0.00	0.03	0.03	0.04	0.03	0.00	0.02	0.02	0.01	0.00	0.02	0.01	0.03
Fe2+	1.85	1.84	1.85	1.86	1.86	1.86	1.87	1.87	1.87	1.85	1.88	1.85	1.85
Mg	0.55	0.52	0.54	0.55	0.54	0.54	0.55	0.56	0.56	0.54	0.54	0.54	0.55
Ca	0.52	0.56	0.55	0.52	0.54	0.54	0.51	0.50	0.52	0.52	0.51	0.54	0.52
Mn	0.09	0.08	0.08	0.08	0.08	0.08	0.08	0.08	0.08	0.08	0.08	0.07	0.08
Total cat	7.99	8.01	8.01	8.02	8.02	8.00	8.01	8.01	8.01	7.99	8.01	8.01	8.02
Andradite	0.00	1.97	2.24	2.71	2.25	0.23	1.73	1.34	1.12	0.00	1.82	0.89	2.58
Pyrope	18.35	17.49	17.92	18.41	17.83	18.04	18.20	18.82	18.64	18.27	18.16	18.06	18.45
Spessartine	2.89	2.81	2.70	2.79	2.71	2.74	2.52	2.77	2.58	2.65	2.60	2.47	2.55
Grossular	17.38	16.88	15.98	14.63	15.69	17.80	15.41	15.38	16.21	17.73	15.28	17.25	14.99
Almandine	61.38	60.85	61.16	61.46	61.53	61.19	62.14	61.70	61.44	61.34	62.14	61.33	61.43
% Rest	0.93	0.26	0.35	0.61	0.10	0.96	0.30	0.37	0.76	1.61	0.28	0.13	0.89
Xprp = XMg	0.18	0.17	0.18	0.18	0.18	0.18	0.18	0.19	0.18	0.18	0.18	0.18	0.18
Xalm = XFe	0.62	0.61	0.62	0.62	0.62	0.62	0.63	0.62	0.62	0.62	0.63	0.62	0.62
Xsps = XMn	0.03	0.03	0.03	0.03	0.03	0.03	0.02	0.03	0.03	0.03	0.03	0.02	0.03
Xgrs = XCa	0.17	0.19	0.18	0.17	0.18	0.18	0.17	0.16	0.17	0.17	0.17	0.18	0.17
XAl	1.00	1.00	1.00	1.00	1.00	1.00	1.00	1.00	1.00	1.00	1.00	1.00	1.00

Appendix Tab. A2: Electron microprobe analysis of biotite.

Sample	45AnTA	45AnTA	45AnTA	45AnTA	45AnTA	45AnTA	45AnTA	45AnTA	45AnTA	45AnTA	45AnTA	45AnTA	45AnTA	45AnTA	45AnTA	45AnTA	45AnTA	45AnTA	45AnTA
Analysis	bt1-1	bt1-2	bt1-3	bt1-4	bt2-1	bt2-2	bt2-3	bt3-1	bt3-2	bt4-1	bt4-2	bt4-3	bt5-1	bt5-2	bt5-3	bt6-1	bt6-2	bt6-3	bt6-4
SiO2	38.65	38.52	38.93	38.76	38.51	38.19	38.35	38.57	39.18	38.61	38.54	38.42	38.32	38.28	38.54	38.96	39.14	38.44	38.51
TiO2	1.11	1.01	1.06	1.08	0.78	1.11	0.90	0.93	0.87	1.02	1.03	0.97	1.04	1.05	1.08	1.10	1.10	1.12	1.18
Al2O3	18.28	18.32	18.23	18.20	18.71	18.46	18.69	18.75	18.38	18.58	18.33	18.48	18.42	18.33	18.04	17.81	17.80	18.19	18.24
Cr2O3	0.00	0.00	0.00	0.00	0.00	0.00	0.00	0.00	0.00	0.00	0.00	0.00	0.00	0.00	0.00	0.00	0.00	0.00	0.00
FeO	13.61	13.58	13.58	13.74	13.84	14.06	13.92	14.83	14.27	13.47	13.79	13.91	14.38	14.64	14.29	13.45	13.34	13.11	13.62
MnO	0.06	0.09	0.04	0.03	0.08	0.03	0.07	0.10	0.04	0.10	0.08	0.00	0.08	0.08	0.10	0.05	0.03	0.04	0.13
MgO	14.24	14.39	14.42	14.27	13.95	13.74	13.80	13.66	13.78	14.36	14.47	14.05	13.65	13.45	13.65	14.63	14.58	14.40	13.96
CaO	0.00	0.00	0.00	0.01	0.01	0.00	0.00	0.01	0.02	0.00	0.00	0.00	0.00	0.00	0.00	0.01	0.00	0.00	0.00
Na2O	0.37	0.34	0.40	0.48	0.32	0.36	0.32	0.32	0.31	0.36	0.36	0.30	0.40	0.38	0.38	0.41	0.38	0.39	0.42
K2O	8.64	8.65	8.68	8.63	8.77	8.87	8.98	8.79	8.68	8.83	8.66	8.77	8.92	8.82	8.71	8.70	8.63	8.69	8.68
Total	94.96	94.89	95.33	95.21	94.97	94.81	95.03	95.96	95.52	95.33	95.25	94.89	95.20	95.02	94.80	95.12	95.00	94.37	94.74
Number of ions on the basis of 11 O (water-free)																			
Si	2.84	2.83	2.85	2.84	2.83	2.82	2.82	2.82	2.86	2.82	2.82	2.83	2.82	2.83	2.85	2.85	2.87	2.84	2.84
AlIV	1.16	1.17	1.15	1.16	1.17	1.18	1.18	1.18	1.14	1.18	1.18	1.17	1.18	1.17	1.15	1.15	1.13	1.16	1.16
AlVI	0.42	0.42	0.42	0.41	0.45	0.43	0.45	0.44	0.45	0.43	0.41	0.43	0.42	0.42	0.42	0.39	0.40	0.42	0.42
Al tot.	1.58	1.59	1.57	1.57	1.62	1.61	1.62	1.62	1.58	1.60	1.58	1.60	1.60	1.60	1.57	1.54	1.54	1.58	1.58
Ti	0.06	0.06	0.06	0.06	0.04	0.06	0.05	0.05	0.05	0.06	0.06	0.05	0.06	0.06	0.06	0.06	0.06	0.06	0.07
Cr	0.00	0.00	0.00	0.00	0.00	0.00	0.00	0.00	0.00	0.00	0.00	0.00	0.00	0.00	0.00	0.00	0.00	0.00	0.00
Mg	1.56	1.58	1.57	1.56	1.53	1.51	1.51	1.49	1.50	1.57	1.58	1.54	1.50	1.48	1.50	1.60	1.59	1.58	1.53
Fe 2+	0.84	0.83	0.83	0.84	0.85	0.87	0.86	0.91	0.87	0.82	0.85	0.86	0.89	0.90	0.88	0.82	0.82	0.81	0.84
Mn	0.00	0.01	0.00	0.00	0.01	0.00	0.00	0.01	0.00	0.01	0.00	0.00	0.00	0.00	0.01	0.00	0.00	0.00	0.01
Ca	0.00	0.00	0.00	0.00	0.00	0.00	0.00	0.00	0.00	0.00	0.00	0.00	0.00	0.00	0.00	0.00	0.00	0.00	0.00
Na	0.05	0.05	0.06	0.07	0.05	0.05	0.04	0.05	0.04	0.05	0.05	0.04	0.06	0.05	0.05	0.06	0.05	0.06	0.06
K	0.81	0.81	0.81	0.81	0.82	0.84	0.84	0.82	0.81	0.82	0.81	0.82	0.84	0.83	0.82	0.81	0.81	0.82	0.82
Total cat	7.74	7.75	7.74	7.75	7.75	7.76	7.76	7.75	7.72	7.76	7.76	7.75	7.77	7.76	7.75	7.75	7.73	7.75	7.74
Fe/(Fe+Mg)	0.35	0.35	0.35	0.35	0.36	0.36	0.36	0.38	0.37	0.34	0.35	0.36	0.37	0.38	0.37	0.34	0.34	0.34	0.35
Al/(Al+Si)	0.36	0.36	0.36	0.36	0.36	0.36	0.36	0.36	0.36	0.36	0.36	0.36	0.36	0.36	0.36	0.35	0.35	0.36	0.36
Mg/(Mg+Fe)	0.65	0.65	0.65	0.65	0.64	0.64	0.64	0.62	0.63	0.66	0.65	0.64	0.63	0.62	0.63	0.66	0.66	0.66	0.65
XTi	0.02	0.02	0.02	0.02	0.01	0.02	0.02	0.02	0.02	0.02	0.02	0.02	0.02	0.02	0.02	0.02	0.02	0.02	0.02
XAlVI	0.15	0.14	0.14	0.14	0.16	0.15	0.16	0.15	0.16	0.15	0.14	0.15	0.15	0.15	0.15	0.14	0.14	0.15	0.15
XMg	0.54	0.55	0.55	0.54	0.53	0.53	0.53	0.52	0.52	0.54	0.55	0.53	0.52	0.52	0.52	0.56	0.55	0.55	0.53
XFe	0.29	0.29	0.29	0.29	0.30	0.30	0.30	0.31	0.30	0.29	0.29	0.30	0.31	0.31	0.31	0.29	0.28	0.28	0.29

Appendix Tab. A3: Electron microprobe analysis of white mica.

Sample	29AnTA	29AnTA	29AnTA	29AnTA	29AnTA	29AnTA	29AnTA	29AnTA	29AnTA	29AnTA	29AnTA	29AnTA	29AnTA	29AnTA	29AnTA	29AnTA	29AnTA	29AnTA	29AnTA
Analysis	wm1-1	wm1-2	wm1-3	wm1-4	wm1-5	wm1-6	wm1-7	wm1-8	wm1-9	wm2-1	wm2-2	wm2-3	wm2-4	wm2-5	wm2-6	wm3-1	wm3-2	wm3-3	wm4-1
Na2O	0.15	0.15	0.13	0.12	0.10	0.15	0.16	0.12	0.10	0.12	0.16	0.08	0.14	0.18	0.14	0.14	0.18	0.14	0.16
K2O	10.88	10.80	10.95	11.04	10.89	10.87	10.82	10.76	10.95	11.04	10.81	10.77	10.76	10.93	11.00	10.83	10.78	10.76	11.18
CaO	0.08	0.04	0.00	0.07	0.08	0.07	0.03	0.11	0.08	0.02	0.02	0.01	0.02	0.00	0.05	0.02	0.00	0.01	0.04
SiO2	48.37	48.83	49.24	48.33	47.10	46.73	48.60	48.16	47.54	49.78	49.06	49.77	49.66	49.23	50.24	49.61	48.61	49.96	48.30
Al2O3	27.12	26.76	27.49	26.89	26.87	25.88	27.18	26.48	26.42	26.97	27.14	26.03	26.76	26.77	26.53	27.36	27.51	27.88	27.52
TiO2	0.49	0.53	0.50	0.49	0.57	0.55	0.56	0.61	0.37	0.33	0.66	0.48	0.53	0.51	0.45	0.55	0.69	0.56	0.61
FeO	6.08	6.89	6.35	6.12	6.09	7.17	7.11	6.32	5.99	6.47	6.52	6.23	6.85	6.67	7.13	6.21	6.53	5.89	5.55
MgO	1.70	1.64	1.74	1.65	1.57	1.63	1.56	1.76	1.69	1.94	1.66	2.08	1.66	1.58	1.83	1.70	1.57	1.82	1.57
MnO	0.01	0.00	0.00	0.06	0.00	0.05	0.02	0.02	0.01	0.01	0.04	0.04	0.00	0.05	0.02	0.05	0.03	0.02	0.00
Cr2O3	0.00	0.00	0.00	0.00	0.00	0.00	0.00	0.00	0.00	0.00	0.00	0.00	0.00	0.00	0.00	0.00	0.00	0.00	0.00
Total	94.88	95.64	96.40	94.78	93.27	93.08	96.04	94.34	93.15	96.68	96.07	95.48	96.37	95.92	97.39	96.47	95.90	97.04	94.93
Number of ions on the basis of 11 O (water-free)																			
Na	0.02	0.02	0.02	0.02	0.01	0.02	0.02	0.02	0.01	0.02	0.02	0.01	0.02	0.02	0.02	0.02	0.02	0.02	0.02
K	0.95	0.94	0.94	0.97	0.97	0.98	0.94	0.95	0.98	0.95	0.94	0.94	0.93	0.95	0.94	0.93	0.94	0.92	0.98
Ca	0.01	0.00	0.00	0.01	0.01	0.00	0.00	0.01	0.01	0.00	0.00	0.00	0.00	0.00	0.00	0.00	0.00	0.00	0.00
Total	0.98	0.96	0.96	0.99	0.99	1.01	0.96	0.97	1.00	0.97	0.96	0.95	0.95	0.97	0.96	0.95	0.96	0.94	1.00
Si	3.32	3.33	3.33	3.33	3.30	3.30	3.31	3.33	3.33	3.35	3.33	3.39	3.36	3.35	3.37	3.34	3.31	3.34	3.31
AlIV	0.68	0.67	0.67	0.67	0.70	0.70	0.69	0.67	0.67	0.65	0.67	0.61	0.64	0.65	0.63	0.66	0.69	0.66	0.69
AlVI	1.52	1.49	1.51	1.51	1.51	1.46	1.49	1.49	1.51	1.50	1.50	1.48	1.49	1.50	1.47	1.52	1.51	1.53	1.53
Al tot.	2.19	2.15	2.19	2.18	2.22	2.16	2.18	2.16	2.18	2.14	2.17	2.09	2.13	2.15	2.10	2.17	2.21	2.19	2.22
Ti	0.03	0.03	0.03	0.03	0.03	0.03	0.03	0.03	0.02	0.02	0.03	0.02	0.03	0.03	0.02	0.03	0.04	0.03	0.03
Cr3+	0.00	0.00	0.00	0.00	0.00	0.00	0.00	0.00	0.00	0.00	0.00	0.00	0.00	0.00	0.00	0.00	0.00	0.00	0.00
Fe2+	0.35	0.39	0.36	0.35	0.36	0.42	0.41	0.37	0.35	0.36	0.37	0.35	0.39	0.38	0.40	0.35	0.37	0.33	0.32
Mg	0.17	0.17	0.18	0.17	0.16	0.17	0.16	0.18	0.18	0.19	0.17	0.21	0.17	0.16	0.18	0.17	0.16	0.18	0.16
Mn	0.00	0.00	0.00	0.00	0.00	0.00	0.00	0.00	0.00	0.00	0.00	0.00	0.00	0.00	0.00	0.00	0.00	0.00	0.00
Fe + Mg	0.52	0.56	0.53	0.52	0.52	0.59	0.56	0.55	0.53	0.56	0.54	0.57	0.55	0.54	0.58	0.52	0.53	0.51	0.48
Cation ratios																			
Fe/(Fe+Mg)	0.67	0.70	0.67	0.67	0.69	0.71	0.72	0.67	0.67	0.65	0.69	0.63	0.70	0.70	0.69	0.67	0.70	0.64	0.67
Mg/(Mg+Fe)	0.33	0.30	0.33	0.33	0.31	0.29	0.28	0.33	0.33	0.35	0.31	0.37	0.30	0.30	0.31	0.33	0.30	0.36	0.33
Muscovite	0.97	0.98	0.98	0.98	0.98	0.98	0.98	0.97	0.98	0.98	0.98	0.99	0.98	0.98	0.98	0.98	0.97	0.98	0.98
Paragonite	0.02	0.02	0.02	0.02	0.01	0.02	0.02	0.02	0.01	0.02	0.02	0.01	0.02	0.02	0.02	0.02	0.03	0.02	0.02
Margarite	0.01	0.00	0.00	0.01	0.01	0.00	0.00	0.01	0.01	0.00	0.00	0.00	0.00	0.00	0.00	0.00	0.00	0.00	0.00

Appendix Tab. A3: Electron microprobe analysis of white mica.

Sample	29AnTA	29AnTA	29AnTA	29AnTA	29AnTA	29AnTA	29AnTA	29AnTA	29AnTA	29AnTA	29AnTA	29AnTA	29AnTA	2AnTA	2AnTA	2AnTA	2AnTA	2AnTA
Analysis	wm4-2	wm4-3	wm5-1	wm5-2	wm5-3	wm5-4	wm5-5	wm6-1	wm6-2	wm6-3	wm7-1	wm7-2	wm7-3	wm1	wm2	wm3	wm4	wm6
Na2O	0.12	0.11	0.12	0.11	0.16	0.16	0.15	0.13	0.14	0.15	0.11	0.17	0.15	0.12	0.11	0.09	0.07	0.07
K2O	10.71	10.78	11.36	10.96	10.91	11.17	10.93	10.94	10.79	10.95	11.23	11.16	11.08	10.75	10.89	10.81	10.84	11.04
CaO	0.05	0.00	0.00	0.00	0.05	0.01	0.00	0.01	0.03	0.03	0.05	0.01	0.00	0.02	0.00	0.02	0.01	0.02
SiO2	49.48	49.49	49.13	48.72	48.26	46.58	48.82	48.90	48.75	48.57	48.64	48.46	48.42	49.94	47.85	49.35	49.32	49.84
Al2O3	27.90	26.80	27.69	27.76	27.46	27.11	27.64	27.63	27.78	27.74	27.65	27.44	27.89	25.10	26.81	25.02	24.74	25.00
TiO2	0.58	0.43	0.23	0.61	0.55	0.65	0.53	0.42	0.61	0.36	0.24	0.31	0.59	0.85	0.78	0.62	0.64	0.66
FeO	6.59	6.66	5.36	6.03	5.97	5.68	6.03	5.94	5.82	5.87	5.78	5.78	5.99	2.55	3.11	3.17	3.70	2.72
MgO	1.55	1.66	1.87	1.71	1.69	1.55	1.64	1.75	1.67	1.71	1.82	1.74	1.64	3.07	3.19	3.61	3.56	3.59
MnO	0.04	0.05	0.00	0.00	0.00	0.03	0.02	0.00	0.02	0.00	0.00	0.06	0.00	0.01	0.00	0.01	0.05	0.00
Cr2O3	0.00	0.00	0.00	0.00	0.00	0.00	0.00	0.00	0.00	0.00	0.00	0.00	0.00	0.00	0.00	0.00	0.00	0.00
Total	97.01	95.98	95.76	95.90	95.05	92.94	95.76	95.72	95.61	95.38	95.51	95.13	95.75	92.41	92.74	92.69	92.93	92.94
Number of ions on the basis of 11 O (water-free)																		
Na	0.02	0.01	0.02	0.01	0.02	0.02	0.02	0.02	0.02	0.02	0.01	0.02	0.02	0.02	0.01	0.01	0.01	0.01
K	0.92	0.93	0.98	0.95	0.95	1.00	0.95	0.95	0.93	0.95	0.98	0.97	0.96	0.95	0.96	0.95	0.96	0.97
Ca	0.00	0.00	0.00	0.00	0.00	0.00	0.00	0.00	0.00	0.00	0.00	0.00	0.00	0.00	0.00	0.00	0.00	0.00
Total	0.94	0.95	1.00	0.96	0.98	1.03	0.97	0.97	0.96	0.97	0.99	1.00	0.98	0.96	0.98	0.97	0.97	0.98
Si	3.32	3.36	3.33	3.31	3.31	3.27	3.32	3.32	3.31	3.31	3.32	3.32	3.29	3.45	3.32	3.42	3.42	3.43
AlIV	0.68	0.64	0.67	0.69	0.69	0.73	0.68	0.68	0.69	0.69	0.68	0.68	0.71	0.55	0.68	0.58	0.58	0.57
AlVI	1.52	1.50	1.55	1.53	1.52	1.52	1.53	1.53	1.54	1.54	1.54	1.53	1.53	1.49	1.51	1.46	1.44	1.46
Al tot.	2.21	2.14	2.21	2.22	2.22	2.25	2.21	2.21	2.22	2.23	2.22	2.21	2.24	2.04	2.19	2.04	2.02	2.03
Ti	0.03	0.02	0.01	0.03	0.03	0.03	0.03	0.02	0.03	0.02	0.01	0.02	0.03	0.04	0.04	0.03	0.03	0.03
Cr3+	0.00	0.00	0.00	0.00	0.00	0.00	0.00	0.00	0.00	0.00	0.00	0.00	0.00	0.00	0.00	0.00	0.00	0.00
Fe2+	0.37	0.38	0.30	0.34	0.34	0.33	0.34	0.34	0.33	0.33	0.33	0.33	0.34	0.15	0.18	0.18	0.21	0.16
Mg	0.15	0.17	0.19	0.17	0.17	0.16	0.17	0.18	0.17	0.17	0.18	0.18	0.17	0.32	0.33	0.37	0.37	0.37
Mn	0.00	0.00	0.00	0.00	0.00	0.00	0.00	0.00	0.00	0.00	0.00	0.00	0.00	0.00	0.00	0.00	0.00	0.00
Fe + Mg	0.52	0.55	0.49	0.52	0.51	0.50	0.51	0.51	0.50	0.51	0.51	0.51	0.51	0.46	0.51	0.56	0.58	0.53
Cation ratios																		
Fe/(Fe+Mg)	0.71	0.69	0.62	0.66	0.66	0.67	0.67	0.66	0.66	0.66	0.64	0.65	0.67	0.31	0.35	0.33	0.37	0.30
Mg/(Mg+Fe)	0.29	0.31	0.38	0.34	0.34	0.33	0.33	0.34	0.34	0.34	0.36	0.35	0.33	0.69	0.65	0.67	0.63	0.70
Muscovite	0.98	0.98	0.98	0.98	0.97	0.98	0.98	0.98	0.98	0.98	0.98	0.98	0.98	0.98	0.99	0.99	0.99	0.99
Paragonite	0.02	0.02	0.02	0.02	0.02	0.02	0.02	0.02	0.02	0.02	0.01	0.02	0.02	0.02	0.01	0.01	0.01	0.01
Margarite	0.00	0.00	0.00	0.00	0.00	0.00	0.00	0.00	0.00	0.00	0.00	0.00	0.00	0.00	0.00	0.00	0.00	0.00

Appendix Tab. A3: Electron microprobe analysis of white mica.

Sample	2AnTA	2AnTA	2AnTA	45AnTA	45AnTA	45AnTA	45AnTA	45AnTA	45AnTA	45AnTA	45AnTA	45AnTA	45AnTA	51AnTA	51AnTA	51AnTA	51AnTA	51AnTA
Analysis	wm8	wm9	wm10	wm1	wm2	wm3	wm4	wm5	wm6	wm7	wm8	wm9	wm10	wm1	wm2	wm3	wm6	wm7
Na2O	0.07	0.08	0.12	0.98	1.20	1.29	1.26	1.11	1.24	0.89	1.30	0.86	1.08	0.09	0.20	0.15	0.12	0.13
K2O	11.15	11.09	10.50	9.54	9.36	8.56	8.96	9.15	9.26	9.35	9.29	9.41	8.37	10.18	11.15	13.08	11.16	10.96
CaO	0.00	0.01	0.05	0.00	0.01	0.18	0.05	0.00	0.00	0.01	0.00	0.00	0.01	0.02	0.02	0.03	0.02	0.02
SiO2	50.45	49.96	49.37	49.32	47.62	47.16	48.01	48.99	48.53	49.63	48.28	50.06	48.39	55.14	50.32	56.54	48.68	50.50
Al2O3	25.18	26.28	25.22	31.73	33.40	33.90	33.30	33.76	34.31	31.79	34.71	31.65	33.41	24.02	27.11	22.10	28.03	25.99
TiO2	0.68	0.82	0.96	0.47	0.39	0.31	0.40	0.34	0.42	0.39	0.28	0.42	0.45	0.72	0.71	0.47	0.89	0.78
FeO	1.89	1.65	2.21	1.20	1.22	1.08	1.10	1.15	1.01	1.37	1.20	1.36	1.16	1.18	1.23	0.73	0.90	1.42
MgO	3.62	3.43	3.38	1.94	1.20	1.02	1.33	1.31	1.15	1.79	0.98	1.98	1.45	2.98	3.26	1.30	2.92	3.51
MnO	0.00	0.00	0.00	0.00	0.00	0.00	0.00	0.00	0.05	0.00	0.00	0.00	0.00	0.00	0.01	0.00	0.00	0.01
Cr2O3	0.00	0.00	0.00	0.00	0.00	0.00	0.00	0.00	0.00	0.00	0.00	0.00	0.00	0.00	0.00	0.00	0.00	0.00
Total	93.03	93.32	91.81	95.17	94.39	93.51	94.41	95.81	95.97	95.21	96.04	95.74	94.33	94.32	94.00	94.40	92.71	93.31
Number of ions on the basis of 11 O (water-free)																		
Na	0.01	0.01	0.02	0.13	0.16	0.17	0.16	0.14	0.16	0.11	0.16	0.11	0.14	0.01	0.03	0.02	0.02	0.02
K	0.97	0.96	0.93	0.80	0.80	0.73	0.76	0.76	0.77	0.79	0.78	0.79	0.71	0.86	0.96	1.12	0.98	0.95
Ca	0.00	0.00	0.00	0.00	0.00	0.01	0.00	0.00	0.00	0.00	0.00	0.00	0.00	0.00	0.00	0.00	0.00	0.00
Total	0.98	0.98	0.95	0.93	0.95	0.91	0.93	0.91	0.93	0.90	0.94	0.90	0.85	0.87	0.99	1.14	0.99	0.97
Si	3.46	3.41	3.43	3.26	3.18	3.16	3.19	3.21	3.18	3.27	3.16	3.28	3.21	3.66	3.40	3.79	3.33	3.44
AlIV	0.54	0.59	0.57	0.74	0.82	0.84	0.81	0.79	0.82	0.73	0.84	0.72	0.79	0.34	0.60	0.21	0.67	0.56
AlVI	1.49	1.52	1.49	1.73	1.81	1.84	1.80	1.81	1.82	1.75	1.84	1.73	1.81	1.53	1.56	1.54	1.60	1.52
Al tot.	2.03	2.11	2.06	2.47	2.63	2.68	2.61	2.61	2.65	2.47	2.68	2.45	2.61	1.88	2.16	1.77	2.26	2.08
Ti	0.03	0.04	0.05	0.02	0.02	0.02	0.02	0.02	0.02	0.02	0.01	0.02	0.02	0.04	0.04	0.02	0.05	0.04
Cr3+	0.00	0.00	0.00	0.00	0.00	0.00	0.00	0.00	0.00	0.00	0.00	0.00	0.00	0.00	0.00	0.00	0.00	0.00
Fe2+	0.11	0.09	0.13	0.07	0.07	0.06	0.06	0.06	0.06	0.08	0.07	0.07	0.06	0.07	0.07	0.04	0.05	0.08
Mg	0.37	0.35	0.35	0.19	0.12	0.10	0.13	0.13	0.11	0.18	0.10	0.19	0.14	0.29	0.33	0.13	0.30	0.36
Mn	0.00	0.00	0.00	0.00	0.00	0.00	0.00	0.00	0.00	0.00	0.00	0.00	0.00	0.00	0.00	0.00	0.00	0.00
Fe + Mg	0.48	0.44	0.48	0.26	0.19	0.16	0.19	0.19	0.17	0.25	0.16	0.27	0.21	0.36	0.40	0.17	0.35	0.44
Cation ratios																		
Fe/(Fe+Mg)	0.23	0.21	0.27	0.26	0.36	0.37	0.32	0.33	0.33	0.30	0.41	0.28	0.31	0.18	0.17	0.24	0.15	0.19
Mg/(Mg+Fe)	0.77	0.79	0.73	0.74	0.64	0.63	0.68	0.67	0.67	0.70	0.59	0.72	0.69	0.82	0.83	0.76	0.85	0.81
Muscovite	0.99	0.99	0.98	0.86	0.84	0.80	0.82	0.84	0.83	0.87	0.83	0.88	0.84	0.99	0.97	0.98	0.98	0.98
Paragonite	0.01	0.01	0.02	0.14	0.16	0.18	0.18	0.16	0.17	0.13	0.17	0.12	0.16	0.01	0.03	0.02	0.02	0.02
Margarite	0.00	0.00	0.00	0.00	0.00	0.01	0.00	0.00	0.00	0.00	0.00	0.00	0.00	0.00	0.00	0.00	0.00	0.00

Appendix Tab. A3: Electron microprobe analysis of white mica.

Sample	51AnTA	51AnTA	51AnTA
Analysis	wm8	wm9	wm10
Na2O	0.15	0.13	0.11
K2O	11.24	10.88	10.95
CaO	0.01	0.02	0.02
SiO2	49.97	48.16	48.63
Al2O3	27.58	27.29	28.11
TiO2	0.81	0.79	0.68
FeO	1.43	1.80	2.75
MgO	3.08	2.96	2.74
MnO	0.00	0.18	0.00
Cr2O3	0.00	0.00	0.00
Total	94.28	92.21	93.98
Number of ions on the basis of 11 O (water-free)			
Na	0.02	0.02	0.01
K	0.97	0.96	0.95
Ca	0.00	0.00	0.00
Total	0.99	0.98	0.97
Si	3.37	3.33	3.31
AlIV	0.63	0.67	0.69
AlVI	1.56	1.56	1.57
Al tot.	2.19	2.23	2.26
Ti	0.04	0.04	0.03
Cr3+	0.00	0.00	0.00
Fe2+	0.08	0.10	0.16
Mg	0.31	0.31	0.28
Mn	0.01	0.01	0.00
Fe + Mg	0.39	0.41	0.43
Cation ratios			
Fe/(Fe+Mg)	0.22	0.25	0.36
Mg/(Mg+Fe)	0.78	0.75	0.64
Muscovite	0.98	0.98	0.98
Paragonite	0.02	0.02	0.01
Margarite	0.00	0.00	0.00

Appendix Tab. A3.1: End-members of white mica after Schliestedt (1980).

Sample	29AnTA	29AnTA	29AnTA	29AnTA	29AnTA	29AnTA	29AnTA	29AnTA	29AnTA	29AnTA	29AnTA	29AnTA	29AnTA	29AnTA	29AnTA	29AnTA	29AnTA	29AnTA
Analysis	wm1-1	wm1-2	wm1-3	wm1-4	wm1-5	wm1-6	wm1-7	wm1-8	wm1-9	wm2-1	wm2-2	wm2-3	wm2-4	wm2-5	wm2-6	wm3-1	wm3-2	wm3-3
Paragonite	2.05	2.03	1.73	1.56	1.31	2.00	2.22	1.69	1.41	1.65	2.13	1.07	1.91	2.43	1.86	1.93	2.52	1.91
Celadonite	32.06	33.49	32.59	32.64	29.72	30.24	31.04	32.99	32.95	35.45	32.83	38.81	35.84	34.93	37.01	34.25	30.51	33.62
Muscovite	65.89	64.49	65.68	65.80	68.97	67.76	66.73	65.31	65.64	62.90	65.04	60.11	62.25	62.64	61.13	63.82	66.98	64.47

Sample	29AnTA	29AnTA	29AnTA	29AnTA	29AnTA	29AnTA	29AnTA	29AnTA	29AnTA	29AnTA	29AnTA	29AnTA	29AnTA	29AnTA	2AnTA	2AnTA	2AnTA	2AnTA
Analysis	wm4-1	wm4-2	wm4-3	wm5-1	wm5-2	wm5-3	wm5-4	wm5-5	wm6-1	wm6-2	wm6-3	wm7-1	wm7-2	wm7-3	wm1	wm2	wm3	wm4
Paragonite	2.13	1.67	1.54	1.53	1.54	2.13	2.16	2.03	1.72	1.95	2.07	1.45	2.22	1.96	1.60	1.46	1.19	0.97
Celadonite	31.03	31.84	35.86	33.18	30.54	30.57	27.49	31.61	32.08	31.09	31.12	31.51	31.75	29.39	45.12	31.69	41.61	41.66
Muscovite	66.84	66.48	62.60	65.29	67.92	67.30	70.36	66.36	66.20	66.96	66.81	67.04	66.03	68.65	53.37	66.85	57.20	57.37

Sample	2AnTA	2AnTA	2AnTA	2AnTA	2AnTA	45AnTA	45AnTA	45AnTA	45AnTA	45AnTA	45AnTA	45AnTA	45AnTA	45AnTA	45AnTA	51AnTA	51AnTA	51AnTA
Analysis	wm6	wm7	wm8	wm9	wm10	wm1	wm2	wm3	wm4	wm5	wm6	wm7	wm8	wm9	wm10	wm1	wm2	wm3
Paragonite	0.93	1.01	0.88	1.08	1.76	13.52	16.32	18.67	17.60	15.58	16.93	12.59	17.48	12.22	16.38	1.31	2.71	1.87
Celadonite	43.41	41.25	45.56	40.74	43.18	26.07	17.79	16.18	19.29	20.72	17.60	27.49	16.10	28.47	20.51	65.69	39.87	78.49
Muscovite	55.66	57.75	53.56	58.17	55.06	60.41	65.89	65.15	63.12	63.70	65.46	59.93	66.42	59.31	63.11	33.00	57.43	15.64

Sample	51AnTA	51AnTA	51AnTA	51AnTA	51AnTA
Analysis	wm6	wm7	wm8	wm9	wm10
Paragonite	1.57	1.70	1.79	1.81	1.48
Celadonite	33.38	43.57	37.12	33.33	31.26
Muscovite	65.06	54.73	60.84	64.86	67.26

Appendix Tab. A4: Electron microprobe analysis of feldspar.

Sample	2AnTA	2AnTA	2AnTA	2AnTA	2AnTA	2AnTA	2AnTA	2AnTA	2AnTA	2AnTA	2AnTA	2AnTA	2AnTA	2AnTA	2AnTA	2AnTA	2AnTA	2AnTA	2AnTA
Analysis	fsp1-1	fsp1-2	fsp1-3	fsp2-1	fsp2-2	fsp2-3	fsp3-1	fsp3-2	fsp3-3	fsp4-1	fsp4-2	fsp4-3	fsp5-1	fsp5-2	fsp5-3	fsp6-1	fsp6-2	fsp6-3	fsp7-1
Na2O	0.30	0.54	0.40	0.26	0.34	0.34	0.39	0.60	0.51	0.52	0.73	0.52	0.34	0.36	0.32	0.38	0.29	0.29	0.43
K2O	16.52	16.25	16.47	16.43	16.23	16.28	16.14	16.03	16.18	16.11	15.96	16.23	16.50	16.14	16.27	16.34	16.46	16.64	16.12
CaO	0.05	0.09	0.17	0.00	0.05	0.03	0.04	0.05	0.00	0.00	0.00	0.01	0.00	0.04	0.13	0.00	0.02	0.00	0.06
SiO2	66.17	66.16	65.67	66.19	65.39	65.63	65.72	65.56	65.66	65.86	65.51	65.54	66.00	65.89	65.89	65.57	65.92	66.22	65.59
Al2O3	17.87	17.82	17.83	17.80	17.92	17.93	17.92	18.05	17.71	17.67	17.78	17.70	17.76	17.91	17.82	17.83	17.89	17.82	17.98
TiO2	0.00	0.00	0.03	0.00	0.00	0.00	0.06	0.00	0.04	0.00	0.00	0.00	0.00	0.02	0.05	0.02	0.03	0.03	0.00
FeO	0.00	0.01	0.08	0.00	0.00	0.00	0.03	0.00	0.03	0.00	0.00	0.06	0.00	0.00	0.02	0.02	0.05	0.02	0.07
MgO	0.00	0.00	0.00	0.00	0.00	0.01	0.00	0.01	0.00	0.00	0.01	0.01	0.00	0.01	0.01	0.00	0.00	0.00	0.01
MnO	0.00	0.00	0.00	0.00	0.00	0.00	0.00	0.00	0.00	0.00	0.00	0.00	0.00	0.00	0.00	0.00	0.00	0.00	0.00
Cr2O3	0.00	0.00	0.00	0.00	0.00	0.00	0.00	0.00	0.00	0.00	0.00	0.00	0.00	0.00	0.00	0.00	0.00	0.00	0.00
Total	100.92	100.87	100.64	100.68	99.93	100.22	100.31	100.30	100.12	100.16	99.99	100.07	100.60	100.37	100.51	100.16	100.66	101.03	100.26
Number of ions on the basis of 8 O																			
Na	0.03	0.05	0.04	0.02	0.03	0.03	0.03	0.05	0.05	0.05	0.06	0.05	0.03	0.03	0.03	0.03	0.03	0.03	0.04
K	0.96	0.95	0.97	0.96	0.96	0.96	0.95	0.94	0.95	0.95	0.94	0.96	0.97	0.95	0.95	0.96	0.96	0.97	0.95
Ca	0.00	0.00	0.01	0.00	0.00	0.00	0.00	0.00	0.00	0.00	0.00	0.00	0.00	0.00	0.01	0.00	0.00	0.00	0.00
Total	0.99	1.00	1.01	0.98	0.99	0.99	0.98	1.00	1.00	0.99	1.00	1.00	1.00	0.98	0.99	1.00	0.99	1.00	0.99
Si	3.03	3.03	3.02	3.03	3.02	3.02	3.02	3.02	3.03	3.03	3.02	3.03	3.03	3.03	3.03	3.02	3.02	3.03	3.02
AlIV	0.00	0.00	0.00	0.00	0.00	0.00	0.00	0.00	0.00	0.00	0.00	0.00	0.00	0.00	0.00	0.00	0.00	0.00	0.00
AlVI	0.96	0.96	0.97	0.96	0.98	0.97	0.97	0.98	0.96	0.96	0.97	0.96	0.96	0.97	0.96	0.97	0.97	0.96	0.98
Al tot.	0.96	0.96	0.97	0.96	0.98	0.97	0.97	0.98	0.96	0.96	0.97	0.96	0.96	0.97	0.96	0.97	0.97	0.96	0.98
Ti	0.00	0.00	0.00	0.00	0.00	0.00	0.00	0.00	0.00	0.00	0.00	0.00	0.00	0.00	0.00	0.00	0.00	0.00	0.00
Cr3+	0.00	0.00	0.00	0.00	0.00	0.00	0.00	0.00	0.00	0.00	0.00	0.00	0.00	0.00	0.00	0.00	0.00	0.00	0.00
Fe2+	0.00	0.00	0.00	0.00	0.00	0.00	0.00	0.00	0.00	0.00	0.00	0.00	0.00	0.00	0.00	0.00	0.00	0.00	0.00
Mg	0.00	0.00	0.00	0.00	0.00	0.00	0.00	0.00	0.00	0.00	0.00	0.00	0.00	0.00	0.00	0.00	0.00	0.00	0.00
Mn	0.00	0.00	0.00	0.00	0.00	0.00	0.00	0.00	0.00	0.00	0.00	0.00	0.00	0.00	0.00	0.00	0.00	0.00	0.00
Total	3.99	3.99	3.99	3.99	4.00	4.00	4.00	4.00	3.99	3.99	3.99	3.99	3.99	4.00	3.99	3.99	4.00	3.99	4.00
Albite	2.71	4.75	3.52	2.34	3.08	3.08	3.55	5.33	4.55	4.71	6.46	4.61	3.04	3.25	2.92	3.41	2.59	2.60	3.90
Orthoclase	97.03	94.81	95.65	97.66	96.68	96.78	96.23	94.40	95.45	95.29	93.54	95.36	96.96	96.54	96.42	96.59	97.34	97.40	95.81
Anorthite	0.26	0.44	0.83	0.00	0.25	0.13	0.22	0.27	0.00	0.00	0.00	0.03	0.00	0.21	0.66	0.00	0.07	0.00	0.28

Appendix Tab. A4: Electron microprobe analysis of feldspar.

Sample	2AnTA	2AnTA	2AnTA	2AnTA	2AnTA	2AnTA	2AnTA	2AnTA	2AnTA	2AnTA	2AnTA	51AnTA	51AnTA	51AnTA	51AnTA	51AnTA	51AnTA	51AnTA	51AnTA
Analysis	fsp7-2	fsp7-3	fsp8-1	fsp8-2	fsp8-3	fsp9-1	fsp9-2	fsp9-3	fsp10-1	fsp10-2	fsp10-3	fsp1-2	fsp1-2	fsp1-3	fsp2-1	fsp2-2	fsp2-3	fsp3-1	fsp3-2
Na2O	0.46	0.38	0.36	0.37	0.46	0.34	0.32	0.42	0.43	0.42	0.41	0.48	0.54	0.49	0.39	0.38	0.51	0.52	0.48
K2O	15.92	16.43	16.30	16.11	16.25	16.47	16.42	16.21	16.28	16.23	16.11	15.78	15.87	16.00	16.25	16.55	16.20	16.07	16.12
CaO	0.15	0.01	0.04	0.03	0.04	0.00	0.01	0.00	0.03	0.10	0.06	0.10	0.02	0.03	0.02	0.00	0.01	0.09	0.08
SiO2	65.46	65.95	65.63	65.39	65.98	65.86	65.84	65.54	65.81	65.82	65.84	65.46	65.42	65.56	66.06	66.24	65.99	66.04	65.83
Al2O3	18.07	17.84	17.83	17.65	17.94	17.86	18.05	18.06	17.95	17.77	17.74	18.15	18.03	17.95	17.80	17.72	17.82	18.05	18.10
TiO2	0.03	0.00	0.07	0.00	0.06	0.00	0.04	0.00	0.00	0.04	0.00	0.02	0.01	0.00	0.00	0.01	0.02	0.00	0.07
FeO	0.00	0.03	0.02	0.03	0.10	0.00	0.05	0.00	0.00	0.00	0.03	0.06	0.00	0.01	0.04	0.04	0.03	0.00	0.00
MgO	0.00	0.01	0.00	0.00	0.00	0.01	0.00	0.01	0.00	0.00	0.01	0.00	0.02	0.00	0.01	0.00	0.00	0.00	0.00
MnO	0.00	0.00	0.00	0.00	0.00	0.00	0.00	0.00	0.00	0.00	0.00	0.00	0.00	0.00	0.00	0.00	0.00	0.00	0.00
Cr2O3	0.00	0.00	0.00	0.00	0.00	0.00	0.00	0.00	0.00	0.00	0.00	0.00	0.00	0.00	0.00	0.00	0.00	0.00	0.00
Total	100.09	100.65	100.25	99.58	100.83	100.54	100.74	100.24	100.50	100.38	100.20	100.06	99.90	100.05	100.58	100.94	100.58	100.77	100.67
Number of ions on the basis of 8 O																			
Na	0.04	0.03	0.03	0.03	0.04	0.03	0.03	0.04	0.04	0.04	0.04	0.04	0.05	0.04	0.03	0.03	0.05	0.05	0.04
K	0.94	0.96	0.96	0.95	0.95	0.97	0.96	0.95	0.95	0.95	0.95	0.93	0.93	0.94	0.95	0.97	0.95	0.94	0.94
Ca	0.01	0.00	0.00	0.00	0.00	0.00	0.00	0.00	0.00	0.00	0.00	0.00	0.00	0.00	0.00	0.00	0.00	0.00	0.00
Total	0.98	1.00	0.99	0.99	0.99	1.00	0.99	0.99	0.99	0.99	0.99	0.98	0.98	0.99	0.99	1.00	0.99	0.99	0.99
Si	3.02	3.03	3.02	3.03	3.02	3.03	3.02	3.02	3.02	3.03	3.03	3.01	3.02	3.02	3.03	3.03	3.03	3.02	3.02
AlIV	0.00	0.00	0.00	0.00	0.00	0.00	0.00	0.00	0.00	0.00	0.00	0.00	0.00	0.00	0.00	0.00	0.00	0.00	0.00
AlVI	0.98	0.97	0.97	0.96	0.97	0.97	0.98	0.98	0.97	0.96	0.96	0.99	0.98	0.98	0.96	0.96	0.96	0.97	0.98
Al tot.	0.98	0.97	0.97	0.96	0.97	0.97	0.98	0.98	0.97	0.96	0.96	0.99	0.98	0.98	0.96	0.96	0.96	0.97	0.98
Ti	0.00	0.00	0.00	0.00	0.00	0.00	0.00	0.00	0.00	0.00	0.00	0.00	0.00	0.00	0.00	0.00	0.00	0.00	0.00
Cr3+	0.00	0.00	0.00	0.00	0.00	0.00	0.00	0.00	0.00	0.00	0.00	0.00	0.00	0.00	0.00	0.00	0.00	0.00	0.00
Fe2+	0.00	0.00	0.00	0.00	0.00	0.00	0.00	0.00	0.00	0.00	0.00	0.00	0.00	0.00	0.00	0.00	0.00	0.00	0.00
Mg	0.00	0.00	0.00	0.00	0.00	0.00	0.00	0.00	0.00	0.00	0.00	0.00	0.00	0.00	0.00	0.00	0.00	0.00	0.00
Mn	0.00	0.00	0.00	0.00	0.00	0.00	0.00	0.00	0.00	0.00	0.00	0.00	0.00	0.00	0.00	0.00	0.00	0.00	0.00
Total	4.00	3.99	3.99	3.99	4.00	3.99	4.00	4.00	3.99	3.99	3.99	4.00	4.00	4.00	3.99	3.99	3.99	4.00	4.00
Albite	4.21	3.40	3.21	3.38	4.10	3.01	2.90	3.76	3.83	3.77	3.70	4.43	4.88	4.48	3.53	3.37	4.57	4.66	4.27
Orthoclase	95.03	96.56	96.60	96.44	95.69	96.99	97.05	96.24	96.03	95.73	96.01	95.07	95.01	95.37	96.35	96.63	95.37	94.91	95.34
Anorthite	0.76	0.04	0.19	0.17	0.21	0.00	0.05	0.00	0.14	0.50	0.30	0.50	0.11	0.16	0.11	0.00	0.06	0.44	0.39

Appendix Tab. A4: Electron microprobe analysis of feldspar.

Sample	51AnTA	51AnTA	51AnTA	51AnTA	51AnTA	51AnTA	51AnTA	51AnTA	51AnTA	51AnTA	51AnTA	51AnTA	51AnTA	51AnTA	51AnTA	51AnTA	51AnTA	51AnTA	51AnTA
Analysis	fsp3-3	fsp4-1	fsp4-2	fsp4-3	fsp5-1	fsp5-2	fsp5-3	fsp6-1	fsp6-2	fsp6-3	fsp7-1	fsp7-2	fsp7-3	fsp8-1	fsp8-2	fsp8-3	fsp9-1	fsp9-2	fsp9-3
Na2O	0.44	0.46	0.45	0.40	0.47	0.37	0.45	0.34	0.44	0.51	0.44	0.47	0.30	0.54	0.60	0.46	0.30	0.37	0.37
K2O	16.18	16.22	16.24	16.36	16.29	16.42	16.22	16.31	16.24	16.29	16.40	16.28	16.47	15.97	15.99	16.24	16.40	16.36	16.21
CaO	0.00	0.33	0.17	0.11	0.02	0.00	0.07	0.03	0.07	0.00	0.08	0.04	0.03	0.03	0.02	0.00	0.06	0.24	0.00
SiO2	66.43	66.27	66.05	66.29	66.19	66.27	66.35	66.29	66.46	66.35	66.06	66.14	66.27	66.01	65.83	66.21	66.09	65.99	66.14
Al2O3	17.84	17.86	18.07	18.06	18.11	17.82	17.99	18.10	17.93	18.01	18.12	17.93	18.04	18.03	17.94	17.94	17.91	17.71	18.09
TiO2	0.00	0.02	0.00	0.00	0.04	0.04	0.00	0.07	0.05	0.00	0.00	0.02	0.00	0.02	0.00	0.02	0.03	0.02	0.00
FeO	0.07	0.03	0.02	0.01	0.00	0.00	0.06	0.00	0.03	0.00	0.02	0.00	0.06	0.02	0.02	0.00	0.04	0.01	0.00
MgO	0.00	0.00	0.00	0.00	0.01	0.01	0.00	0.00	0.02	0.00	0.00	0.00	0.00	0.00	0.01	0.00	0.00	0.00	0.00
MnO	0.00	0.00	0.00	0.00	0.00	0.00	0.00	0.00	0.00	0.00	0.00	0.00	0.00	0.00	0.00	0.00	0.00	0.00	0.00
Cr2O3	0.00	0.00	0.00	0.00	0.00	0.00	0.00	0.00	0.00	0.00	0.00	0.00	0.00	0.00	0.00	0.00	0.00	0.00	0.00
Total	100.95	101.20	101.00	101.24	101.14	100.94	101.14	101.14	101.23	101.16	101.11	100.87	101.16	100.62	100.41	100.87	100.83	100.70	100.81
Number of ions on the basis of 8 O																			
Na	0.04	0.04	0.04	0.04	0.04	0.03	0.04	0.03	0.04	0.04	0.04	0.04	0.03	0.05	0.05	0.04	0.03	0.03	0.03
K	0.94	0.94	0.95	0.95	0.95	0.96	0.94	0.95	0.94	0.95	0.96	0.95	0.96	0.93	0.94	0.95	0.96	0.96	0.95
Ca	0.00	0.02	0.01	0.01	0.00	0.00	0.00	0.00	0.00	0.00	0.00	0.00	0.00	0.00	0.00	0.00	0.00	0.01	0.00
Total	0.98	1.00	1.00	0.99	0.99	0.99	0.99	0.98	0.99	0.99	1.00	0.99	0.99	0.98	0.99	0.99	0.99	1.00	0.98
Si	3.03	3.02	3.02	3.02	3.02	3.03	3.03	3.02	3.03	3.03	3.02	3.03	3.02	3.02	3.02	3.03	3.03	3.03	3.02
AlIV	0.00	0.00	0.00	0.00	0.00	0.00	0.00	0.00	0.00	0.00	0.00	0.00	0.00	0.00	0.00	0.00	0.00	0.00	0.00
AlVI	0.96	0.96	0.97	0.97	0.97	0.96	0.97	0.97	0.96	0.97	0.98	0.97	0.97	0.97	0.97	0.97	0.97	0.96	0.98
Al tot.	0.96	0.96	0.97	0.97	0.97	0.96	0.97	0.97	0.96	0.97	0.98	0.97	0.97	0.97	0.97	0.97	0.97	0.96	0.98
Ti	0.00	0.00	0.00	0.00	0.00	0.00	0.00	0.00	0.00	0.00	0.00	0.00	0.00	0.00	0.00	0.00	0.00	0.00	0.00
Cr3+	0.00	0.00	0.00	0.00	0.00	0.00	0.00	0.00	0.00	0.00	0.00	0.00	0.00	0.00	0.00	0.00	0.00	0.00	0.00
Fe2+	0.00	0.00	0.00	0.00	0.00	0.00	0.00	0.00	0.00	0.00	0.00	0.00	0.00	0.00	0.00	0.00	0.00	0.00	0.00
Mg	0.00	0.00	0.00	0.00	0.00	0.00	0.00	0.00	0.00	0.00	0.00	0.00	0.00	0.00	0.00	0.00	0.00	0.00	0.00
Mn	0.00	0.00	0.00	0.00	0.00	0.00	0.00	0.00	0.00	0.00	0.00	0.00	0.00	0.00	0.00	0.00	0.00	0.00	0.00
Total	4.00	3.99	3.99	3.99	4.00	3.99	4.00	4.00	3.99	3.99	3.99	3.99	4.00	4.00	4.00	3.99	3.99	3.99	4.00
Albite	3.93	4.06	4.02	3.59	4.21	3.30	4.06	3.07	3.92	4.52	3.88	4.15	2.66	4.84	5.41	4.14	2.73	3.26	3.37
Orthoclase	96.07	94.30	95.13	95.86	95.70	96.70	95.60	96.79	95.75	95.48	95.73	95.65	97.19	95.00	94.49	95.86	96.98	95.56	96.63
Anorthite	0.00	1.63	0.84	0.55	0.10	0.00	0.35	0.14	0.34	0.00	0.39	0.20	0.15	0.16	0.10	0.00	0.29	1.18	0.00

Appendix Tab. A4: Electron microprobe analysis of feldspar.

Sample	51AnTA	51AnTA	51AnTA
Analysis	fsp10-1	fsp10-2	fsp10-3
Na2O	0.41	0.51	0.33
K2O	16.28	16.12	16.42
CaO	0.00	0.00	0.17
SiO2	66.24	66.19	65.74
Al2O3	18.06	18.00	17.88
TiO2	0.00	0.00	0.00
FeO	0.01	0.00	0.00
MgO	0.00	0.00	0.00
MnO	0.00	0.00	0.00
Cr2O3	0.00	0.00	0.00
Total	101.01	100.82	100.54
Number of ions on the basis of 8 O			
Na	0.04	0.05	0.03
K	0.95	0.94	0.96
Ca	0.00	0.00	0.01
Total	0.98	0.99	1.00
Si	3.02	3.03	3.02
AlIV	0.00	0.00	0.00
AlVI	0.97	0.97	0.97
Al tot.	0.97	0.97	0.97
Ti	0.00	0.00	0.00
Cr3+	0.00	0.00	0.00
Fe2+	0.00	0.00	0.00
Mg	0.00	0.00	0.00
Mn	0.00	0.00	0.00
Total	4.00	4.00	3.99
Albite	3.72	4.57	2.93
Orthoclase	96.28	95.43	96.22
Anorthite	0.00	0.00	0.85

Appendix Tab. A5: Garnet-biotite geothermometer.

Sample	45AnTA	45AnTA	45AnTA	45AnTA
Garnet	grt1-1 rim	grt1-86 rim	grt3-1 rim	grt3-36 rim
Biotite	bt3-1 rim	bt2-1 rim	bt5-1 rim	bt4-3 rim
Ferry and Spear (1978)				
ln KD	-1.674	-1.704	-1.696	-1.732
Temp(°C) 4kb	593	583	585	573
Temp(°C) 6kb	601	590	593	581
Temp(°C) 7kb	605	594	597	585
Perchuk and Lavrent'eva (1983)				
ln KD	1.674	1.704	1.696	1.732
Temp(°C) 6kb	596	590	592	585
Hoinkes (1986)				
ln KD	-1.674	-1.704	-1.696	-1.732
Temp(°C) 4kb	725	716	715	704
Temp(°C) 6kb	734	725	724	712
Temp(°C) 7kb	739	729	728	717
Indares and Martignole (1985)				
ln KD	-1.674	-1.704	-1.696	-1.732
Temp(°C) 4kb	624	638	616	616
Temp(°C) 6kb	632	645	624	623
Temp(°C) 7kb	636	649	628	627

Appendix Tab. B1: Electron microprobe analysis of apatite.

Sample	Apatit A	Apatit S	Theorie	2AnTA	2AnTA	2AnTA	2AnTA	2AnTA	2AnTA	2AnTA	2AnTA	18AnTA	18AnTA	18AnTA	18AnTA	18AnTA	18AnTA	18AnTA	18AnTA
Analysis				2-1	2-2	2-2	2-5	2-6	2-7	2-8	2-9	18-3	18-4	18-5	18-6	18-7	18-8	18-9	18-10
CaO	55.81	53.30	54.74	55.69	55.64	54.22	54.67	54.96	55.25	55.22	54.56	52.19	51.99	52.43	52.51	52.38	52.38	51.79	52.00
P2O5	42.39	40.95	41.56	44.56	44.83	43.22	45.10	45.39	45.16	44.54	44.36	44.49	44.46	44.51	45.34	44.37	45.48	45.26	44.88
SrO	0.00	0.00	0.00	0.00	0.19	0.05	0.03	0.06	0.10	0.12	0.05	0.17	0.18	0.09	0.25	0.12	0.13	0.31	0.05
SiO2	0.00	0.90	0.00	0.06	0.00	0.02	0.03	0.04	0.04	0.00	0.01	0.25	0.25	0.19	0.15	0.21	0.06	0.06	0.19
MnO	0.00	0.00	0.00	0.08	0.00	0.10	0.13	0.05	0.06	0.00	0.04	0.06	0.04	0.05	0.06	0.03	0.04	0.01	0.05
Y2O3	0.00	0.00	0.00	0.11	0.09	0.17	0.18	0.09	0.17	0.21	0.12	0.18	0.16	0.03	0.22	0.17	0.08	0.03	0.07
Ce2O3	0.00	1.21	0.00	0.00	0.02	0.07	0.13	0.02	0.01	0.14	0.06	0.08	0.18	0.06	0.12	0.13	0.05	0.15	0.15
F	0.00	3.55	3.70	3.58	3.65	3.00	3.56	3.28	3.58	2.94	3.10	3.62	3.96	3.50	3.73	3.44	3.53	4.00	3.34
Cl	0.00	0.02	0.00	0.01	0.01	0.01	0.01	0.01	0.00	0.01	0.00	0.01	0.00	0.01	0.01	0.01	0.01	0.00	0.00
Total	98.20	99.93	100.00	104.10	104.43	100.86	103.83	103.89	104.36	103.16	102.30	101.07	101.22	100.86	102.38	100.86	101.75	101.60	100.73
O=F	0.00	1.49	1.56	1.51	1.54	1.26	1.50	1.38	1.51	1.24	1.31	1.53	1.67	1.47	1.57	1.45	1.49	1.68	1.41
O=Cl	0.00	0.00	0.00	0.00	0.00	0.00	0.00	0.00	0.00	0.00	0.00	0.00	0.00	0.00	0.00	0.00	0.00	0.00	0.00
Total	98.20	98.43	98.44	102.59	102.89	99.60	102.33	102.51	102.85	101.92	100.99	99.54	99.55	99.38	100.81	99.41	100.26	99.91	99.32
Number of ions on the basis of 26 O																			
Ca	10.40	9.78	10.00	9.70	9.66	9.77	9.52	9.55	9.57	9.71	9.65	9.28	9.23	9.34	9.21	9.34	9.22	9.13	9.25
P	6.24	5.94	6.00	6.13	6.15	6.15	6.20	6.23	6.18	6.19	6.20	6.25	6.24	6.26	6.28	6.25	6.32	6.30	6.31
Sr	0.00	0.00	0.00	0.00	0.02	0.00	0.00	0.01	0.01	0.01	0.00	0.02	0.02	0.01	0.02	0.01	0.01	0.03	0.00
Si	0.00	0.15	0.00	0.01	0.00	0.00	0.00	0.01	0.01	0.00	0.00	0.04	0.04	0.03	0.02	0.04	0.01	0.01	0.03
Mn	0.00	0.00	0.00	0.01	0.00	0.01	0.02	0.01	0.01	0.00	0.01	0.01	0.01	0.01	0.01	0.00	0.01	0.00	0.01
Y	0.00	0.00	0.00	0.01	0.01	0.02	0.02	0.01	0.01	0.02	0.01	0.02	0.01	0.00	0.02	0.02	0.01	0.00	0.01
Ce	0.00	0.08	0.00	0.00	0.00	0.00	0.01	0.00	0.00	0.01	0.00	0.01	0.01	0.00	0.01	0.01	0.00	0.01	0.01
F	0.00	1.92	2.00	1.84	1.87	1.60	1.83	1.68	1.83	1.53	1.62	1.90	2.08	1.84	1.93	1.81	1.84	2.08	1.76
Cl	0.00	0.01	0.00	0.00	0.00	0.00	0.00	0.00	0.00	0.00	0.00	0.00	0.00	0.00	0.00	0.00	0.00	0.00	0.00
Total cat	16.64	17.87	18.00	17.71	17.71	17.56	17.60	17.49	17.63	17.47	17.50	17.52	17.63	17.49	17.51	17.48	17.42	17.57	17.38
A	6.24	6.09	6.00	6.14	6.15	6.15	6.21	6.24	6.19	6.19	6.20	6.29	6.28	6.29	6.31	6.29	6.33	6.31	6.34
B	10.40	9.85	10.00	9.72	9.68	9.81	9.56	9.57	9.61	9.75	9.68	9.33	9.28	9.36	9.27	9.38	9.25	9.17	9.28
C	0.00	1.93	2.00	1.85	1.87	1.60	1.83	1.68	1.83	1.53	1.62	1.91	2.08	1.84	1.93	1.82	1.84	2.08	1.76

Appendix Tab. B1: Electron microprobe analysis of apatite.

Sample	22AnTA	22AnTA	22AnTA	22AnTA	22AnTA	31AnTA	31AnTA	31AnTA	31AnTA	31AnTA	31AnTA	31AnTA	31AnTA	31AnTA	32AnTA	32AnTA	32AnTA	32AnTA	32AnTA
Analysis	22-2	22-5	22-7	22-9	22-10	31-1	31-2	31-3	31-4	31-6	31-7	31-8	31-9	31-10	32-1	32-2	32-3	32-4	32-5
CaO	56.07	55.91	55.50	55.66	55.43	54.49	54.47	54.47	54.95	55.46	54.65	54.72	54.54	54.18	54.96	54.91	55.09	54.74	54.34
P2O5	44.69	44.78	45.43	45.14	44.94	45.70	43.30	44.57	45.98	45.00	44.61	44.75	45.31	44.84	45.46	44.38	44.69	44.10	44.45
SrO	0.03	0.07	0.07	0.04	0.01	0.13	0.02	0.06	0.07	0.07	0.11	0.05	0.09	0.04	0.11	0.20	0.05	0.04	0.19
SiO2	0.00	0.01	0.00	0.04	0.04	0.07	0.10	0.41	0.06	0.05	0.06	0.14	0.21	0.07	0.00	0.11	0.00	0.03	0.02
MnO	0.11	0.09	0.08	0.06	0.10	0.03	0.00	0.07	0.00	0.11	0.00	0.00	0.07	0.08	0.09	0.06	0.08	0.12	0.01
Y2O3	0.02	0.07	0.08	0.06	0.17	0.03	0.08	0.13	0.02	0.04	0.08	0.05	0.25	0.06	0.03	0.10	0.09	0.06	0.07
Ce2O3	0.00	0.15	0.11	0.11	0.09	0.08	0.00	0.10	0.15	0.06	0.03	0.12	0.11	0.15	0.07	0.02	0.00	0.09	0.07
F	3.60	3.61	3.48	3.53	3.39	2.45	2.30	2.70	2.37	2.75	2.44	2.44	2.33	2.38	3.14	2.89	3.09	2.98	2.58
Cl	0.00	0.00	0.00	0.00	0.00	0.13	0.15	0.14	0.13	0.15	0.13	0.14	0.14	0.15	0.01	0.00	0.01	0.00	0.01
Total	104.53	104.67	104.75	104.64	104.15	103.08	100.43	102.65	103.73	103.68	102.12	102.41	103.07	101.95	103.87	102.67	103.10	102.15	101.73
O=F	1.52	1.52	1.47	1.49	1.43	1.03	0.97	1.14	1.00	1.16	1.03	1.03	0.98	1.00	1.32	1.22	1.30	1.26	1.09
O=Cl	0.00	0.00	0.00	0.00	0.00	0.03	0.03	0.03	0.03	0.03	0.03	0.03	0.03	0.03	0.00	0.00	0.00	0.00	0.00
Total	103.01	103.15	103.28	103.16	102.72	102.02	99.43	101.48	102.71	102.49	101.06	101.35	102.05	100.91	102.54	101.45	101.80	100.90	100.64
Number of ions on the basis of 26 O																			
Ca	9.73	9.69	9.69	9.74	9.64	9.52	9.85	9.59	9.55	9.69	9.68	9.66	9.56	9.60	9.55	9.69	9.67	9.71	9.66
P	6.13	6.14	6.16	6.13	6.18	6.31	6.19	6.20	6.31	6.21	6.25	6.24	6.28	6.28	6.24	6.19	6.20	6.18	6.25
Sr	0.00	0.01	0.01	0.00	0.00	0.01	0.00	0.01	0.01	0.01	0.01	0.01	0.01	0.00	0.01	0.02	0.00	0.00	0.02
Si	0.00	0.00	0.00	0.01	0.01	0.01	0.02	0.07	0.01	0.01	0.01	0.02	0.03	0.01	0.00	0.02	0.00	0.00	0.00
Mn	0.02	0.01	0.01	0.01	0.01	0.00	0.00	0.01	0.00	0.01	0.00	0.00	0.01	0.01	0.01	0.01	0.01	0.02	0.00
Y	0.00	0.01	0.01	0.01	0.01	0.00	0.01	0.01	0.00	0.00	0.01	0.00	0.02	0.01	0.00	0.01	0.01	0.01	0.01
Ce	0.00	0.01	0.01	0.01	0.01	0.00	0.00	0.01	0.01	0.00	0.00	0.01	0.01	0.01	0.00	0.00	0.00	0.01	0.00
F	1.85	1.85	1.76	1.79	1.74	1.26	1.23	1.40	1.22	1.42	1.28	1.27	1.21	1.24	1.61	1.50	1.60	1.56	1.35
Cl	0.00	0.00	0.00	0.00	0.00	0.03	0.04	0.04	0.04	0.04	0.04	0.04	0.04	0.04	0.00	0.00	0.00	0.00	0.00
Total cat	17.73	17.71	17.64	17.69	17.59	17.17	17.33	17.34	17.14	17.40	17.27	17.26	17.16	17.21	17.44	17.44	17.50	17.50	17.30
A	6.13	6.14	6.16	6.14	6.18	6.32	6.20	6.27	6.32	6.22	6.26	6.27	6.31	6.29	6.24	6.21	6.20	6.19	6.25
B	9.75	9.73	9.72	9.76	9.67	9.55	9.86	9.63	9.56	9.72	9.70	9.68	9.61	9.63	9.58	9.73	9.69	9.75	9.69
C	1.85	1.85	1.76	1.79	1.74	1.30	1.27	1.44	1.25	1.46	1.31	1.31	1.25	1.28	1.61	1.51	1.60	1.56	1.36

Appendix Tab. B1: Electron microprobe analysis of apatite.

Sample	32AnTA	32AnTA	32AnTA	32AnTA	32AnTA	35AnTA	35AnTA	35AnTA	35AnTA	35AnTA	35AnTA	35AnTA	35AnTA	41 AnTA	41 AnTA	41 AnTA	41 AnTA	41 AnTA	41 AnTA
Analysis	32-6	32-7	32-8	32-9	32-10	35-1	35-4	35-5	35-6	35-7	35-8	35-9	35-10	41-1	41-2	41-3	41-4	41-5	41-6
CaO	55.02	54.48	54.41	54.39	55.03	54.45	54.87	55.11	54.75	55.16	54.41	54.80	55.87	54.62	53.86	55.11	54.79	54.78	54.04
P2O5	44.42	44.17	43.65	44.57	44.50	43.82	44.74	44.51	44.63	45.66	44.40	45.30	44.37	44.76	44.80	43.65	44.57	45.37	44.98
SrO	0.10	0.02	0.01	0.49	0.04	0.00	0.00	0.01	0.05	0.08	0.05	0.05	0.03	0.07	0.13	0.05	0.23	0.04	0.23
SiO2	0.03	0.02	0.11	0.01	0.04	0.04	0.04	0.05	0.03	0.02	0.00	0.01	0.00	0.24	0.20	0.22	0.14	0.20	0.07
MnO	0.15	0.01	0.07	0.08	0.03	0.10	0.13	0.06	0.03	0.08	0.03	0.05	0.08	0.00	0.00	0.04	0.07	0.02	0.03
Y2O3	0.11	0.01	0.23	0.00	0.09	0.03	0.03	0.00	0.02	0.00	0.03	0.07	0.03	0.05	0.06	0.10	0.09	0.03	0.04
Ce2O3	0.02	0.12	0.15	0.00	0.07	0.03	0.16	0.00	0.08	0.02	0.00	0.00	0.00	0.24	0.22	0.24	0.10	0.31	0.09
F	2.91	2.46	2.41	2.52	2.67	1.98	1.96	1.98	1.89	2.22	2.03	2.07	2.11	3.91	3.69	3.32	3.52	3.49	3.41
Cl	0.00	0.00	0.00	0.01	0.00	0.05	0.04	0.02	0.05	0.08	0.06	0.04	0.04	0.00	0.01	0.01	0.01	0.01	0.00
Total	102.76	101.29	101.05	102.07	102.48	100.50	101.96	101.75	101.52	103.32	101.01	102.38	102.53	103.88	102.96	102.73	103.51	104.25	102.87
O=F	1.23	1.04	1.02	1.06	1.13	0.83	0.82	0.83	0.80	0.93	0.85	0.87	0.89	1.65	1.55	1.40	1.48	1.47	1.44
O=Cl	0.00	0.00	0.00	0.00	0.00	0.01	0.01	0.00	0.01	0.02	0.01	0.01	0.01	0.00	0.00	0.00	0.00	0.00	0.00
Total	101.53	100.25	100.03	101.00	101.35	99.66	101.13	100.91	100.71	102.37	100.14	101.50	101.63	102.24	101.40	101.33	102.03	102.78	101.43
Number of ions on the basis of 26 O																			
Ca	9.71	9.74	9.77	9.65	9.73	9.82	9.74	9.81	9.76	9.63	9.74	9.66	9.90	9.50	9.44	9.75	9.59	9.49	9.48
P	6.19	6.24	6.20	6.25	6.21	6.25	6.28	6.26	6.28	6.30	6.28	6.31	6.21	6.15	6.20	6.10	6.16	6.21	6.23
Sr	0.01	0.00	0.00	0.05	0.00	0.00	0.00	0.00	0.00	0.01	0.00	0.00	0.00	0.01	0.01	0.00	0.02	0.00	0.02
Si	0.01	0.00	0.02	0.00	0.01	0.01	0.01	0.01	0.00	0.00	0.00	0.00	0.00	0.04	0.03	0.04	0.02	0.03	0.01
Mn	0.02	0.00	0.01	0.01	0.00	0.01	0.02	0.01	0.00	0.01	0.00	0.01	0.01	0.00	0.00	0.01	0.01	0.00	0.00
Y	0.01	0.00	0.02	0.00	0.01	0.00	0.00	0.00	0.00	0.00	0.00	0.01	0.00	0.00	0.01	0.01	0.01	0.00	0.00
Ce	0.00	0.01	0.01	0.00	0.00	0.00	0.01	0.00	0.00	0.00	0.00	0.00	0.00	0.01	0.01	0.01	0.01	0.02	0.01
F	1.52	1.30	1.28	1.32	1.40	1.05	1.03	1.04	0.99	1.14	1.07	1.08	1.10	2.01	1.91	1.73	1.82	1.79	1.77
Cl	0.00	0.00	0.00	0.00	0.00	0.01	0.01	0.01	0.01	0.02	0.02	0.01	0.01	0.00	0.00	0.00	0.00	0.00	0.00
Total cat	17.46	17.29	17.31	17.28	17.36	17.16	17.09	17.13	17.07	17.13	17.12	17.07	17.24	17.73	17.61	17.66	17.64	17.54	17.52
A	6.20	6.24	6.22	6.25	6.22	6.25	6.28	6.27	6.29	6.31	6.28	6.31	6.21	6.19	6.23	6.14	6.18	6.24	6.24
B	9.75	9.75	9.82	9.71	9.75	9.84	9.77	9.82	9.77	9.65	9.75	9.68	9.91	9.53	9.47	9.79	9.63	9.51	9.51
C	1.52	1.30	1.28	1.32	1.40	1.07	1.04	1.05	1.01	1.17	1.09	1.09	1.12	2.01	1.91	1.74	1.82	1.79	1.77

Appendix Tab. B1: Electron microprobe analysis of apatite.

Sample	41 AnTA	41 AnTA	41 AnTA	43AnTA	43AnTA	43AnTA	43AnTA	43AnTA	43AnTA	43AnTA	43AnTA	43AnTA	44AnTA	44AnTA	44AnTA	44AnTA	44AnTA	44AnTA	44AnTA
Analysis	41-7	41-8	41-9	43-1	43-2	43-3	43-5	43-6	43-7	43-8	43-9	43-10	44-2	44-3	44-4	44-5	44-6	44-7	44-8
CaO	55.31	54.61	54.37	54.00	54.27	54.92	54.52	55.07	54.69	54.18	54.79	53.88	54.88	55.13	55.18	54.92	55.02	55.02	54.02
P2O5	45.02	45.02	44.48	44.79	45.84	44.79	45.20	44.81	44.43	45.27	44.55	44.84	45.55	44.00	45.10	45.02	44.60	45.45	44.03
SrO	0.31	0.06	0.11	0.02	0.08	0.04	0.06	0.11	0.06	0.02	0.05	0.03	0.03	0.05	0.00	0.03	0.04	0.01	0.01
SiO2	0.02	0.19	0.19	0.10	0.04	0.02	0.04	0.02	0.03	0.01	0.00	0.00	0.09	0.12	0.07	0.03	0.08	0.04	0.05
MnO	0.06	0.02	0.02	0.05	0.02	0.11	0.00	0.14	0.01	0.02	0.08	0.05	0.06	0.02	0.05	0.05	0.07	0.00	0.04
Y2O3	0.09	0.07	0.04	0.00	0.00	0.00	0.02	0.04	0.02	0.02	0.00	0.03	0.17	0.14	0.23	0.15	0.09	0.16	0.23
Ce2O3	0.09	0.30	0.33	0.13	0.10	0.06	0.04	0.23	0.04	0.10	0.07	0.09	0.00	0.03	0.03	0.06	0.04	0.07	0.03
F	3.43	4.00	3.50	3.31	3.69	3.62	3.40	3.72	3.45	3.36	3.41	3.79	3.00	2.94	3.49	3.33	3.05	3.04	2.98
Cl	0.01	0.01	0.00	0.00	0.01	0.01	0.00	0.00	0.00	0.00	0.00	0.00	0.02	0.02	0.03	0.03	0.01	0.03	0.02
Total	104.33	104.27	103.05	102.39	104.05	103.57	103.28	104.12	102.73	103.00	102.93	102.71	103.79	102.46	104.17	103.61	103.00	103.81	101.41
O=F	1.44	1.68	1.47	1.39	1.55	1.52	1.43	1.56	1.45	1.41	1.43	1.60	1.26	1.24	1.47	1.40	1.28	1.28	1.26
O=Cl	0.00	0.00	0.00	0.00	0.00	0.00	0.00	0.00	0.00	0.00	0.00	0.00	0.00	0.00	0.01	0.01	0.00	0.01	0.01
Total	102.89	102.58	101.57	101.00	102.49	102.04	101.84	102.56	101.27	101.58	101.50	101.11	102.52	101.22	102.69	102.20	101.71	102.52	100.15
Number of ions on the basis of 26 O																			
Ca	9.61	9.46	9.55	9.51	9.38	9.59	9.52	9.58	9.63	9.47	9.63	9.45	9.54	9.76	9.58	9.58	9.67	9.57	9.64
P	6.18	6.16	6.17	6.23	6.26	6.18	6.23	6.16	6.18	6.26	6.19	6.22	6.25	6.16	6.19	6.21	6.19	6.24	6.21
Sr	0.03	0.01	0.01	0.00	0.01	0.00	0.01	0.01	0.01	0.00	0.00	0.00	0.00	0.00	0.00	0.00	0.00	0.00	0.00
Si	0.00	0.03	0.03	0.02	0.01	0.00	0.01	0.00	0.01	0.00	0.00	0.00	0.01	0.02	0.01	0.00	0.01	0.01	0.01
Mn	0.01	0.00	0.00	0.01	0.00	0.01	0.00	0.02	0.00	0.00	0.01	0.01	0.01	0.00	0.01	0.01	0.01	0.00	0.01
Y	0.01	0.01	0.00	0.00	0.00	0.00	0.00	0.00	0.00	0.00	0.00	0.00	0.01	0.01	0.02	0.01	0.01	0.01	0.02
Ce	0.01	0.02	0.02	0.01	0.01	0.00	0.00	0.01	0.00	0.01	0.00	0.01	0.00	0.00	0.00	0.00	0.00	0.00	0.00
F	1.76	2.04	1.81	1.72	1.88	1.86	1.75	1.91	1.80	1.73	1.77	1.97	1.54	1.54	1.79	1.71	1.58	1.56	1.57
Cl	0.00	0.00	0.00	0.00	0.00	0.00	0.00	0.00	0.00	0.00	0.00	0.00	0.01	0.01	0.01	0.01	0.00	0.01	0.01
Total cat	17.60	17.73	17.60	17.49	17.54	17.66	17.52	17.70	17.62	17.48	17.60	17.65	17.37	17.51	17.60	17.54	17.48	17.40	17.46
A	6.18	6.19	6.20	6.25	6.27	6.18	6.24	6.16	6.19	6.26	6.19	6.22	6.27	6.18	6.20	6.21	6.21	6.25	6.22
B	9.66	9.49	9.59	9.52	9.39	9.61	9.53	9.63	9.64	9.49	9.65	9.47	9.56	9.79	9.61	9.61	9.69	9.59	9.67
C	1.76	2.05	1.81	1.72	1.88	1.87	1.75	1.91	1.80	1.74	1.77	1.97	1.54	1.54	1.79	1.72	1.58	1.57	1.58

Appendix Tab. B1: Electron microprobe analysis of apatite.

Sample	44AnTA	44AnTA	51AnTA	51AnTA	51AnTA	51AnTA	51AnTA	51AnTA	51AnTA	55AnTA	55AnTA	55AnTA	55AnTA	55AnTA	55AnTA	55AnTA	55AnTA	55AnTA	58AnTA
Analysis	44-9	44-10	51-1	51-2	51-3	51-4	51-5	51-7	51-9	55-1	55-2	55-3	55-4	55-5	55-6	55-8	55-9	55-10	58-1
CaO	55.53	55.06	55.15	54.83	55.58	54.70	55.54	55.23	55.16	54.68	53.92	54.08	54.17	53.37	54.71	54.25	54.89	54.80	54.85
P2O5	45.14	44.83	45.17	45.55	44.17	44.19	44.94	44.59	43.46	45.99	44.05	44.73	44.93	44.62	44.58	43.79	45.25	44.77	45.69
SrO	0.07	0.06	0.01	0.22	0.09	0.08	0.06	0.25	0.26	0.15	0.15	0.24	0.02	0.03	0.00	0.12	0.14	0.16	0.24
SiO2	0.14	0.09	0.00	0.00	0.00	0.01	0.00	0.00	0.00	0.00	0.02	0.02	0.00	0.00	0.00	0.00	0.00	0.00	0.00
MnO	0.04	0.04	0.13	0.00	0.00	0.00	0.05	0.00	0.03	0.00	0.03	0.03	0.00	0.02	0.09	0.00	0.05	0.02	0.05
Y2O3	0.19	0.17	0.21	0.14	0.21	0.22	0.09	0.13	0.12	0.14	0.15	0.22	0.20	0.48	0.45	0.04	0.18	0.10	0.05
Ce2O3	0.00	0.06	0.01	0.00	0.05	0.10	0.08	0.13	0.08	0.07	0.11	0.11	0.20	0.10	0.20	0.09	0.06	0.00	0.00
F	3.16	3.21	3.52	3.23	3.22	3.13	3.31	3.30	3.39	3.26	3.49	3.81	3.84	3.29	3.61	3.74	3.38	3.51	3.28
Cl	0.03	0.00	0.00	0.01	0.01	0.00	0.01	0.01	0.01	0.00	0.00	0.00	0.00	0.01	0.00	0.00	0.01	0.00	0.04
Total	104.28	103.51	104.19	103.99	103.32	102.45	104.08	103.64	102.50	104.29	101.91	103.23	103.37	101.91	103.63	102.02	103.95	103.37	104.19
O=F	1.33	1.35	1.48	1.36	1.36	1.32	1.39	1.39	1.43	1.37	1.47	1.60	1.62	1.38	1.52	1.57	1.42	1.48	1.38
O=Cl	0.01	0.00	0.00	0.00	0.00	0.00	0.00	0.00	0.00	0.00	0.00	0.00	0.00	0.00	0.00	0.00	0.00	0.00	0.01
Total	102.95	102.16	102.71	102.63	101.96	101.13	102.68	102.24	101.07	102.91	100.44	101.63	101.75	100.52	102.11	100.45	102.53	101.90	102.80
Number of ions on the basis of 26 O																			
Ca	9.63	9.62	9.57	9.51	9.78	9.68	9.67	9.67	9.80	9.44	9.58	9.47	9.46	9.45	9.57	9.63	9.54	9.59	9.50
P	6.19	6.19	6.19	6.25	6.14	6.18	6.18	6.17	6.10	6.28	6.18	6.19	6.20	6.24	6.16	6.14	6.22	6.19	6.25
Sr	0.01	0.01	0.00	0.02	0.01	0.01	0.01	0.02	0.03	0.01	0.01	0.02	0.00	0.00	0.00	0.01	0.01	0.02	0.02
Si	0.02	0.01	0.00	0.00	0.00	0.00	0.00	0.00	0.00	0.00	0.00	0.00	0.00	0.00	0.00	0.00	0.00	0.00	0.00
Mn	0.01	0.01	0.02	0.00	0.00	0.00	0.01	0.00	0.00	0.00	0.00	0.00	0.00	0.00	0.01	0.00	0.01	0.00	0.01
Y	0.02	0.01	0.02	0.01	0.02	0.02	0.01	0.01	0.01	0.01	0.01	0.02	0.02	0.04	0.04	0.00	0.02	0.01	0.00
Ce	0.00	0.00	0.00	0.00	0.00	0.01	0.00	0.01	0.01	0.00	0.01	0.01	0.01	0.01	0.01	0.01	0.00	0.00	0.00
F	1.62	1.66	1.80	1.65	1.67	1.64	1.70	1.71	1.78	1.66	1.83	1.97	1.98	1.72	1.86	1.96	1.73	1.81	1.68
Cl	0.01	0.00	0.00	0.00	0.00	0.00	0.00	0.00	0.00	0.00	0.00	0.00	0.00	0.00	0.00	0.00	0.00	0.00	0.01
Total cat	17.50	17.52	17.60	17.45	17.62	17.53	17.57	17.59	17.73	17.41	17.63	17.68	17.68	17.47	17.66	17.76	17.53	17.62	17.47
A	6.21	6.21	6.19	6.25	6.14	6.18	6.18	6.17	6.10	6.28	6.18	6.19	6.20	6.24	6.16	6.14	6.22	6.19	6.25
B	9.66	9.65	9.61	9.55	9.80	9.71	9.69	9.71	9.85	9.47	9.61	9.52	9.49	9.50	9.64	9.65	9.58	9.61	9.53
C	1.63	1.66	1.80	1.66	1.68	1.64	1.70	1.71	1.78	1.66	1.83	1.97	1.98	1.72	1.86	1.96	1.74	1.81	1.69

Appendix Tab. B1: Electron microprobe analysis of apatite.

Sample	58AnTA	58AnTA	58AnTA	58AnTA	58AnTA	58AnTA	58AnTA	58AnTA
Analysis	58-3	58-4	58-5	58-6	58-7	58-8	58-9	58-10
CaO	54.95	54.86	54.71	55.28	55.27	54.30	54.43	54.37
P2O5	45.01	44.37	45.37	45.13	45.61	45.01	44.18	44.98
SrO	0.00	0.10	0.06	0.00	0.14	0.28	0.14	0.16
SiO2	0.00	0.00	0.00	0.04	0.00	0.00	0.09	0.00
MnO	0.07	0.09	0.02	0.06	0.02	0.07	0.04	0.00
Y2O3	0.02	0.02	0.00	0.17	0.09	0.01	0.11	0.05
Ce2O3	0.02	0.02	0.06	0.03	0.00	0.11	0.00	0.00
F	3.10	3.01	3.19	3.27	2.85	2.79	3.20	2.75
Cl	0.03	0.02	0.05	0.02	0.05	0.06	0.02	0.05
Total	103.20	102.49	103.45	103.99	104.02	102.64	102.20	102.36
O=F	1.30	1.27	1.34	1.37	1.20	1.17	1.35	1.16
O=Cl	0.01	0.00	0.01	0.00	0.01	0.01	0.00	0.01
Total	101.89	101.22	102.09	102.61	102.81	101.45	100.85	101.19
Number of ions on the basis of 26 O								
Ca	9.62	9.70	9.54	9.61	9.60	9.56	9.64	9.59
P	6.22	6.20	6.25	6.20	6.26	6.26	6.18	6.27
Sr	0.00	0.01	0.01	0.00	0.01	0.03	0.01	0.02
Si	0.00	0.00	0.00	0.01	0.00	0.00	0.01	0.00
Mn	0.01	0.01	0.00	0.01	0.00	0.01	0.01	0.00
Y	0.00	0.00	0.00	0.01	0.01	0.00	0.01	0.00
Ce	0.00	0.00	0.00	0.00	0.00	0.01	0.00	0.00
F	1.60	1.57	1.64	1.68	1.46	1.45	1.67	1.43
Cl	0.01	0.00	0.01	0.00	0.01	0.02	0.01	0.01
Total cat	17.47	17.49	17.45	17.52	17.35	17.33	17.54	17.32
A	6.22	6.20	6.25	6.21	6.26	6.26	6.20	6.27
B	9.63	9.72	9.55	9.64	9.62	9.61	9.67	9.61
C	1.61	1.57	1.66	1.68	1.47	1.47	1.68	1.45

Sample	9AnTA	9AnTA	9AnTA	9AnTA	12AnTA	12AnTA	12AnTA	12AnTA	12AnTA	12AnTA
Analysis	9-3	9-4	9-5	9-8	12-1	12-3	12-4	12-6	12-7	12-8
CaO	54.89	55.29	54.45	55.13	55.62	54.95	55.58	54.89	54.87	55.25
P2O5	45.06	45.27	44.01	44.76	43.43	44.72	43.89	44.00	45.53	44.94
SrO	0.07	0.10	0.03	0.08	0.06	0.05	0.01	0.04	0.04	0.08
SiO2	0.05	0.01	0.08	0.03	0.01	0.00	0.02	0.00	0.02	0.03
MnO	0.04	0.16	0.07	0.08	0.03	0.03	0.10	0.05	0.16	0.09
Y2O3	0.14	0.17	0.19	0.16	0.08	0.07	0.13	0.08	0.19	0.09
Ce2O3	0.00	0.10	0.00	0.05	0.03	0.02	0.09	0.00	0.11	0.00
F	3.41	3.71	3.72	4.08	4.05	3.80	3.49	3.56	2.94	3.29
Cl	0.01	0.00	0.00	0.00	0.04	0.06	0.12	0.12	0.14	0.05
Total	103.66	104.80	102.55	104.36	103.34	103.69	103.42	102.73	103.98	103.82
O=F	1.44	1.56	1.57	1.72	1.70	1.60	1.47	1.50	1.24	1.39
O=Cl	0.00	0.00	0.00	0.00	0.01	0.01	0.03	0.03	0.03	0.01
Total	102.22	103.24	100.98	102.65	101.63	102.07	101.92	101.20	102.71	102.42
Number of ions on the basis of 26 O										
Ca	9.57	9.55	9.61	9.56	9.80	9.59	9.78	9.69	9.53	9.63
P	6.20	6.18	6.14	6.14	6.05	6.16	6.10	6.14	6.25	6.19
Sr	0.01	0.01	0.00	0.01	0.01	0.00	0.00	0.00	0.00	0.01
Si	0.01	0.00	0.01	0.00	0.00	0.00	0.00	0.00	0.00	0.01
Mn	0.00	0.02	0.01	0.01	0.00	0.00	0.01	0.01	0.02	0.01
Y	0.01	0.01	0.02	0.01	0.01	0.01	0.01	0.01	0.02	0.01
Ce	0.00	0.01	0.00	0.00	0.00	0.00	0.01	0.00	0.01	0.00
F	1.75	1.89	1.94	2.09	2.10	1.96	1.81	1.86	1.51	1.69
Cl	0.00	0.00	0.00	0.00	0.01	0.02	0.03	0.03	0.04	0.01
Total cat	17.56	17.67	17.74	17.83	17.98	17.74	17.76	17.73	17.38	17.56
A	6.21	6.18	6.15	6.14	6.05	6.16	6.10	6.14	6.25	6.19
B	9.59	9.60	9.64	9.60	9.82	9.60	9.81	9.71	9.58	9.66
C	1.76	1.89	1.94	2.09	2.12	1.97	1.85	1.89	1.55	1.71

Appendix Tab. B1: Electron microprobe analysis of apatite.

Sample	12AnTA	12AnTA	17AnTA	17AnTA	17AnTA	17AnTA	17AnTA	17AnTA	17AnTA	17AnTA	17AnTA	25AnTA	25AnTA	25AnTA	25AnTA	25AnTA	25AnTA	25AnTA	25AnTA
Analysis	12-9	12-10	17-1	17-2	17-4	17-5	17-6	17-7	17-8	17-9	17-10	25-1	25-2	25-3	25-4	25-5	25-6	25-7	25-10
CaO	54.97	54.71	54.02	55.06	54.31	54.64	54.37	54.40	54.02	54.50	54.31	54.28	55.35	55.12	54.56	54.72	54.47	54.98	54.71
P2O5	44.95	44.27	42.80	43.02	43.76	43.48	44.45	44.58	42.21	45.31	44.44	45.19	43.15	44.16	43.67	45.27	45.95	44.37	45.39
SrO	0.00	0.05	0.01	0.03	0.02	0.08	0.06	0.39	0.02	0.02	0.12	0.01	0.00	0.03	0.05	0.02	0.01	0.10	0.02
SiO2	0.00	0.00	0.25	0.00	0.02	0.03	0.05	0.02	0.07	0.37	0.04	0.05	0.04	0.05	0.06	0.06	0.00	0.04	0.04
MnO	0.05	0.27	0.13	0.05	0.01	0.02	0.04	0.00	0.06	0.04	0.15	0.06	0.11	0.09	0.18	0.08	0.11	0.06	0.07
Y2O3	0.15	0.13	0.08	0.05	0.05	0.07	0.09	0.17	0.09	0.08	0.19	0.17	0.17	0.24	0.21	0.31	0.25	0.17	0.17
Ce2O3	0.06	0.02	0.41	0.12	0.14	0.27	0.13	0.04	0.07	0.46	0.15	0.02	0.05	0.05	0.00	0.00	0.10	0.00	0.02
F	2.95	3.14	3.17	4.03	3.47	4.00	4.13	4.11	3.92	3.29	3.96	3.93	3.29	3.51	3.99	3.36	3.60	3.80	3.61
Cl	0.11	0.05	0.01	0.01	0.01	0.01	0.00	0.01	0.01	0.00	0.00	0.00	0.00	0.01	0.00	0.01	0.01	0.01	0.01
Total	103.23	102.65	100.88	102.38	101.79	102.59	103.31	103.70	100.47	104.08	103.35	103.70	102.16	103.25	102.72	103.83	104.48	103.52	104.04
O=F	1.24	1.32	1.34	1.70	1.46	1.68	1.74	1.73	1.65	1.39	1.67	1.66	1.39	1.48	1.68	1.41	1.52	1.60	1.52
O=Cl	0.02	0.01	0.00	0.00	0.00	0.00	0.00	0.00	0.00	0.00	0.00	0.00	0.00	0.00	0.00	0.00	0.00	0.00	0.00
Total	101.97	101.32	99.54	100.68	100.32	100.90	101.57	101.97	98.82	102.69	101.68	102.04	100.77	101.77	101.04	102.42	102.96	101.92	102.52
Number of ions on the basis of 26 O																			
Ca	9.63	9.66	9.75	9.79	9.67	9.68	9.52	9.50	9.79	9.45	9.51	9.43	9.87	9.69	9.64	9.51	9.39	9.62	9.48
P	6.22	6.18	6.10	6.05	6.16	6.09	6.15	6.15	6.04	6.21	6.15	6.20	6.08	6.13	6.10	6.22	6.26	6.14	6.22
Sr	0.00	0.01	0.00	0.00	0.00	0.01	0.01	0.04	0.00	0.00	0.01	0.00	0.00	0.00	0.00	0.00	0.00	0.01	0.00
Si	0.00	0.00	0.04	0.00	0.00	0.00	0.01	0.00	0.01	0.06	0.01	0.01	0.01	0.01	0.01	0.01	0.00	0.01	0.01
Mn	0.01	0.04	0.02	0.01	0.00	0.00	0.01	0.00	0.01	0.01	0.02	0.01	0.02	0.01	0.02	0.01	0.01	0.01	0.01
Y	0.01	0.01	0.01	0.00	0.00	0.01	0.01	0.01	0.01	0.01	0.02	0.01	0.01	0.02	0.02	0.03	0.02	0.01	0.01
Ce	0.00	0.00	0.03	0.01	0.01	0.02	0.01	0.00	0.00	0.03	0.01	0.00	0.00	0.00	0.00	0.00	0.01	0.00	0.00
F	1.53	1.64	1.69	2.12	1.82	2.09	2.13	2.12	2.10	1.69	2.05	2.02	1.73	1.82	2.08	1.72	1.83	1.97	1.85
Cl	0.03	0.02	0.00	0.00	0.00	0.00	0.00	0.00	0.00	0.00	0.00	0.00	0.00	0.00	0.00	0.00	0.00	0.00	0.00
Total cat	17.44	17.55	17.64	17.98	17.67	17.90	17.83	17.82	17.97	17.45	17.78	17.69	17.73	17.69	17.87	17.51	17.52	17.77	17.59
A	6.22	6.18	6.14	6.05	6.16	6.09	6.15	6.15	6.06	6.27	6.16	6.21	6.09	6.14	6.11	6.23	6.26	6.14	6.22
B	9.65	9.72	9.80	9.82	9.68	9.71	9.54	9.55	9.81	9.49	9.57	9.46	9.91	9.73	9.69	9.55	9.43	9.65	9.51
C	1.56	1.65	1.69	2.12	1.83	2.10	2.13	2.12	2.10	1.69	2.05	2.02	1.73	1.82	2.08	1.73	1.83	1.97	1.85

Appendix Tab. B1: Electron microprobe analysis of apatite.

Sample	38AnTA	38AnTA	38AnTA	38AnTA	38AnTA	38AnTA	57AnTA	57AnTA	57AnTA	57AnTA	57AnTA	57AnTA	23AnTA	23AnTA	23AnTA	23AnTA	23AnTA	23AnTA
Analysis	38-1	38-3	38-5	38-7	38-8	38-9	57-1	57-4	57-5	57-6	57-9	57-10	23-1	23-2	23-3	23-4	23-5	23-6
CaO	55.38	54.53	54.98	55.22	54.62	55.26	54.86	54.79	54.26	54.39	54.42	54.72	54.91	54.75	54.94	54.32	54.39	54.01
P2O5	44.88	45.22	44.51	44.04	45.21	45.00	43.04	44.91	43.89	45.32	44.48	45.51	43.95	45.76	44.55	45.76	45.38	45.33
SrO	0.43	0.50	0.31	0.27	0.37	0.48	0.36	0.13	0.38	0.30	0.21	0.35	0.16	0.16	0.15	0.18	0.12	0.25
SiO2	0.00	0.00	0.00	0.00	0.00	0.00	0.11	0.00	0.45	0.06	0.00	0.02	0.01	0.00	0.00	0.00	0.02	0.00
MnO	0.03	0.01	0.00	0.00	0.06	0.02	0.00	0.00	0.04	0.00	0.00	0.03	0.00	0.05	0.00	0.02	0.00	0.04
Y2O3	0.02	0.02	0.00	0.17	0.02	0.05	0.09	0.04	0.05	0.02	0.04	0.01	0.01	0.05	0.03	0.05	0.00	0.05
Ce2O3	0.00	0.11	0.02	0.00	0.11	0.01	0.00	0.02	0.00	0.09	0.09	0.04	0.04	0.05	0.00	0.00	0.10	0.00
F	4.25	4.37	3.70	4.21	4.04	3.64	3.81	3.92	3.58	3.68	3.86	3.66	3.69	3.34	3.23	3.22	3.16	3.19
Cl	0.00	0.01	0.00	0.00	0.01	0.00	0.01	0.01	0.01	0.01	0.02	0.02	0.02	0.00	0.01	0.00	0.01	0.00
Total	104.99	104.76	103.51	103.89	104.43	104.46	102.28	103.84	102.66	103.87	103.12	104.34	102.79	104.15	102.91	103.53	103.17	102.86
O=F	1.79	1.84	1.56	1.77	1.70	1.53	1.60	1.65	1.51	1.55	1.63	1.54	1.55	1.41	1.36	1.35	1.33	1.34
O=Cl	0.00	0.00	0.00	0.00	0.00	0.00	0.00	0.00	0.00	0.00	0.00	0.00	0.00	0.00	0.00	0.00	0.00	0.00
Total	103.20	102.92	101.95	102.12	102.73	102.92	100.67	102.19	101.15	102.32	101.48	102.80	101.23	102.74	101.55	102.18	101.84	101.52
Number of ions on the basis of 26 O																		
Ca	9.56	9.41	9.62	9.66	9.45	9.59	9.77	9.53	9.57	9.45	9.55	9.47	9.69	9.47	9.66	9.44	9.50	9.46
P	6.12	6.17	6.16	6.08	6.18	6.17	6.06	6.17	6.12	6.22	6.17	6.22	6.13	6.26	6.19	6.28	6.26	6.27
Sr	0.04	0.05	0.03	0.03	0.03	0.05	0.03	0.01	0.04	0.03	0.02	0.03	0.02	0.01	0.01	0.02	0.01	0.02
Si	0.00	0.00	0.00	0.00	0.00	0.00	0.02	0.00	0.07	0.01	0.00	0.00	0.00	0.00	0.00	0.00	0.00	0.00
Mn	0.00	0.00	0.00	0.00	0.01	0.00	0.00	0.00	0.01	0.00	0.00	0.00	0.00	0.01	0.00	0.00	0.00	0.01
Y	0.00	0.00	0.00	0.01	0.00	0.00	0.01	0.00	0.00	0.00	0.00	0.00	0.00	0.00	0.00	0.00	0.00	0.00
Ce	0.00	0.01	0.00	0.00	0.01	0.00	0.00	0.00	0.00	0.01	0.01	0.00	0.00	0.00	0.00	0.00	0.01	0.00
F	2.17	2.23	1.91	2.17	2.06	1.86	2.00	2.02	1.86	1.89	2.00	1.87	1.92	1.71	1.68	1.65	1.63	1.65
Cl	0.00	0.00	0.00	0.00	0.00	0.00	0.00	0.00	0.00	0.00	0.00	0.00	0.00	0.00	0.00	0.00	0.00	0.00
Total cat	17.90	17.86	17.72	17.95	17.75	17.67	17.89	17.74	17.68	17.60	17.75	17.60	17.77	17.47	17.55	17.40	17.41	17.41
A	6.12	6.17	6.16	6.08	6.18	6.17	6.08	6.18	6.19	6.23	6.17	6.22	6.13	6.26	6.19	6.28	6.27	6.27
B	9.61	9.47	9.65	9.69	9.51	9.64	9.81	9.55	9.62	9.48	9.58	9.50	9.71	9.50	9.68	9.46	9.52	9.49
C	2.17	2.23	1.91	2.17	2.06	1.86	2.00	2.02	1.87	1.89	2.01	1.88	1.93	1.71	1.68	1.65	1.63	1.65

Appendix Tab. B1: Electron microprobe analysis of apatite.

Sample	23AnTA	23AnTA	23AnTA	23AnTA	26AnTA	26AnTA	26AnTA	26AnTA	26AnTA	26AnTA	26AnTA	26AnTA	6AnTA	6AnTA	6AnTA	6AnTA	6AnTA	6AnTA
Analysis	23-7	23-8	23-9	23-10	26-1	26-2	26-5	26-6	26-7	26-8	26-9	26-10	6-1	6-2	6-3	6-4	6-5	6-6
CaO	54.99	54.25	54.26	54.70	55.30	54.43	54.41	54.19	53.64	54.99	54.41	53.99	54.58	53.73	54.73	54.41	55.01	55.12
P2O5	45.92	45.13	44.95	46.11	45.37	44.67	45.07	44.56	43.88	46.36	44.15	45.05	44.43	45.09	44.76	46.02	44.59	44.86
SrO	0.14	0.19	0.21	0.13	0.11	0.08	0.19	0.12	0.24	0.14	0.06	0.05	0.00	0.06	0.05	0.07	0.05	0.00
SiO2	0.00	0.02	0.00	0.00	0.00	0.24	0.02	0.00	0.39	0.00	0.00	0.17	0.03	0.09	0.06	0.08	0.11	0.10
MnO	0.06	0.08	0.06	0.00	0.00	0.04	0.00	0.00	0.00	0.01	0.00	0.07	0.12	0.01	0.00	0.10	0.04	0.11
Y2O3	0.10	0.00	0.10	0.05	0.11	0.23	0.06	0.08	0.09	0.13	0.14	0.21	0.06	0.06	0.00	0.01	0.07	0.07
Ce2O3	0.00	0.05	0.04	0.06	0.00	0.13	0.09	0.00	0.34	0.00	0.00	0.25	0.22	0.16	0.10	0.21	0.23	0.21
F	3.27	3.61	3.30	3.27	3.20	3.32	3.49	3.31	3.14	3.72	3.08	3.53	2.98	2.73	3.10	2.65	2.66	2.86
Cl	0.01	0.01	0.00	0.01	0.00	0.00	0.01	0.00	0.00	0.01	0.01	0.01	0.04	0.04	0.02	0.07	0.04	0.02
Total	104.48	103.33	102.92	104.33	104.10	103.14	103.35	102.26	101.73	105.36	101.84	103.33	102.45	101.96	102.82	103.62	102.79	103.34
O=F	1.38	1.52	1.39	1.38	1.35	1.40	1.47	1.40	1.32	1.57	1.30	1.49	1.25	1.15	1.30	1.12	1.12	1.20
O=Cl	0.00	0.00	0.00	0.00	0.00	0.00	0.00	0.00	0.00	0.00	0.00	0.00	0.01	0.01	0.01	0.02	0.01	0.00
Total	103.10	101.81	101.53	102.95	102.75	101.74	101.87	100.86	100.41	103.79	100.55	101.84	101.19	100.80	101.51	102.49	101.66	102.14
Number of ions on the basis of 26 O																		
Ca	9.49	9.47	9.52	9.43	9.60	9.54	9.50	9.57	9.55	9.39	9.67	9.43	9.65	9.49	9.62	9.45	9.70	9.66
P	6.26	6.22	6.23	6.28	6.22	6.19	6.22	6.22	6.17	6.26	6.20	6.22	6.21	6.29	6.22	6.32	6.21	6.21
Sr	0.01	0.02	0.02	0.01	0.01	0.01	0.02	0.01	0.02	0.01	0.01	0.00	0.00	0.01	0.01	0.01	0.00	0.00
Si	0.00	0.00	0.00	0.00	0.00	0.04	0.00	0.00	0.07	0.00	0.00	0.03	0.01	0.01	0.01	0.01	0.02	0.02
Mn	0.01	0.01	0.01	0.00	0.00	0.01	0.00	0.00	0.00	0.00	0.00	0.01	0.02	0.00	0.00	0.01	0.01	0.02
Y	0.01	0.00	0.01	0.00	0.01	0.02	0.01	0.01	0.01	0.01	0.01	0.02	0.01	0.01	0.00	0.00	0.01	0.01
Ce	0.00	0.00	0.00	0.00	0.00	0.01	0.01	0.00	0.02	0.00	0.00	0.01	0.01	0.01	0.01	0.01	0.01	0.01
F	1.66	1.86	1.71	1.66	1.64	1.72	1.80	1.73	1.65	1.88	1.61	1.82	1.55	1.42	1.61	1.36	1.38	1.48
Cl	0.00	0.00	0.00	0.00	0.00	0.00	0.00	0.00	0.00	0.00	0.00	0.00	0.01	0.01	0.01	0.02	0.01	0.01
Total cat	17.44	17.59	17.50	17.40	17.48	17.53	17.56	17.53	17.49	17.55	17.50	17.54	17.46	17.25	17.47	17.19	17.35	17.40
A	6.26	6.23	6.23	6.28	6.22	6.23	6.22	6.22	6.24	6.26	6.20	6.24	6.21	6.31	6.23	6.33	6.23	6.23
B	9.51	9.50	9.56	9.45	9.62	9.58	9.53	9.59	9.60	9.42	9.69	9.48	9.68	9.51	9.63	9.48	9.73	9.69
C	1.67	1.86	1.71	1.67	1.64	1.72	1.80	1.73	1.65	1.88	1.62	1.82	1.57	1.43	1.61	1.38	1.40	1.48

Appendix Tab. B1: Electron microprobe analysis of apatite.

Sample	6AnTA	6AnTA	6AnTA	MA36	MA36	MA36	MA36	MA36	MA36	MA36	MA36	MA36	MA36
Analysis	6-7	6-9	6-10	MA36-1	MA36-2	MA36-3	MA36-4	MA36-5	MA36-6	MA36-7	MA36-8	MA36-9	MA36-10
CaO	54.98	54.83	55.09	54.92	54.80	54.69	55.44	55.04	55.19	54.45	54.55	54.81	55.24
P2O5	45.74	44.41	45.22	45.25	45.22	44.61	44.47	44.47	44.61	44.10	44.48	44.48	44.81
SrO	0.00	0.01	0.01	0.11	0.08	0.10	0.04	0.00	0.03	0.03	0.00	0.09	0.02
SiO2	0.04	0.03	0.08	0.03	0.06	0.04	0.00	0.03	0.03	0.04	0.02	0.02	0.06
MnO	0.06	0.10	0.04	0.14	0.18	0.21	0.17	0.17	0.21	0.15	0.19	0.23	0.19
Y2O3	0.03	0.11	0.01	0.00	0.04	0.01	0.00	0.04	0.06	0.00	0.09	0.05	0.07
Ce2O3	0.10	0.19	0.35	0.19	0.00	0.09	0.14	0.13	0.12	0.00	0.15	0.14	0.06
F	2.61	2.83	2.82	2.73	2.67	2.67	2.71	2.83	2.79	2.71	2.68	2.97	2.67
Cl	0.03	0.03	0.02	0.01	0.00	0.01	0.01	0.02	0.01	0.01	0.01	0.01	0.01
Total	103.59	102.55	103.66	103.37	103.05	102.43	102.96	102.72	103.05	101.48	102.17	102.80	103.13
O=F	1.10	1.19	1.19	1.15	1.13	1.12	1.14	1.19	1.18	1.14	1.13	1.25	1.12
O=Cl	0.01	0.01	0.00	0.00	0.00	0.00	0.00	0.00	0.00	0.00	0.00	0.00	0.00
Total	102.48	101.35	102.46	102.22	101.92	101.30	101.82	101.53	101.87	100.34	101.04	101.55	102.00
Number of ions on the basis of 26 O													
Ca	9.57	9.69	9.61	9.60	9.60	9.67	9.77	9.71	9.71	9.71	9.67	9.66	9.70
P	6.29	6.20	6.24	6.25	6.26	6.23	6.19	6.20	6.20	6.22	6.23	6.20	6.22
Sr	0.00	0.00	0.00	0.01	0.01	0.01	0.00	0.00	0.00	0.00	0.00	0.01	0.00
Si	0.01	0.01	0.01	0.00	0.01	0.01	0.00	0.00	0.01	0.01	0.00	0.00	0.01
Mn	0.01	0.01	0.01	0.02	0.03	0.03	0.02	0.02	0.03	0.02	0.03	0.03	0.03
Y	0.00	0.01	0.00	0.00	0.00	0.00	0.00	0.00	0.01	0.00	0.01	0.00	0.01
Ce	0.01	0.01	0.02	0.01	0.00	0.01	0.01	0.01	0.01	0.00	0.01	0.01	0.00
F	1.34	1.48	1.46	1.41	1.38	1.39	1.41	1.47	1.45	1.43	1.40	1.55	1.38
Cl	0.01	0.01	0.01	0.00	0.00	0.00	0.00	0.00	0.00	0.00	0.00	0.00	0.00
Total cat	17.23	17.42	17.35	17.32	17.29	17.34	17.41	17.43	17.41	17.38	17.35	17.47	17.35
A	6.30	6.21	6.25	6.26	6.27	6.24	6.19	6.20	6.21	6.22	6.23	6.20	6.23
B	9.58	9.73	9.64	9.65	9.64	9.71	9.81	9.75	9.75	9.74	9.71	9.72	9.74
C	1.35	1.49	1.46	1.41	1.38	1.40	1.41	1.48	1.45	1.43	1.40	1.55	1.39

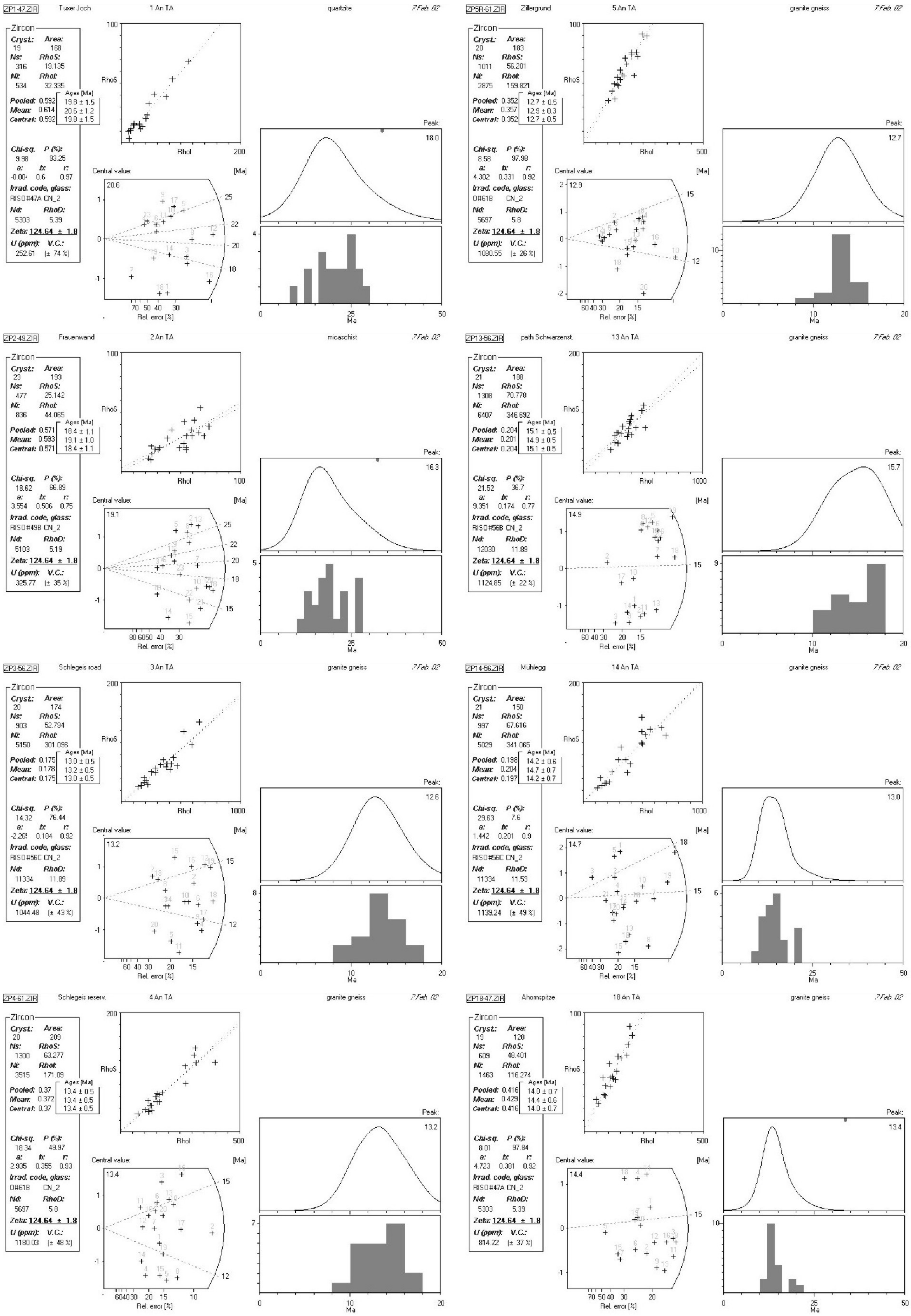

Appendix Fig. B1:

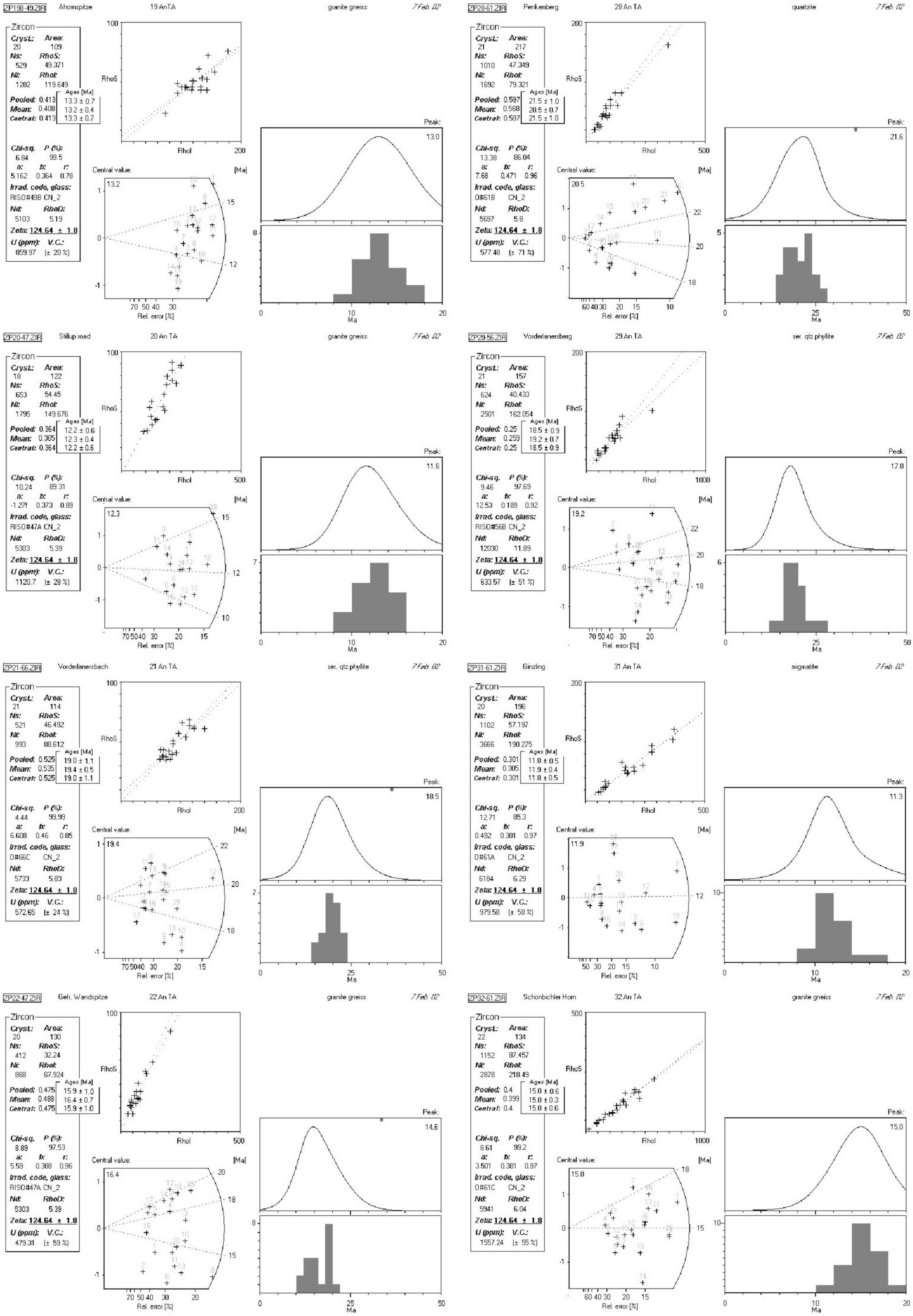

Appendix Fig. B1:

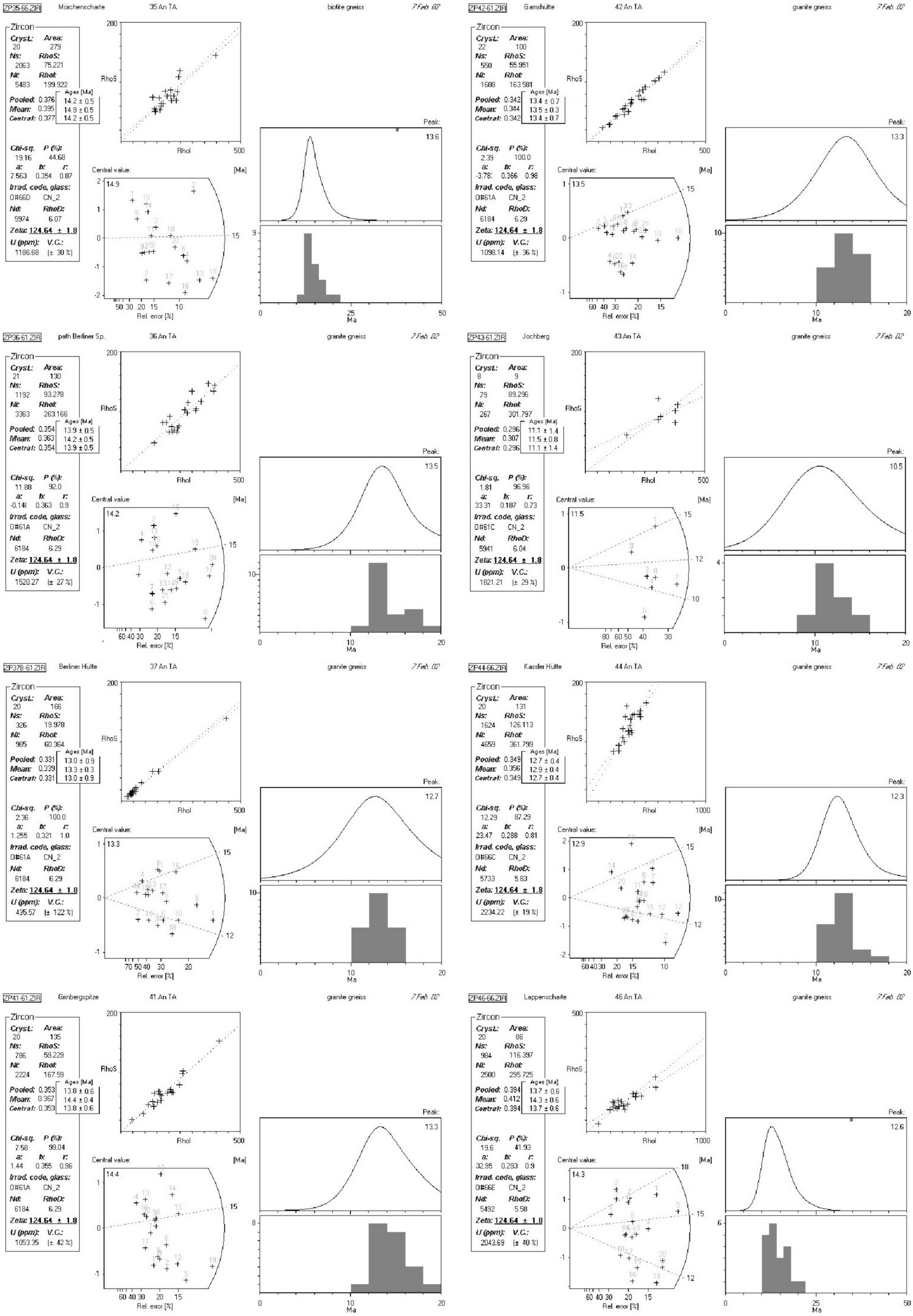

Appendix Fig. B1:

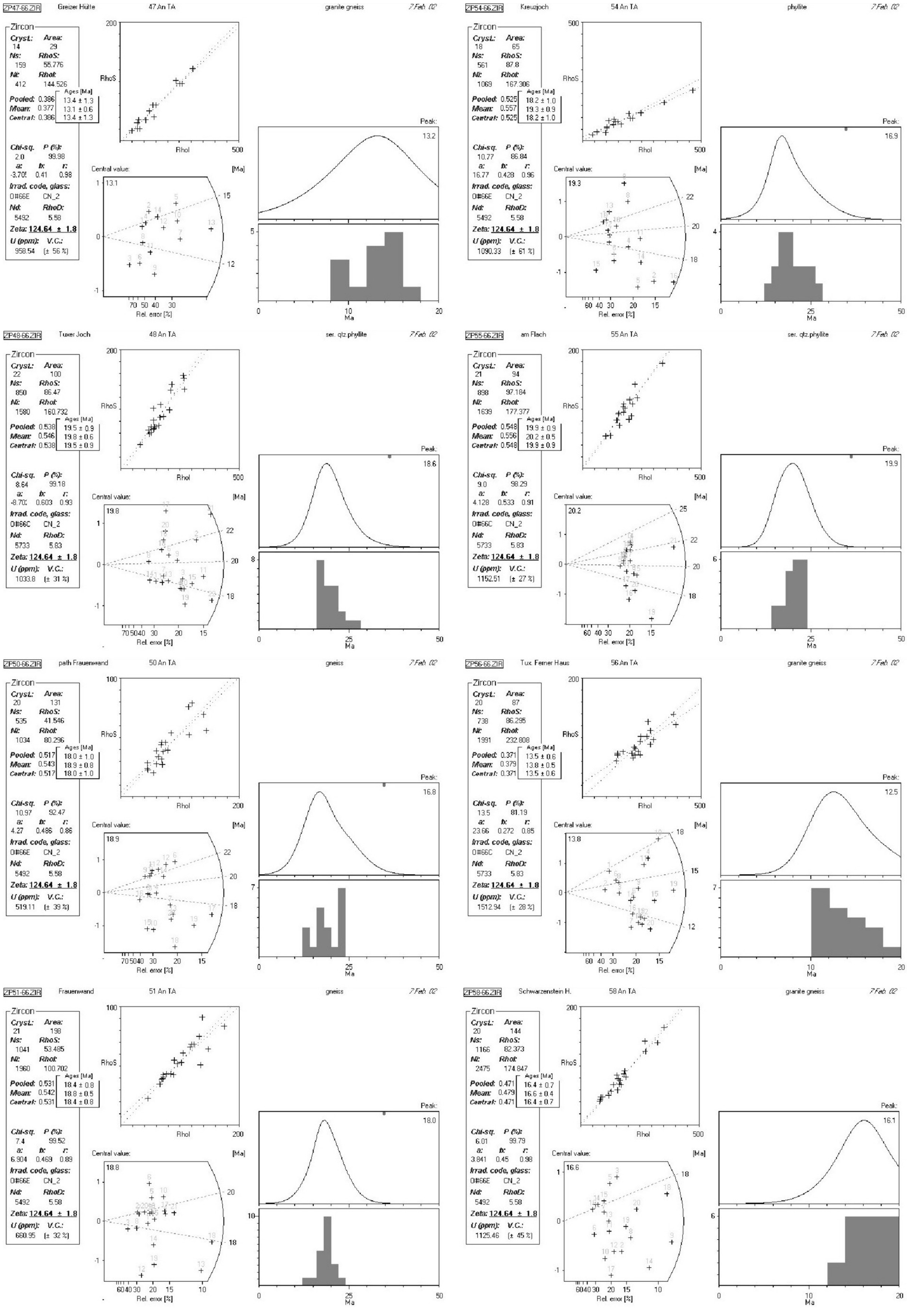

Appendix Fig. B1:

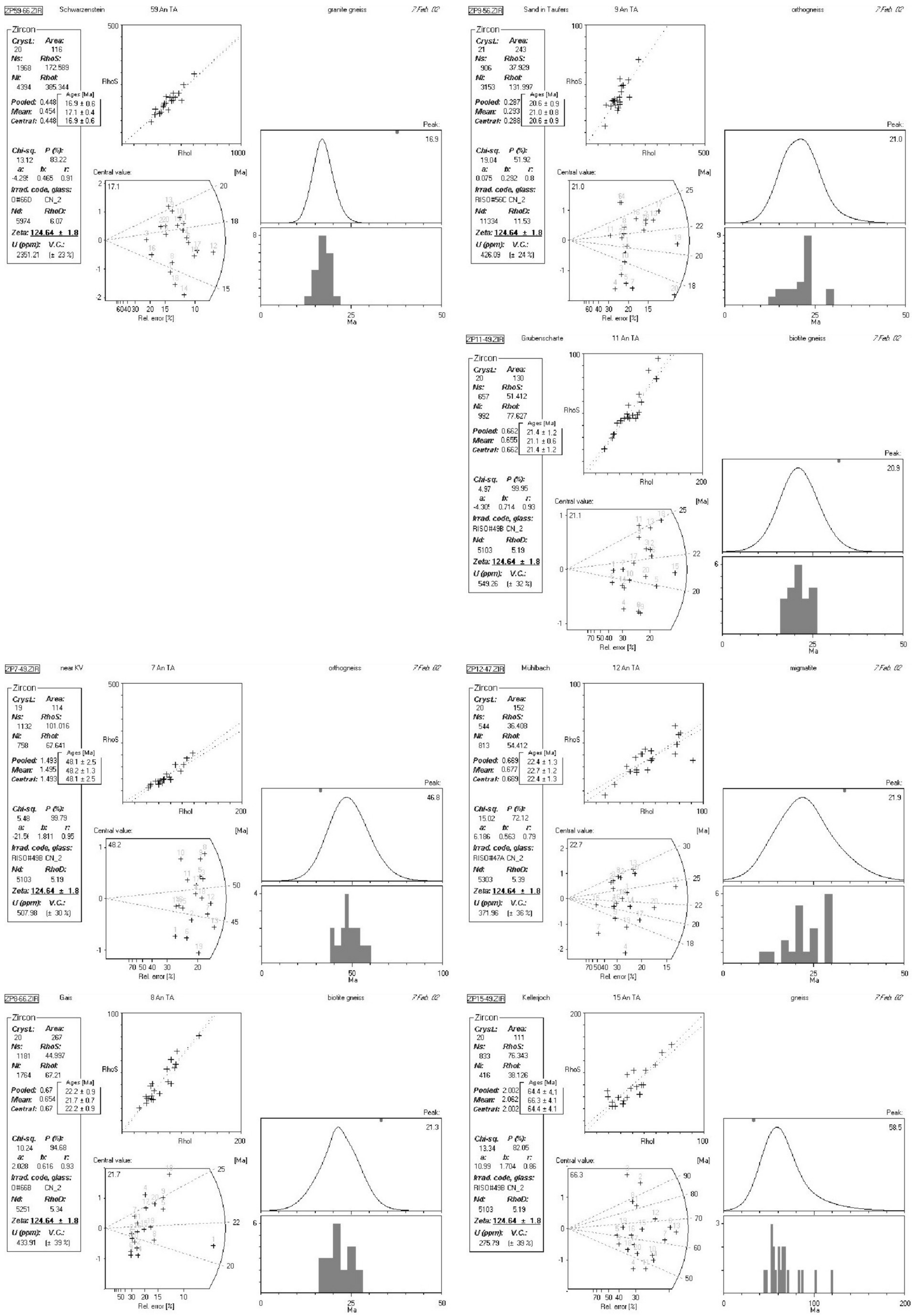

Appendix Fig. B1:

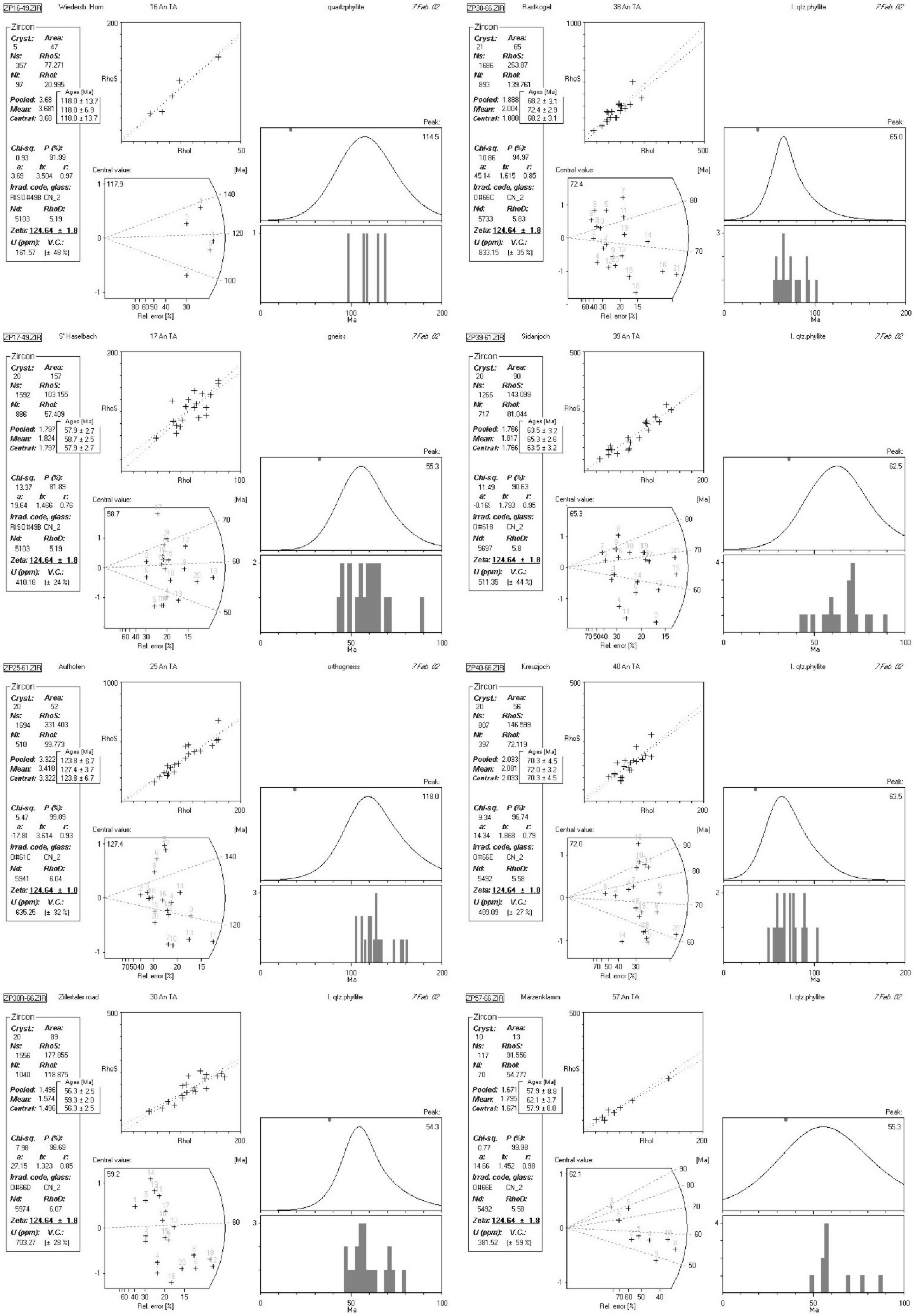

Appendix Fig. B1:

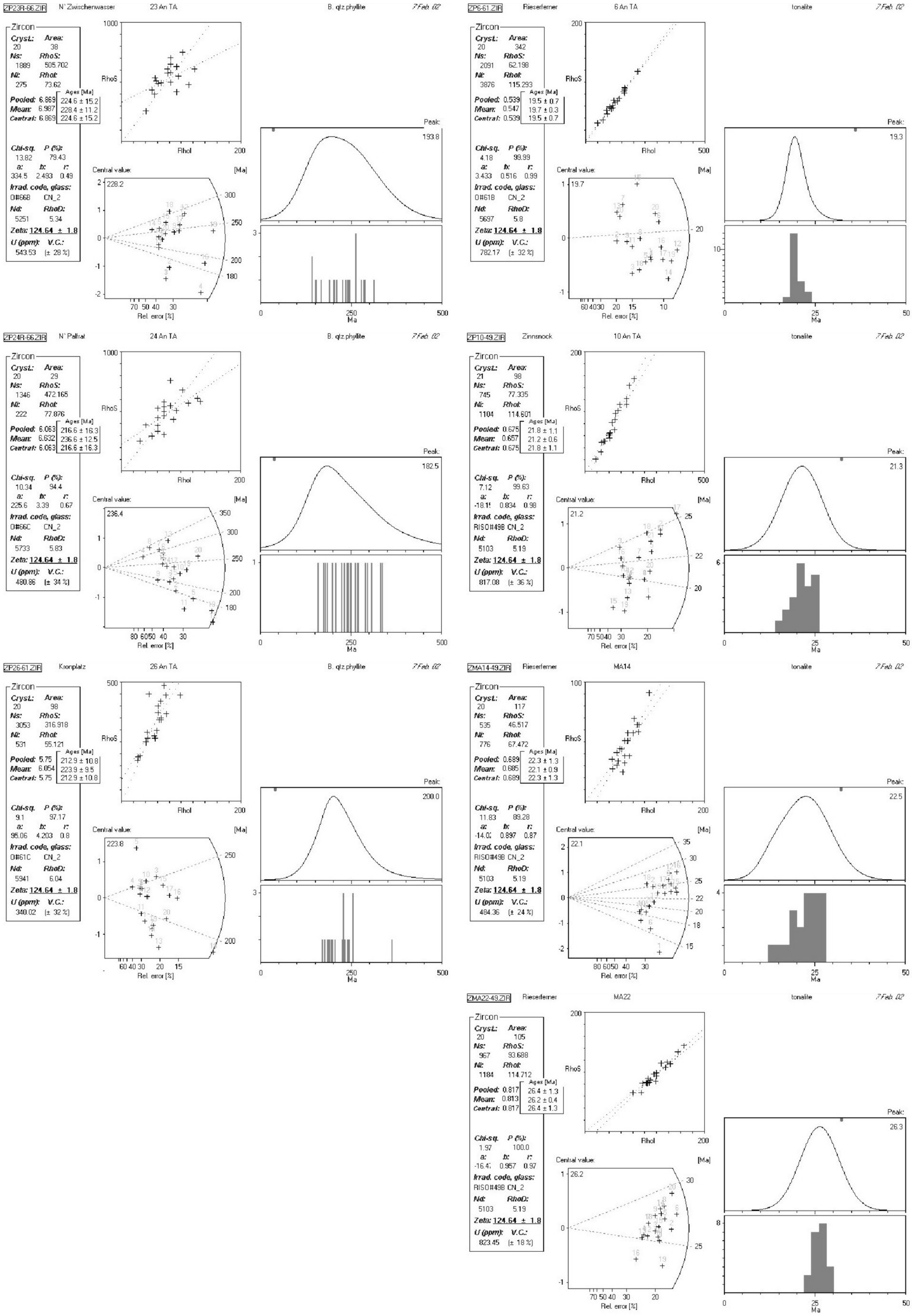

Appendix Fig. B1:

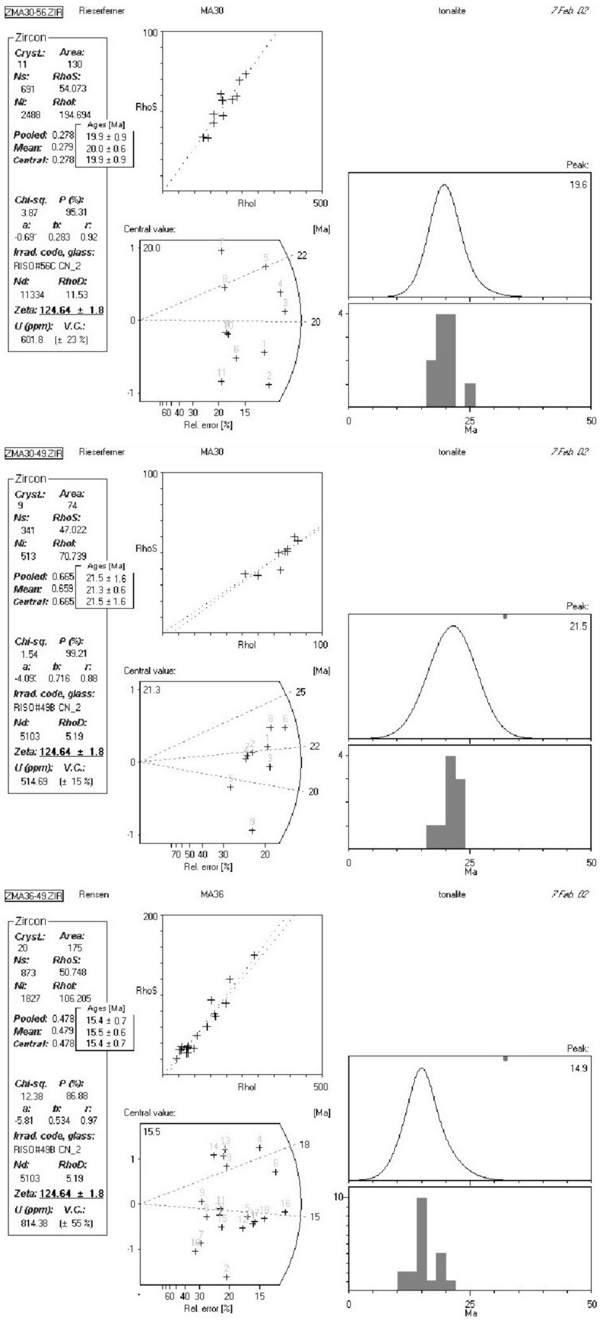

Appendix Fig. B1:

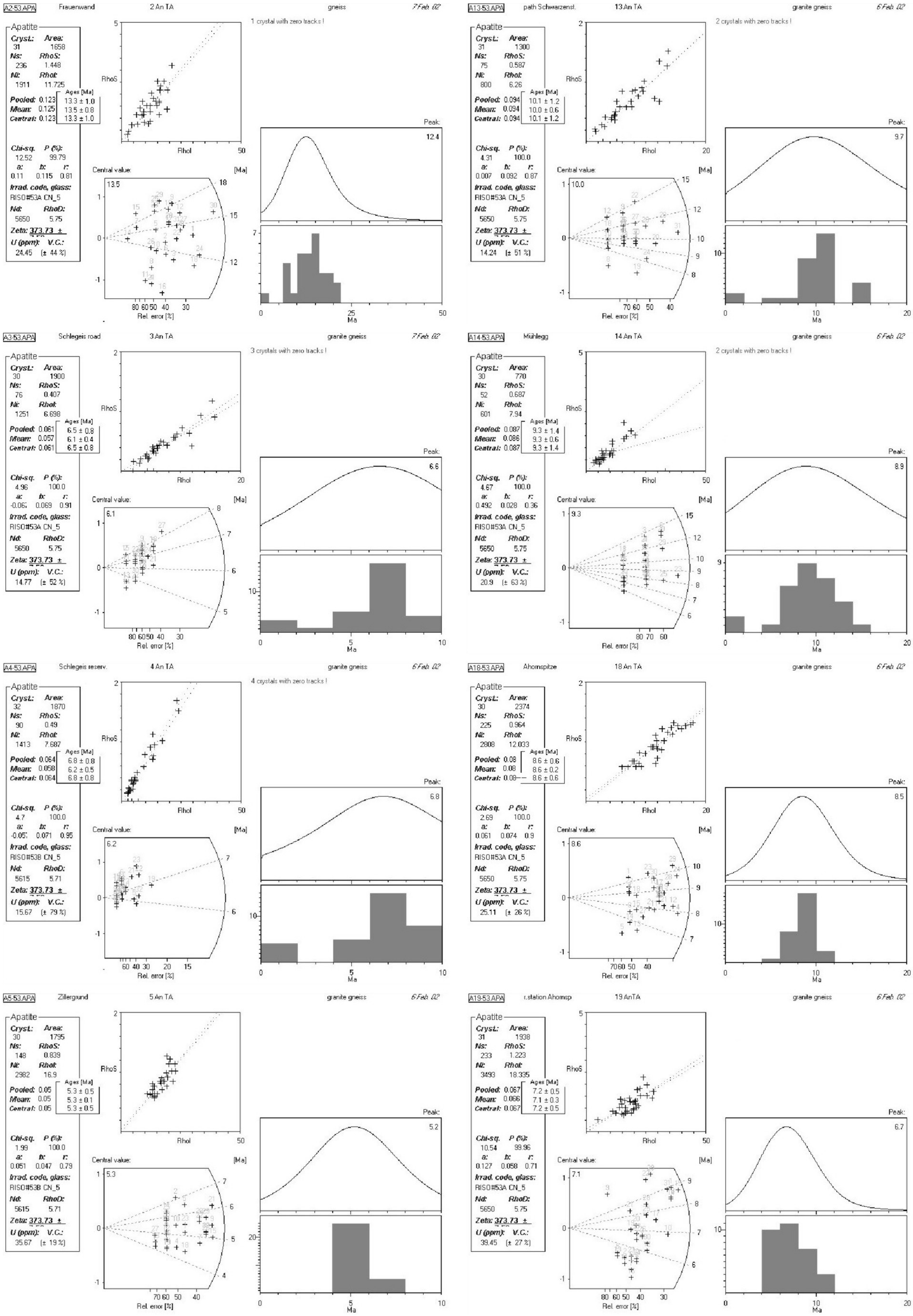

Appendix Fig. B2:

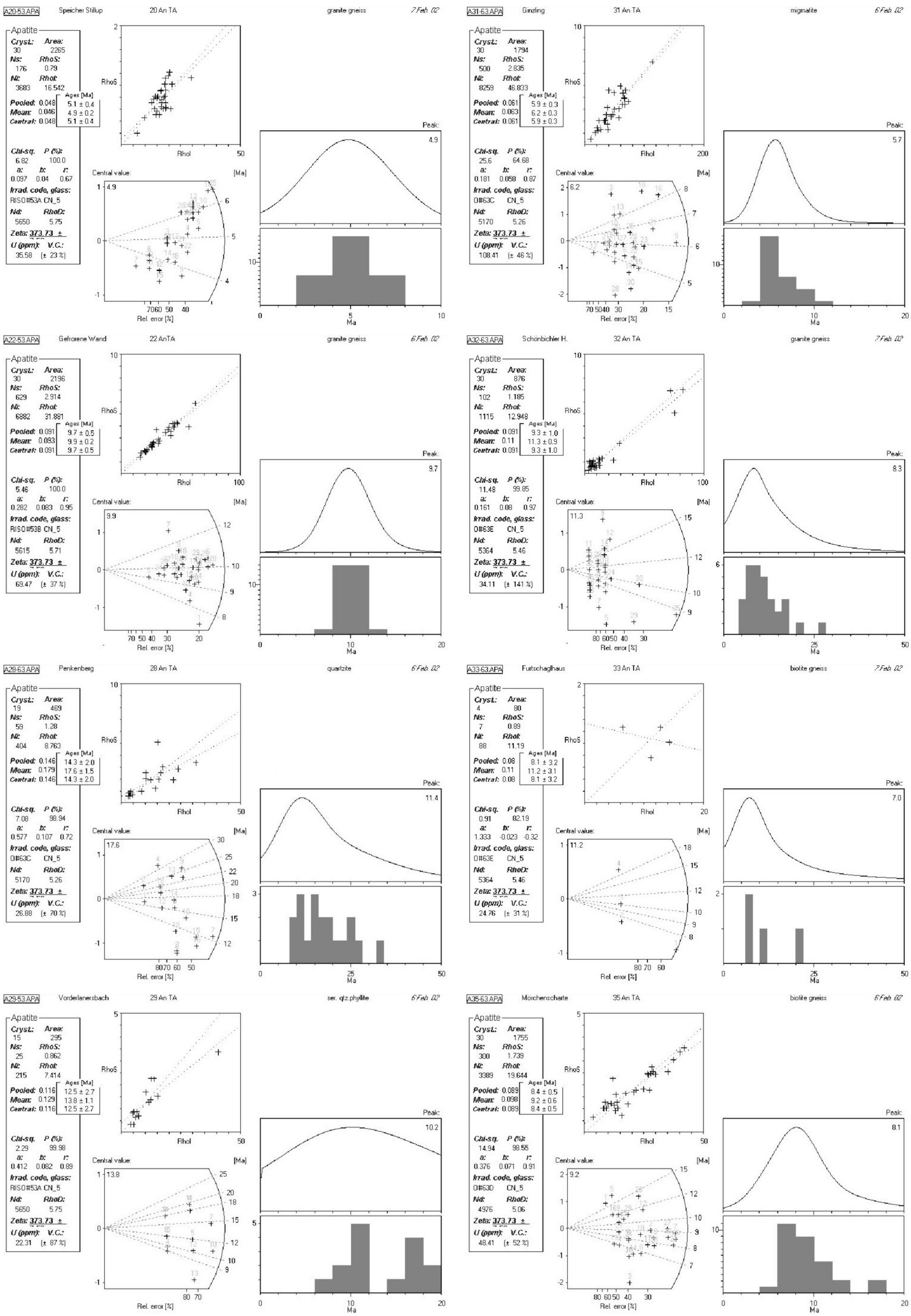

Appendix Fig. B2:

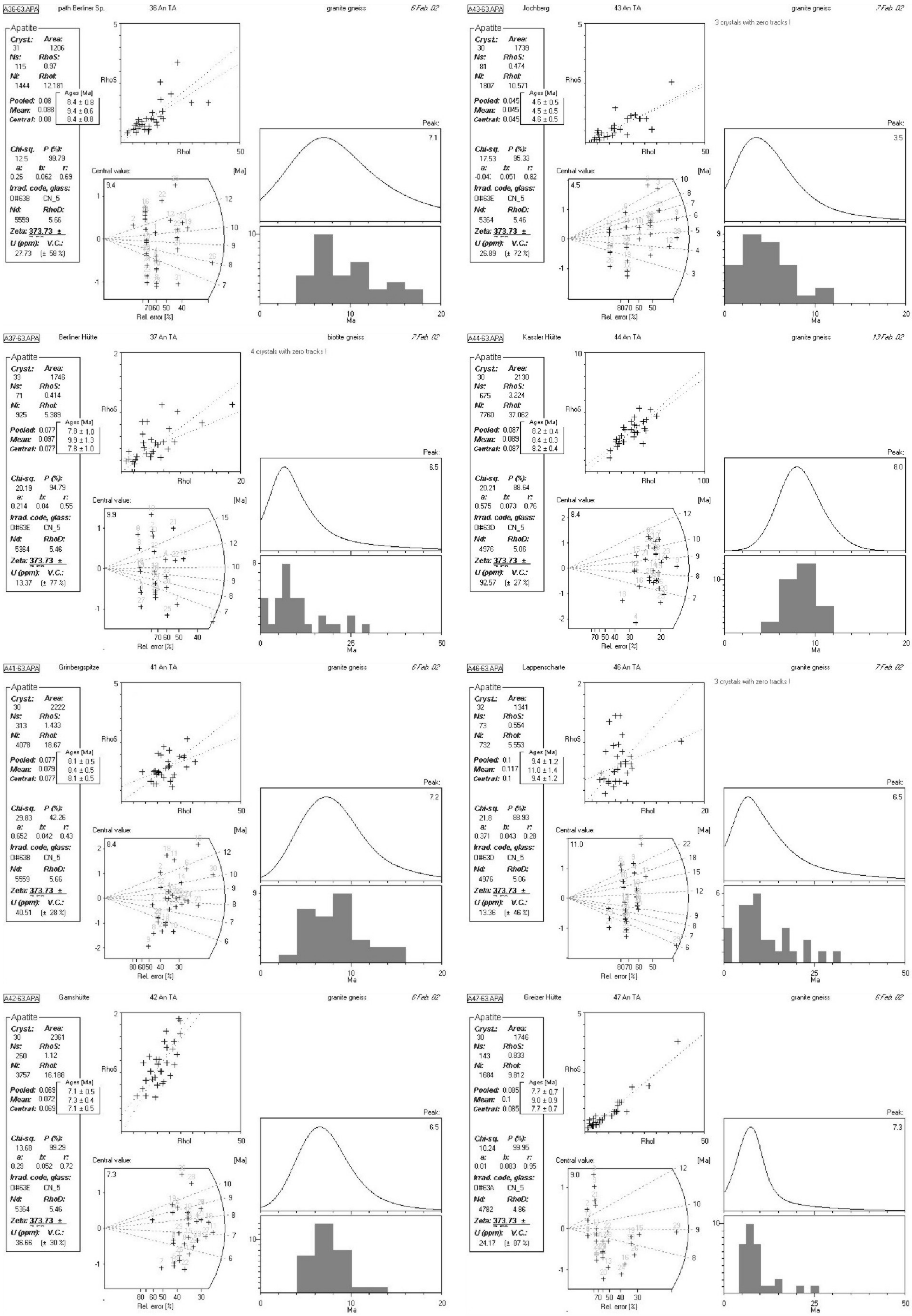

Appendix Fig. B2:

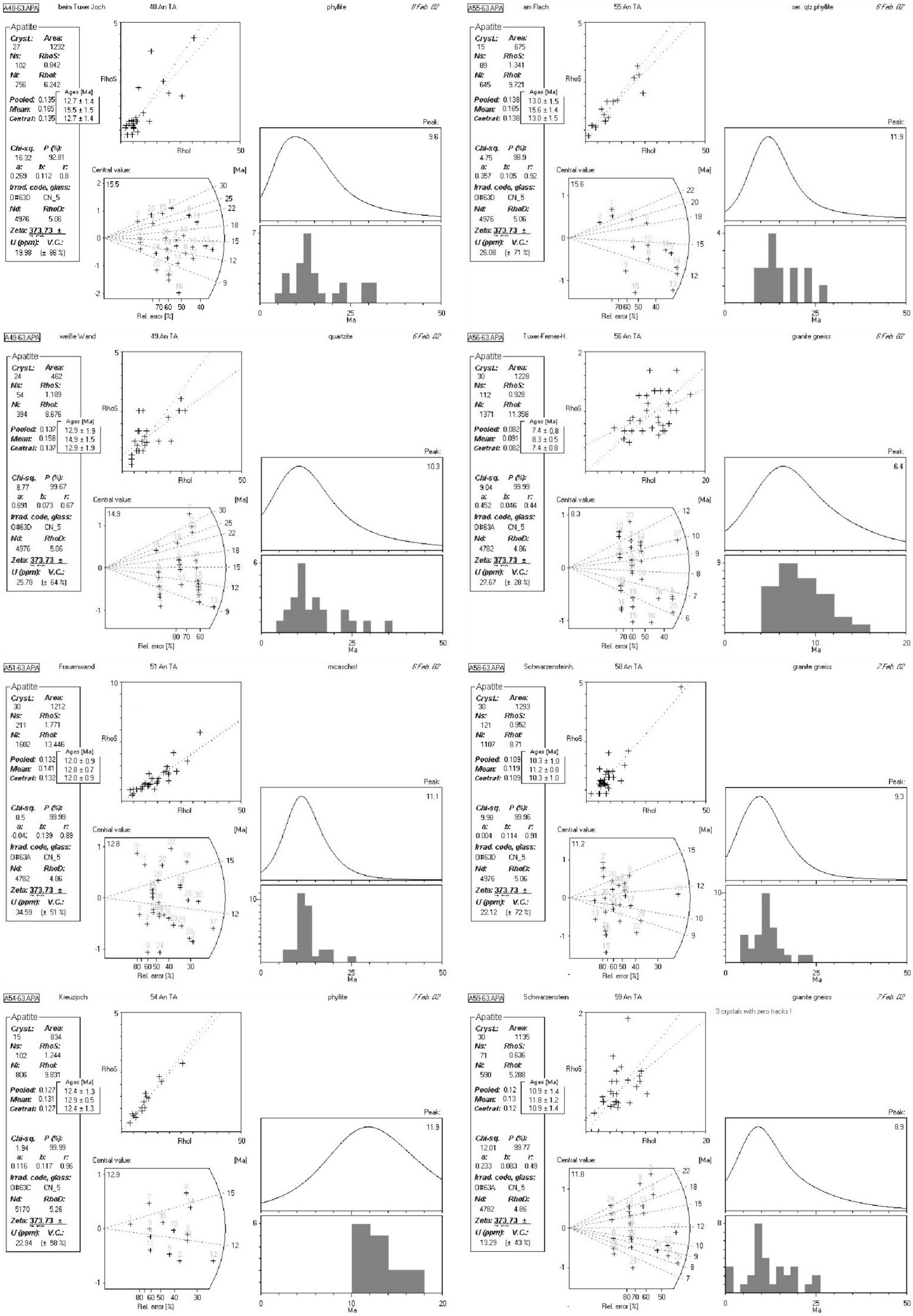

Appendix Fig. B2:

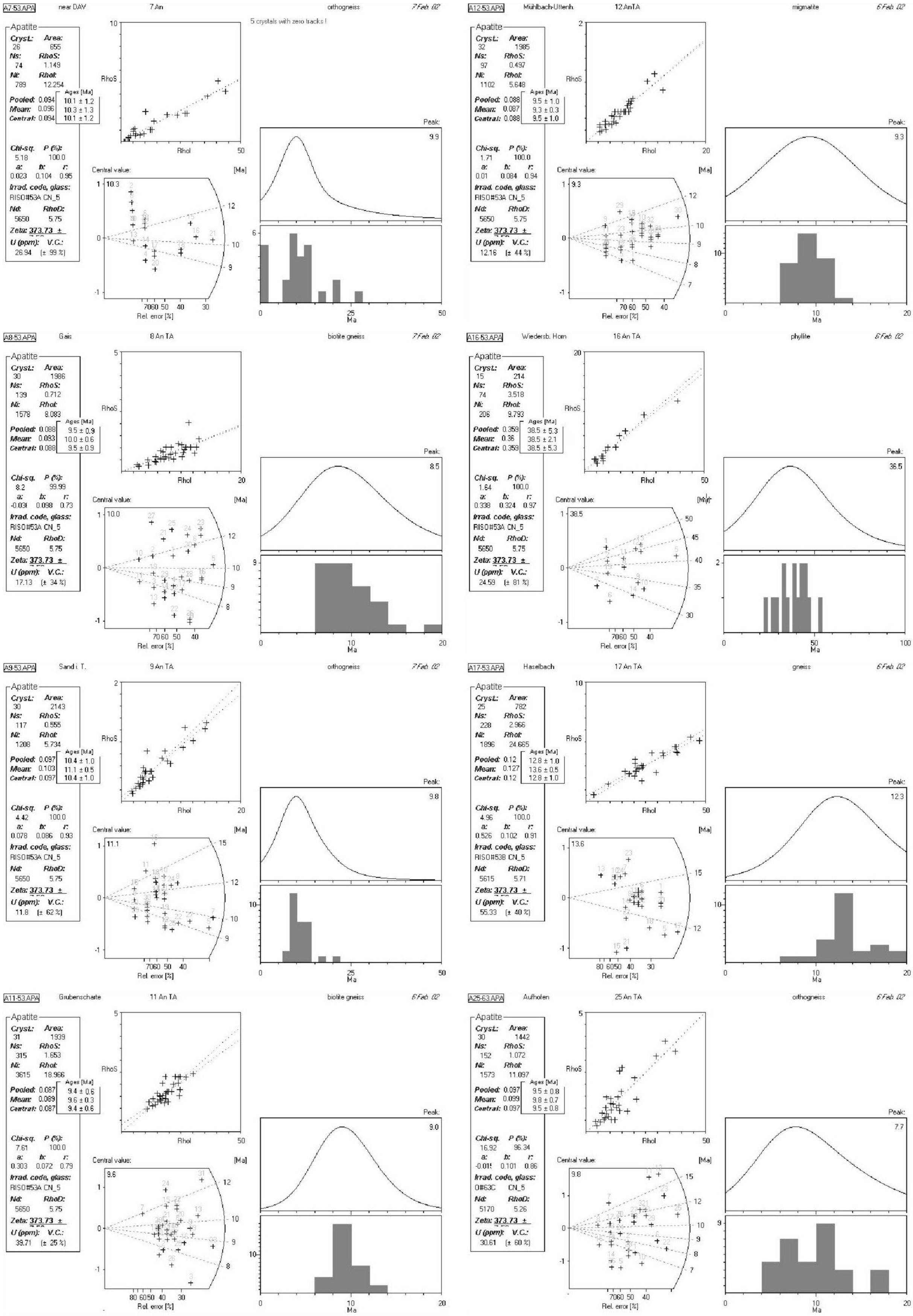

Appendix Fig. B2:

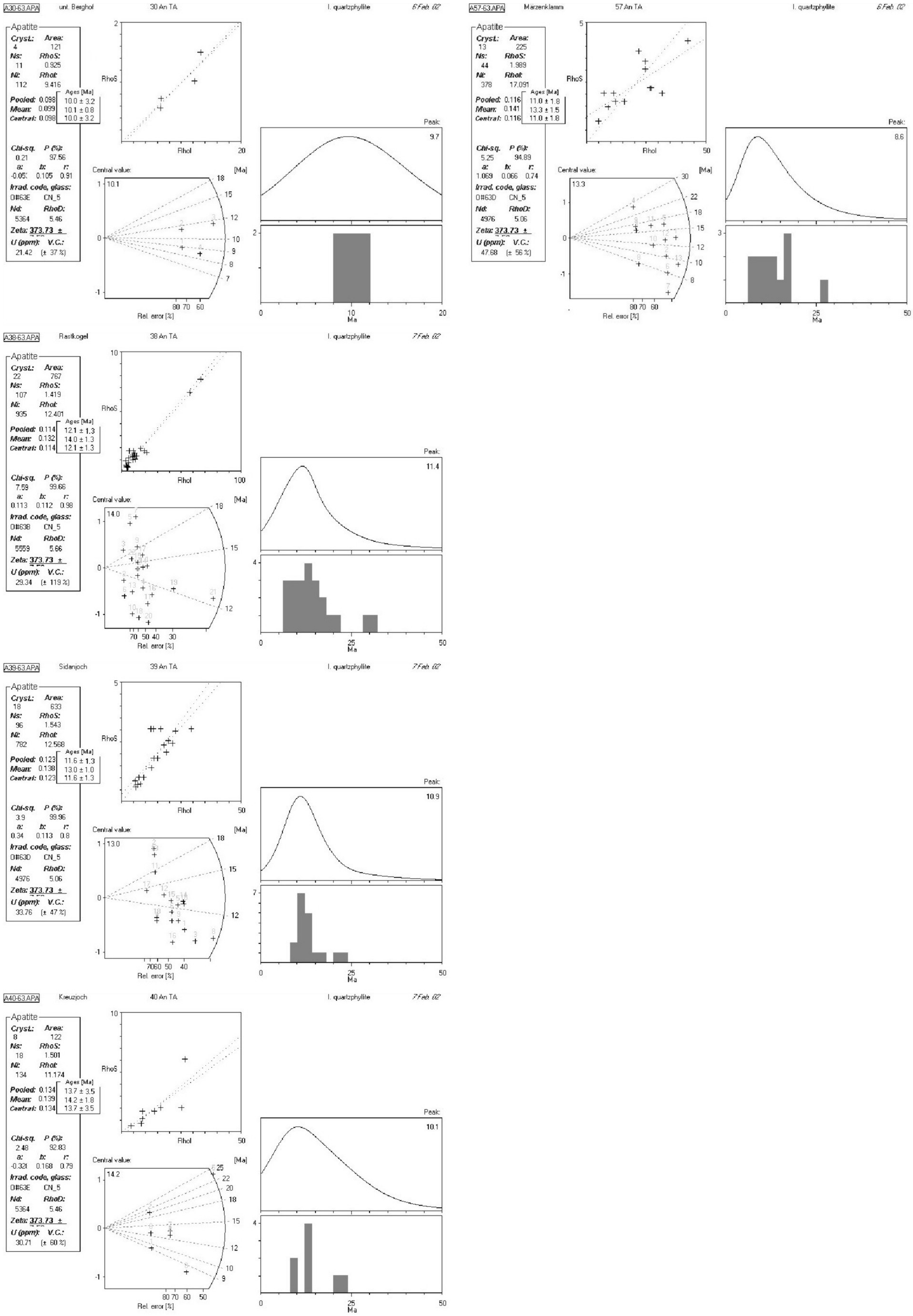

Appendix Fig. B2:

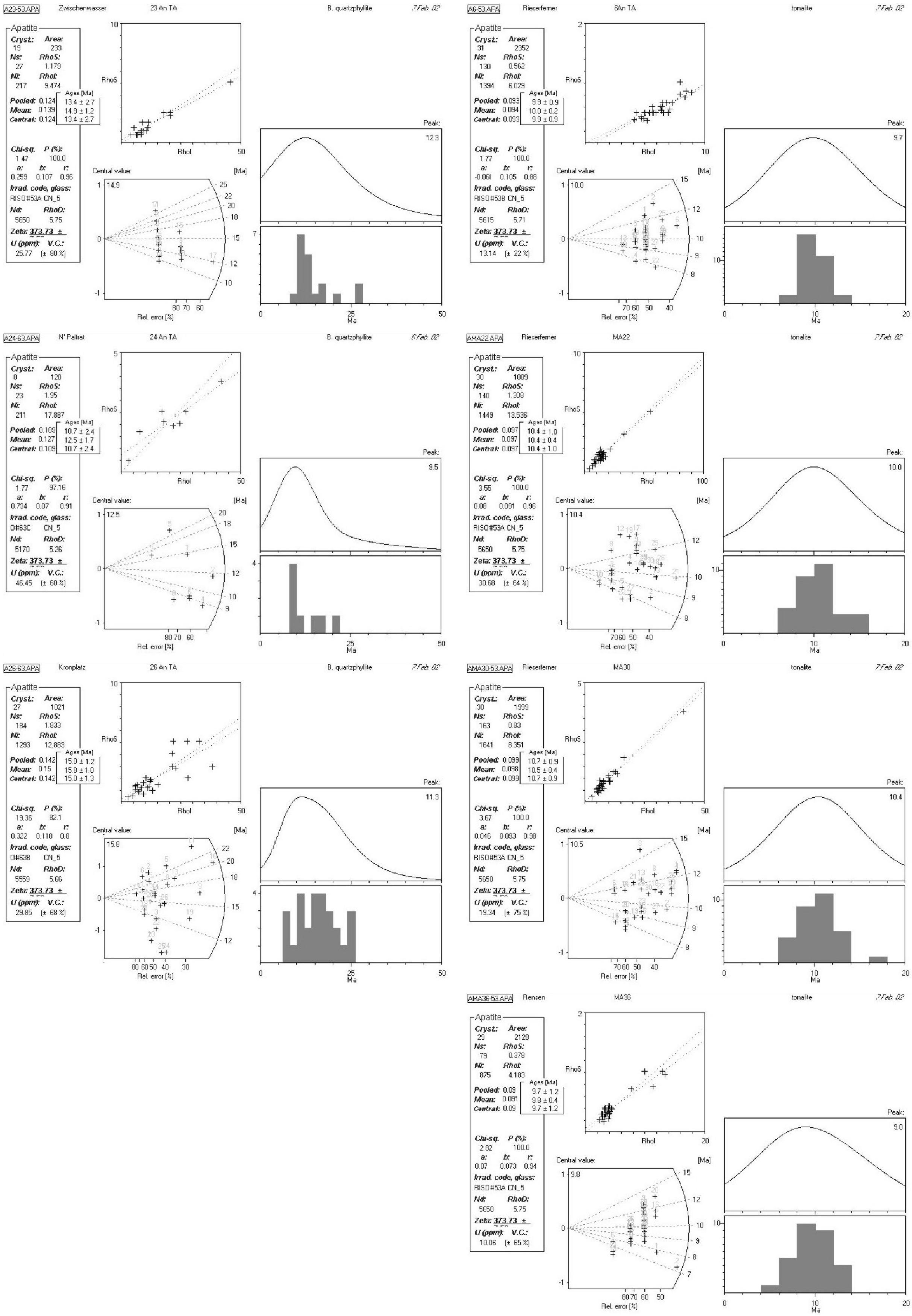

Appendix Fig. B2:

CURRICULUM VITAE

Name:	Petra Most
Geburtsdatum / -ort:	15. November 1971, Göppingen

Schule:

1978 – 1982	Grundschule Wangen
1982 – 1991	Mörike Gymnasium Göppingen

Studium:

1991 – 1997	Studium der Geologie / Paläontologie an der Geowissenschaftlichen Fakultät der Georg-August Universität, Göttingen. Abschluß: Diplom-Geologin.
1998 – 2003	Promotionsstudium am Institut für Geowissenschaften der Eberhardt-Karls Universität Tübingen.